Double emulsion microdroplets for high-throughput yeast single-cell analysis

By

Hangrui Liu

A Thesis submitted to Macquarie University

for the Degree Of

Doctor of Philosophy

Department of Physics and Astronomy

September 2021

MACQUARIE
University

Statement of Originality

This work has not previously been submitted for a degree or diploma in any university. To the best of my knowledge and belief, the thesis contains no material previously published or written by another person except where due reference is made in the thesis itself.

(Signed)_____ Date: 03/09/2021

Acknowledgements

These past three years have seen numerous transitions in my life, which have been extremely significant in my future life, career, and research. I would like to express my deepest gratitude to my supervisors, Emeritus Prof. James Piper AM and Dr. Ming Li, for the success of my journey here. They have helped me in all aspects of my study and taught me the lessons to be a competent PhD student, not only on how to interpret an elusive phenomenon in experiments, also how to capture every fleeting inspiration and opportunity with sensitivity. I'm proud of, and grateful for, my time working with them.

Second, I greatly acknowledge the International Macquarie University Research Excellence Scholarships (iMQRES) and ARC Centre of Excellence for Nanoscale BioPhotonics (CNBP) to provide support for my graduate study and the achievement of this project.

Third, my sincere thanks also go to Macquarie researchers who offered me valuable ideas, suggestions, and experiences, Prof. Ian Paulsen, Prof. David Inglis, Dr. Mohsen Asadnia, Dr. Amy Cain, Dr. Thomas Williams, Dr. Heinrich Kroukamp, Dr. Lianmei Jiang, Dr. Lucie Semenec, Dr. Xin Xu, Dr. Chao Shen, Mr. Arthur Chien, and Mr. Peng Kai. I am also very thankful to Prof. Polly Fordyce and Dr. Kara Brower from Stanford University who generously shared their work that inspired me to finish this project. Thank you all for the time and effort you put into answering my questions and demonstrating!

I earnestly thank my dear friends in Sydney. We had many great moments and memories in Australia and have grown together. I will treasure these experiences forever.

I am extremely grateful to my family for the continuous support along the way, and especially to my partner, Dr. Yu Chen, for the encouragement and inspiration from her.

Last but not least, I express my sincere gratitude to my thesis examiners for reviewing my thesis and giving their valuable comments on this project.

List of publications

Publications included in the thesis

1. **Liu, H.**; Li, M.; Wang, Y.; Piper, J. A.; Jiang, L., Improving single-cell encapsulation efficiency and reliability through neutral buoyancy of suspension. *Micromachines* **2020**, *11* (1), 94. **(chapter 3**)

2. **Liu, H.**; Xu, X.; Peng, K.; Zhang, Y.; Jiang, L.; Williams, T. C.; Paulsen, I. T.; Piper, J. A.; Li, M., Microdroplet enabled cultivation of single yeast cells correlates with bulk growth and reveals subpopulation phenomena. *Biotechnology and Bioengineering* **2021**, 118: 647– 658. (**chapter 4**)

3. **Liu, H.**; Piper, J. A.; Li, M., Rapid, simple and inexpensive spatial patterning of wettability in microfluidic devices for double emulsion generation. *Analytical Chemistry* **2021,** 93, 31, 10955–10965. (**chapter 5**)

4. **Liu, H.**; Piper, J. A.; Li, M., High-throughput microfluidics for the screening and sorting of superior cellulase activity in yeast. Palm Springs, California, USA, *MicroTAS* **2021.** (**chapter 6)**

Other Publications

1. Liu, P. *; **Liu, H.** * (*Joint first author); Semenec L.; Yuan D.; Yan S.; Cain A. K.; Li, M., Length-based separation of *Bacillus subtilis* bacterial populations by viscoelastic microfluidics. *Microsystems & Nanoengineering* **2021.**

2. Liu, P. *; **Liu, H.**; * Yuan, D.; Jang, D.; Yan, S.; Li, M., Separation and enrichment of yeast *Saccharomyces cerevisiae* by shape using viscoelastic microfluidics. *Analytical Chemistry* **2021,** 93, 3, 1586–1595.

3. Li M.; **Liu, H**.; Zhuang, S.; Goda, K., Droplet flow cytometry for single-cell analysis. *RSC Advances* **2021,** 11, 20944-20960.

4. **Liu, H.**; Piper, J. A.; Li, M., A rapid and inexpensive wettability patterning method for generating double emulsions by microfluidics. Palm Springs, California, USA, *MicroTAS* **2021.**

5. Zhuang, S.; **Liu, H.**; Li, M., Enhancing the detection signals of cell-laden microdroplets by osmosis. Palm Springs, California, USA, *MicroTAS* **2021.**

6. Cheng H.; **Liu, H**.; Li W.; Li M., Recent advances in magnetic digital microfluidic platforms. *Electrophoresis* **2021,** 42: 2329-2346.

7. Zhao, Y.; Gao, C.; Liu, H.; **Liu, H.**; Feng, Y.; Li, Z.; Liu, H.; Wang, J.; Yang, B.; Lin, Q., Infliximab-based self-healing hydrogel composite scaffold enhances stem cell survival, engraftment, and function in rheumatoid arthritis treatment. *Acta Biomaterialia* **2021**, 121, 653-664.

8. Lin, Y.; Villacanas, M.; Zou, H.; **Liu, H**.; Carcedo, I.; Wu, Y.; Sun, B.; Wu, X.; Prasadam, I.; Monteiro, M.; Li, L.; Xu, Z.; Gu, W., A new calcium-bisphosphonate nanoparticle platform as a prolonged nano-drug and bone targeted delivery system for bone diseases and cancers. *ACS Applied Bio Materials* **2021**, 4, 3, 2490–2501.

9. Zhang, Y.; Zhao, Q.; Yuan, D.; **Liu, H.**; Yun, G.; Lu, H.; Li, M.; Guo, J.; Li, W.; Tang, S.-Y., Modular off-chip emulsion generator enabled by a revolving needle. *Lab on a Chip* **2020**, *20*, 4592-4599.

10. Akhter, F.; Nag, A.; Alahi, M. E. E.; **Liu, H.**; Mukhopadhyay, S. C., Electrochemical detection of calcium and magnesium in water bodies. *Sensors & Actuators A: Physical* **2020**, *305*, 111949.

11. Sayem, A. S. M.; Simorangkir, R. B. V. B.; Esselle, K. P.; Hashmi, R. M.; **Liu, H.**, A Method to develop flexible robust optically transparent unidirectional antennas utilizing pure water, PDMS, and transparent conductive mesh. *IEEE Transactions on Antennas and Propagation* **2020**, *68* (10), 6943-6952.

12. Sayem, A. S. M.; Esselle, K. P.; Hashmi, R. M.; **Liu, H.**, Experimental studies of the robustness of the conductive-mesh-polymer composite towards the development of conformal and transparent antennas. *Smart Materials and Structures* **2020**, *29* (8), 085015.

13. Han, T.; Nag, A.; Simorangkir, R. B. V. B.; Afsarimanesh, N.; **Liu, H.**; Mukhopadhyay, S. C.; Xu, Y.; Zhadobov, M.; Sauleau, R., Multifunctional flexible sensor based on laser-induced graphene. *Sensors* **2019**, *19* (16), 3477.

14. Han, T.; Nag, A.; Afsarimanesh, N.; Akhter, F.; **Liu, H**.; Sapra, S.; Mukhopadhyay, S.; Xu, Y., Gold/Polyimide-based resistive strain sensors. *Electronics* **2019**, *8* (5), 565.

List of acronyms

(In Alphabetic Order)

AA	Acetic Acid
AADS	Absorbance-Activated Droplet Sorting
AFM	Atomic Force Microscopy
ALE	Adaptive Laboratory Evolution
AMI	Amicoumacin A
ANOVA	Analysis of Variance
aTC	Anhydrotetracycline
BSA	Bovine Serum Albumin
BGL	β-glucosidase
Ca	Capillary Number
CA	Contact Angle
C.V.	Coefficient of Variation
ddPCR	Droplet Digital Polymerase Chain Reaction
DE	Double Emulsion
DEP	Dielectrophoresis
DI	Deionised
FACS	Fluorescence-Activated Cell Sorting
FADS	Fluorescence-Activated Droplet Sorting
FBS	Fetal Bovine Serum
FC	Flow Cytometry
FEP	Fluorinated Ethylene Propylene
FITC	Fluorescein Isothiocyanate
FLADS	Lifetime-Activated Droplet Sorting
FSC	Forward Scatter
HLB	Hydrophilic–Lipophilic Balance
IACS	Image-Activated Cell Sorting
IFC	Imaging Flow Cytometry
IQR	Interquartile Range
LBL	Layer-By-Layer Deposition
LCM	Laser Capture Microdissection
LSC	Laser Scanning Cytometry
NIH	National Institutes of Health

OD	Optical Density
OTS	Trichloro(Octadecyl)Silane
O/W	Oil-in-Water
PA	Propionic Acid
PAA	Poly(Acrylic Acid)
PBS	Phosphate-Buffered Saline
PCR	Polymerase Chain Reaction
PDMS	Polydimethylsiloxane
PEG	Poly(Ethylene Glycol)
PFEP	Perfluoropolyether
PFOH	(1H,1H,2H,2H-Perfluoro-1-Octanol)
PMMA	Poly(Methyl Methacrylate)
PON	Paraoxonase
PVA	Poly(Vinyl Alcohol)
Re	Reynolds Number
RGD	Alginate-Arginine-Glycine-Aspartic
R^2	The Coefficient of Determination
SAW	Surface Acoustic Wave
SCRaMbLE	Synthetic Chromosome Rearrangement and Modification by LoxPsym-mediated Evolution
SSC	Side Scatter
UV	Ultraviolet
w/o	Water-in-Oil
w/o/w	Water-in-Oil-in-Water
YNB	Yeast Nitrogen Base
2D	Two Dimensional
3D	Three Dimensional

Abstract

Saccharomyces cerevisiae is the most successful eukaryotic organism acting as a cell factory for producing a wide range of value-added products in an economical and environmental-friendly manner. To acquire desirable phenotypes (e.g., high biomass and metabolite productivity, and high acid tolerance) for large-scale industrial production, directed evolution has been widely used, by mimicking the natural selection of rare variants from random mutant libraries. However, traditional directed evolution of variants is performed in bulk, obscuring cell-to-cell heterogeneity and slowing evolution efficiency. Fluorescence-activated cell sorting (FACS) can perform high-throughput single-cell analyses; however, it can only analyse biomarkers that are intracellular or expressed on cell surface.

The advent of droplet microfluidics opens avenues for the analysis of individual cells encapsulated within picoliter microdroplets, based on extracellular activities (e.g., secreted protein production). Particularly, water-in-oil-in-water (w/o/w) double emulsions (DEs) are compatible with commercial flow cytometric instruments, allowing the characterisation and selection of single cells exhibiting desirable properties. Although there exist a few studies on the use of the integrated DE and FACS approach for directed evolution of enzymes in microorganisms, several practical challenges have prevented its widespread adoption and applications. Therefore, the thesis aims to optimise DE-FACS methods in differing aspects, for a high-throughput directed evolution of enzymes in yeast.

First, the use of a density-matching reagent, OptiPrep™, for acquiring high-efficiency single-cell encapsulation in droplets has been quantitatively characterised. OptiPrep™ creates a neutral buoyance of cell suspension, making distribution of cell numbers in droplets fit closely to the Poisson distribution. In addition, there was no obvious decrease in cell viability

after 24 h cultivation when different concentrations of OptiPrep™ of different concentrations were used.

To investigate yeast single-cell growth and physiological behaviours in droplets, yeast single cell cultures were compared with corresponding bulk cultures using different cell strains and environmental conditions. It was found that *S. cerevisiae* single cells in droplets have a similar growth rate to that of bulk cultures in the exponential phase and can reveal subpopulation behaviours obscured in bulk cultures. Moreover, the effect of acids on cell growth, and these effects of potassium ion and mutation on cell resistance to PA at the single-cell level were studied, showing similar trends to bulk cultures.

To achieve a rapid, simple, and inexpensive generation of monodisperse DEs, a method to prepare PDMS devices with local wettability has been developed. A convenient hand-held corona treater that can generate local corona discharge was used to render microchannels hydrophilic at target regions. In addition, a specific customised channel (i.e., a serpentine narrow channel as a plasma resistor) was designed to prevent the diffusion of corona discharge to unwanted regions. With this approach, I achieved the generation of DEs with multiple structures and morphologies. Furthermore, I demonstrated the abilities of generated DEs for microgel synthesis and yeast single cell culture and its downstream flow cytometric screening.

Lastly, the improved DE-FACS platform technology was applied to screening and selection of extracellular enzymatic activities in yeast cells. As a proof of concept, an artificial library of wild type and cellulase-secreting mutant cells were mixed with a ratio of 1:1 and encapsulated in DEs. Mutant cells showing a high level of extracellular enzymatic activity were successfully selected by FACS, with an accuracy of up to 92%.

In summary, this thesis has studied different approaches to improving the performance of integrated DE-FACS platform technology for single-cell analysis. These results have shown great potential for directed evolution of extracellular enzymes in yeast for industrial production.

Table of contents

Chapter 1. Introduction

1.1 Background

Baker's yeast, *Saccharomyces cerevisiae*, has been traditionally used for the production of bread, alcohols, and bioethanol in biotechnological industries. Nowadays, *S. cerevisiae* has become the most popular eukaryotic organism as a cell factory for the production of a wide range of value-added biochemicals, e.g., lipids, organic acids, pharmaceutical proteins, natural enzymes, and so on[1]. Due to its versatile capacity of producing bio-products in an economical and eco-friendly manner, yeast cell factory has been widely used in manufacturing, pharmaceutical, cosmetic, food, textile, and chemical industries. Producing commercial products by a yeast cell factory avoids the processes of chemical synthesis or oil refining that require toxic solvent, complex reaction conditions, and mass generation of by-products.

Although there exist a lot of host organisms suitable for the heterologous production of bio-products, including *Escherichia coli*, microalgae, and plants, *S. cerevisiae* is the most popular with many advantages. *S. cerevisiae* is resistant to low pH, and high ethanol and sugar concentrations; can grow anaerobically or with inhibitors present in biomass hydrolysates during fermentation; and requires low-cost growth media[2, 3]. These properties reduce the risk of contamination and make the process convenient and robust in industrial fermentation. Besides, *S. cerevisiae,* which firstly has eukaryotic complete genome, hosts an extensive repertoire of genetic resources[4]. A large amount of data for *S. cerevisiae* genes, open reading frames, gene networks, and gene products can be found in several databases such as the General Repository of Interaction Datasets and the Comprehensive Yeast Genome Database[2].

Directed evolution strategy plays an important role in metabolic engineering[5], intentionally redirecting the metabolic productivity (e.g., the amount and catalytic properties of enzymes)[5] in yeast strains for most industrial applications. In practise, directed evolution artificially

induces mutations in yeast cells, by mimicking the process of natural selection through random mutagenesis to direct evolution at the protein level[6, 7]. After this, the cells exhibiting desired traits are isolated and an iterative process is undertaken including several rounds of directed evolution of metabolic fluxes to generate the final novel variants. The screening and selection of potential variants are performed on the phenotypes, while the evolutionary information is included in the genotypes. Therefore, the identification of novel genes or metabolic pathways associated with desired traits normally requires a compartment to establish a linkage between the phenotype and genotype[6]. When the desired cells are sorted from a phenotypic screening, downstream analysis, e.g., tandem genomic, transcriptomic, and metabolomic analyses, can act on the same target or clusters, revealing genes or genetic pathways associated with the phenotypic functions.

Apparently, the successful acquisition of the superior variants requires cell-to-cell screening and selection from large heterogenous populations or libraries. Traditional directed evolution approaches, e.g., adaptive laboratory evolution (ALE), for vast screening and selection for enzymatic activity are based on the assays of isolated cell cultures on agar plates or microtiter plates[8]. Unfortunately, the frequency typically falls in the range of 10^3–10^4, and rarely above 10^5 with the help of the automated liquid handling systems[9]. Therefore, the process is lab-intensive, which can take hundreds of generations and even several years until desired strains are selected. Flow cytometric instruments (e.g., Fluorescence-activated cell sorting (FACS)) has been developed as powerful single-cell research tools, allowing a high-throughput screening and selection (i.e., over 10^7 events per hour) using fluorescence intensity as an indicator of metabolic activity levels[10]. Although a cell links genotype and phenotype for intracellular or cell surface products, many other properties cannot be interrogated by single-cell FACS: these include extracellular metabolites, catalytic properties of enzymes that are generally measured by surrounding substrates, and cell concentrations reflecting the growth

rate of producers[11]. This calls for a high-throughput platform technology that can screen and isolate on *S. cerevisiae* single cells based on extracellular enzymatic activities, which will open avenues for next-generation applications in fundamental biological research, food industry, and metabolic engineering, and so on. In recent decades, the development of miniaturised screening systems substantially circumvents this issue by creating millions of man-made compartments[12], i.e., aqueous droplets, suitable for single-cell encapsulation, long-term cell culture, and screening of biochemical reactions. The aqueous phase of a droplet is generally encapsulated within an oil phase, preventing the efflux or diffusion of polar substances between neighbouring droplets. Therefore, droplets acting as bioreactors spatially and temporally separate the dynamics of biochemical activities of individual cells and provides the linkages of the phenotype and genotype. To date, microfluidic devices have been widely used for the generation of monodisperse single-cell laden droplets at a rate of up to several kHz, off-chip cell-laden droplet incubation, reinjection of droplets into a device integrated with functionalised electrodes for sorting[13]. Fluorescence-activated droplet sorting (FADS), first developed by Baret et al.[14], enabled the sorting of water-in-oil droplets in a microfluidic device using dielectrophoresis (DEP), which has been adapted for successful evolution of variants[6].

Besides the water-in-oil droplet on-chip sorting, some forms of droplets can be screened and sorted off-chip, water-in-oil-in-water (w/o/w) double emulsions (DEs) and hydrogel droplets[15]. For simplicity, I refer to w/o/w DE as DE in the following discussions, as it is the most frequently used format of DEs to trap small molecules in droplets for single-cell analysis[11, 15, 16]. Unlike the conventional water-in-oil droplets that are carried by an oil phase, the DEs can be suspended in an aqueous phase, which makes them compatible with commercial flow cytometry instruments. The integrated DE and FACS approach has many advantages for single-cell assays compared with on-chip droplet sorting: 1) the state-of-the-art FACS enables the screening with a rate of at least an order of magnitude faster than on-chip sorting systems (⩽

2 kHz)[6, 17]; 2) commercial instruments avoid the manual adjustment and installation of complex DEP sorter and associated control modules, making the platform user-friendly to operators who do not have an engineering background. A few studies have demonstrated FACS screening of DEs as *in vitro* compartmentalisation for directed evolution of enzymes[9, 18, 19].

Despite the great promise, the integrated DE-FACS platform technology has not been as widely adopted as expected. A few key challenges below have inhibited potential broader applications:

1) unreliable passive encapsulation of single cells. In general, the ratios of droplets containing different numbers of cells are dictated by Poisson distribution. Although the portion of single-cell droplets can be ideally acquired by adjusting the initial cell concentrations, the intrinsic cell sedimentation and aggregation affect the neutrally buoyant cell suspension in practise, resulting in an unreliable estimation of a portion of single-cell laden droplets.

2) a correlation between cell culture in droplets and in bulk remains a gap. Although there are lots of investigations on cell culture in droplets, few studies have investigated the relation between single-cell culture in microdroplets and in bulk cell culture, especially under the effects of environmental factors.

3) the lack of convenient methods for monodisperse DE generation. The process of DE generation is more complicated than that of single emulsions. Traditional bulk methods are straightforward but result in highly polydisperse DE. The emerging microfluidic devices can hierarchically generate monodisperse DEs, however, they always require complicated spatially patterning of wettability in devices for DE generation.

4) it is unclear if the integrated DE-FACS approach can be used for yeast single-cell assays of β-glucosidases enzymatic activities. Even though *S. cerevisiae* has been considered as the most popular microorganism for directed evolution of enzymes, there are very few studies on using this platform for improved bio-product production by yeast. Particularly, the studies on

screening and sorting of cellulase production by yeast single cells using DE-FACS have not ever been reported.

1.2 Objectives and structure of the thesis

This thesis aims to develop an integrated platform technology, single-cell DEs combining with FACS, for a high-throughput directed evolution of enzymes in yeast. The specific objectives of the thesis are as below:

(1) Improve the single-cell encapsulation efficiency in DEs,

(2) Understand yeast single-cell behaviours in DEs,

(3) Generate single-cell laden DEs in a simple and cost-effective manner,

(4) Perform the screening and sorting of yeast single-cell assays of enzyme activity using an integrated DE and FACS approach.

The thesis consists of the following sections: introduction (Chapter 1), literature review (Chapter 2), four research projects (Chapter 3-6), conclusions and future work (Chapter 7). Specifically, the thesis is organised as follows:

Chapter 1 summarises the background, including the current methods for single-cell analysis, the importance of yeast research, the reasons for using the integrated DE-FACS approach, and the scope of the thesis.

Chapter 2 gives a literature review on the importance of single-cell analysis, fundamentals of DEs, different methods for generating DEs, materials and chemicals used for DEs, applications of DEs in single-cell based applications, especially in a high-throughput analysis.

Chapter 3 describes a quantitative characterisation of the effect of the density-matching reagent, OptiPrep™, on improving the efficiency and reliability of single-cell encapsulation in DEs.

Chapter 4 reports the investigation of the relation between yeast single-cell growth in droplet and cell growth in bulk. Two types of organic acids of different concentrations were added to microdroplets to compare the yeast cell resistance.

Chapter 5 explores a method employing localised corona discharge in a customised-built microfluidic device to achieve spatially patterned wettability for generating monodisperse DEs.

Chapter 6 presents the use of this integrated DE and FACS approach for high-throughput screening and sorting of *S. cerevisiae* single-cell cellulase activities.

Chapter 7 summarises the major outcomes of the thesis, and discusses prospects and opportunities of improving this platform technology.

References

1. Liu, H.; Xu, X.; Peng, K.; Zhang, Y.; Jiang, L.; Williams, T. C.; Paulsen, I. T.; Piper, J. A.; Li, M., Microdroplet enabled cultivation of single yeast cells correlates with bulk growth and reveals subpopulation phenomena. *Biotechnol. Bioeng.* **2021,** *118* (2), 647-658.
2. Chang, J.-J.; Ho, C.-Y.; Ho, F.-J.; Tsai, T.-Y.; Ke, H.-M.; Wang, C. H. T.; Chen, H.-L.; Shih, M.-C.; Huang, C.-C.; Li, W.-H., PGASO: A synthetic biology tool for engineering a cellulolytic yeast. *Biotechnol. Biofuels* **2012,** *5* (1), 53.
3. Walker, R. S. K.; Pretorius, I. S., Applications of Yeast Synthetic Biology Geared towards the Production of Biopharmaceuticals. *Genes* **2018,** *9* (7).
4. Goffeau, A.; Barrell, B. G.; Bussey, H.; Davis, R. W.; Dujon, B.; Feldmann, H.; Galibert, F.; Hoheisel, J. D.; Jacq, C.; Johnston, M.; Louis, E. J.; Mewes, H. W.; Murakami, Y.; Philippsen, P.; Tettelin, H.; Oliver, S. G., Life with 6000 Genes. *Science* **1996,** *274* (5287), 546.
5. Abatemarco, J.; Hill, A.; Alper, H. S., Expanding the metabolic engineering toolbox with directed evolution. *Biotechnol. J.* **2013,** *8* (12), 1397-1410.
6. Agresti, J. J.; Antipov, E.; Abate, A. R.; Ahn, K.; Rowat, A. C.; Baret, J.-C.; Marquez, M.; Klibanov, A. M.; Griffiths, A. D.; Weitz, D. A., Ultrahigh-throughput screening in drop-based microfluidics for directed evolution. *Proc. Nat.l Acad. Sci. U. S. A.* **2010,** *107* (9), 4004.
7. Weng, L.; Spoonamore, J. E., Droplet microfluidics-enabled high-throughput screening for protein engineering. *Micromachines* **2019,** *10* (11).
8. Almario, M. P.; Reyes, L. H.; Kao, K. C., Evolutionary engineering of Saccharomyces cerevisiae for enhanced tolerance to hydrolysates of lignocellulosic biomass. *Biotechnol. Bioeng.* **2013,** *110* (10), 2616-2623.
9. Aharoni, A.; Amitai, G.; Bernath, K.; Magdassi, S.; Tawfik, D. S., High-throughput screening of enzyme libraries: thiolactonases evolved by fluorescence-activated sorting of single cells in emulsion compartments. *Chem. Biol.* **2005,** *12* (12), 1281-9.
10. Stucki, A.; Vallapurackal, J.; Ward, T. R.; Dittrich, P. S., Droplet Microfluidics and Directed Evolution of Enzymes: An Intertwined Journey. *Angew. Chem. Int. Ed.* **2021,** *n/a* (n/a).
11. Bowman, E. K.; Alper, H. S., Microdroplet-Assisted Screening of Biomolecule Production for Metabolic Engineering Applications. *Trends Biotechnol.* **2020,** *38* (7), 701-714.
12. Tawfik, D. S.; Griffiths, A. D., Man-made cell-like compartments for molecular evolution. *Nat. Biotechnol.* **1998,** *16* (7), 652-656.
13. Matuła, K.; Rivello, F.; Huck, W. T. S., Single-Cell Analysis Using Droplet Microfluidics. *Adv. Biosyst.* **2020,** *4* (1), 1900188.
14. Baret, J.-C.; Miller, O. J.; Taly, V.; Ryckelynck, M.; El-Harrak, A.; Frenz, L.; Rick, C.; Samuels, M. L.; Hutchison, J. B.; Agresti, J. J.; Link, D. R.; Weitz, D. A.; Griffiths, A. D., Fluorescence-activated droplet sorting (FADS): efficient microfluidic cell sorting based on enzymatic activity. *Lab Chip* **2009,** *9* (13), 1850-1858.

15. Li, M.; Liu, H.; Zhuang, S.; Goda, K., Droplet flow cytometry for single-cell analysis. *RSC Adv.* **2021,** *11* (34), 20944-20960.
16. van Tatenhove-Pel, R. J.; Hernandez-Valdes, J. A.; Teusink, B.; Kuipers, O. P.; Fischlechner, M.; Bachmann, H., Microdroplet screening and selection for improved microbial production of extracellular compounds. *Curr. Opin. Biotechnol.* **2020,** *61*, 72-81.
17. Mazutis, L.; Gilbert, J.; Ung, W. L.; Weitz, D. A.; Griffiths, A. D.; Heyman, J. A., Single-cell analysis and sorting using droplet-based microfluidics. *Nat. Protoc.* **2013,** *8* (5), 870-891.
18. Aharoni, A.; Griffiths, A. D.; Tawfik, D. S., High-throughput screens and selections of enzyme-encoding genes. *Curr. Opin. Chem. Biol.* **2005,** *9* (2), 210-6.
19. Mastrobattista, E.; Taly, V.; Chanudet, E.; Treacy, P.; Kelly, B. T.; Griffiths, A. D., High-throughput screening of enzyme libraries: in vitro evolution of a beta-galactosidase by fluorescence-activated sorting of double emulsions. *Chem. Biol.* **2005,** *12* (12), 1291-300.

Chapter 2 Literature review

2.1 Importance of single-cell analysis

A cell is the most fundamental structural, functional, and physiological unit of all living organisms ranging from microbes to human beings. Cells synthesise genetic materials, proteins, and metabolites that are responsible for functions and activities of living organisms. The study of cells plays an essential role in many fields, e.g., cancer diagnosis and therapy, drug discovery and delivery, and metabolic engineering. To date, most of cellular studies are performed in bulk based on population-averaged assays, assuming that ensemble averages reflect the main mechanism of individual cells in a population.

However, heterogeneity is inherent in a cell population. Cellular heterogeneities can be caused by different factors, such as intrinsic stochasticity in genes and proteins[1,2] and extrinsic factors[1-4]. Cell genomes, especially microbial genomes, can change substantially within a short period of time. The stochasticity in gene expression and protein synthesis can account for the cell-to-cell variations in macromolecular composition or activity. The progression through the cell cycle or external stimuli can result in the differences in cell morphologies including size, shape, structure, and internal characteristics. These factors result in genetic, biochemical, and physiological heterogeneities as well as behavioural heterogeneities in a cell population.

Unfortunately, these heterogeneities are normally obscured by conventional population-averaged assays. This may result in the loss of important information originating from relevant subpopulations or rare events, particularly in cases where small subpopulations or rare events determine the behaviour of the whole population. Cell heterogeneity can lead to an evolutionary, positive characteristic in microbiology[5]. For example, some microbial populations can accommodate to new environment, survive and evolve stress resistance, when subjected to a rapid change in environmental factors (e.g., temperature, pH, antibiotics)[5]. In

addition, cell heterogeneities can cause the development of malfunction in organisms, since the high level of noise is likely to disable or reduce the efficiency of signalling in organisms. For instance, tumour microenvironment is heterogenous[6], which consists of multiple intricate interactions between tumour cells and their neighbouring non-cancerous stromal cells[7].

Therefore, investigating the heterogeneity in a massive cell population via single-cell analysis can elucidate cellular functions and is subsequently essential for different applications in microbiology, medicine, pharmaceutical industry. Recent advances in single-cell analysis technologies have enabled the characterisation of phenotypes and profiling of the genome, transcriptome, epigenome, proteome, and metabolome, along with temporal and spatial information of individual cells[8-11].

2.2 Methods of single-cell isolation and analysis

An upstream single-cell isolation step is crucial prior to the analysis for many analytical and bioinformatics tools that have been applied for the identification and quantitative analysis of single cells. Limiting dilution and light microscopy represent the original set of tools for single-cell analysis, which remain the most available methods in biological laboratories for isolating monoclonal cell cultures[8, 9]. To achieve single-cell isolation by serial limiting dilution, a highly diluted cell suspension is seeded into separate micro-volume compartments by pipetting (see Fig. 2.1A). However, this method is costly, time-consuming, and inefficient, since the probability of achieving a single cell in an aliquot follows the Poisson distribution by which the cell suspension has to be strongly diluted. For example, the cell concentration of 1 cell/mL is needed if the aliquot volume is 100 μL, otherwise, the probability of multiple cells in an aliquot is relatively high. For example, the probability of $\geqslant 1$ cells encapsulated in droplets is ~4.0% when cell concentration is 3 cells/mL, decreasing the accuracy of single-cell analysis.

Recent advances in imaging, optics, automation, chemistry, engineering, and computation technologies have driven the development of new tools for single-cell isolation and analysis,

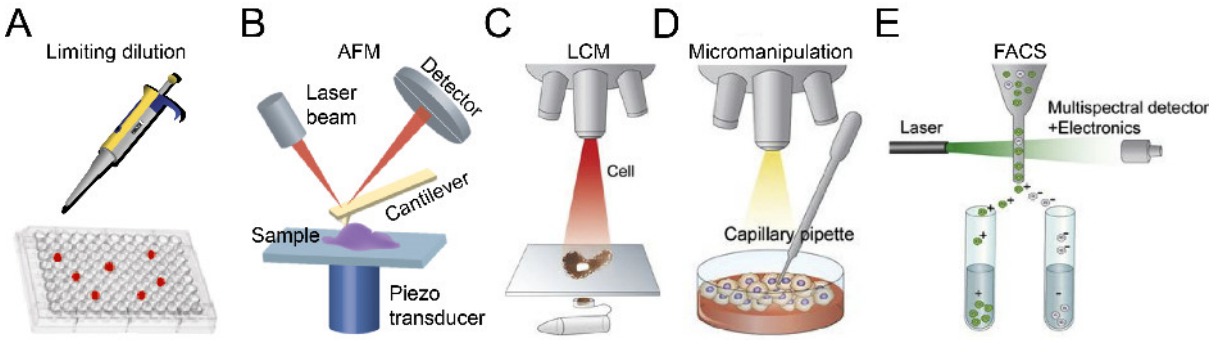

Figure 2.1 An overview of conventional and traditional approaches for single-cell analysis. A) Limiting dilution, B) Atomic force microscope (AFM). Reprinted from Ref.[15] with permission of Future Medicine Ltd. C) Laser capture microdissection (LCM). D) Micromanipulation. E) Fluorescence-activated cell sorting (FACS). Reprinted from Ref.[14].

significantly improving the efficiency, throughput, purity, and recovery rate of assays[8-10]. These single-cell analysis tools allow the observation of discrete and dynamic events occurring on or within living cells with high spatial and/or temporal resolution. As a result, scientists have been able to characterise cellular phenotypes and perform downstream omics studies, i.e., genomics, transcriptomics, epigenomics, proteomics, and metabolomics at the resolution of single cells[5, 6, 11-14]. The existing and commonly used single-cell isolation and analytical technologies include atomic force microscopy (AFM), laser capture microdissection (LCM) micromanipulation, cytometry, and microfluidics, which are listed and presented below.

2.2.1 Atomic force microscopy

AFM technologies have been recognised as a powerful tool to characterise biological materials, by investigating the structures and properties of native biological samples at the micro/nanoscale under near-physiological conditions at a single-cell resolution[15] (see Fig. 2.1B). The main component of an AFM is a cantilever acting as an arm, which is attached with a very sharp probe. As the tip is scanned across a surface in the x-y plane, probe-sample direct or atomic force interactions cause z-plane deviations of the cantilever, which are detected and amplified by a laser. These deviations can reveal topographical details in the biological samples

at atomic resolution. Although AFM is highly useful in revealing single-cell morphology, probing cellular mechanics, and performing cellular manipulation for physicochemical assays due to its high accuracy, the throughput of single-cell analysis is relatively low.

2.2.2 Laser capture microdissection

LCM is an advanced technique to rapidly and reliably isolate individual cells from a wide range of tissue samples via microscopic visualisation[8, 9, 12, 16, 17] (see Fig. 2.1C). The LCM system consists of an inverted microscope, a solid-state near-infrared laser, a laser control unit, a joystick, a controllable microscope stage with a vacuum chuck, a charge-coupled device camera, and a color monitor. Cells of interest are visualised through an inverted microscope, then a fixed-position, short and focused laser pulse is delivered to melt the thin transparent thermoplastic film on a cap above the targeted cells. The film melts and fuses with the underlying cells of interest. When the film is removed, the target cells remain bound to the film while the rest of the tissue is left behind. Finally, cells are transferred to a microcentrifuge tube containing buffer solutions for downstream analysis. LCM has relatively high speed while maintaining its precision and versatility, but it requires highly trained researchers to identify cells of interest through visual microscopic inspection[9, 18]. Moreover, LCM has the potential to cause ultraviolet (UV) damage on cell integrity, depending on the degree of cell fixation and extraction[18, 19].

2.2.3 Micromanipulation

Micromanipulation, or so-called manual cell picking, is a simple, convenient, and efficient physical method for isolating single cells[7-9]. This method has become more accurate and cost-effective with the advent of automation and computation technologies as well as more sensitive methods for fluid aspiration and deposition (see Fig. 2.1D). Besides ultrathin glass capillaries coupled with an aspiration and dispensation unit for controlled cell separation, electrorotation, optical, acoustic, and magnetic forces can be used to trap, move, pull, twist, or cut individual

cells without any physical contact. Once a cell is immobilised in a field of view, its response to environmental changes, e.g., nutrients, antibiotics, or enzymes can be monitored with quantitative measurements. To date, many noncontact methods, such as patch-clamp, optical tweezer, magnetic tweezer, acoustic force spectroscopy, and dielectrophoresis (DEP) have been widely used for the accurate, non-invasive single-cell manipulation and analysis. However, the throughput remains limited and they always require highly skilled professionals to operate. Additionally, they cannot detect complex changes in properties and dynamics of single cells.

2.2.4 Cytometry

"Cytometry" is a general term that may apply to any technology used to measure, count, compare, or characterise a wide range of cells. This general term is nearly synonymous with flow cytometry (FC), due to the popularity of FC technique[20]. Different forms of cytometry that have specialised advantages for single-cell studies and, along with FC, are discussed below.

FC is a powerful diagnostic tool dependent on visible light scattering and fluorescence for rapid analysis of entire cell populations at single-cell resolution. Multiple traits, including cell number, cell size or structure, and responses to fluorescent probes are collected simultaneously by this method[2, 9]. Unlike the aforementioned static methods, i.e., AFM, LCM, and micromanipulation, a flow cytometer generally involves the hydrodynamic module to isolate fluorescently labelled individual cells suspending in a buffered saline solution. The information about cell morphologies and biomolecules of interest within or attached to cells are automatically collected in a high-throughput manner. Additionally, a specialised type of flow cytometer, FACS, incorporates an electrostatic deflection module to sort and collect desired cells for further analysis[14] (see Fig. 2.1E).

FC has been recognised as a gold standard for single-cell analysis because of its automation, massive throughput, cellular characterisation by fluorescent labelling, allowing a simple, rapid,

and quantitative determination of various proteins cell populations[21]. However, FC is not designed to observe the temporal and spatial dynamics of individual cells, because cells pass through the system only once[2, 21, 22]. Also, the single-cell detection by FC mainly relies on cell-surface markers or intracellular information, lacking the ability to analyse extracellular molecules. Some modified forms of cytometry integrate with custom modules, e.g., optics, light microscopy, motorised control, and computational analytical tools to broaden the scope of single-cell analysis. Imaging flow cytometry (IFC) and laser scanning cytometry (LSC) are two main techniques that have been developed and used for single-cell analysis[21, 23].

IFC combines the advanced image analysis with the hydrodynamic module to obtain two-dimensional images of individual cells in suspensions, resulting in real-time single-cell detection and sorting[24, 25]. Compared with FC, IFC enables high flexibility in data acquisition, data processing, and sorting. But similar to FC, it can only provide a one-time cellular measurement[26]. LSC is a solid-phase cytometric technology for collecting laser-excited fluorescence associated with immobilised cells[17]. LSC instruments allow rapid counting, quantification, and recording of the distribution of fluorescent events on a filter. Microscope-based LSC instruments can provide visual information on both cell morphology and the spatial distribution of fluorescence within each cell. Unlike FC and IFC, they can also repeatedly interrogate the same cell over time. Despite its ability of continuous screening, the efficiency is relatively low, making it unsuitable for high-throughput analysis (i.e., screening millions of cells). Moreover, LSC may involve the exposure of the sample to the excitation source for a relatively long period. This may result in the photobleaching of fluorescent labels that could be problematic for some applications, particularly if multiple scans are required.

2.2.5 Microfluidics

Microfluidics technologies have many advantages over conventional approaches for single-cell isolation and analysis, and have been widely applied to a number of research and industrial

fields. In detail, microfluidics-based methods offer the following advantages[7, 12, 16, 21, 23, 27, 28]: 1) the miniaturised system can operate with picoliter to nanoliter liquid volumes and cells ranging from the sub-micron metre to millimetre level, which reduces sample loss and the cost of reagents while improving the sensitivity of biochemical assays, 2) they are highly automatable with the ability to perform multiplexed, high-throughput assays, enabling statistically significant single-cell analysis, and 3) a microfluidic system is highly flexible, and can be adjusted to fulfil the demands of diverse cell manipulation and analysis tasks. Different mechanical components, external fields (e.g., hydrodynamic, electrical, optical, magnetic, and acoustic fields), detection approaches (e.g., imaging-based microscopy, fluorescence microscopy, fluorometry, absorbance spectrophotometry, and mass spectroscopy) have been integrated with microfluidic devices to perform diversified tasks. These features make microfluidic device an ideal platform to analyse the heterogeneity of single cells. In recent years, a variety of microfluidic platforms have been developed for single-cell isolation and analysis, which can be classified into three main groups: 1) microstructure-based methods, 2) external force-based methods, and 3) droplet-based microfluidics.

2.3.5.1 Methods based on microstructures

Single-cell manipulation can be achieved by physical constrictions (e.g. microtraps, microwells and microvalves) that form individual cell traps when cell suspension passes through the microchannel. These microstructures have been widely used for single-cell in situ analysis, including proliferation, lysis, reaction, differentiation, metabolism, migration, pairing, and fusion[12].

The use of microtraps and microwells requires researchers to design microstructures having a similar size to a single cell. After injection into the microdevices, cells flowing along the streamlines of the laminar flow can be trapped by the shear force generated by microstructures. Di Carlo et al.[22], for the first time, proposed a classical U-shaped microtrap array for capturing

Hela cells (see Fig. 2.2A). A high-density array of U-shaped traps was fabricated within a Polydimethylsiloxane (PDMS) based device by soft lithography, creating a high channel for flowing cell suspension and a low channel for cell capture. A hollow in the middle trap was introduced to direct fluid streamlines to facilitate the capture of single cells[22]. Based on the principles of this study, multiple variant designs have been developed afterwards[29-31], e.g., an asymmetrical microtrap designed to capture single cells more efficiently for genome sequencing[31].

A similar microstructure, an array of properly designed microwells, was also used for single-cell isolation and analysis in a microdevice [32-34]. After flowing a cell suspension through the microdevice, single cells were retained inside the wells while the redundant cells can be flushed away, as demonstrated by Park et al.[33] (see Fig. 2.2B). The roofless microwell structure allows rapid and direct sample retrieval, and capture and detection of metabolites or genetic materials[34]. In addition, the concave wells can be chemically modified to enhance the robustness and specificity of cell capture[35, 36]. Similarly, other types of surface-modified microstructures, e.g., microposts[37] and herringbone patterns[38], have been integrated within

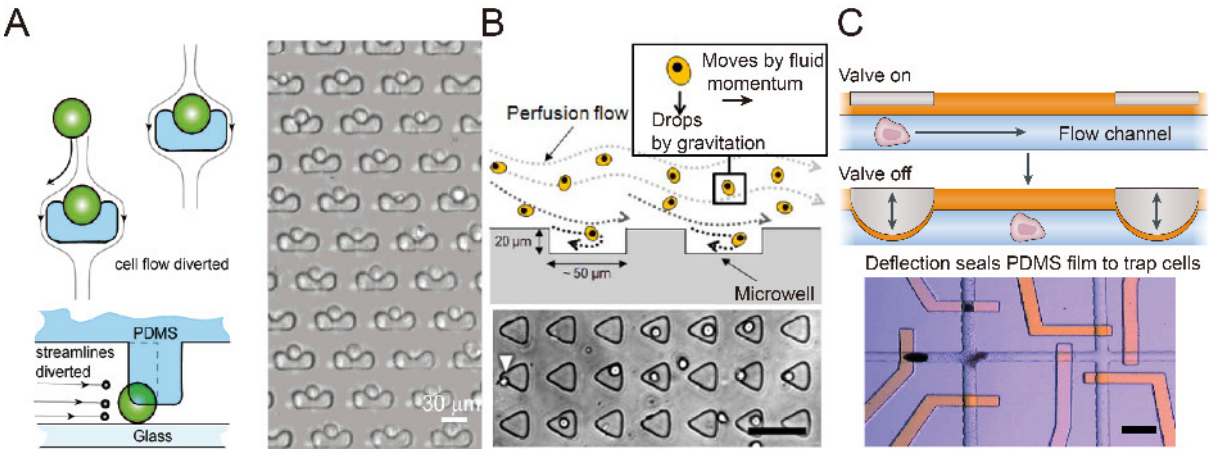

Figure 2.2 Microstructure based microfluidic approaches for single-cell isolation and analysis. A) Hydrodynamic microtraps. Reprinted from Ref.[22]. B) Microwells. Reprinted from Ref.[33]. C) Microvalves. Reprinted from Ref.[40].

microfluidic chips for single-cell capture with high-yield and high-purity, due to the increased interactions between cells and modified surface[38].

Another type of microstructure, pressure-controlled on-off microvalves, is integrated with valve-based microfluidics for flow control. The microdevice containing these valves has at least two crossed layers, one as a main flow channel and the other as a valve-control channel, and a deformable film is inserted between two layers. When pressure is applied from the control channel, the film is deformed and blocks the flow in the main channel; while without pressure, the flow layer is open for flowing cell suspension. By controlling the timing of film deformation, isolation of single cells from the passing cell suspensions can be achieved. This approach was invented by Quake's group[21, 39] and has been upgraded and adapted for many purposes. For example, Hong et al.[40] demonstrated automated single-cell isolation, lysis, nucleic acid purification using a valve-based microfluidic device (see Fig. 2.2C).

These methods based on the physical properties of microdevices allow label-free single-cell isolation with high accuracy. However, these methods generally require complicated structure design and multi-step fabrication processes. Moreover, the number of traps, wells, or channels is highly restricted in a given limited space, resulting in low-throughput assays.

2.3.5.2 Methods based on external forces

Microfluidic microdevices can be integrated with various external fields (e.g., electrical, optical, magnetic, and acoustic fields) for advanced single-cell manipulation. Different methods based on external forces, such as DEP, optical traps, immunomagnetic beads and acoustic radiation force[41], have been developed. The advantages and disadvantages of methods based on external fields have been summarised in previous review articles[7, 21, 42, 43].

DEP is regarded as the most popular electrical approach integrated with microfluidic systems for single-cell trapping, due to its label-free nature, low cell damage, and high specificity[12, 21]. DEP forces that are dependent on cell size, dielectric properties of cells and

surrounding medium, and the properties of electric fields, i.e., voltage, gradient, and frequency, are used to manipulate cells. Polarisable cells are directed toward higher or lower electric field regions with positive or negative DEP forces, respectively. Therefore, cells with the distinct

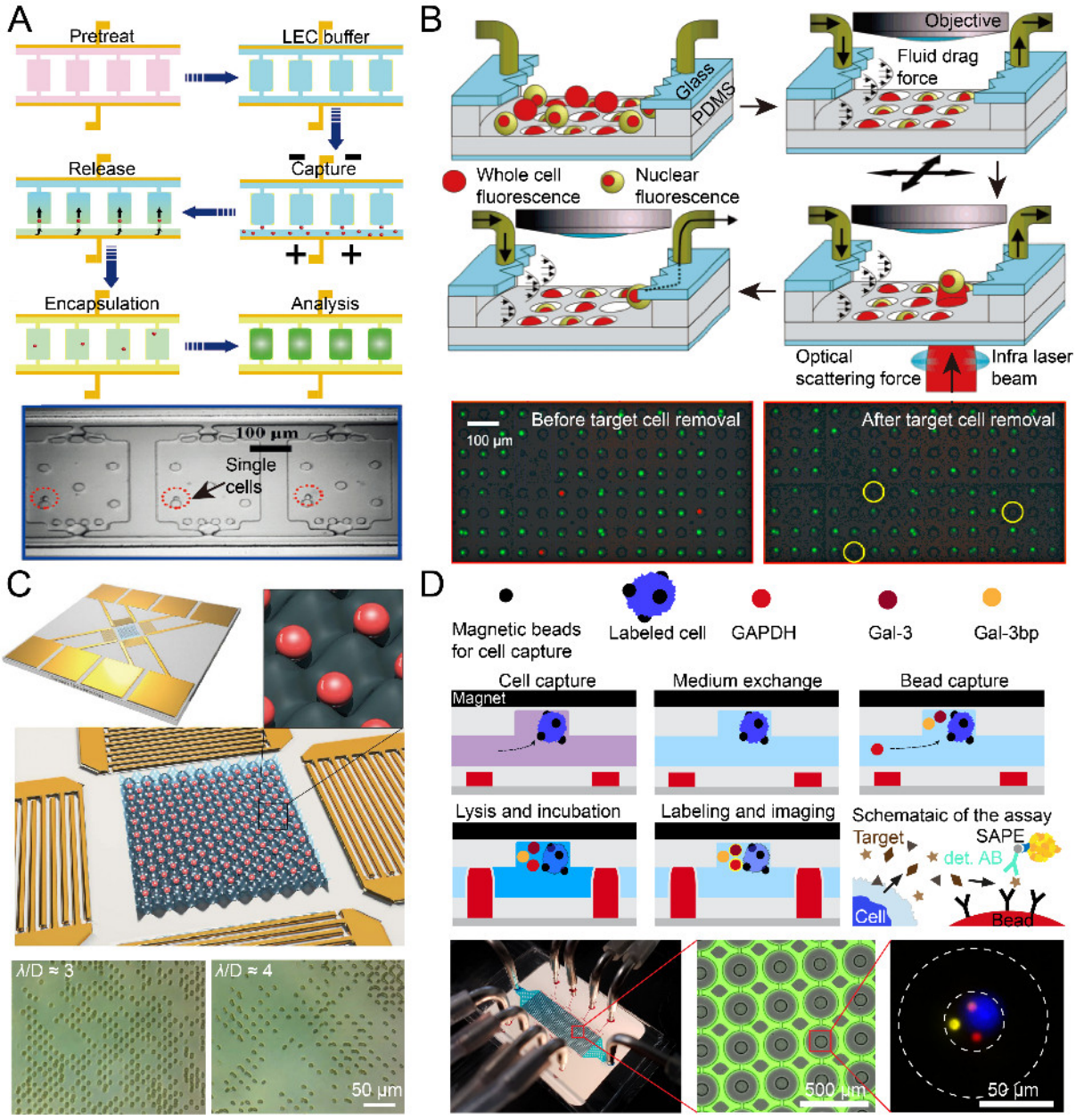

Figure 2.3 Microfluidic approaches integrated with external fields for single-cell isolation and analysis. A) Dielectrophoretic (DEP) traps for single-cell isolation and nucleic acid analysis. Reprinted from Ref.[44]. B) Optical scattering force and microwells for single-cell sorting. Reprinted from Ref.[25]. C) Surface acoustic waves for two-dimensional spatial patterning of single cells, which is dependent by acoustic wavelengths and cell diameters. Reprinted from Ref.[45]. D) Magnetic forces for immobilising single cells and superparamagnetic barcode beads in microchambers, enabling single-cell protein profiling. Reprinted from Ref.[46].

dielectric properties can be selected and manipulated by DEP-based microfluidic systems. Moreover, microarrays are normally integrated with DEP for precise cell isolation, allowing the monitoring and analysis of individual cells without contamination[44]. Towards this end, a self-digitisation dielectrophoretic chip was designed for single-cell isolation and nucleic acid analysis, in which each cell was trapped within a chamber by positive DEP, sealed by an immiscible fluid to prevent contamination, and then lysed for further assays (see Fig. 2.3A).

Microfluidic optical single-cell trapping platforms can be categorised into different types, e.g., optical tweezer, optically-induced-DEP, optically-induced mechanical manipulation, and opto-thermocapillary. Among these platforms, optical tweezer based on either gradient or scattering forces is the most popular one due to its high specificity and spatial resolution, non-intrusiveness, and the capacity of single-cell trapping. Compared with the gradient force, scattering force is weaker and more biocompatible for cell manipulation and can be easier to be integrated with a microfluidics system[10]. For instance, Kovac et al.[25] developed an optical trapping and sorting platform with 10,000 microwells (see Fig. 2.3B). Individual cells were passively trapped in microwell arrays, monitored by fluorescence microscope, and extracted optical scattering force based on subcellular events, e.g., localised protein expression.

Microfluidic acoustic cell manipulation is based on the interactions between a cell flow and a microstructure, which is initiated by acoustic waves in a microfluidic channel. This method acquires single-cell isolation in a biocompatible manner, avoiding the possible photobleaching and local heat stress[45]. There are two forms of acoustic waves, body and surface waves. Surface acoustic wave (SAW) has been widely used for single-cell manipulation in microfluidic chips, due to its high frequency, high energy density, excellent penetrability, and compatibility with microfluidics. For example, Collins et al.[45] introduced high-frequency SAWs to create a two-dimensional (2D) acoustic force field in a microfluidic device to pattern multiple spatially isolated single human lymphocytes and red blood cells (see Fig. 2.3C). Furthermore, the

relation between a feasible patterning and a ratio of the acoustic wavelength, λ, to the cell diameter, D, has been investigated.

Magnetic microfluidics integrates magnets or electromagnets to facilitate the cell trapping and immunoassays. In general, immunomagnetic beads are labelled to the surface of cells by antigen-antibody interactions. For instance, Armbrecht et al.[46] developed a microfluidic platform consisting of 1,026 microchambers controlled by microvalves and a permanent magnet placed on top of the device (see Fig. 2.3D). Magnetic beads for cell capture were firstly injected and remained within the microchambers due to the existence of magnets, allowing individual cells to be trapped in the microchambers. To achieve multiplexed protein analysis at a single-cell level, magnetic beads functionalised with different antibodies for specific protein sites were infused and incubated with lysed cells. Finally, a in situ sandwich fluorescence-based immunoassay was quantitively performed by image analysis.

2.3.5.3 Droplet-based microfluidics

Droplet-based microfluidics, the method that was adopted in the current study, which has become increasingly popular due to its capability to encapsulate cells and reagents in isolated compartments. Three types of microfluidic droplet generation approaches are usually used: T-junction, flow focusing, and co-flow[11, 21, 47] (see Fig. 2.4A). When two immiscible liquids meet at a junction, one fluid shears the other one into segments in the form of droplets[12]. Apart from the above-mentioned advantages of microfluidics, droplet-based microfluidics has been widely utilised for time-dependent cellular analysis for multiple reasons[11, 48-51]. The microfluidic microdevice can quickly create a large number of uniform and parallel microcompartments (normally w/o droplets) to harmonise the environment and encapsulate cells. The oil phase of droplets provides unique confinement to eliminate the cross-contamination between droplets. The encapsulated content, such as cells, cell lysis, secreted metabolites, genetic materials, and fluorescence staining dye, can remain inside the droplets for downstream analysis. Additionally,

many studies have been dedicated to the development of droplet manipulation, including but not limited to merging, splitting, re-loading, incubation, detection, and sorting[11] (see Fig. 2.4B). Hence, a wide range of cellular analyses requiring external stimuli, multiple operational procedures, long-term culture, and recovery of ingredients have been achieved[52, 53].

One of the most important applications of single-cell analysis by droplet-based microfluidics is linking genotypes to phenotypes, as the droplets encapsulating cells with desired properties can be sorted for downstream analysis[48-51]. Generally, an automated system can recognise the signals of individual droplets when they pass through the detection site one by one, which can trigger a downstream dielectrophoretic force to direct droplets into different outlet channels. Many custom-built systems have been developed, including FADS[54-58], fluorescence lifetime-activated droplet sorting (FLADS)[59], and absorbance-activated droplet

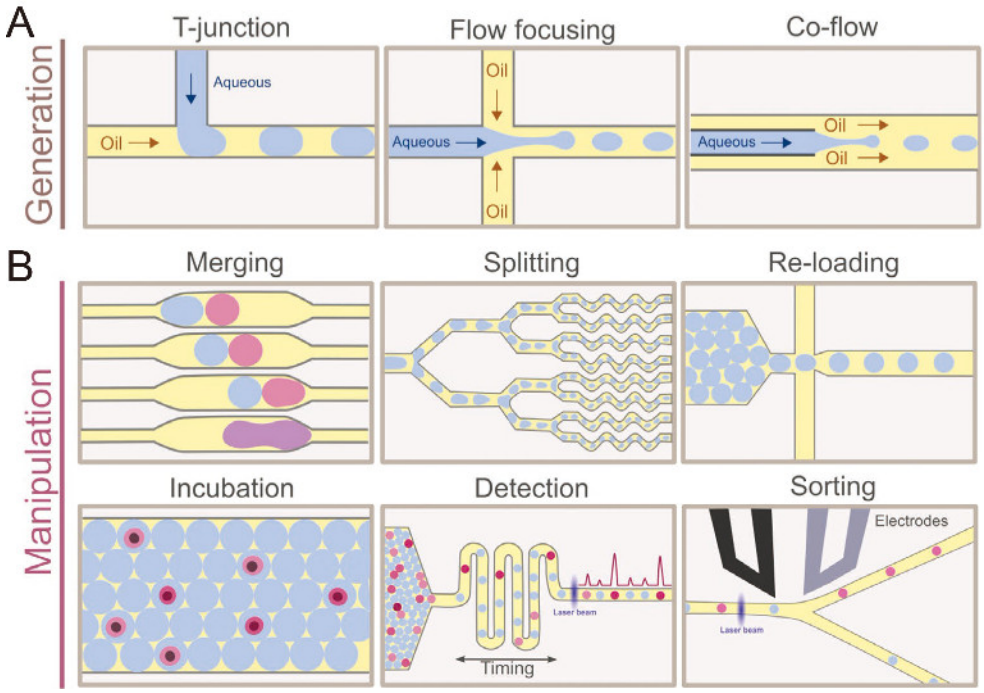

Figure 2.4 Generation and manipulation of microdroplets in microfluidic devices for single-cell analysis. A) Three main geometries, T-junction, flow focusing, and co-flow, for generating droplets in microfluidics. B) Modules for the manipulation of droplets in microfluidics: merging, splitting, re-loading, on-chip incubation, detection, and sorting. Reprinted from Ref[11].

sorting (AADS)[60], and so on[61]. These droplet sorting systems are flexible, allowing versatile screening assays in a relatively short timeframe, including discovery of rare cells and variants, metabolic engineering, and other biomedical applications. For example, Qiao et al.[58] developed a customised FADS and demonstrated the discovery of 47 lipase-producing bacterial strains from environmental soil, with a throughput of 2×10^6/h. However, the systems are complex and require professional operators, hindering the rapid spread and adoption of this method. The sorting process is highly sensitive to flow turbulence at the sorting regions, and most of droplet sorting systems perform a binary decision-making for droplets, lacking capacities of multiplex assays. Additionally, the sorting throughputs are normally at rates of hundreds of events per second, rarely above 1 kHz, which are an order of magnitude slower than commercial instruments[55, 62].

Besides on-chip droplet sorting platforms, an off-chip screening and sorting approach based on commercial flow cytometric instruments (e.g., FACS) has enabled the sorting of two main forms of droplets, i.e., hydrogel droplets and DEs[63]. The conventional w/o single emulsions carried by an oil phase can only be used in the on-chip droplet sorting platforms, whereas hydrogels and DEs can be suspended in an aqueous phase and are suitable for flow cytometers[26, 64]. Hydrogels are three-dimensional cross-linked hydrophilic polymer networks, which can be generated using w/o droplets as a template and transferred from an oil suspension into an aqueous solution (e.g., buffer or cell culture medium) after gelation for use in FC. A recent review on the use of hydrogels with FC can be found elsewhere[26].

2.3 Structures and fundamentals of DEs

Compared with single emulsions, a DE is a complex soft colloidal core-shell system, in which an aqueous core or multiple aqueous cores are separated from the outer carrier aqueous phase by an immiscible oil phase[65, 66]. This system is stabilised by two sets of surface-active agents, i.e., surfactants. Surfactants in an oil phase and an outer water phase stabilise the

interface of the water-in-oil internal emulsion and that of the oil-in-water emulsion, respectively.

The inner core, an encapsulated w/o emulsion, is generally recognised as an isolated reservoir for encapsulating cells and water-soluble active ingredients, such as vitamins, vaccines, enzymes, nucleic acids, and hydrophilic metabolites. The middle oil shell acts as a semi-permeable selective membrane that allows the transport of specific substances, thus it controls the behaviours of the inner core, including reaction, culture, storage, rupture, and so on. In the meanwhile, hydrophilic compounds (e.g., charged molecules, nucleic acids, peptides, and sugars) are entrapped in the inner core, providing the accumulated signals of the cells[64]. In addition, unlike single w/o emulsions, the outer phase and carrier phase of DEs are aqueous, allowing a mass transfer between the inner core and external environment through the selective oil shell. These traits empower a DE with many capacities as a core-shell system for single-cell analysis.

Firstly, DE is a highly controllable bioreactor for biochemical studies and industrial applications[67]. Nutrients and oxygen in the continuous aqueous phase can enter the inner core where cell cultures are located, and thus enhances the viability, growth and metabolisms of cells, reduces droplet shrinkage, and elongates the achievable culture time. Similarly, chemical inducers and drugs can be added after encapsulation to study complex biological processes that involve the communication with external molecular stimuli and drugs[67, 68].

Secondly, the composition of a DE is flexible. The liquid middle phase can convert into solidified shells to create microcapsules[69, 70], which can enhance the stability of encapsulation and allow applications with better control of bioactive preservation and release. Also, a 3D solid matrix as an inner core can enable cells to form specific structures or enhance cellular functions. Notably, the DE inner core volume is dependent on the osmotic pressure between the inner phase and carrier phase, which can be used for shrinking or swelling inner cores to

ensure a stable flow cytometric screening[71], enhancing the indicative fluorescence signalling of a DE[72], and spontaneously releasing ingredients into the carrier phase or environment[73-75].

Thirdly, the outer aqueous phase of a DE allows are suitable for single-cell analysis it to integrate with commercial flow cytometric instruments, e.g., FACS[26], for quantitative high-throughput assays necessary in a user-friendly manner. The traditional screening methods based on microtiter plates can only measure 10,000 events per day[76-78], even with the aid of automated liquid handling and dispensing. In contrast, this DE-FACS methodology can routinely analyse and sort $>10^7$ events per hour, facilitating its applications in biological and biomedical fields where high-throughput screening and sorting are desirable[63].

Lastly, a DE system is regarded as metastable with two protective shells[79, 80], which offers protection against oxidation, degradation, and corrosion[69, 70]. The structure of DEs remains stable without a loss of inner ingredients after experiencing high-temperature inactivation[71], PCR thermal cycling[81], lysis procedures and frozen storage (i.e., at −20 °C or −80 °C for one month) [71]; the multi-layer structure can protect encapsulated cells from harsh conditions[82-84] (e.g., low pH, *in vivo* degradation, mixture with external substances). Also, the burst of inner cores and the resultant release of encapsulated actives, and cells can be triggered by several biofriendly factors, e.g., osmotic imbalance[85, 86], pH change, and an alternating current electric field[87].

With the advent of microfluidic technologies for generating DEs, the size of emulsions, number of inner cores, and the composition and properties of each layer can be manipulated[66]. As a result, a DE has a highly tailorable structure that can be adjusted for various food, cosmetic, pharmaceutical, chemical, and biological applications, including the production of food with sustained probiotics, controllable release of nutrients and flavours, programmable drug delivery, material synthesis, medical diagnostics, drug discovery, and directed evolution of molecules.

2.4 Generation of DEs by microfluidic devices

Since the 1980s, there is an increasing number of theoretical and experimental studies on the generation of DEs, as DEs have shown significant promise in extensive research areas[65]. In the early stage of the development of microfluidics, DEs are prepared by two-step batch approaches, such as stirring[88], high shear homogenisation[89, 90], and membrane extrusion[89-97]. In general, single w/o emulsions are prepared by vigorous mixing with high shear stress or membrane extrusion; then the single emulsions are further emulsified in another immiscible liquid phase by gentle mixing or multiple rounds of membrane extrusion. The batch emulsification is implemented for rapidly generating DEs, but it generates highly polydisperse droplets due to the random shear[98]. Moreover, the high shear results in the rupture of DEs, leading to low encapsulation efficiency[66]. For single-cell assays using DEs, polydisperse emulsions can exhibit dramatically different assay outcomes (e.g., varying fluorescence intensity) depending on the size of inner cores, and randomly occurring large droplets can potentially cause the blockage of nozzles of flow cytometry instruments.

Accurate and independent control of the size and number of inner cores and the shell thickness of DEs can result in controllable characteristics of DEs for more efficient and precise quantitative single-cell assays. Various one-step methods have emerged over the past two decades. The coaxial jet electrospray technology has been used to generate DEs by controlling the electric potential between an inner liquid and a surrounding fluid[99-101]. The size of DEs can be adjusted from tens of nanometers to hundreds of micrometers with a minimum C.V. of 15% by tuning the flow rates of each phase and applied voltage [99]. However, this relatively large variation of size is problematic for quantitative cellular assays. Additionally, this method requires conductive liquids and high voltage that can adversely affect cells or other actives[66], limiting the usage of this method. Therefore, an alternative one-step method that can provide well-defined size distribution of DEs has emerged with the rapid advance of microfluidic

technologies. Within the microchannels of fixed geometries or capillaries at a micrometre level, the one-step continuous flow method uses a relatively high flow rate of oil phase to cut an aqueous phase with a low rate to generate w/o droplets, and a second aqueous flow with a much higher rate is applied to cut the oil-water flow. Finally, DEs with a single core are generated with a drop-by-drop ordered feature. This microfluidic approach effectively confines either the disperse phase or w/o single emulsions before encountering the downstream carrier phase, and forms highly monodisperse DEs that are suitable for single-cell analysis.

Wettability is the most curtail property of one-step microfluidic devices for generating DEs[66, 102], which requires a high level of control to determine the type of emulsions formed. The droplet generator that forms w/o droplets dispersed in oil, has to be hydrophobic, whereas the droplet generator that sequentially encapsulates w/o droplets within the outer aqueous phase has to be hydrophilic. However, selective control over the wettability of microchannel surfaces has been challenging, and precludes the further use of microfluidics to produce monodisperse DEs[66, 102, 103]. A wide range of strategies have been explored to prepare microfluidic devices with spatially patterned wettability.

PDMS, polymethyl methacrylate (PMMA), and glass have been used as main materials for fabricating microfluidic components for DE generation. Hydrophobic materials, i.e., PDMS and PMMA[104], are more preferable for w/o droplet generation due to their intrinsic hydrophobic properties, while hydrophilic glass is suitable for generating w/o droplets dispersed in aqueous phase[105]. The properties of microchannel surface can be modified by various approaches, e.g., self-assembly monolayers formed by chemicals, plasma treatment, and UV exposure. Once a mould has been obtained, a PDMS device is relatively easy to fabricate by standard soft lithography, with high flexibility, rapid manufacture, and cost-effectiveness. Regarding the fabrication of PMMA and glass-based devices, multiple direct machining (which removes unnecessary parts using mechanical and energy-assisted methods)

and replications methods (which makes moulds with fine features and performs replication, including casting, hot embossing, micro-injection, etc) have been employed[106]. Some of these methods are able to achieve mass production of devices in industries, with an advantage over the soft lithography[107]. However, these methods are normally considered more complex and costly[106, 107].

Besides the materials of devices, the design of device plays an important role in the spatial patterning of wettability in microchannels. Two main types of microfluidic devices, multi-module and single-module microfluidics, have been used for DE generation. The multi-module microfluidics requires three or more co-axial capillaries, cascading T-junction and/or flow-focusing droplet generators in separate modules, whereas single-module microfluidics integrates cascading droplet generators in a single device.

2.4.1 Multi-module microfluidics

The multi-module microfluidic approach adopts two or more modules in which the entire channel surface has different wettability intrinsically or after treatment. Thus, this method satisfies the requirement of hydrophilic and hydrophobic surfaces for different droplet generators and is more straightforward for producing DEs than single-module approach. Two-chip module or co-axial glass capillary based microfluidic devices are most widely used for DE generation.

2.4.1.1. Two-chip microfluidic devices

Two separate microfluidic chips can be physically connected to generate DEs[103, 108-120]. The preparation of two modules can be performed separately by researchers with less experience in microfluidics. Also, it is possible to change the morphology and size of droplets using devices with different channel dimensions[109, 110]. Otherwise, channels with different depths can be obtained using dual-layer soft lithography processes or coaxial flow-focusing.

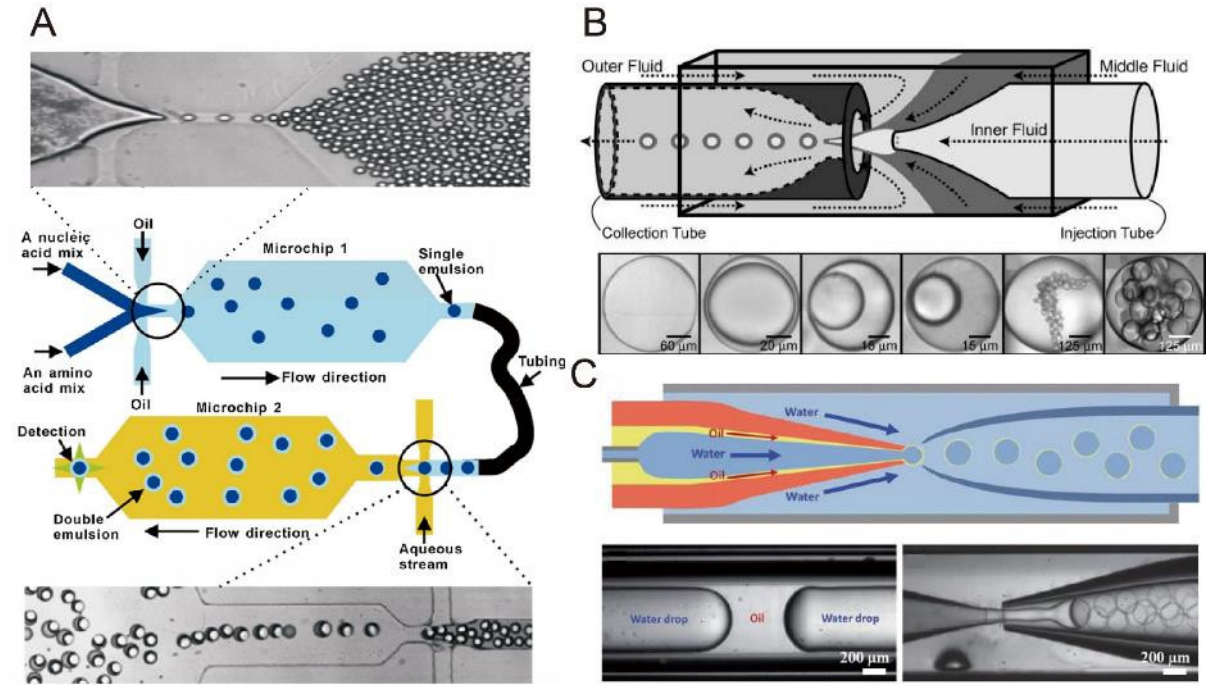

Figure 2.5 Multi-module microfluidic devices for double emulsion (DE) generation. A) Two separate microfluidic devices with reverse wettability are connected by an inert tubing. Reprinted from Ref.[114]. B) A reverse-flow capillary microfluidic device consisting of a tapered and a cylindrical capillary, nested within a square one. Reprinted from Ref.[124]. C) A co-flow capillary microfluidic device with three tapered capillaries nested within a square one. Reprinted from Ref.[127].

Okushima et al.[113] firstly developed the two-chip modules with sequential T-junctions fabricated by isotropic etching on quartz glass. The microchannel in the first chip was modified to hydrophobic using a silane coupling agent and the microchannel in the second chip was kept hydrophilic (i.e., intrinsic property of glass). The outlet of the first chip and the inlet of the second chip were connected by a short poly(tetrafluoroethylene) (PTFE) tube. Droplet formation at each junction was reproducible, and the resulting droplets had a small variation in size. By adjusting the flow rate of each phase and the breakup rates at the two junctions, the morphology and number of generated droplets can be controlled. Similarly, Wu et al.[114] reported a two-chip module device consisting of a PMMA chip and PDMS chip connected by a PTFE tube for the generation and encapsulation of w/o droplets, respectively (See Fig. 2.5A). The hydrophobic PMMA chip is suitable for w/o droplet generation, while PDMS surface in

the second chip is converted to hydrophilic by coating with acrylic acid via a two-step sol-gel method. Moreover, Zhang et al.[109] used two PDMS chips to achieve similar results. The second PDMS chip was modified by a sol-gel coating procedure[121]. Notably, the first PDMS chip was converted to highly hydrophobic by silane coupling reagents, as fluorinated oil phase requires fluorophilicity to reduce the tension at interfaces[122]. Fluorinated oil-based emulsions are very useful for microfluidic applications in biology, due to their stability, inertness, impermeability to small molecules, and permeability to gases[123]. Zinchenko et al.[110] demonstrated that a two-chip module allows the off-chip storage and reinjection of w/o droplets into the second chip after incubation. The w/o droplets were collected in a sterile syringe, incubated under various conditions, and reinjected into the second chip in a uniformly distributed manner by co-injecting a spacing oil, resulting in the generation of single-core DEs at a high rate.

This two-chip module-based design not only makes it easy to prepare surfaces of wettability in microfluidic chips but also makes single-cell assays more flexible. However, the number of inner cores droplets varies, because the array of to-be-enclosed droplets formed in the first chip is likely to collapse before reaching the second chip. This is because of the sudden change in flow speed at the junction between the two chips. In addition, gravity influences the distribution of primary droplets before entering into the second chip. A smoother connection between the two chips would allow more precise control of the encapsulation.

2.4.1.2. Capillary microfluidic devices

Co-axial capillary devices for DE generation consist of two or three circular, internal capillaries with tapered orifice dimensions [73-75, 87, 124-149]. There are always one or two internal capillaries for injection and another one for collection, whose surface can be modified to either hydrophobic or hydrophilic. In this way, the oil and aqueous phases can flow smoothly through each capillary. Internal capillaries are precisely aligned with each other, and nested within an external square capillary. With the well-aligned capillary microfluidic device, inner aqueous

and oil phases are injected into the device through the innermost injection capillary and surrounding injection capillary, respectively. The flow condition changes with the cross-sectional area of tapered glass capillary in the focusing section. Due to the Rayleigh–Plateau instability, the drag force applied by the continuous phase and the interfacial tension by disperse phase[74], the coaxial mixed-flow breaks up into uniform droplets at the end of the focusing section. Simultaneously, continuous phase is injected through the square capillary to encapsulate the formed droplets, resulting in the formation of DEs. Two different flow configurations have been used in co-axial capillary device, i.e., reverse-flow and co-flow configuration, depending on the flow directions of the outer aqueous phase and the middle oil phase.

Utada et al.[124] firstly developed an co-axial capillary device with a reverse-flow configuration of three capillaries. The inner fluid was injected into the tapered glass capillary, while the middle fluid was injected into the square channel surrounded with the inner fluid, forming the co-axial stream at the tip of the conical capillary. The outer fluid was injected into the outer region from the reverse direction, and all fluids passed through the outlet of the capillary and consequently broke up to form droplets (see Fig. 2.5B). This device has been used to synthesise hydrogel microbeads using DEs as a template[75, 129]. Oh et al.[125] firstly reported the use of an co-axial capillary device with a co-flow configuration for DE generation. The assembly was constructed by arranging three capillaries in a PDMS block where a central hole was pre-punched. The inner and middle fluids were injected into channel separately, and travelled through the intermediate capillary to form the coaxial jet. The coaxial jet flow was focused at the exit of the capillary and subsequently split into DEs in the continuous phase. Afterwards, a device having the co-flow configuration, but without the external block, was demonstrated by Chu et al.[126]. Two square capillaries were used to infuse the middle phase and outer phase, respectively, which were connected by a cylindrical capillary with a tapered end.

The co-axial capillary device designed by Kim et al.[127] has been widely used to date. A hydrophobic tapered glass capillary for injecting oil phase was inserted into a square capillary for injecting outer aqueous phase, and a small tapered glass capillary was inserted into the injection capillary to simultaneously inject an inner aqueous phase. Another circular capillary was inserted into the square capillary from the other side to confine the flow at the injection tip (see Fig. 2.5C).

Multi-module capillary microfluidic device makes it easy to obtain spatially patterned wettability. However, the manufacture of capillary devices lacks flexible and reproducible methods for capillary alignment (especially for two tapered glass capillaries) and sealing[102, 105, 150], and glass capillaries need extra hydrophobic silane coatings compared with intrinsically hydrophobic PDMS devices.

2.4.2 Single-module microfluidic device

Compared with multi-module microfluidic devices, the single-module microfluidic device integrating two sequential droplet generators in one chip reduces the shear turbulence occurred in connection and avoids misalignment of different modules. However, this method requires precise control of wettability at different regions within the same device, except three-dimensional (3D) PDMS microfluidic device that can avoid the contact between engulfed phases and channel walls at the droplet generators. A wide range of methods have been used to prepare a microfluidic device with spatially patterned wettability, such as localised polymer grafting, localised layer-by-layer deposition (LbL), and surface activation with a blocking phase. Besides, there exists other strategies to generate DEs in a single-module microfluidics device, e.g., by employing moving-wall, mass transfer, and phase transfer.

2.4.2.1 3D PDMS microfluidic devices

Similar to multi-module capillary microfluidic devices, a 3D PDMS microfluidic device also generates DEs in a co-axial manner. The device is fabricated by three layers of SU-8 photo-

resist structures that form coaxial embedded orifices at the centre of the microchannel. Similar to the tapered end of the circular capillaries, the flow-focusing orifice is narrow (e.g., a 50 × 50 μm orifice, compared with a surrounding 320 μm tall junction[151]). The liquid thread of the inner fluid breaks into droplets by the middle phase due to Rayleigh–Plateau hydrodynamic instability under the competition of viscous and capillary forces. Then the stream of generated primary droplets stays confined to the central axis of the microchannel and encapsulated by the continuous phase in the downstream wide channels[152, 153]. Using a sheath fluid of a high flow rate can prevent the w/o stream from touching the channel wall downstream, allowing the formation of either w/o or O/W emulsions, irrespective of channel wettability. Similarly, wettability of co-axial capillary device for DE generation are ignored in some cases.

Takeuchi et al.[152] and Yobas et al.[153] have developed 3D flow-focusing devices made of PDMS and silicon, respectively, for the generation of w/o droplets. The generated droplets can be confined in the central axis of the channel to prevent the dispersed phase from wetting the channel wall. Huang et al[154] for the first time introduced a 3D PDMS microfluidic device with a narrow coaxial orifice between two spacious microchannels for generating DEs. Chang et al.[155] reported a 3D PDMS microfluidic device for generating DEs by an assembly of two PDMS slabs: one with two different depths (200 μm and 20 μm) and the other with a uniform depth (200 μm), which were fabricated using three-layer SU-8 microstructures as a master (see Fig. 2.6A).

This method has been widely used for the generation of DEs with different morphologies and properties[151, 154-164]. The size of an inner core and outer droplets can be accurately and independently manipulated by adjusting orifice size, channel dimensions, and flow rates. However, unlike the planar microchannels that can be manufactured by one-step soft

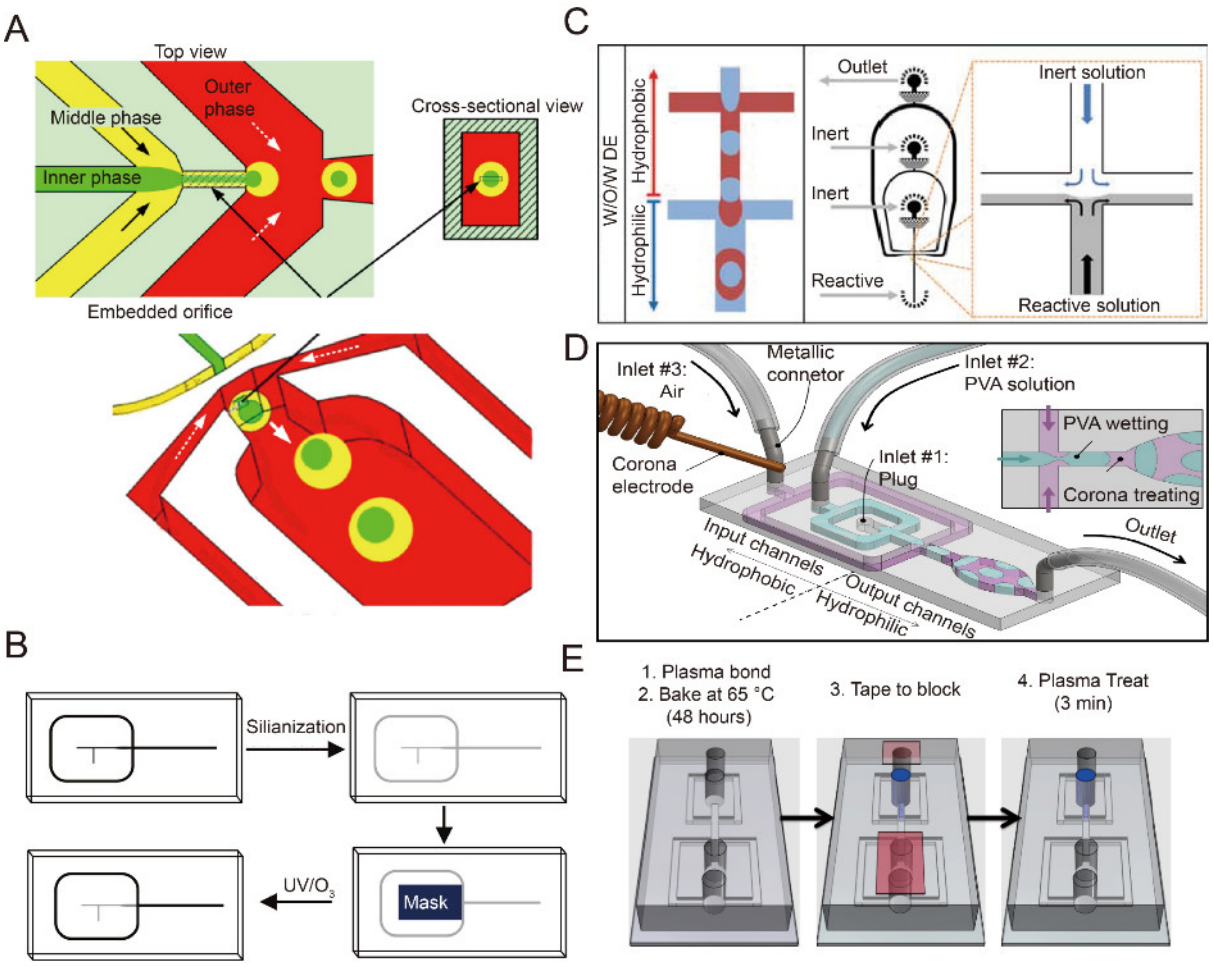

Figure 2.6 Single-module microfluidic devices for DE generation. A) 3D Polydimethylsiloxane (PDMS) co-flow microfluidic device, without any hydrophilic surface treatment. Reprinted from Ref.[155]. B) Glass microfluidic devices with localised silianisation by protecting target regions from UV/O_3. Reprinted from Ref.[105]. C) PDMS microfluidic devices, confining the reactive solution at the second droplet generator by simultaneously infusing the first hydrophobic droplet generator with inert solution. Reprinted from Ref.[121]. D) Localised corona air plasma treatment to spatially pattern hydrophilicity at the second PDMS droplet generator, confined by polyvinyl alcohol (PVA) solution. Reprinted from Ref.[178]. E) Localised oxygen plasma used to treat the second PDMS droplet generator hydrophilic with a narrow channel as physical confinement. Reprinted from Ref.[102].

lithography, the fabrication and assembly of 3D structures are more complex and less reliable, as two models are manufactured separately and then manually aligned[159]. Meanwhile, successful production of DEs requires a high flow rate of a sheath fluid, nevertheless, the

process is inefficient and has a high likelihood of leakage[102]. Therefore, the practical applications of these devices are limited.

2.4.2.2 Localised polymer grafting

For microfluidic devices made of glass, hydrophilic surface treatment is not necessary in general but hydrophobic modification of surface (e.g., silanisation) is typically required for generating w/o droplets. For PDMS devices, conversely, the hydrophilic surface is crucial for encapsulating primary droplets. The most common method used to acquire hydrophilic PDMS surface is oxygen plasma treatment[165-167]. However, the intrinsic hydrophobic property of PDMS recovers within several hours, due to the continuous migration of uncross-linked PDMS monomer from bulk to the surface[165, 167]. Chemical modification, e.g., UV, plasma, and thermal polymer grafting, silanisation, sol-gel, and LbL, can circumvent this issue by covalently bonding polymer layers onto PDMS surface. Such a polymer layer acts as a film to prevent the uncross-linked PDMS monomer from migrating towards the treated surface, maintaining the gained surface hydrophilicity for a long period of time (months or even years)[165, 166, 168]. There exist many studies to achieve localised polymers grafting at target regions in sealed PDMS channels.

To the best of our knowledge, precise polymerisation initialised by plasma is first used by Barbier et al.[168] to generate DEs in a PDMS microfluidic device. The device was composed of two T-junction droplet generators. The long-lasting (i.e., several weeks) hydrophilic PDMS surface of the second droplet generator was achieved by depositing plasma-initialised Poly(acrylic acid) (PAA) coating. During the grafting process, the first droplet generator was covered with a glass slide, left ungrafted and hydrophobic. Seo et al.[169] used a similar process to prepare a sealed PDMS microfluidic device. The whole device was filled up with a monomer acrylic acid solution, and the hydrophilic part was modified by exposure to UV light for up to 15 min, whereas the rest was protected by a black electrical tape as a photomask. After this,

the channels were cleaned and washed with deionised (DI) water. Due to the precision and flexibility of controlling the region experiencing UV exposure, Abate et al.[170, 171] fabricated a series of devices consisting of two, three, four, and even five droplet generators with either hydrophobic or hydrophilic properties for the generation of DEs and higher-order multiple emulsions (i.e., triple, quadruple, and quintuple emulsions). Moreover, Bai et al.[105] demonstrated that UV-initiated photodegrading process can be used for preparing glass microfluidic devices. Firstly, a silane solution was used to covert the surface of the whole glass device to hydrophobic. Then the final hydrophobic area was covered by a photomask, while the target hydrophilic part was exposed to long-term (i.e., at least 60 min) UV radiation that degrades the hydrophobic self-assembly layer (see Fig. 2.6B).

This method based on the chemical grafting controlled by localised plasma or UV generally can generate a long-lasting modified surface, however, the use of different solvents can easily cause contamination. Moreover, multi-step manual processing achieved with relatively long-time treatment and complex external apparatus (e.g., the low-pressure plasma polymerisation system[168] and the UV photo surface processors[105]) make this method rather tedious and labour intensive.

2.4.2.3 Localised chemical modification using inert phases

The key part of this method is that when the target area is being treated to render hydrophobic or hydrophilic, an inert liquid or gaseous phase can be used to fill up the rest area to maintain its original properties[68, 104, 108, 113, 121, 172-182].

Nisisako et al.[108] have demonstrated the hydrophobic modification of the surface of the first droplet generator in a glass device. The surface of the whole device is firstly converted to hydrophobic by silanisation. Then an immiscible organic fluid, i.e., an inert phase, was infused to fill up the first droplet generator. Simultaneously, a sodium hydroxide solution was continuously infused into the downstream channels where the second droplet generator was

located. This sodium hydroxide solution removed the formed hydrophobic layer and converted the surface of downstream channel to hydrophilic; and the hydrophobic surface of the first droplet generator remained. Bauer et al.[172] demonstrated the use of flow confinement to prepare a PDMS microfluidic device by LbL deposition technique and a commercial water repellent agent Aquapel at different regions. Immediately after the bonding of the device, a polyelectrolyte sequence was injected through the outlet, with the rest parts being protected with DI water. As a result, only the surface of the second droplet generator was rendered hydrophilic. Thereafter, a reverse setup is used to selectively render the surface of the first droplet generator hydrophobic. The Aquapel solution is slowly injected from inner phase inlet and the hydrophilic channels were protected by infusing a stream of air. Abate et al.[121] developed a similar approach using flow confinement. The surface of the whole device was converted to superhydrophobic using a vaporised sol-gel coating. PAA monomer solution was injected from the outlet and exited from the outer phase inlet, which experienced photo/thermal-initiated polymerisation reactions to make the surface of the second droplet generator hydrophilic; meanwhile, the hydrophobic part was protected by injecting an inert fluid (see Fig. 2.6C). It is worth noting that, the flow rate of the reactive fluid is much lower than that of the inertial fluid during the flow confinement. The reactive and inert fluids always meet in the second droplet generator, so that a stable interface can form between these two fluids. It is preferable to have a sharp interface to prevent diffusion, which can be controlled by the flow rates of the two phases[121].

This chemical-based method is relatively slow and failure-prone. This is because it requires operators with hands-on experience to keep the interface between the reactive and inert regions steady in a microchannel, otherwise, it may result in irreversible chemical contamination of microchannels.

2.4.2.4 Localised surface activation

The most widely used method for modifying the surface of PDMS is surface activation, including direct oxygen plasma[167], corona discharge[183], and UV-ozone exposure[184]. These methods make PDMS surface hydrophilic due to the oxidation of surface siloxane groups into silanols[167]. Tan et al.[185] for the first time investigated the use of oxygen plasma to render PDMS surface hydrophilic in sealed microchannels. The effect was confirmed to last for at least six hours, suitable for continuous droplet generation. Compared with chemical modification, localised surface activation in a sealed microchannel can be highly simple and time-saving, with a processing time ranging from a few seconds to minutes. More importantly, it is an ideal method that avoids the introduction of liquids into the device, enabling a simple, reliable, and scalable wettability patterning.

Davies et al.[157] have achieved spatially patterned wettability in PDMS devices using corona discharge, based on the confinement by an inertial phase. Similar to localised chemical modification by flow-confinement, the hydrophobic droplet generator was filled an inert phase, i.e., oleic acid. Then the corona discharge was initiated and merely oxidised the unblocked outer channels. Also, Samandari et al.[178] achieved spatially patterned wettability in PDMS devices and further elongated the lifetime of hydrophilic surface by polymeric grafting (e.g., polymerisation of PAA and polyvinyl alcohol (PVA)) on the localised surface after treatment (see Fig. 2.6D).

Kim et al.[102] avoided the introduction of chemicals into a device by confining oxygen plasma using a long, narrow, serpentine channel for surface activation. This channel acted as a barrier to prevent the ionised gas from entering the target hydrophobic area (see Fig. 2.6E). During the oxygen plasma, only the outlet closest to the second droplet generator was open. As a result, the target hydrophilic area was exposed to the oxygen plasma in a controllable manner.

This method is free of chemicals usage and possible contamination, and has commercial potential for spatial patterning in devices in parallel instead of one by one.

In summary, the localised surface activation method in a sealed channel avoids the processing of wet chemistry, which is highly efficient to achieve a superhydrophilic surface. One drawback of this method is that the resultant hydrophilicity cannot last for a long time [186]. Many studies showed that filling up the hydrophilic part and storing treated devices in DI water can make the surface modification effect last for at least several days.

2.4.3 Other methods

Table 2.1 A summary of different methods used for DE generation in multi-module microfluidic devices

Method	Material	Surface treatment	Reagent	Time*	Stable time
Two-chip	Glass	Silanisation	Y	N.A.	N.A.[108, 113]
		N.A.	N	N.A.	N.A.[120]
	PMMA; PDMS	Silanisation; UV grafting	Y	7.5 min	>45 h[114]
	PDMS	Sol-gel; thermal grafting	Y	> 9 min	>45 h[114, 117-119]
		Plasma grafting	Y	9-11 min	A few weeks[103]
		Silanisation; LbL	Y	>30 min	N.A.[110]
		Silanisation; Plasma	Y	N.A.	N.A.[115, 116]
		Silanisation; thermal grafting	Y	4 min	1 year[109, 111, 112, 117, 118]
Capillaries	Glass	Not necessary	N	N.A.	N.A.[75, 124-126, 133, 138, 141, 145-149]
		Silanisation	Y	>10 min	N.A.[74, 87, 127-132, 134-137, 139, 140, 142-144]
3D PDMS	Glass	Silanisation	Y	10 min	N.A.[159]
	PDMS	Not necessary	N	N.A.	N.A.[154, 155, 160-163]
		Silanisation	Y	10 min	N.A.[158, 159, 164]

Table 2.2 A summary of different methods used for DE generation in single-module microfluidic devices

Method	Material	Surface treatment	Reagent	Time*	Stable time
Localise grafting	Glass	Silanisation; UV/O3	Y	150 min	1 month (water) [105]
	PDMS	Plasma grafting	Y	30 s	A few weeks[168]
		UV grafting	Y	15 min	>10 weeks[169]
		Sol-gel; UV grafting	Y	10 min	N.A.[170, 171, 187, 188]
Chemical modification	Glass	Silanisation	Y	N.A.	N.A.[108, 113]
	Polycarbonate	Organic coating; LbL	Y	>4 h	A few weeks (water) [173]

		Silanisation; LbL	Y	>10 min	> 90 min[172, 174, 182]
	PDMS	LbL	Y	>10 min	N.A.[189]
		Sol-gel; thermal/UV grafting	Y	N.A.	N.A.[121]
		UV grafting	Y	5.5 min	N.A.[176, 180]
		Plasma grafting	Y	9 min	weeks[103]
		Thermal grafting	Y	20-25 min	1 month[68, 177, 181, 190]
		Silanisation; thermal grafting	Y	40 min	N.A.[179]
Localised surface activation	PDMS	Corona plasma	Y	3 s	6 h[157]
		Corona plasma; thermal grafting;	Y	15 min	A few weeks[178]
		Oxygen plasma	N	0.5-4.5 min	A few weeks (water)[102, 191, 192]

Note: * excluding fabrication of devices, recovery to PDMS hydrophobicity, and preparation, injection, and washing of reagents.

Besides the discussed methods, there exist other approaches to generate DEs in microfluid devices, e.g., integrating microfluidic T-junction with electrohydrodynamic focusing[193], squeezing the pre-focused w/o droplet stream by controllable pneumatic choppers[194], deforming a w/o coaxial jet by air bubbles[195], spontaneous phase transfer after w/o droplet generation[196, 197], and adjusting the interfacial tensions between two immiscible droplets in contact with each other[198].

These methods are under-used due to different reasons[66], e.g., polydispersity, low reproducibility, low droplet generation frequency, low inner core encapsulation efficiency, lack of flexibility, and difficulty of device fabrication.

All the methods used for generating DEs in microfluidics are summarised and compared in Table 2.1&Table 2.2.

2.5 Materials of DEs

In the sections above, the state-of-art approaches for generating monodisperse DEs are discussed. Besides the emulsification methods, a large variety of material formulas, including various aqueous phases, oils, and surfactants, decide the structures, morphologies, properties of resultant DEs and their functionalities. This allows the use of DEs for various applications, including long-term cell culture, alteration of cellular phenotypes, controlling the behaviours

of encapsulated or surrounding molecules (e.g., mass-transport, release, preservation, and absorption), microcapsule fabrication, self-separation of the microgels, and so on.

The liquid cores and oil shells are converted into microgels, solidified or high-density shells, respectively, through polymerisation. Natural macromolecules (e.g., natural polysaccharides or proteins including alginate, dextran, gelatin, and so on) and synthetic polymers (e.g., poly(ethylene glycol (PEG)) and PVA) have been used with proper polymerisation, e.g., temperature or pH change, light illumination, ionic or chemical initiation, and solvent evaporation[199].

The combination of oils and surfactants plays an essential role in the stability, selective permeability, and biocompatibility of a DE[48]. Oils generally used for DEs are hydrocarbon and fluorinated oils. In early studies of DEs, hydrocarbon oils, e.g., mineral oil or hexadecane, were widely used, emulsified by commercial surfactants, e.g., Span™ 80 or Abil™ EM[48]. However, as the increasing demand for the use of DEs in cellular research, fluorinated oils (e.g., HFE 7500 and FC 40 oils (3M)) have been adopted as an alternative. Fluorinated oils have high chemical inertness, high biocompatibility with high oxygen transport; and limited solubility for organic and aqueous actives, enabling effective isolation between neighbouring DEs during biochemical assays.

Moreover, the type and concentration of surfactants significantly affect the properties of DEs. A surfactant with a low hydrophilic-lipophilic balance (HLB) is soluble in oil and can be used to generate w/o emulsions. Conversely, one with a high HLB in aqueous phases is used for generating O/W emulsions[79, 80]. The interplay of the two types of surfactants determines the stability of DEs. Apart from stability, the selection of the oil and surfactant depends on 1) the nature of encapsulated small molecules (which are of either hydrophilicity or lipophilicity); 2) the capacity of preventing non-specific adsorption of proteins from the water-oil interface; 3) the possibility of forming reverse micelle, which is dependent on properties of oils and

surfactants and serves as carriers for either organic or inorganic substance through oils[48, 50, 65, 79, 80, 200, 201]. Moreover, minimising the use of surfactants is desirable in cellular research due to the high cost and slight toxicity to organisms[202].

Fluorocarbon surfactants are needed for fluorinated oils in DE generation. There exist quite a few commercial fluorocarbon surfactants, e.g., 008-FluoroSurfactant (RAN Biotechnologies), and PicoSurf™ (Sphere Fluidics). In addition, many attempts have been made to develop a range of fluorocarbon surfactants based on Krytox (DuPont) oils, fluorocarbon ether polymers containing perfluoropolyether (PFEP) tails. The heads were replaced by various functional groups for specific properties, resulting in the development of PEG-PFPE, poly-l-lysine-PFPE, and so on[160, 203, 204]. Different combinations of oils and surfactants for monodisperse DEs of different sizes for corresponding applications are listed in Table 2.3.

Table 2.3 A summary of materials for generating monodisperse DEs in microfluidic devices

Applicat-ion	Inner phase*	Oil/Surfactant	Outer phase†	Size (ID/OD, μm)
Biology	N.A.	Mineral oil/Abil® EM90&Span™ 80	Tween® 20	28-40/N.A.[114]
	N.A.	HFE7500/PEG-PFPE	Pluronic® F-127	80/100[109]
	PVA	PMX200 silicone oil&liquid PDMS	PVA	100/120[68]
	N.A.	DC200 silicone oil/DC749	PVA	20-200/N.A.[133]
	N.A.	HFE7500/PicoSurf™ 1	Pluronic® F-127	50/N.A.[119]
	Tween® 20	HFE7500/PEG-PFPE	Pluronic® F-68 &Tween®20	16-29/28-48[81]; 34/47[192]
Tissue engineering	Pluronic® F-127	HFE7500/PicoSurf™ 1	Pluronic® F127	65 ~90, 150~210/N.A.;[117] 122, 200/N.A.[118]
	N.A.	HFE7500/PicoSurf™ 1	Pluronic® F-127	~150/174[180]
Metabolic Engineering	Triton™ x-100	HFE7500/PicoSurf™ 1	Tween® 80	~14/N.A.[120]
	N.A.	HFE7500/008FluoroSurfactant	Tween® 80	35-40/50[115]
	N.A.	QX200™ DG Oil for EvaGreen	Tween® 80	~28/42[179]
	N.A.	QX200 ™ DG Oil for EvaGreen	Tween® 80	17-33/22-51[116]
	N.A.	HFE7500 & FC-40/EA or AZ2C	Tween® 80	20-100/40-110[71]
Drug discovery	N.A.	Mineral oil /Abil® EM 180 or HFE7500/PicoSurf™ 2	Pluronic® F-127&PVA	~40/N.A.[111, 112]

* and † indicate surfactants used for inner phase and outer phase, respectively.

2.6 Applications of DEs

DEs have been widely used for single-cell analysis in different fields, including but not limited to cell biology, food industry, tissue engineering, metabolic engineering, and drug discovery. Additionally, the integration of DEs with flow cytometric instruments enables high-throughput screening and selection of cell-laden DE compartments. Hence, rare but valuable cells exhibiting desirable properties can be measured and isolated from large heterogeneous cell populations.

2.6.1 Cell biology

The droplets generally integrate biological, chemical, and mechanical functionalities to mimic in bulk or *in vivo* microenvironments for cell growth. Due to its ability for selective mass transfer of molecules (including inducible nutrients, chemical cues, oxygen, etc.) between the inner core and the exterior environment, a DE system can be regulated to provide a well-controlled microenvironment for cellular assays with defined dimensions. Also, the structure of DEs can be maintained in a continuous phase or in microstructural traps for long-term or in situ analysis. Thus, it is convenient for probing cellular expressions, cellular heterogeneities, and cell-to-cell interactions, under distinct environments. Furthermore, a DE can be easily triggered to release the trapped ingredients for downstream applications. To date, DEs have been used for studying various cellular behaviours, including cell morphology, migration, proliferation, differentiation, and response to stimuli, which possess great importance for biological, medical, and ecological applications.

Chang et al.[133] applied DEs to study the development and structure of biofilms, using *Bacillus subtilis* and *Pseudomonas aeruginosa* as models (see Fig. 2.7A). The morphology, migration, proliferation, and differentiation of cells were observed. For example, cyan *B. subtilis* initially stayed and proliferated at the w/o interface. After 12 h culture, the cyan rod-

shaped, motile *B. subtilis* single cells differentiated and formed chains of matrix-forming cells showing yellow fluorescence. After 48 h, all bacterial cells evolved into non-fluorescence spores and sunk at the bottom of DEs.

Moreover, Zhang et al.[109] demonstrated the use of DEs to study complex biological processes in a cell population that involved communication with external environments (see Fig. 2.7B). This study tracked the growth of GFP-expressing *E. coli* both qualitatively and quantitatively to study cell signalling. The author cultured inducible GFP-expressing *E. coli* encapsulated in DEs with medium including inducible factors, i.e., anhydrotetracycline (aTC).

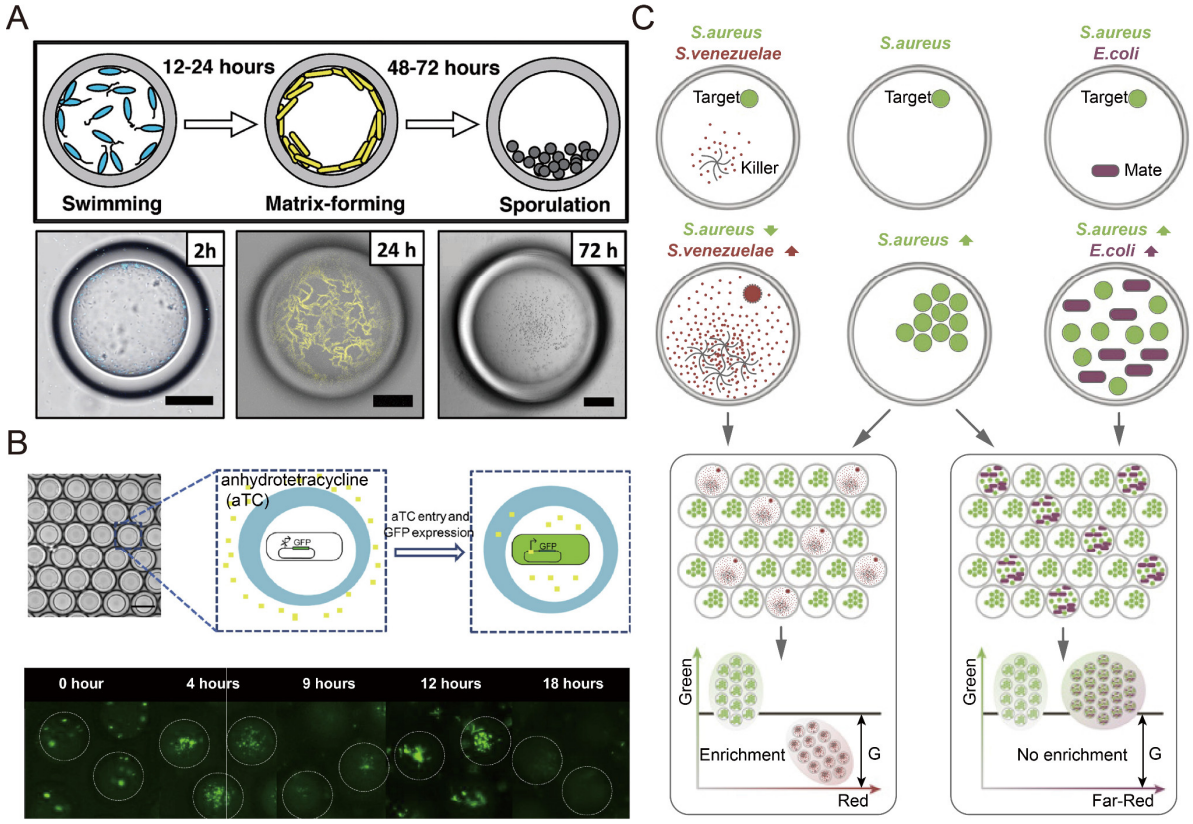

Figure 2.7 Applications of DEs in fundamental cell biology. A) Monitoring of the differentiating behaviours of *B. subtilis* in DEs for 72 h, revealing the formation and degradation of biofilms. Reprinted from Ref.[133]. B) Screening of *E. coli* expressing GFP encapsulated in DEs, revealing the transport of nutrients and quorum-sensing activities. Reprinted from Ref.[109]. C) Screening of cell-to-cell interactions between *S. aureus* (secreting green fluorescent reporters) with either *S. venezuelae* (secreting red fluorescent extracellular proteins) or *E.coli* (secreting far-red fluorescent reporters) using DE-FACS. Reprinted from Ref.[111].

Then FC screening and microscopic observation were performed to identify DEs with high fluorescence intensity, indicating a nutrient transport through the oil shell. In addition, the quorum sensing phenomenon was studied. The GFP-expressing bacteria were co-cultured with bacteria expressing quorum-sensing circuit. When the culture reached a specific concentration, chemical signals were released from quorum-sensing bacteria to affect the neighbouring cells, controlling cell population size and cellular behaviours. The usage of DEs enabled a quantitative measurement of this cellular process and revealed the occurrence of the quorum-sensing activity.

Characterisation of the cell-to-cell interaction networks within DEs across different community states, population sizes, and external environmental factors can reveal critical parameters shaping the structures and functions of microbial communities[205]. Chan et al.[118] demonstrated that the functions of hepatocyte spheroids were significantly improved when co-culturing with supporting cells (endothelial progenitor cells). Terekhov et al.[111, 112] have co-encapsulated two bacterial strains (*Streptomyces venezuelae* and *E. coli*) in DEs to identify killer cells and inactive cells for a target cell, *Staphylococcus aureus*, which is achieved by flow cytometric screening of the survival cells in DEs (see Fig. 2.7C). After this, a naturally sourced microbial consortium containing a large number of variants were co-encapsulated with *S. aureus* to find out antibiotic producers and the underlying mechanisms of antibiotic resistance. Moreover, different cell strains were cultured in different layers of a DE to control interaction rate and investigate the conditions needed to improve cell viability metabolic activities[206-208].

2.6.2 Food industry

Traditional food ingredients include flavouring agents, food acids and bases, lipids, vitamins, minerals, and other food additives. Recently, bioactive food ingredients, such as omega-3 oils, plant phytonutrients, and probiotic bacteria, have attracted increasing interest in

food processing industry[209], due to their significance in health. Since bioactive substances are generally sensitive and unstable, the long-term retention of these substances requires a suitable container that can protect the inner ingredients from heat, oxidation, moisture, low-pH, antagonism, and *in vivo* environment, till the release at destination sites. A multi-layered DE emulsion enhances the robustness of the interface for long-term storage and allows the controlled release of inner ingredients, which has great potential in food industry.

Shima et al.[84], for the first time, created DEs to encapsulate a lactic acid bacterium, *Lactobacillus acidophilus*, found in digestive tracts and known as probiotics, whose components and fermentation products are beneficial to human health. Due to the low pH in gastric juice and bile acid, only 1.3% of the bacteria were viable after a short time. However, around 50% of the bacteria remained alive after 2 h if encapsulated in DEs and immersed in gastric juice. Van der Ark et al.[210] investigated the viability of *Akkermansia muciniphila,* between unencapsulated and encapsulated in DEs in simulated digestion (incubated in gastric juice and subsequent intestinal fluid for 2 h, respectively). After the digestion, the viability of encapsulated *A. muciniphila* was 6.6%, significantly higher than the viability of free cells, 0.4% (see Fig. 2.8A). Upon the introduction of intestinal liquid, the emulsion is digested and the bacteria are released. Other probiotics, including *Lactobacillus dellbrueckii*[90], *Lactobacillus rhamnosus*[211], *Lactobacillus paracasei*[85], *Lactobacillus casei*[82, 212], and *Bifidobacterium subsp. lactis*[213], also showed improved viability or preserved functional properties in simulated digestive processes. Moreover, it is found that the gelation occurred in the outer aqueous phase of DEs further protect probiotics against heat treatment and long-term freeze-dried storage [82, 212].

DE system has also been used in fermentation process control, due to its ability to release encapsulated ingredients in a controllable manner. Devanthi et al.[206, 207], demonstrated that DEs encapsulated with two fermentation microorganisms have controllable release and activity (see

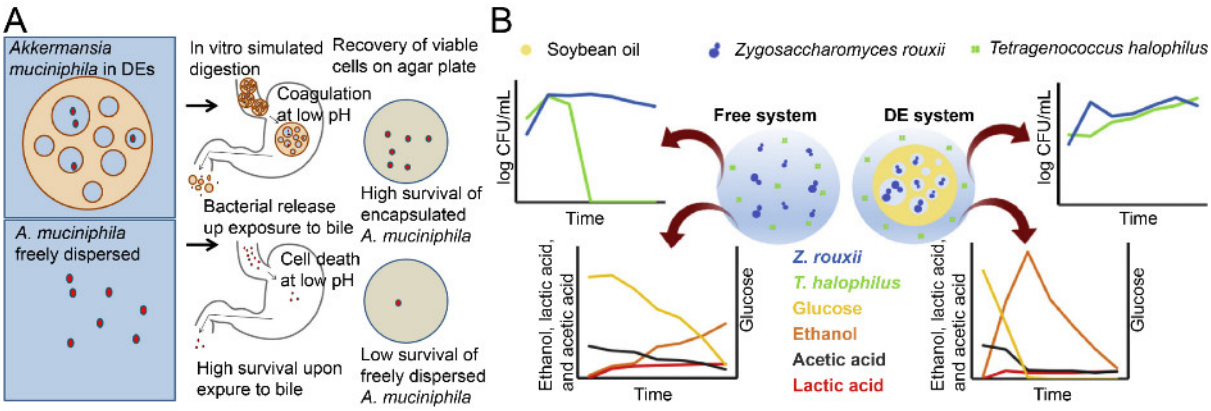

Figure 2.8 Applications of DEs in food industry. A) Encapsulation of *A.muciniphila* in DE enhances cell viability in gastric juice and after recovery. Reprinted from Ref.[210]. B) Co-culture of *Z. rouxii* and *T. halophilus* in DEs improves cell viability and metabolitesecretion. Reprinted from Ref.[206].

Fig. 2.8B). *Zygosaccharomyces rouxii* and *Tetragenococcus halophilus,* entrapped in the inner core and external aqueous phase, respectively, were delivered in a culture broth. The interactions of these two fermentation microbes within a DE were studied. The viabilities of the two microbes and their physicochemical dynamics (including the levels of glucose, ethanol, lactic acid, and acetic acid) were monitored between free cells and cells encapsulated in DEs. As a result, the presence of DEs significantly changed the microbial activities of the two species during the fermentation and induced a higher viability of *Z. rouxii* (~3 log).

2.6.3 Tissue engineering

Tissue engineering is related to the generation of biological tissue replacements that can be injected, grafted, or implanted into the diseased or injured area of a patient's body. In realistic body tissues, an agglomeration containing multiple types of cells resides in a 3D extracellular matrix. The function of a tissue, multicellular spheroids, is highly dependent on multiple factors, such as cell-to-cell interactions and cellular interactions with the surrounding extracellular matrix.

Traditionally, cells are suspended in a spinner flask to make a functional tissue, especially multicellular spheroids, resulting in a wide size distribution and inconvenience to change the

growth environment. In contrast, constructing an artificial tissue scaffold using biocompatible microparticles (e.g., DEs and hydrogel microgels) as building blocks can confine cells of different types and provide an alterable 3D matrix to mimic different tissues. It is noteworthy that both DEs and microgels can protect the inner contents from a harsh environment, resulting in a high viability of encapsulated spheroids. A microgel as a semi-open vessel enables live spheroid culture in a medium a long period of time (e.g., two weeks in the medium at 37 °C), due to its superior mechanical properties and high permeability to external nutrients. The applications of microgels in tissue engineering have been discussed in recent review articles[69,

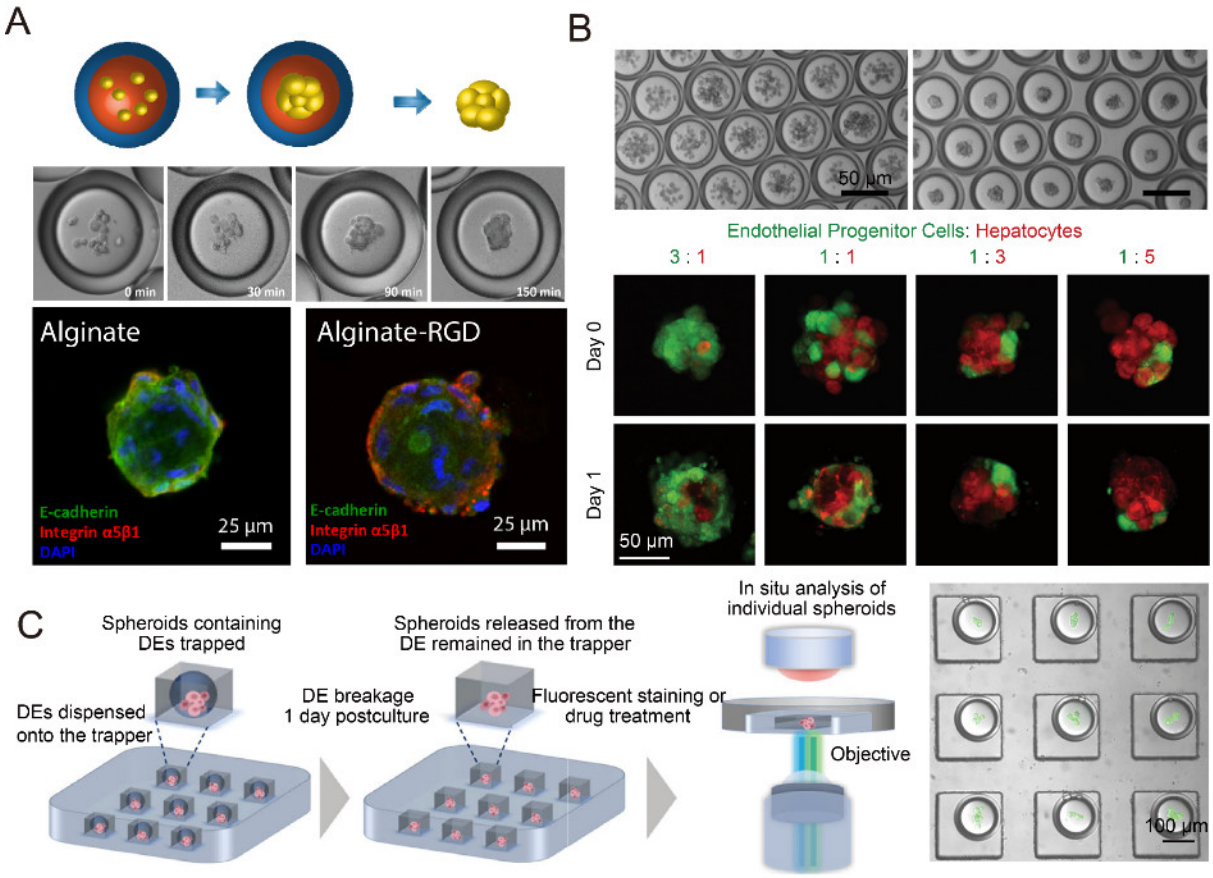

Figure 2.9 Applications of DEs in tissue engineering. A) Generation of stem cell spheroids. Reprinted from Ref.[117]. B) Generation of hepatocyte spheroids and composite spheroids consisting of two types of cells. Reprinted from Ref.[118], Inc. C) In situ drug treatment, observation, and analysis of individual tumour cell spheroids by microscopy and Raman spectroscopy. Reprinted from Ref.[180].

[70]. Moreover, a DE with a liquid core improves the interactions between the cells therefore, the functions, e.g., cell differentiation, are achieved more quickly.

Chan et al.[117] for the first time demonstrated the use of a DE for the formation of human mesenchymal stem cells spheroids (see Fig. 2.9A). Although spheroids of tumour cells have been constructed in microgels previously, the spheroids of stem cells have not been achieved yet. Using a DE as a 3D matrix, the stem cells spheroids were rapidly established within 150 min, while traditional methods take 1 to 4 days. Moreover, enhanced osteogenic differentiation was found by using a microgel precursor as the inner phase and solidifying the inner core after the formation of spheroids. The osteogenic differentiation is controllable by modulating the composition of the microgel, e.g., using alginate-arginine-glycine-aspartic acid (-RGD) instead of alginate to enhance the expression of integrin a5b1. Similarly, the same group demonstrated the use of DEs with a liquid core to form human embryonic kidney 293 and hepatocytes spheroids in 4 h[118] (see Fig. 2.9B). The effects of different biochemical formulas of the inner phase and the ratio of a supporting cell, human endothelial progenitor cells, to hepatocytes have been investigated to enhance the hepatocyte functions.

Recently, Qu et al.[180] reported a microwell platform to perform a long-term in-situ characterisation of the formation and functionality of spheroids of individual human lung adenocarcinoma cells, Calu-3, by microscopy and Raman spectroscopy (see Fig. 2.9C). The growth dynamics of Calu-3 spheroids have been recorded, and Raman spectroscopy showed that the formed Calu-3 spheroids exhibit elevated ordered lipid structures in the apical membrane. Moreover, the response of spheroids to a drug was analysed by microscopic observations and Raman spectroscopy.

2.6.4 Metabolic engineering

Microbial production of industrial enzymes and other value-added bioproducts has attract growing interest due to its advantages over conventional chemical syntheses, such as

sustainability, reduction in environmental pollution, and cost-effectiveness. Due to the limited knowledge of complicated cellular networks, directed evolution has played an essential role in improving the performance and functionality of industrially important microbes. ALE has been a powerful tool in metabolic engineering for the development of superior industrial microbial strains. However, ALE experiments are lab-intensive and time-consuming, requiring the evaluation of the growth and metabolic kinetics of intermediate populations and numerous

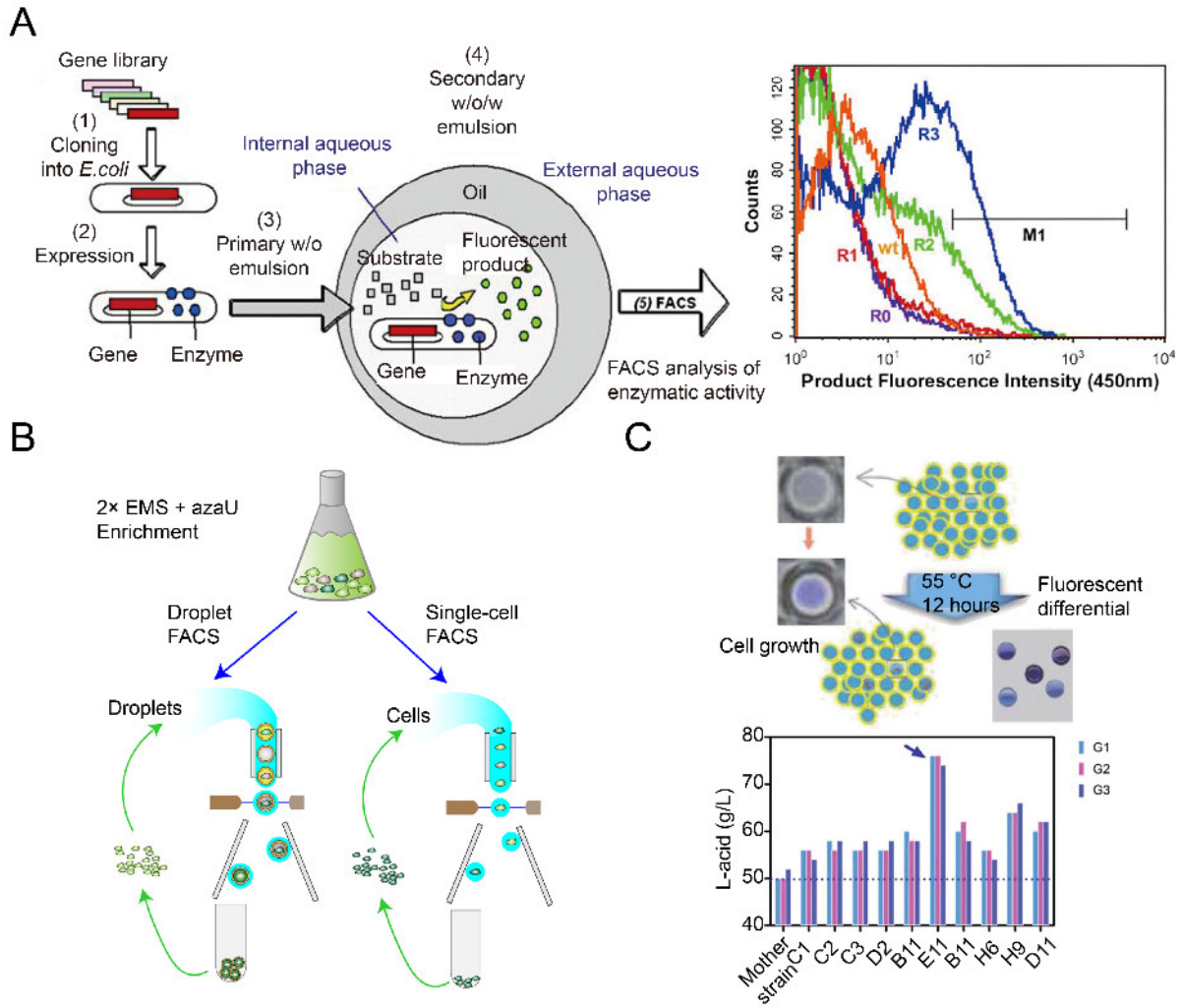

Figure 2.10 Applications of DEs in metabolic engineering. A) Directed enzyme evolution by iterative rounds of screening and selection of positive DEs encapsulating *E.coli* variant libraries via FACS. Reprinted from Ref.[78]. B) Comparison of DE-FACS and single-cell FACS for improving the production of self-fluorescent Riboflavin in *Y. lipolytica*. Reprinted from Ref. [115]. C) Selection of *B. coagulans* strains with high yield of lactic acids by FACS. Reprinted from Ref.[179].

candidate strains to select an ideal strain with improved phenotypes. In addition, this process lacks the ability to track the growth of cells at a single-cell level. Therefore, it calls for a high-throughput and cost-effective screening and selection tool to select superior variant with desired traits.

Single-cell FACS has already demonstrated its capability to select individual cells exhibiting desired properties from a heterogeneous cell population in a high throughput format (>10^7 events per hour). Nevertheless, single-cell FACS for enzyme selection is limited to intracellular molecules or adhesive molecules on the cell surface. In addition, single-cell FACS can only perform screening based on the amount of secreted enzyme rather than enzymatic activity, due to the lack of substrates as an indicator. The limitations of single-cell FACS can be overcome by encapsulating single cells within DEs, which restricts the diffusion of products by compartmentalisation using fluorinated oils as a barrier. By flow cytometric screening and sorting of cell-laden DEs based on the fluorescence intensity, cells with high productivity encapsulated in DEs can be isolated. Moreover, cells are viable after recovering from sorted DEs, which can be re-encapsulated in DEs for further rounds of selection. Similar to the ALE process, a few rounds of iterative rounds of mutagenesis and phenotypic selection by a DE-FACS can result in successful evolution of industrial strains with desired traits.

To date, a wide range of industrially important microorganisms (both eukaryotes and prokaryotes) have been cultivated in a DE for strain evolution, including *S. cerevisiae*[214, 215], *E. coli*[78, 92, 216-218], *Bacillus subtilis*[219], *Bacillus coagulans*[179], and *Yarrowia lipolytica*[115]. Notably, a mutagenesis library can be transcribed and translated either in a cell-free system[220], i.e., *in vitro* compartmentalisation or within single cells (i.e., model organism cells transformed with plasmids carrying gene variants[78, 216, 219, 221]). For example, Mastrobattista et al.[222] achieved the directed evolution of b-galactosidase from a random mutagenesis library constructed by error-prone polymerase chain reaction (PCR) using DE-FACS. The positive individual genes among

the library went through *in vitro* transcription and translation and converted the fluorogenic substrates into recognisable fluorescent signals. After two rounds of selection, novel mutations accounting for the enzyme activity were identified by coupling the genotypes with phenotypes.

Aharoni et al.[78] for the first time proposed to use DE-FACS for high-throughput screening of enzyme libraries (see. Fig. 2.10A). A gene variant library was transformed and cloned into *E. coli*, and the encoded protein, paraoxonase (PON)-1, was allowed to translate in the *E. coli*. By cultivating individual *E. coli* in DEs and the three rounds of DE selection by FACS, the isolated PON-1 variants exhibited 100-fold improvements in enzymatic activity.

Ideally, if the product of interest is intrinsically fluorescent, the encapsulation of fluorescent indicators within DEs can be avoided. For instance, Wagner et al.[115] have demonstrated the evolution of *Y. lipolytica* that can produce 54-fold higher riboflavin (which is auto-fluorescent) than the parent strain (see Fig. 2.10B). Moreover, traditional single-cell FACS was compared with DE-FACS in terms of the improvement of riboflavin secretion. The results showed that the mutants isolated by DE-FACS produced more net and extracellular products than those selected by single-cell FACS.

Another product detection approach is using fluorescent dyes that are not significantly quenched upon exposure and can specifically reflect the production levels. Zhu et al.[179] selected a *B. coagulans* mutant with a 52% higher yield of lactic acid production than its parent strain (see Fig. 2.10C). A pH-sensitive probe was co-encapsulated with cells to detect low pH and indicate the level of lactic acid production, allowing the selection of DEs containing high-yielding mutants by FACS.

To date, DE-FACS has facilitated the directed evolution of different types of enzymes and other bioproducts, including cellulase[92], protease[219], polymerase[120], cutinase[217], butyrylcholinesterase[111], glucose oxidase[215], esterase[218], riboflavin[115], and lactic acid[179]. By sequencing and analysing the isolated mutants, mapping sequence-function relationships can

provide novel insights into the underlying mechanisms of molecular evolution and reveal new functional gene clusters and functional protein sites, opening avenues to perform function genomics and combinatorial protein engineering[223].

2.6.5 Drug discovery

Due to the emergence of new diseases caused by pathogens with multidrug resistance, it calls for next-generation antibiotics for treating pathogen infections. Traditional antibiotic discovery mainly depends on the exploration and purification of natural products that are secreted by the e33cological competitors of target pathogens or their derivatives. Hence, scrutinizing the environmental microbiota containing a plethora of microorganisms continues to be important in modern drug discovery. However, many natural resources are under-used

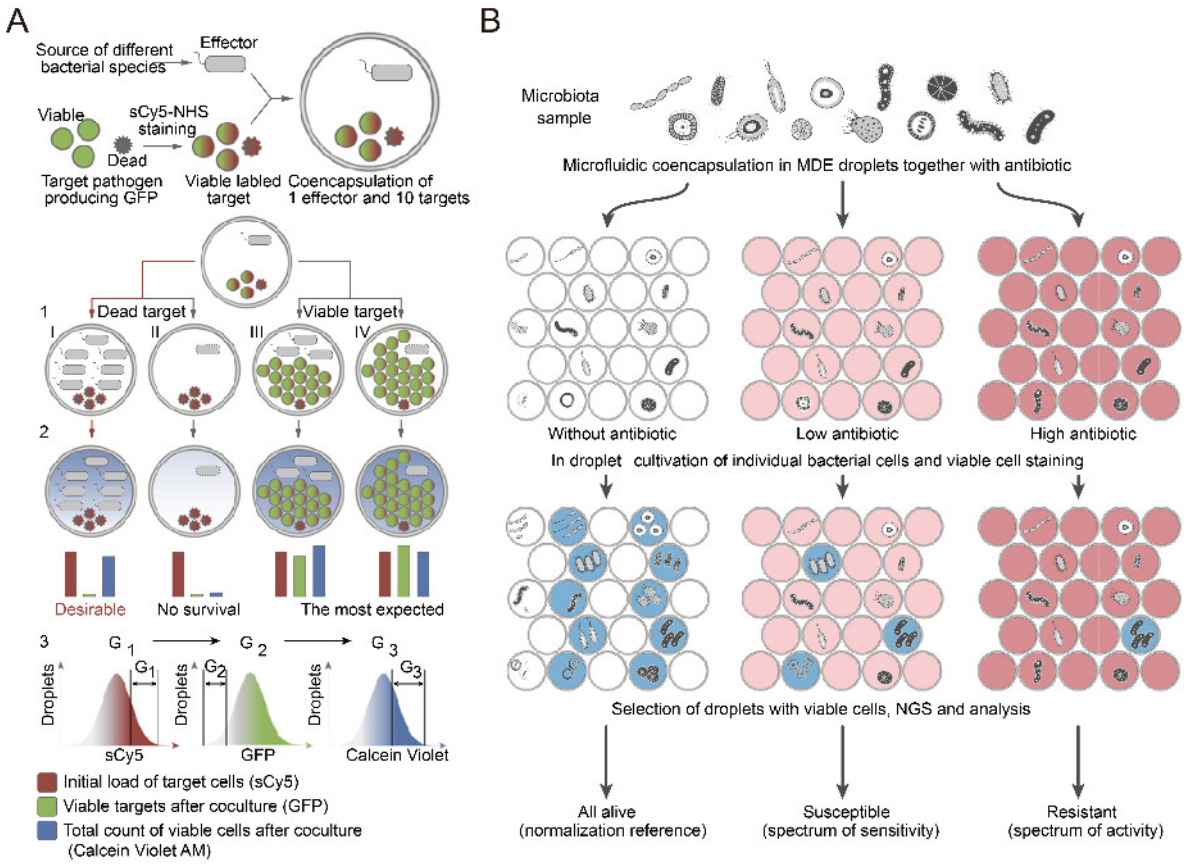

Figure 2.11 Applications of DEs in drug discovery. A) High-throughput screening of desired cells inhibiting bacterial growth via DE-FACS. Reprinted from Ref.[111]. B) Profiling of the activity and sensitivity spectrum of a natural microbiota to a discovered antibiotic, amicoumacin A (Ami) via high-throughput screening of DE-FACS. Reprinted from Ref.[112].

due to the inefficiency of the traditional screening methodologies, which are based on miscellaneous population signals and might ignore rare or slow-growing microbiota sources.

A high-throughput drug screening method plays a critical role in discovering new drugs from natural resources as cures against certain pathogens and diseases. DE-FACS not only offers a high-throughput screening method but also empowers a high-throughput functional profiling of microbiota through the integration with downstream analytical tools, i.e., sequencing, bioinformatics, and metabolomic analysis. In addition, a DE acts as a constriction to fast-growing species, thus the minority of slow-growing microbiota species accounting for less than 0.1% of the whole population can be assessed[111].

Terekhov et al.[111] established a workflow of a DE-FACS screening (see Fig. 2.11A). In their study, antibiotic-resistant pathogen, *S. aureus*, were co-cultured with a host of microorganisms originating from human oral microbiota in DEs. FACS was used to isolate DEs containing inhibited *S. aureus* and a cultivatable killer organism, indicated by a specific combination of three fluorescence reporters. By next-generation sequencing, bioinformatics, and mass spectrometry, both slow-growing and culturable oral microbiota species as killers to *S. aureus* were identified, a genus associated with this antibiotics effect was revealed, and some compounds, e.g., Pyocyanin and phenazine-1-carboxylic acid were recognised as the principal functional bioactives to perform a synergetic inhibition of *S. aureus*.

Later on, the same group demonstrated in the discovery of probiotics and physiologically active compounds from Siberian bear microbiota using a similar DE-FACS approach[112] (see Fig. 2.11B). An active compound, amicoumacin A (Ami), and its culturable producer, *Bacillus pumilus*, were isolated. Functional gene clusters of Ami were subsequently recognised and characterised by proteomics and heterologous expression, revealing the mechanism of Ami activity. Moreover, a quantitative single-cell analysis was performed to evaluate the probiotic

susceptibility and resistance activities toward different microbiomes, i.e., the oral microbiota from the Siberian bear and human fecal microbiota.

2.7 Challenges

As discussed above, using DEs as microbioreactors has many advantages for cellular assays (e.g., high-throughput single-cell isolation, high controllability, and integration with FC) compared with traditional methods. Therefore, DEs have been used for a wide range of applications in biological, biomedical and industrial fields. However, there still exist some limitations, which hinder the adoption of DEs by wider communities, including single-cell encapsulation rate and generation, stability, and the molecule leakage of DEs.

2.7.1 Single-cell encapsulation

Droplet-based microfluidics has been considered as a powerful tool to rapidly encapsulate a large number of single cells in parallel compartments, i.e., single emulsions and DEs. Individual cells are encapsulated within droplets when they arrive at the water-oil interface. However, the travelling time of cells in microchannels to reach the interface is random, resulting in passive encapsulation that follows the statistical model, Poisson distribution.

Deterministic cell encapsulation methods include hydrodynamic methods and printed droplet microfluidics. Hydrodynamic methods (e.g., inertial focusing) allow individual cells to reach the interface at the same rate and with uniform spacing[224-226]. Printed droplet microfluidics technology can automatically control the dispensing of droplets and cells to ensure single-cell encapsulation[227]. Despite the high efficiency of single-cell encapsulation, the first method requires specific configurations of cells and high flow rates[47] while the second method requires a complex setup and has low throughput. In non-deterministic cell encapsulation, there are some inaccuracies in predicting the portion of droplets containing various numbers of cells via Poisson distribution, due to the cell sedimentation and aggregation.

Cell sedimentation changes the uniformity of cell distribution within the suspension (in the syringe, tubing, and microchannels), and therefore, increases the chance of aggregation. Finally, cell sedimentation and the resultant aggregation decrease the reliability of the droplet generation system. Therefore, sedimentation effects must be suppressed in the microfluidic droplet systems to improve single-cell encapsulation efficiency.

Magnetic stirring has been often used to prevent cell sedimentation and aggregation[228, 229]. However, this method may cause cell volume fraction, cell damage, and cell physiological fluctuations. A simpler and gentler method is the use of biocompatible density-matching reagents to balance the density of cell suspensions and suspending medium before cell injection. Also, it calls for a detailed report that quantitatively evaluates the effect of density-matching reagents on single-cell encapsulation efficiency. Notably, a high cell concentration in a droplet at the beginning is desired for some applications, e.g., food industry[206, 207] and tissue engineering[118]. For high cell concentrations and large droplets with large λ values, the random distribution of cells is not a significant issue to encapsulate an approximately equal number of cells per droplet. The number of cells encapsulated in a droplet in these cases follows Gaussian distribution[47].

2.7.2 Generation

Passive methods for generating DEs with microfluidic devices can rapidly generate monodisperse DEs with good control of droplet size and single-cell encapsulation efficiency. However, some technological limitations still exist in the fabrication and generation of DEs. The wettability of the microdevices significantly affect the robustness of the high-throughput generation of DEs, and the geometry plays an important role in determining the pattern of wettability in the devices. Besides 3D PDMS microfluidics that requires multiple fabrications and alignments, most microchannels or microcapillaries need surface treatment at target regions using either chemicals modification or surface activation methods based on plasma,

discharge, or UV/O_3. For multi-module microfluidics connecting more than one separate microdevices or glass capillaries, the patterning of either hydrophobicity or hydrophilicity can be achieved separately in different devices, which may cause turbulence due to the unstable shear force at the connection and suffer from the difficulty of the precise alignment. Although single-module microfluidics avoids these issues, it requires a high degree of spatial control of wettability in one microdevice. Different approaches based on the use of controllable initiators (e.g., temperature, UV, and plasma), inert phase or diffusion barrier channels can confine the surface treatment at target regions, but they suffer from either relatively long treatment time or labour-intensive processes.

2.7.3 Stability

In practice, DEs are thermodynamically unstable systems and tend to rupture during storage[65]. The reasons for the inherent instability have been investigated, which are attributed to the polydispersity of DEs, the size of inner cores, mass transfer between inner and outer layers, and reverse micellar mechanisms. This leads to an uncontrollable release of the inner ingredients to the environment, restricting its commercial production and potential applications[80, 230]. The uniformity of DEs and the reduced size of inner cores can be resolved by improving the generation methods[80]. Notably, the size of generated DEs should be less than one-third of the nozzle diameter to prevent the collapse of DE under a high shear force during the flow cytometric screening and sorting[71].

Two main approaches without changing the entrapped actives have been proposed to improve DE stability[65, 79, 80]. First, the osmotic pressure gradience should be balanced between the inner phase and outer phase to prevent the occurrence of osmosis. Second, an alternative composition of a DE (e.g., an alginate core instead of a liquid core) can enhance its mechanical, thermal, chemical stabilities[69]. Monomeric surfactants in aqueous phases should be avoided as they can immigrate to the oil layer and form reverse micelles that dissolve aqueous

compounds[231]. Towards this end, a large number of oils, aqueous cosolvents, combinations of ionic or non-ionic surfactants have been explored[69, 80, 230-232] to enhance DE stability. The use of polymeric amphiphiles (synthetic tailored or natural macromolecules), e.g., proteins and polysaccharides[231] in each phase can either increase the viscosity of each phase or form complex oils or surfactants to enable a DE to behave like a more stable solid core-shell system[69] (i.e., microcapsules or microspheres), significantly reducing the mass transport between layers and reverse micellar transport. It's worth noting that the concentrations of amphiphiles can be optimised and the selection of materials for each phase is based on the applications.

2.7.4 Molecule restriction

As mentioned above, DEs generally allow the mass transfer of small molecules, ions, and gas between their interior and exterior, selectively or at a low rate. This trait has been utilised for introducing the reagents for stimulating cells or analysing cellular behaviours after encapsulation for real-time cell screening[70, 109, 117, 132]. However, to ensure an accurate and effective cellular analysis, it is crucial to maintain all the molecules within the inner core of DEs for a long period in many cases, during the incubation, relocation, screening, and sorting without any cross-contamination or analyte leakage[51]. There are two main mechanisms caused the unwanted mass transport[200]: the diffusion of trapped molecules into the oil, and formation and transport of reverse micellular.

To date, several approaches have been used to facilitate the retention of small-molecule analytes within DEs. Biopolymers such as BSA and carboxymethyl cellulose can form a complex at the interface that can reduce the leakage of molecules [160, 191, 192, 200, 233]. Moreover, fluorinated oils are widely used in current droplet-based microfluidics instead of mineral oils, whose fluorocarbon group is immiscible with organic molecules and hence reduces the molecule leakage. Some approaches are based on the use of indirect reporters to circumvent the intrinsic permeability of a DE, opening up avenues to screen a broader range of analytes.

For example, a hydrophobic substrate is engineered, which can diffuse into the inner core of a DE. After reacting with the entrapped enzymes, its products have a reverse polarity and can be retained inside the oil shell[234]. Furthermore, biosensor cells and high-molecular-weight reporters (e.g., responsive proteins and RNA aptamers) have been integrated with DEs to capture small molecules, avoiding possible leakage[63].

2.8 Summary

In summary single-cell analysis has attracted increasing attention to reveal cell-to-cell heterogeneity for many applications from both the academic and industrial perspectives. Different approaches have been developed for single-cell isolation and subsequent analysis, including AFM, LCM, micromanipulation, cytometry, and microfluidics. I mainly focus on droplet-based microfluidics for single-cell analysis, due to its intrinsic advantage of high-throughput generation of a large number of single-cell compartments. A DE system is a highly tailorable, semi-permeable core-shell system, which is compatible with commercial flow cytometers for single-cell screening and sorting. The inner phase contains functional cells or actives for various applications; the middle shell acts as a selective barrier that controls the mass transport; and the outer phase determines the composition and morphology of the whole system and provides the compatibility with FC setup. These traits empower a DE with a lot of advantages as a micro-bioreactor: for single-cell analysis. I highlight the generation and composition of DEs, the applications of DEs for single-cell analysis in various areas, as well as current challenges and opportunities for DE technology.

References

1. Wang, D.; Bodovitz, S., Single cell analysis: the new frontier in 'omics'. *Trends Biotechnol.* **2010,** *28* (6), 281-290.
2. Schmid, A.; Kortmann, H.; Dittrich, P. S.; Blank, L. M., Chemical and biological single cell analysis. *Curr. Opin. Biotechnol.* **2010,** *21* (1), 12-20.
3. Kærn, M.; Elston, T. C.; Blake, W. J.; Collins, J. J., Stochasticity in gene expression: from theories to phenotypes. *Nat. Rev. Genet.* **2005,** *6* (6), 451-464.

4. Metzler, R., The Future is Noisy: The Role of Spatial Fluctuations in Genetic Switching. *Phys. Rev. Lett.* **2001,** *87* (6), 068103.
5. Zare, R. N.; Kim, S., Microfluidic Platforms for Single-Cell Analysis. *Annu. Rev. Biomed. Eng.* **2010,** *12* (1), 187-201.
6. Stuart, T.; Satija, R., Integrative single-cell analysis. *Nat. Rev. Genet.* **2019,** *20* (5), 257-272.
7. Hao, Y.; Cheng, S.; Tanaka, Y.; Hosokawa, Y.; Yalikun, Y.; Li, M., Mechanical properties of single cells: Measurement methods and applications. *Biotechnol. Adv.* **2020,** *45*, 107648.
8. Hu, P.; Zhang, W.; Xin, H.; Deng, G., Single Cell Isolation and Analysis. *Front. Cell Dev. Biol.* **2016,** *4*, 116.
9. Gross, A.; Schoendube, J.; Zimmermann, S.; Steeb, M.; Zengerle, R.; Koltay, P., Technologies for Single-Cell Isolation. *Int. J. Mol. Sci.* **2015,** *16* (8).
10. Huang, N.-T.; Zhang, H.-l.; Chung, M.-T.; Seo, J. H.; Kurabayashi, K., Recent advancements in optofluidics-based single-cell analysis: optical on-chip cellular manipulation, treatment, and property detection. *Lab Chip* **2014,** *14* (7), 1230-1245.
11. Matuła, K.; Rivello, F.; Huck, W. T. S., Single-Cell Analysis Using Droplet Microfluidics. *Adv. Biosyst.* **2020,** *4* (1), 1900188.
12. Xu, X.; Wang, J.; Wu, L.; Guo, J.; Song, Y.; Tian, T.; Wang, W.; Zhu, Z.; Yang, C., Microfluidic Single-Cell Omics Analysis. *Small* **2020,** *16* (9), 1903905.
13. Blainey, P. C.; Quake, S. R., Dissecting genomic diversity, one cell at a time. *Nat. Meth.* **2014,** *11* (1), 19-21.
14. Mehmood, S.; Bilal, M.; Manzoor, R.; Iqbal, H. M. N., Deciphering the adult brain development complexity by single-cell transcriptome analysis—a review. *Mater. Today Chem.* **2019,** *13*, 88-97.
15. Shi, X.; Zhang, X.; Xia, T.; Fang, X., Living cell study at the single-molecule and single-cell levels by atomic force microscopy. *Nanomed.* **2012,** *7* (10), 1625-1637.
16. Murphy, T. W.; Zhang, Q.; Naler, L. B.; Ma, S.; Lu, C., Recent advances in the use of microfluidic technologies for single cell analysis. *Analyst* **2018,** *143* (1), 60-80.
17. Revzin, A.; Sekine, K.; Sin, A.; Tompkins, R. G.; Toner, M., Development of a microfabricated cytometry platform for characterization and sorting of individual leukocytes. *Lab Chip* **2005,** *5* (1), 30-37.
18. Chen Gonzalez, E.; McGee, J. S., Research Techniques Made Simple: Laser Capture Microdissection in Cutaneous Research. *J. Invest. Dermatol.* **2016,** *136* (10), e99-e103.
19. Allard, W. J.; Matera, J.; Miller, M. C.; Repollet, M.; Connelly, M. C.; Rao, C.; Tibbe, A. G. J.; Uhr, J. W.; Terstappen, L. W. M. M., Tumor Cells Circulate in the Peripheral Blood of All Major Carcinomas but not in Healthy Subjects or Patients With Nonmalignant Diseases. *Clin. Cancer Res.* **2004,** *10* (20), 6897.
20. Brehm-Stecher Byron, F.; Johnson Eric, A., Single-Cell Microbiology: Tools, Technologies, and Applications. *Microbiol. Mol. Biol. Rev.* **2004,** *68* (3), 538-559.
21. Luo, T.; Fan, L.; Zhu, R.; Sun, D., Microfluidic Single-Cell Manipulation and Analysis: Methods and Applications. *Micromachines* **2019,** *10* (2).
22. Di Carlo, D.; Aghdam, N.; Lee, L. P., Single-Cell Enzyme Concentrations, Kinetics, and Inhibition Analysis Using High-Density Hydrodynamic Cell Isolation Arrays. *Anal. Chem.* **2006,** *78* (14), 4925-4930.
23. Gao, D.; Jin, F.; Zhou, M.; Jiang, Y., Recent advances in single cell manipulation and biochemical analysis on microfluidics. *Analyst* **2019,** *144* (3), 766-781.
24. Nitta, N.; Sugimura, T.; Isozaki, A.; Mikami, H.; Hiraki, K.; Sakuma, S.; Iino, T.; Arai, F.; Endo, T.; Fujiwaki, Y.; Fukuzawa, H.; Hase, M.; Hayakawa, T.; Hiramatsu, K.; Hoshino, Y.; Inaba, M.; Ito, T.; Karakawa, H.; Kasai, Y.; Koizumi, K.; Lee, S.; Lei, C.; Li, M.; Maeno, T.; Matsusaka, S.; Murakami, D.; Nakagawa, A.; Oguchi, Y.; Oikawa, M.; Ota, T.; Shiba, K.; Shintaku, H.; Shirasaki, Y.; Suga, K.; Suzuki, Y.; Suzuki, N.; Tanaka, Y.; Tezuka, H.; Toyokawa, C.; Yalikun, Y.; Yamada, M.; Yamagishi, M.; Yamano, T.; Yasumoto, A.; Yatomi, Y.; Yazawa, M.; Di Carlo, D.; Hosokawa, Y.; Uemura, S.; Ozeki, Y.; Goda, K., Intelligent Image-Activated Cell Sorting. *Cell* **2018,** *175* (1), 266-276.e13.
25. Kovac, J. R.; Voldman, J., Intuitive, Image-Based Cell Sorting Using Optofluidic Cell Sorting. *Anal. Chem.* **2007,** *79* (24), 9321-9330.
26. Li, M.; Liu, H.; Zhuang, S.; Goda, K., Droplet flow cytometry for single-cell analysis. *RSC Adv.* **2021,** *11* (34), 20944-20960.
27. Fung, C. W.; Chan, S. N.; Wu, A. R., Microfluidic single-cell analysis—Toward integration and total on-chip analysis. *Biomicrofluidics* **2020,** *14* (2), 021502.
28. Yousuff, C. M.; Ho, E. T.; Hussain K, I.; Hamid, N. H. B., Microfluidic Platform for Cell Isolation and Manipulation Based on Cell Properties. *Micromachines* **2017,** *8* (1).
29. Chen, J.; Chen, D.; Yuan, T.; Xie, Y.; Chen, X., A microfluidic chip for direct and rapid trapping of white blood cells from whole blood. *Biomicrofluidics* **2013,** *7* (3), 034106.
30. Jin, D.; Deng, B.; Li, J. X.; Cai, W.; Tu, L.; Chen, J.; Wu, Q.; Wang, W. H., A microfluidic device enabling high-efficiency single cell trapping. *Biomicrofluidics* **2015,** *9* (1), 014101.

31. Marie, R.; Pødenphant, M.; Koprowska, K.; Bærlocher, L.; Vulders, R. C. M.; Wilding, J.; Ashley, N.; McGowan, S. J.; van Strijp, D.; van Hemert, F.; Olesen, T.; Agersnap, N.; Bilenberg, B.; Sabatel, C.; Schira, J.; Kristensen, A.; Bodmer, W.; van der Zaag, P. J.; Mir, K. U., Sequencing of human genomes extracted from single cancer cells isolated in a valveless microfluidic device. *Lab Chip* **2018,** *18* (13), 1891-1902.
32. Rettig, J. R.; Folch, A., Large-Scale Single-Cell Trapping And Imaging Using Microwell Arrays. *Anal. Chem.* **2005,** *77* (17), 5628-5634.
33. Park, J. Y.; Morgan, M.; Sachs, A. N.; Samorezov, J.; Teller, R.; Shen, Y.; Pienta, K. J.; Takayama, S., Single cell trapping in larger microwells capable of supporting cell spreading and proliferation. *Microfluid. Nanofluidics* **2010,** *8* (2), 263-268.
34. Wood, D. K.; Weingeist, D. M.; Bhatia, S. N.; Engelward, B. P., Single cell trapping and DNA damage analysis using microwell arrays. *Proc. Nat.l Acad. Sci. U. S. A.* **2010,** *107* (22), 10008.
35. Breukers, J.; Horta, S.; Struyfs, C.; Spasic, D.; Feys, H. B.; Geukens, N.; Thevissen, K.; Cammue, B. P. A.; Vanhoorelbeke, K.; Lammertyn, J., Tuning the Surface Interactions between Single Cells and an OSTE+ Microwell Array for Enhanced Single Cell Manipulation. *ACS Appl. Mater. Interfaces* **2021,** *13* (2), 2316-2326.
36. Shah, P.; Zhu, X.; Chen, C.; Hu, Y.; Li, C.-Z., Lab-on-chip device for single cell trapping and analysis. *Biomed. Microdevices* **2014,** *16* (1), 35-41.
37. Nagrath, S.; Sequist, L. V.; Maheswaran, S.; Bell, D. W.; Irimia, D.; Ulkus, L.; Smith, M. R.; Kwak, E. L.; Digumarthy, S.; Muzikansky, A.; Ryan, P.; Balis, U. J.; Tompkins, R. G.; Haber, D. A.; Toner, M., Isolation of rare circulating tumour cells in cancer patients by microchip technology. *Nature* **2007,** *450* (7173), 1235-1239.
38. Stott, S. L.; Hsu, C.-H.; Tsukrov, D. I.; Yu, M.; Miyamoto, D. T.; Waltman, B. A.; Rothenberg, S. M.; Shah, A. M.; Smas, M. E.; Korir, G. K.; Floyd, F. P.; Gilman, A. J.; Lord, J. B.; Winokur, D.; Springer, S.; Irimia, D.; Nagrath, S.; Sequist, L. V.; Lee, R. J.; Isselbacher, K. J.; Maheswaran, S.; Haber, D. A.; Toner, M., Isolation of circulating tumor cells using a microvortex-generating herringbone-chip. *Proc. Nat.l Acad. Sci. U. S. A.* **2010,** *107* (43), 18392.
39. Unger, M. A.; Chou, H.-P.; Thorsen, T.; Scherer, A.; Quake, S. R. J. S., Monolithic microfabricated valves and pumps by multilayer soft lithography. *Science* **2000,** *288* (5463), 113-116.
40. Hong, J. W.; Studer, V.; Hang, G.; Anderson, W. F.; Quake, S. R., A nanoliter-scale nucleic acid processor with parallel architecture. *Nat. Biotechnol.* **2004,** *22* (4), 435-439.
41. Weser, R.; Winkler, A.; Weihnacht, M.; Menzel, S.; Schmidt, H., The complexity of surface acoustic wave fields used for microfluidic applications. *Ultrasonics* **2020,** *106*, 106160.
42. Yuan, G.-C.; Cai, L.; Elowitz, M.; Enver, T.; Fan, G.; Guo, G.; Irizarry, R.; Kharchenko, P.; Kim, J.; Orkin, S.; Quackenbush, J.; Saadatpour, A.; Schroeder, T.; Shivdasani, R.; Tirosh, I., Challenges and emerging directions in single-cell analysis. *Genome Biol.* **2017,** *18* (1), 84.
43. Shen, Y.; Yalikun, Y.; Tanaka, Y., Recent advances in microfluidic cell sorting systems. *Sens. Actuators B Chem.* **2019,** *282*, 268-281.
44. Qin, Y.; Wu, L.; Schneider, T.; Yen, G. S.; Wang, J.; Xu, S.; Li, M.; Paguirigan, A. L.; Smith, J. L.; Radich, J. P.; Anand, R. K.; Chiu, D. T., A Self-Digitization Dielectrophoretic (SD-DEP) Chip for High-Efficiency Single-Cell Capture, On-Demand Compartmentalization, and Downstream Nucleic Acid Analysis. *Angew. Chem. Int. Ed.* **2018,** *57* (35), 11378-11383.
45. Collins, D. J.; Morahan, B.; Garcia-Bustos, J.; Doerig, C.; Plebanski, M.; Neild, A., Two-dimensional single-cell patterning with one cell per well driven by surface acoustic waves. *Nat. Commun.* **2015,** *6* (1), 8686.
46. Armbrecht, L.; Müller, R. S.; Nikoloff, J.; Dittrich, P. S., Single-cell protein profiling in microchambers with barcoded beads. *Microsyst. Nanoeng.* **2019,** *5* (1), 55.
47. Collins, D. J.; Neild, A.; deMello, A.; Liu, A.-Q.; Ai, Y., The Poisson distribution and beyond: methods for microfluidic droplet production and single cell encapsulation. *Lab Chip* **2015,** *15* (17), 3439-3459.
48. Joensson, H. N.; Andersson Svahn, H., Droplet Microfluidics—A Tool for Single-Cell Analysis. *Angew. Chem. Int. Ed.* **2012,** *51* (49), 12176-12192.
49. Guo, M. T.; Rotem, A.; Heyman, J. A.; Weitz, D. A., Droplet microfluidics for high-throughput biological assays. *Lab Chip* **2012,** *12* (12), 2146-2155.
50. Theberge, A. B.; Courtois, F.; Schaerli, Y.; Fischlechner, M.; Abell, C.; Hollfelder, F.; Huck, W. T. S., Microdroplets in Microfluidics: An Evolving Platform for Discoveries in Chemistry and Biology. *Angew. Chem. Int. Ed.* **2010,** *49* (34), 5846-5868.
51. Liu, H.; Li, M.; Wang, Y.; Piper, J.; Jiang, L., Improving Single-Cell Encapsulation Efficiency and Reliability through Neutral Buoyancy of Suspension. *Micromachines* **2020,** *11* (1).
52. Kaushik, A. M.; Hsieh, K.; Wang, T.-H., Droplet microfluidics for high-sensitivity and high-throughput detection and screening of disease biomarkers. *WIREs Nanomed. Nanobiotechnol.* **2018,** *10* (6), e1522.
53. Rakszewska, A.; Tel, J.; Chokkalingam, V.; Huck, W. T. S., One drop at a time: toward droplet microfluidics as a versatile tool for single-cell analysis. *NPG Asia Mater.* **2014,** *6* (10), e133-e133.

54. Agresti, J. J.; Antipov, E.; Abate, A. R.; Ahn, K.; Rowat, A. C.; Baret, J.-C.; Marquez, M.; Klibanov, A. M.; Griffiths, A. D.; Weitz, D. A., Ultrahigh-throughput screening in drop-based microfluidics for directed evolution. *Proc. Nat.l Acad. Sci. U. S. A.* **2010,** *107* (9), 4004.
55. Mazutis, L.; Gilbert, J.; Ung, W. L.; Weitz, D. A.; Griffiths, A. D.; Heyman, J. A., Single-cell analysis and sorting using droplet-based microfluidics. *Nat. Protoc.* **2013,** *8* (5), 870-891.
56. Wang, B. L.; Ghaderi, A.; Zhou, H.; Agresti, J.; Weitz, D. A.; Fink, G. R.; Stephanopoulos, G., Microfluidic high-throughput culturing of single cells for selection based on extracellular metabolite production or consumption. *Nat. Biotechnol.* **2014,** *32* (5), 473-8.
57. Vallejo, D.; Nikoomanzar, A.; Paegel, B. M.; Chaput, J. C., Fluorescence-Activated Droplet Sorting for Single-Cell Directed Evolution. *ACS Synth. Biol.* **2019,** *8* (6), 1430-1440.
58. Qiao, Y.; Zhao, X.; Zhu, J.; Tu, R.; Dong, L.; Wang, L.; Dong, Z.; Wang, Q.; Du, W., Fluorescence-activated droplet sorting of lipolytic microorganisms using a compact optical system. *Lab Chip* **2018,** *18* (1), 190-196.
59. Hasan, S.; Geissler, D.; Wink, K.; Hagen, A.; Heiland, J. J.; Belder, D., Fluorescence lifetime-activated droplet sorting in microfluidic chip systems. *Lab Chip* **2019,** *19* (3), 403-409.
60. Gielen, F.; Hours, R.; Emond, S.; Fischlechner, M.; Schell, U.; Hollfelder, F., Ultrahigh-throughput–directed enzyme evolution by absorbance-activated droplet sorting (AADS). *Proc. Nat.l Acad. Sci. U. S. A.* **2016,** *113* (47), E7383.
61. Fu, X.; Zhang, Y.; Xu, Q.; Sun, X.; Meng, F., Recent Advances on Sorting Methods of High-Throughput Droplet-Based Microfluidics in Enzyme Directed Evolution. *Front. Chem.* **2021,** *9*, 168.
62. Weng, L.; Spoonamore, J. E., Droplet microfluidics-enabled high-throughput screening for protein engineering. *Micromachines* **2019,** *10* (11).
63. Bowman, E. K.; Alper, H. S., Microdroplet-Assisted Screening of Biomolecule Production for Metabolic Engineering Applications. *Trends Biotechnol.* **2020,** *38* (7), 701-714.
64. van Tatenhove-Pel, R. J.; Hernandez-Valdes, J. A.; Teusink, B.; Kuipers, O. P.; Fischlechner, M.; Bachmann, H., Microdroplet screening and selection for improved microbial production of extracellular compounds. *Curr. Opin. Biotechnol.* **2020,** *61*, 72-81.
65. Garti, N.; Bisperink, C., Double emulsions: Progress and applications. *Curr. Opin. Colloid Interface Sci.* **1998,** *3* (6), 657-667.
66. Chong, D.; Liu, X.; Ma, H.; Huang, G.; Han, Y. L.; Cui, X.; Yan, J.; Xu, F., Advances in fabricating double-emulsion droplets and their biomedical applications. *Microfluid. Nanofluidics* **2015,** *19* (5), 1071-1090.
67. Duncanson, W. J.; Lin, T.; Abate, A. R.; Seiffert, S.; Shah, R. K.; Weitz, D. A., Microfluidic synthesis of advanced microparticles for encapsulation and controlled release. *Lab Chip* **2012,** *12* (12), 2135-2145.
68. Cai, B.; Ji, T.-T.; Wang, N.; Li, X.-B.; He, R.-X.; Liu, W.; Wang, G.; Zhao, X.-Z.; Wang, L.; Wang, Z., A microfluidic platform utilizing anchored water-in-oil-in-water double emulsions to create a niche for analyzing single non-adherent cells. *Lab Chip* **2019,** *19* (3), 422-431.
69. Galogahi, F. M.; Zhu, Y.; An, H.; Nguyen, N.-T., Core-shell microparticles: Generation approaches and applications. *J. Sci.: Adv. Mater. Devices* **2020,** *5* (4), 417-435.
70. Li, W.; Zhang, L.; Ge, X.; Xu, B.; Zhang, W.; Qu, L.; Choi, C.-H.; Xu, J.; Zhang, A.; Lee, H.; Weitz, D. A., Microfluidic fabrication of microparticles for biomedical applications. *Chem. Soc. Rev.* **2018,** *47* (15), 5646-5683.
71. Zinchenko, A.; Devenish, S. R.; Kintses, B.; Colin, P. Y.; Fischlechner, M.; Hollfelder, F., One in a million: flow cytometric sorting of single cell-lysate assays in monodisperse picolitre double emulsion droplets for directed evolution. *Anal. Chem.* **2014,** *86* (5), 2526-33.
72. Tu, F.; Lee, D., Controlling the Stability and Size of Double-Emulsion-Templated Poly(lactic-co-glycolic) Acid Microcapsules. *Langmuir* **2012,** *28* (26), 9944-9952.
73. Liu, E. Y.; Jung, S.; Weitz, D. A.; Yi, H.; Choi, C. H., High-throughput double emulsion-based microfluidic production of hydrogel microspheres with tunable chemical functionalities toward biomolecular conjugation. *Lab Chip* **2018,** *18* (2), 323-334.
74. Kim, B.; Jeon, T. Y.; Oh, Y. K.; Kim, S. H., Microfluidic Production of Semipermeable Microcapsules by Polymerization-Induced Phase Separation. *Langmuir* **2015,** *31* (22), 6027-34.
75. Martinez, C. J.; Kim, J. W.; Ye, C.; Ortiz, I.; Rowat, A. C.; Marquez, M.; Weitz, D., A microfluidic approach to encapsulate living cells in uniform alginate hydrogel microparticles. *Macromol. Biosci.* **2012,** *12* (7), 946-51.
76. Garabedian, B. M.; Meadows, C. W.; Mingardon, F.; Guenther, J. M.; de Rond, T.; Abourjeily, R.; Lee, T. S., An automated workflow to screen alkene reductases using high-throughput thin layer chromatography. *Biotechnol. Biofuels* **2020,** *13* (1), 184.
77. Pereira, S. A. P.; Dyson, P. J.; Saraiva, M. L. M. F. S., Miniaturized technologies for high-throughput drug screening enzymatic assays and diagnostics – A review. *TrAC - Trends Anal. Chem.* **2020,** *126*, 115862.

78. Aharoni, A.; Amitai, G.; Bernath, K.; Magdassi, S.; Tawfik, D. S., High-throughput screening of enzyme libraries: thiolactonases evolved by fluorescence-activated sorting of single cells in emulsion compartments. *Chem. Biol.* **2005,** *12* (12), 1281-9.
79. Garti, N., Progress in Stabilization and Transport Phenomena of Double Emulsions in Food Applications. *LWT - Food Sci. Technol.* **1997,** *30* (3), 222-235.
80. Garti, N., Double emulsions — scope, limitations and new achievements. *Colloids Surf. A Physicochem. Eng. Asp.* **1997,** *123-124*, 233-246.
81. Brower, K. K.; Carswell-Crumpton, C.; Klemm, S.; Cruz, B.; Kim, G.; Calhoun, S. G. K.; Nichols, L.; Fordyce, P. M., Double emulsion flow cytometry with high-throughput single droplet isolation and nucleic acid recovery. *Lab Chip* **2020,** *20* (12), 2062-2074.
82. Beldarrain-Iznaga, T.; Villalobos-Carvajal, R.; Sevillano-Armesto, E.; Leiva-Vega, J., Functional properties of Lactobacillus casei C24 improved by microencapsulation using multilayer double emulsion. *Int. Food Res. J.* **2021,** *141*, 110136.
83. Wang, L.; Song, M.; Zhao, Z.; Chen, X.; Cai, J.; Cao, Y.; Xiao, J., Lactobacillus acidophilus loaded pickering double emulsion with enhanced viability and colon-adhesion efficiency. *LWT* **2020,** *121*, 108928.
84. Shima, M.; Morita, Y.; Yamashita, M.; Adachi, S., Protection of Lactobacillus acidophilus from the low pH of a model gastric juice by incorporation in a W/O/W emulsion. *Food Hydrocoll.* **2006,** *20* (8), 1164-1169.
85. El Kadri, H.; Lalou, S.; Mantzouridou, F.; Gkatzionis, K., Utilisation of water-in-oil-water (W1/O/W2) double emulsion in a set-type yogurt model for the delivery of probiotic Lactobacillus paracasei. *Int. Food Res. J.* **2018,** *107*, 325-336.
86. El Kadri, H.; Overton, T.; Bakalis, S.; Gkatzionis, K., Understanding and controlling the release mechanism of Escherichia coli in double W1/O/W2emulsion globules in the presence of NaCl in the W2phase. *RSC Adv.* **2015,** *5* (127), 105098-105110.
87. Jia, Y.; Ren, Y.; Hou, L.; Liu, W.; Jiang, T.; Deng, X.; Tao, Y.; Jiang, H., Electrically controlled rapid release of actives encapsulated in double-emulsion droplets. *Lab Chip* **2018,** *18* (7), 1121-1129.
88. Sukovich, D. J.; Kim, S. C.; Ahmed, N.; Abate, A. R., Bulk double emulsification for flow cytometric analysis of microfluidic droplets. *Analyst* **2017,** *142* (24), 4618-4622.
89. Shima, M.; Kobayashi, Y.; Fujii, T.; Tanaka, M.; Kimura, Y.; Adachi, S.; Matsuno, R., Preparation of fine W/O/W emulsion through membrane filtration of coarse W/O/W emulsion and disappearance of the inclusion of outer phase solution. *Food Hydrocoll.* **2004,** *18* (1), 61-70.
90. Eslami, P.; Davarpanah, L.; Vahabzadeh, F., Encapsulating role of β-cyclodextrin in formation of pickering water-in-oil-in-water (W1/O/W2) double emulsions containing Lactobacillus dellbrueckii. *Food Hydrocoll.* **2017,** *64*, 133-148.
91. Mastrobattista, E.; Taly, V.; Chanudet, E.; Treacy, P.; Kelly, B. T.; Griffiths, A. D., High-throughput screening of enzyme libraries: in vitro evolution of a beta-galactosidase by fluorescence-activated sorting of double emulsions. *Chem. Biol.* **2005,** *12* (12), 1291-300.
92. Korfer, G.; Pitzler, C.; Vojcic, L.; Martinez, R.; Schwaneberg, U., In vitro flow cytometry-based screening platform for cellulase engineering. *Sci. Rep.* **2016,** *6*, 26128.
93. Nakashima, T.; Shimizu, M.; Kukizaki, M., Particle control of emulsion by membrane emulsification and its applications. *Adv. Drug Delivery Rev.* **2000,** *45* (1), 47-56.
94. Sugiura, S.; Nakajima, M.; Iwamoto, S.; Seki, M., Interfacial Tension Driven Monodispersed Droplet Formation from Microfabricated Channel Array. *Langmuir* **2001,** *17* (18), 5562-5566.
95. Ma, G.-H.; Sone, H.; Omi, S., Preparation of Uniform-Sized Polystyrene−Polyacrylamide Composite Microspheres from a W/O/W Emulsion by Membrane Emulsification Technique and Subsequent Suspension Polymerization. *Macromolecules* **2004,** *37* (8), 2954-2964.
96. Liu, R.; Ma, G.; Meng, F.-T.; Su, Z.-G., Preparation of uniform-sized PLA microcapsules by combining Shirasu Porous Glass membrane emulsification technique and multiple emulsion-solvent evaporation method. *J. Control. Release* **2005,** *103* (1), 31-43.
97. Matos, M.; Gutiérrez, G.; Iglesias, O.; Coca, J.; Pazos, C., Enhancing encapsulation efficiency of food-grade double emulsions containing resveratrol or vitamin B12 by membrane emulsification. *J. Food Eng.* **2015,** *166*, 212-220.
98. Wang, W.; Zhang, M.-J.; Chu, L.-Y., Microfluidic approach for encapsulation via double emulsions. *Curr. Opin. Pharmacol.* **2014,** *18*, 35-41.
99. Loscertales, I. G.; Barrero, A.; Guerrero, I.; Cortijo, R.; Marquez, M.; Gañán-Calvo, A. M., Micro/Nano Encapsulation via Electrified Coaxial Liquid Jets. *Science* **2002,** *295* (5560), 1695.
100. Jaworek, A., Electrospray droplet sources for thin film deposition. *J. Mater. Sci.* **2007,** *42* (1), 266-297.
101. Marín, Á. G.; Loscertales, I. G.; Márquez, M.; Barrero, A., Simple and Double Emulsions via Coaxial Jet Electrosprays. *Phys. Rev. Lett.* **2007,** *98* (1), 014502.
102. Kim, S. C.; Sukovich, D. J.; Abate, A. R., Patterning microfluidic device wettability with spatially-controlled plasma oxidation. *Lab Chip* **2015,** *15* (15), 3163-9.

103. Bashir, S.; Bashir, M.; Solvas, X.; Rees, J.; Zimmerman, W., Hydrophilic Surface Modification of PDMS Microchannel for O/W and W/O/W Emulsions. *Micromachines* **2015,** *6* (10), 1445-1458.
104. Nisisako, T.; Torii, T.; Higuchi, T., Droplet formation in a microchannel network. *Lab Chip* **2002,** *2* (1), 24-26.
105. Bai, Z.; Wang, B.; Chen, H.; Wang, M., Spatial wettability patterning of glass microchips for water-in-oil-in-water (W/O/W) double emulsion preparation. *Sens. Actuators B Chem.* **2015,** *215*, 330-336.
106. Scott, S. M.; Ali, Z., Fabrication Methods for Microfluidic Devices: An Overview. *Micromachines* **2021,** *12* (3).
107. Wang, T.; Chen, J.; Zhou, T.; Song, L., Fabricating Microstructures on Glass for Microfluidic Chips by Glass Molding Process. *Micromachines* **2018,** *9* (6).
108. Nisisako, T.; Okushima, S.; Torii, T., Controlled formulation of monodisperse double emulsions in a multiple-phase microfluidic system. *Soft Matter* **2005,** *1* (1), 23-27.
109. Zhang, Y.; Ho, Y. P.; Chiu, Y. L.; Chan, H. F.; Chlebina, B.; Schuhmann, T.; You, L.; Leong, K. W., A programmable microenvironment for cellular studies via microfluidics-generated double emulsions. *Biomaterials* **2013,** *34* (19), 4564-72.
110. Zinchenko, A.; Devenish, S. R.; Kintses, B.; Colin, P. Y.; Fischlechner, M.; Hollfelder, F., One in a million: flow cytometric sorting of single cell-lysate assays in monodisperse picolitre double emulsion droplets for directed evolution. *Anal. Chem.* **2014,** *86* (5), 2526-33.
111. Terekhov, S. S.; Smirnov, I. V.; Stepanova, A. V.; Bobik, T. V.; Mokrushina, Y. A.; Ponomarenko, N. A.; Belogurov, A. A., Jr.; Rubtsova, M. P.; Kartseva, O. V.; Gomzikova, M. O.; Moskovtsev, A. A.; Bukatin, A. S.; Dubina, M. V.; Kostryukova, E. S.; Babenko, V. V.; Vakhitova, M. T.; Manolov, A. I.; Malakhova, M. V.; Kornienko, M. A.; Tyakht, A. V.; Vanyushkina, A. A.; Ilina, E. N.; Masson, P.; Gabibov, A. G.; Altman, S., Microfluidic droplet platform for ultrahigh-throughput single-cell screening of biodiversity. *Proc. Natl. Acad. Sci. U. S. A.* **2017,** *114* (10), 2550-2555.
112. Terekhov, S. S.; Smirnov, I. V.; Malakhova, M. V.; Samoilov, A. E.; Manolov, A. I.; Nazarov, A. S.; Danilov, D. V.; Dubiley, S. A.; Osterman, I. A.; Rubtsova, M. P.; Kostryukova, E. S.; Ziganshin, R. H.; Kornienko, M. A.; Vanyushkina, A. A.; Bukato, O. N.; Ilina, E. N.; Vlasov, V. V.; Severinov, K. V.; Gabibov, A. G.; Altman, S., Ultrahigh-throughput functional profiling of microbiota communities. *Proc. Natl. Acad. Sci. U. S. A.* **2018,** *115* (38), 9551-9556.
113. Okushima, S.; Nisisako, T.; Torii, T.; Higuchi, T., Controlled Production of Monodisperse Double Emulsions by Two-Step Droplet Breakup in Microfluidic Devices. *Langmuir* **2004,** *20* (23), 9905-9908.
114. Wu, N.; Oakeshott, J. G.; Easton, C. J.; Peat, T. S.; Surjadi, R.; Zhu, Y., A double-emulsion microfluidic platform forin vitrogreen fluorescent protein expression. *J. Micromech. Microeng.* **2011,** *21* (5), 054032.
115. Wagner, J. M.; Liu, L.; Yuan, S. F.; Venkataraman, M. V.; Abate, A. R.; Alper, H. S., A comparative analysis of single cell and droplet-based FACS for improving production phenotypes: Riboflavin overproduction in Yarrowia lipolytica. *Metab. Eng.* **2018,** *47*, 346-356.
116. Ma, F.; Guo, T.; Zhang, Y.; Bai, X.; Li, C.; Lu, Z.; Deng, X.; Li, D.; Kurabayashi, K.; Yang, G. Y., An ultrahigh-throughput screening platform based on flow cytometric droplet sorting for mining novel enzymes from metagenomic libraries. *Environ. Microbiol.* **2021,** *23* (2), 996-1008.
117. Chan, H. F.; Zhang, Y.; Ho, Y. P.; Chiu, Y. L.; Jung, Y.; Leong, K. W., Rapid formation of multicellular spheroids in double-emulsion droplets with controllable microenvironment. *Sci. Rep.* **2013,** *3*, 3462.
118. Chan, H. F.; Zhang, Y.; Leong, K. W., Efficient One-Step Production of Microencapsulated Hepatocyte Spheroids with Enhanced Functions. *Small* **2016,** *12* (20), 2720-30.
119. Chan, H. F.; Ma, S.; Tian, J.; Leong, K. W., High-throughput screening of microchip-synthesized genes in programmable double-emulsion droplets. *Nanoscale* **2017,** *9* (10), 3485-3495.
120. Larsen, A. C.; Dunn, M. R.; Hatch, A.; Sau, S. P.; Youngbull, C.; Chaput, J. C., A general strategy for expanding polymerase function by droplet microfluidics. *Nat. Commun.* **2016,** *7*, 11235.
121. Abate, A. R.; Thiele, J.; Weinhart, M.; Weitz, D. A., Patterning microfluidic device wettability using flow confinement. *Lab Chip* **2010,** *10* (14), 1774-6.
122. Abate, A. R.; Lee, D.; Do, T.; Holtze, C.; Weitz, D. A., Glass coating for PDMS microfluidic channels by sol–gel methods. *Lab Chip* **2008,** *8* (4), 516-518.
123. Studer, A.; Hadida, S.; Ferritto, R.; Kim, S.-Y.; Jeger, P.; Wipf, P.; Curran, D. P., Fluorous Synthesis: A Fluorous-Phase Strategy for Improving Separation Efficiency in Organic Synthesis. *Science* **1997,** *275* (5301), 823.
124. Utada, A. S.; Lorenceau, E.; Link, D. R.; Kaplan, P. D.; Stone, H. A.; Weitz, D. A., Monodisperse Double Emulsions Generated from a Microcapillary Device. *Science* **2005,** *308* (5721), 537.
125. Oh, H.-J.; Kim, S.-H.; Baek, J.-Y.; Seong, G.-H.; Lee, S.-H., Hydrodynamic micro-encapsulation of aqueous fluids and cells via 'on the fly' photopolymerization. *J. Micromech. Microeng.* **2006,** *16* (2), 285-291.

126. Chu, L.-Y.; Utada, A. S.; Shah, R. K.; Kim, J.-W.; Weitz, D. A., Controllable Monodisperse Multiple Emulsions. *Angew. Chem. Int. Ed.* **2007,** *46* (47), 8970-8974.
127. Kim, S.-H.; Kim, J. W.; Cho, J.-C.; Weitz, D. A., Double-emulsion drops with ultra-thin shells for capsule templates. *Lab Chip* **2011,** *11* (18), 3162-3166.
128. Choi, C. H.; Wang, H.; Lee, H.; Kim, J. H.; Zhang, L.; Mao, A.; Mooney, D. J.; Weitz, D. A., One-step generation of cell-laden microgels using double emulsion drops with a sacrificial ultra-thin oil shell. *Lab Chip* **2016,** *16* (9), 1549-55.
129. Ekanem, E. E.; Zhang, Z.; Vladisavljevic, G. T., Facile microfluidic production of composite polymer core-shell microcapsules and crescent-shaped microparticles. *J. Colloid Interface Sci.* **2017,** *498*, 387-394.
130. Nabavi, S. A.; Vladisavljević, G. T.; Gu, S.; Ekanem, E. E., Double emulsion production in glass capillary microfluidic device: Parametric investigation of droplet generation behaviour. *Chem. Eng. Sci.* **2015,** *130*, 183-196.
131. Nabavi, S. A.; Vladisavljević, G. T.; Gu, S.; Manović, V., Semipermeable Elastic Microcapsules for Gas Capture and Sensing. *Langmuir* **2016,** *32* (38), 9826-9835.
132. Barlow, J.; Gozzi, K.; Kelley, C. P.; Geilich, B. M.; Webster, T. J.; Chai, Y.; Sridhar, S.; van de Ven, A. L., High throughput microencapsulation of Bacillus subtilis in semi-permeable biodegradable polymersomes for selenium remediation. *Appl. Microbiol. Biotechnol.* **2017,** *101* (1), 455-464.
133. Chang, C. B.; Wilking, J. N.; Kim, S.-H.; Shum, H. C.; Weitz, D. A., Monodisperse Emulsion Drop Microenvironments for Bacterial Biofilm Growth. *Small* **2015,** *11* (32), 3954-3961.
134. Zhang, W.; Abbaspourrad, A.; Chen, D.; Campbell, E.; Zhao, H.; Li, Y.; Li, Q.; Weitz, D. A., Osmotic Pressure Triggered Rapid Release of Encapsulated Enzymes with Enhanced Activity. *Adv. Funct. Mater.* **2017,** *27* (29), 1700975.
135. Lee, T. Y.; Ku, M.; Kim, B.; Lee, S.; Yang, J.; Kim, S.-H., Microfluidic Production of Biodegradable Microcapsules for Sustained Release of Hydrophilic Actives. *Small* **2017,** *13* (29), 1700646.
136. Deng, N.-N.; Yelleswarapu, M.; Huck, W. T. S., Monodisperse Uni- and Multicompartment Liposomes. *J. Am. Chem. Soc.* **2016,** *138* (24), 7584-7591.
137. Datta, S. S.; Abbaspourrad, A.; Amstad, E.; Fan, J.; Kim, S.-H.; Romanowsky, M.; Shum, H. C.; Sun, B.; Utada, A. S.; Windbergs, M.; Zhou, S.; Weitz, D. A., 25th Anniversary Article: Double Emulsion Templated Solid Microcapsules: Mechanics And Controlled Release. *Adv. Mater.* **2014,** *26* (14), 2205-2218.
138. Shah, R. K.; Kim, J.-W.; Agresti, J. J.; Weitz, D. A.; Chu, L.-Y., Fabrication of monodisperse thermosensitive microgels and gel capsules in microfluidic devices. *Soft Matter* **2008,** *4* (12), 2303-2309.
139. Deng, N.-N.; Yelleswarapu, M.; Zheng, L.; Huck, W. T. S., Microfluidic Assembly of Monodisperse Vesosomes as Artificial Cell Models. *J. Am. Chem. Soc.* **2017,** *139* (2), 587-590.
140. Xie, X.; Zhang, W.; Abbaspourrad, A.; Ahn, J.; Bader, A.; Bose, S.; Vegas, A.; Lin, J.; Tao, J.; Hang, T.; Lee, H.; Iverson, N.; Bisker, G.; Li, L.; Strano, M. S.; Weitz, D. A.; Anderson, D. G., Microfluidic Fabrication of Colloidal Nanomaterials-Encapsulated Microcapsules for Biomolecular Sensing. *Nano Lett.* **2017,** *17* (3), 2015-2020.
141. Liu, D.; Zhang, H.; Herranz-Blanco, B.; Mäkilä, E.; Lehto, V.-P.; Salonen, J.; Hirvonen, J.; Santos, H. A., Microfluidic Assembly of Monodisperse Multistage pH-Responsive Polymer/Porous Silicon Composites for Precisely Controlled Multi-Drug Delivery. *Small* **2014,** *10* (10), 2029-2038.
142. Choi, C.-H.; Lee, H.; Abbaspourrad, A.; Kim, J. H.; Fan, J.; Caggioni, M.; Wesner, C.; Zhu, T.; Weitz, D. A., Triple Emulsion Drops with An Ultrathin Water Layer: High Encapsulation Efficiency and Enhanced Cargo Retention in Microcapsules. *Adv. Mater.* **2016,** *28* (17), 3340-3344.
143. Zhao, Y.; Xie, Z.; Gu, H.; Jin, L.; Zhao, X.; Wang, B.; Gu, Z., Multifunctional photonic crystal barcodes from microfluidics. *NPG Asia Mater.* **2012,** *4* (9), e25-e25.
144. Amato, D. V.; Lee, H.; Werner, J. G.; Weitz, D. A.; Patton, D. L., Functional Microcapsules via Thiol–Ene Photopolymerization in Droplet-Based Microfluidics. *ACS Appl. Mater. Interfaces* **2017,** *9* (4), 3288-3293.
145. Zhao, Y.; Shum, H. C.; Adams, L. L. A.; Sun, B.; Holtze, C.; Gu, Z.; Weitz, D. A., Enhanced Encapsulation of Actives in Self-Sealing Microcapsules by Precipitation in Capsule Shells. *Langmuir* **2011,** *27* (23), 13988-13991.
146. Sun, B. J.; Shum, H. C.; Holtze, C.; Weitz, D. A., Microfluidic Melt Emulsification for Encapsulation and Release of Actives. *ACS Appl. Mater. Interfaces* **2010,** *2* (12), 3411-3416.
147. Ren, P.-W.; Ju, X.-J.; Xie, R.; Chu, L.-Y., Monodisperse alginate microcapsules with oil core generated from a microfluidic device. *J. Colloid Interface Sci.* **2010,** *343* (1), 392-395.
148. Liu, L.; Wu, F.; Ju, X. J.; Xie, R.; Wang, W.; Niu, C. H.; Chu, L. Y., Preparation of monodisperse calcium alginate microcapsules via internal gelation in microfluidic-generated double emulsions. *J. Colloid Interface Sci.* **2013,** *404*, 85-90.
149. Kim, S.-H.; Shum, H. C.; Kim, J. W.; Cho, J.-C.; Weitz, D. A., Multiple Polymersomes for Programmed Release of Multiple Components. *J. Am. Chem. Soc.* **2011,** *133* (38), 15165-15171.

150. Li, S.; Gong, X.; Mc Nally, C. S.; Zeng, M.; Gaule, T.; Anduix-Canto, C.; Kulak, A. N.; Bawazer, L. A.; McPherson, M. J.; Meldrum, F. C., Rapid preparation of highly reliable PDMS double emulsion microfluidic devices. *RSC Adv.* **2016,** *6* (31), 25927-25933.
151. Cole, R. H.; Tran, T. M.; Abate, A. R., Double Emulsion Generation Using a Polydimethylsiloxane (PDMS) Co-axial Flow Focus Device. *J. Vis. Exp.* **2015,** (106), e53516.
152. Takeuchi, S.; Garstecki, P.; Weibel, D. B.; Whitesides, G. M., An Axisymmetric Flow-Focusing Microfluidic Device. *Adv. Mater.* **2005,** *17* (8), 1067-1072.
153. Yobas, L.; Martens, S.; Ong, W.-L.; Ranganathan, N., High-performance flow-focusing geometry for spontaneous generation of monodispersed droplets. *Lab Chip* **2006,** *6* (8), 1073-1079.
154. Huang, S.-H.; Tan, W.-H.; Tseng, F.-G.; Takeuchi, S., A monolithically three-dimensional flow-focusing device for formation of single/double emulsions in closed/open microfluidic systems. *J. Micromech. Microeng.* **2006,** *16* (11), 2336-2344.
155. Chang, F.-C.; Su, Y.-C., Controlled double emulsification utilizing 3D PDMS microchannels. *J. Micromech. Microeng.* **2008,** *18* (6).
156. Sim, S. P. C.; Kang, T. G.; Yobas, L.; Holtze, C.; Weitz, D. A., The shape of a step structure as a design aspect to control droplet generation in microfluidics. *J. Micromech. Microeng.* **2010,** *20* (3), 035010.
157. Davies, R. T.; Kim, D.; Park, J., Formation of liposomes using a 3D flow focusing microfluidic device with spatially patterned wettability by corona discharge. *J. Micromech. Microeng.* **2012,** *22* (5).
158. Romanowsky, M. B.; Abate, A. R.; Rotem, A.; Holtze, C.; Weitz, D. A., High throughput production of single core double emulsions in a parallelized microfluidic device. *Lab Chip* **2012,** *12* (4), 802-807.
159. Rotem, A.; Abate, A. R.; Utada, A. S.; Van Steijn, V.; Weitz, D. A., Drop formation in non-planar microfluidic devices. *Lab Chip* **2012,** *12* (21), 4263-4268.
160. Lim, S. W.; Abate, A. R., Ultrahigh-throughput sorting of microfluidic drops with flow cytometry. *Lab Chip* **2013,** *13* (23), 4563-72.
161. Tran, T. M.; Cater, S.; Abate, A. R., Coaxial flow focusing in poly(dimethylsiloxane) microfluidic devices. *Biomicrofluidics* **2014,** *8* (1), 016502.
162. Castro-Hernández, E.; Kok, M. P.; Versluis, M.; Fernandez Rivas, D., Study of the geometry in a 3D flow-focusing device. *Microfluid. Nanofluidics* **2016,** *20* (2), 40.
163. Saeki, D.; Sugiura, S.; Kanamori, T.; Sato, S.; Ichikawa, S., Microfluidic preparation of water-in-oil-in-water emulsions with an ultra-thin oil phase layer. *Lab Chip* **2010,** *10* (3), 357-362.
164. Abate, A. R.; Kutsovsky, M.; Seiffert, S.; Windbergs, M.; Pinto, L. F. V.; Rotem, A.; Utada, A. S.; Weitz, D. A., Synthesis of Monodisperse Microparticles from Non-Newtonian Polymer Solutions with Microfluidic Devices. *Adv. Mater.* **2011,** *23* (15), 1757-1760.
165. Hillborg, H.; Ankner, J. F.; Gedde, U. W.; Smith, G. D.; Yasuda, H. K.; Wikström, K., Crosslinked polydimethylsiloxane exposed to oxygen plasma studied by neutron reflectometry and other surface specific techniques. *Polymer* **2000,** *41* (18), 6851-6863.
166. Bodas, D.; Khan-Malek, C., Formation of more stable hydrophilic surfaces of PDMS by plasma and chemical treatments. *Microelectron. Eng.* **2006,** *83* (4-9), 1277-1279.
167. Duffy, D. C.; McDonald, J. C.; Schueller, O. J. A.; Whitesides, G. M., Rapid Prototyping of Microfluidic Systems in Poly(dimethylsiloxane). *Anal. Chem.* **1998,** *70* (23), 4974-4984.
168. Barbier, V.; Tatoulian, M.; Li, H.; Arefi-Khonsari, F.; Ajdari, A.; Tabeling, P., Stable Modification of PDMS Surface Properties by Plasma Polymerization: Application to the Formation of Double Emulsions in Microfluidic Systems. *Langmuir* **2006,** *22* (12), 5230-5232.
169. Seo, M.; Paquet, C.; Nie, Z.; Xu, S.; Kumacheva, E., Microfluidic consecutive flow-focusing droplet generators. *Soft Matter* **2007,** *3* (8), 986-992.
170. Abate, A. R.; Krummel, A. T.; Lee, D.; Marquez, M.; Holtze, C.; Weitz, D. A., Photoreactive coating for high-contrast spatial patterning of microfluidic device wettability. *Lab Chip* **2008,** *8* (12), 2157-2160.
171. Abate, A. R.; Weitz, D. A., High-order multiple emulsions formed in poly(dimethylsiloxane) microfluidics. *Small* **2009,** *5* (18), 2030-2.
172. Bauer, W. A.; Fischlechner, M.; Abell, C.; Huck, W. T., Hydrophilic PDMS microchannels for high-throughput formation of oil-in-water microdroplets and water-in-oil-in-water double emulsions. *Lab Chip* **2010,** *10* (14), 1814-9.
173. Jankowski, P.; Ogończyk, D.; Derzsi, L.; Lisowski, W.; Garstecki, P., Hydrophilic polycarbonate chips for generation of oil-in-water (O/W) and water-in-oil-in-water (W/O/W) emulsions. *Microfluid. Nanofluidics* **2012,** *14* (5), 767-774.
174. Yan, J.; Bauer, W.-A.; Fischlechner, M.; Hollfelder, F.; Kaminski, C.; Huck, W., Monodisperse Water-in-Oil-in-Water (W/O/W) Double Emulsion Droplets as Uniform Compartments for High-Throughput Analysis via Flow Cytometry. *Micromachines* **2013,** *4* (4), 402-413.
175. Zhang, L.; Feng, Q.; Wang, J.; Sun, J.; Shi, X.; Jiang, X., Microfluidic synthesis of rigid nanovesicles for hydrophilic reagents delivery. *Angew. Chem. Int. Ed. Engl.* **2015,** *54* (13), 3952-6.

176. Ma, X.; Jepsen, M. L.; Ivarsen, A. K. R.; Knudsen, B. R.; Ho, Y.-P., Molecular and functional assessment of multicellular cancer spheroids produced in double emulsions enabled by efficient airway resistance based selective surface treatment. *J. Micromech. Microeng.* **2017,** *27* (9), 095014.
177. Liao, Q.-Q.; Zhao, S.-K.; Cai, B.; He, R.-X.; Rao, L.; Wu, Y.; Guo, S.-S.; Liu, Q.-Y.; Liu, W.; Zhao, X.-Z., Biocompatible fabrication of cell-laden calcium alginate microbeads using microfluidic double flow-focusing device. *Sens. Actuators, A* **2018,** *279*, 313-320.
178. Samandari, M.; Alipanah, F.; Haghjooy Javanmard, S.; Sanati-Nezhad, A., One-step wettability patterning of PDMS microchannels for generation of monodisperse alginate microbeads by in Situ external gelation in double emulsion microdroplets. *Sens. Actuators B Chem.* **2019,** *291*, 418-425.
179. Zhu, X.-D.; Shi, X.; Wang, S.-W.; Chu, J.; Zhu, W.-H.; Ye, B.-C.; Zuo, P.; Wang, Y.-H., High-throughput screening of high lactic acid-producing Bacillus coagulans by droplet microfluidic based flow cytometry with fluorescence activated cell sorting. *RSC Adv.* **2019,** *9* (8), 4507-4513.
180. Qu, F.; Zhao, S.; Cheng, G.; Rahman, H.; Xiao, Q.; Chan, R. W. Y.; Ho, Y.-P., Double emulsion-pretreated microwell culture for the in vitro production of multicellular spheroids and their in situ analysis. *Microsyst. Nanoeng.* **2021,** *7* (1), 38.
181. Trantidou, T.; Elani, Y.; Parsons, E.; Ces, O., Hydrophilic surface modification of PDMS for droplet microfluidics using a simple, quick, and robust method via PVA deposition. *Microsyst. Nanoeng.* **2017,** *3* (1), 16091.
182. Hutter, T.; Bauer, W.-A. C.; Elliott, S. R.; Huck, W. T. S., Formation of Spherical and Non-Spherical Eutectic Gallium-Indium Liquid-Metal Microdroplets in Microfluidic Channels at Room Temperature. *Adv. Funct. Mater.* **2012,** *22* (12), 2624-2631.
183. Hillborg, H.; Gedde, U. W., Hydrophobicity recovery of polydimethylsiloxane after exposure to corona discharges. *Polymer* **1998,** *39* (10), 1991-1998.
184. Efimenko, K.; Wallace, W. E.; Genzer, J., Surface Modification of Sylgard-184 Poly(dimethyl siloxane) Networks by Ultraviolet and Ultraviolet/Ozone Treatment. *J. Colloid Interface Sci.* **2002,** *254* (2), 306-315.
185. Tan, S. H.; Nguyen, N. T.; Chua, Y. C.; Kang, T. G., Oxygen plasma treatment for reducing hydrophobicity of a sealed polydimethylsiloxane microchannel. *Biomicrofluidics* **2010,** *4* (3), 32204.
186. Wong, I.; Ho, C.-M., Surface molecular property modifications for poly(dimethylsiloxane) (PDMS) based microfluidic devices. *Microfluid. Nanofluidics* **2009,** *7* (3), 291.
187. Romanowsky, M. B.; Heymann, M.; Abate, A. R.; Krummel, A. T.; Fraden, S.; Weitz, D. A., Functional patterning of PDMS microfluidic devices using integrated chemo-masks. *Lab Chip* **2010,** *10* (12), 1521-1524.
188. Thiele, J.; Abate, A. R.; Shum, H. C.; Bachtler, S.; Förster, S.; Weitz, D. A., Fabrication of Polymersomes using Double-Emulsion Templates in Glass-Coated Stamped Microfluidic Devices. *Small* **2010,** *6* (16), 1723-1727.
189. Mohd Isa, N. S.; El Kadri, H.; Vigolo, D.; Gkatzionis, K., Optimisation of bacterial release from a stable microfluidic-generated water-in-oil-in-water emulsion. *RSC Adv.* **2021,** *11* (13), 7738-7749.
190. Wu, W.; Zhou, S.; Hu, J.; Wang, G.; Ding, X.; Gou, T.; Sun, J.; Zhang, T.; Mu, Y., A Thermosetting Oil for Droplet-Based Real-Time Monitoring of Digital PCR and Cell Culture. *Adv. Funct. Mater.* **2018,** *28* (39), 1803559.
191. Brower, K. K.; Carswell-Crumpton, C.; Klemm, S.; Cruz, B.; Kim, G.; Calhoun, S. G. K.; Nichols, L.; Fordyce, P. M., Double emulsion flow cytometry with high-throughput single droplet isolation and nucleic acid recovery. *Lab Chip* **2020,** *20* (12), 2062-2074.
192. Brower, K. K.; Khariton, M.; Suzuki, P. H.; Still, C., 2nd; Kim, G.; Calhoun, S. G. K.; Qi, L. S.; Wang, B.; Fordyce, P. M., Double Emulsion Picoreactors for High-Throughput Single-Cell Encapsulation and Phenotyping via FACS. *Anal. Chem.* **2020,** *92* (19), 13262-13270.
193. Parhizkar, M.; Stride, E.; Edirisinghe, M., Preparation of monodisperse microbubbles using an integrated embedded capillary T-junction with electrohydrodynamic focusing. *Lab Chip* **2014,** *14* (14), 2437-2446.
194. Lin, Y.; Lee, C.; Lee, G., Droplet Formation Utilizing Controllable Moving-Wall Structures for Double-Emulsion Applications. *J. Microelectromech. Syst.* **2008,** *17* (3), 573-581.
195. Abate, A. R.; Weitz, D. A., Air-bubble-triggered drop formation in microfluidics. *Lab Chip* **2011,** *11* (10), 1713-1716.
196. Zhao, C.-X.; Middelberg, A. P. J., Microfluidic Mass-Transfer Control for the Simple Formation of Complex Multiple Emulsions. *Angew. Chem. Int. Ed.* **2009,** *48* (39), 7208-7211.
197. Choi, C.-H.; Weitz, D. A.; Lee, C.-S., One Step Formation of Controllable Complex Emulsions: From Functional Particles to Simultaneous Encapsulation of Hydrophilic and Hydrophobic Agents into Desired Position. *Adv. Mater.* **2013,** *25* (18), 2536-2541.
198. Deng, N.-N.; Wang, W.; Ju, X.-J.; Xie, R.; Weitz, D. A.; Chu, L.-Y., Wetting-induced formation of controllable monodisperse multiple emulsions in microfluidics. *Lab Chip* **2013,** *13* (20), 4047-4052.

199. Yuan, Q.; Williams, R. A., Precision emulsification for droplet and capsule production. *Adv. Powder Technol.* **2014,** *25* (1), 122-135.
200. Courtois, F.; Olguin, L. F.; Whyte, G.; Theberge, A. B.; Huck, W. T. S.; Hollfelder, F.; Abell, C., Controlling the Retention of Small Molecules in Emulsion Microdroplets for Use in Cell-Based Assays. *Anal. Chem.* **2009,** *81* (8), 3008-3016.
201. Cheng, J.; Chen, J.-F.; Zhao, M.; Luo, Q.; Wen, L.-X.; Papadopoulos, K. D., Transport of ions through the oil phase of W1/O/W2 double emulsions. *J. Colloid Interface Sci.* **2007,** *305* (1), 175-182.
202. van der Graaf, S.; Schroën, C. G. P. H.; Boom, R. M., Preparation of double emulsions by membrane emulsification—a review. *J. Membr. Sci.* **2005,** *251* (1), 7-15.
203. Sukovich, D. J.; Lance, S. T.; Abate, A. R., Sequence specific sorting of DNA molecules with FACS using 3dPCR. *Sci. Rep.* **2017,** *7*, 39385.
204. Clausell-Tormos, J.; Lieber, D.; Baret, J.-C.; El-Harrak, A.; Miller, O. J.; Frenz, L.; Blouwolff, J.; Humphry, K. J.; Köster, S.; Duan, H.; Holtze, C.; Weitz, D. A.; Griffiths, A. D.; Merten, C. A., Droplet-Based Microfluidic Platforms for the Encapsulation and Screening of Mammalian Cells and Multicellular Organisms. *Chem. Biol.* **2008,** *15* (5), 427-437.
205. Hsu, R. H.; Clark, R. L.; Tan, J. W.; Ahn, J. C.; Gupta, S.; Romero, P. A.; Venturelli, O. S., Microbial Interaction Network Inference in Microfluidic Droplets. *Cell System* **2019,** *9* (3), 229-242 e4.
206. Devanthi, P. V. P.; El Kadri, H.; Bowden, A.; Spyropoulos, F.; Gkatzionis, K., Segregation of Tetragenococcus halophilus and Zygosaccharomyces rouxii using W1/O/W2 double emulsion for use in mixed culture fermentation. *Int. Food Res. J.* **2018,** *105*, 333-343.
207. Devanthi, P. V. P.; Linforth, R.; El Kadri, H.; Gkatzionis, K., Water-in-oil-in-water double emulsion for the delivery of starter cultures in reduced-salt moromi fermentation of soy sauce. *Food Chem.* **2018,** *257*, 243-251.
208. Šipailienė, A.; Šlimaitė, G.; Jeznienė, S.; Venskutonis, P. R.; Leskauskaitė, D., W/O/W double emulsion-loaded alginate capsules containing Lactobacillus plantarum and lipophilic sea buckthorn (Hippophae rhamnoides L.) pomace extract in different phases. *Food Sci. Technol. Int.* **2021**, 10820132211018036.
209. Augustin, M. A.; Hemar, Y., Nano- and micro-structured assemblies for encapsulation of food ingredients. *Chem. Soc. Rev.* **2009,** *38* (4), 902-912.
210. van der Ark, K. C. H.; Nugroho, A. D. W.; Berton-Carabin, C.; Wang, C.; Belzer, C.; de Vos, W. M.; Schroen, K., Encapsulation of the therapeutic microbe Akkermansia muciniphila in a double emulsion enhances survival in simulated gastric conditions. *Int. Food Res. J.* **2017,** *102*, 372-379.
211. Pimentel-González, D. J.; Campos-Montiel, R. G.; Lobato-Calleros, C.; Pedroza-Islas, R.; Vernon-Carter, E. J., Encapsulation of Lactobacillus rhamnosus in double emulsions formulated with sweet whey as emulsifier and survival in simulated gastrointestinal conditions. *Int. Food Res. J.* **2009,** *42* (2), 292-297.
212. Beldarrain-Iznaga, T.; Villalobos-Carvajal, R.; Leiva-Vega, J.; Sevillano Armesto, E., Influence of multilayer microencapsulation on the viability of Lactobacillus casei using a combined double emulsion and ionic gelation approach. *Food Bioprod. Process.* **2020,** *124*, 57-71.
213. Frakolaki, G.; Katsouli, M.; Giannou, V.; Tzia, C., Novel encapsulation approach for Bifidobacterium subsp. lactis (BB-12) viability enhancement through its incorporation into a double emulsion prior to the extrusion process. *LWT* **2020,** *130*, 109671.
214. Ostafe, R.; Prodanovic, R.; Commandeur, U.; Fischer, R., Flow cytometry-based ultra-high-throughput screening assay for cellulase activity. *Anal. Biochem.* **2013,** *435* (1), 93-8.
215. Ostafe, R.; Prodanovic, R.; Nazor, J.; Fischer, R., Ultra-high-throughput screening method for the directed evolution of glucose oxidase. *Chem. Biol.* **2014,** *21* (3), 414-21.
216. Gupta, R. D.; Goldsmith, M.; Ashani, Y.; Simo, Y.; Mullokandov, G.; Bar, H.; Ben-David, M.; Leader, H.; Margalit, R.; Silman, I.; Sussman, J. L.; Tawfik, D. S., Directed evolution of hydrolases for prevention of G-type nerve agent intoxication. *Nat. Chem. Biol.* **2011,** *7* (2), 120-5.
217. Hwang, B.-Y., Directed evolution of cutinase using in vitro compartmentalization. *Biotechnol. Bioprocess Eng.* **2012,** *17* (3), 500-505.
218. Ma, F.; Xie, Y.; Huang, C.; Feng, Y.; Yang, G., An improved single cell ultrahigh throughput screening method based on in vitro compartmentalization. *PLoS ONE* **2014,** *9* (2), e89785.
219. Tu, R.; Martinez, R.; Prodanovic, R.; Klein, M.; Schwaneberg, U., A flow cytometry-based screening system for directed evolution of proteases. *J. Biomol. Screen.* **2011,** *16* (3), 285-94.
220. Aharoni, A.; Griffiths, A. D.; Tawfik, D. S., High-throughput screens and selections of enzyme-encoding genes. *Curr. Opin. Chem. Biol.* **2005,** *9* (2), 210-6.
221. Hardiman, E.; Gibbs, M.; Reeves, R.; Bergquist, P., Directed evolution of a thermophilic beta-glucosidase for cellulosic bioethanol production. *Appl. Biochem. Biotechnol.* **2010,** *161* (1-8), 301-12.
222. Mastrobattista, E.; Taly, V.; Chanudet, E.; Treacy, P.; Kelly, B. T.; Griffiths, A. D., High-throughput screening of enzyme libraries: in vitro evolution of a beta-galactosidase by fluorescence-activated sorting of double emulsions. *Chem. Biol.* **2005,** *12* (12), 1291-300.

223. Romero, P. A.; Tran, T. M.; Abate, A. R., Dissecting enzyme function with microfluidic-based deep mutational scanning. *Proc. Nat.l Acad. Sci. U. S. A.* **2015,** *112* (23), 7159.
224. Kemna, E. W. M.; Schoeman, R. M.; Wolbers, F.; Vermes, I.; Weitz, D. A.; van den Berg, A., High-yield cell ordering and deterministic cell-in-droplet encapsulation using Dean flow in a curved microchannel. *Lab Chip* **2012,** *12* (16), 2881-2887.
225. Di Carlo, D., Inertial microfluidics. *Lab Chip* **2009,** *9* (21), 3038-3046.
226. Edd, J. F.; Di Carlo, D.; Humphry, K. J.; Köster, S.; Irimia, D.; Weitz, D. A.; Toner, M., Controlled encapsulation of single-cells into monodisperse picolitre drops. *Lab Chip* **2008,** *8* (8), 1262-1264.
227. Schoendube, J.; Wright, D.; Zengerle, R.; Koltay, P., Single-cell printing based on impedance detection. *Biomicrofluidics* **2015,** *9* (1), 014117.
228. Rotem, A.; Ram, O.; Shoresh, N.; Sperling, R. A.; Schnall-Levin, M.; Zhang, H.; Basu, A.; Bernstein, B. E.; Weitz, D. A., High-Throughput Single-Cell Labeling (Hi-SCL) for RNA-Seq Using Drop-Based Microfluidics. *PLoS ONE* **2015,** *10* (5), e0116328.
229. Sollier, E.; Amini, H.; Go, D. E.; Sandoz, P. A.; Owsley, K.; Di Carlo, D., Inertial microfluidic programming of microparticle-laden flows for solution transfer around cells and particles. *Microfluid. Nanofluidics* **2015,** *19* (1), 53-65.
230. Ficheux, M. F.; Bonakdar, L.; Leal-Calderon, F.; Bibette, J., Some Stability Criteria for Double Emulsions. *Langmuir* **1998,** *14* (10), 2702-2706.
231. Benichou, A.; Aserin, A.; Garti, N., Double emulsions stabilized with hybrids of natural polymers for entrapment and slow release of active matters. *Adv. Colloid Interface Sci.* **2004,** *108-109*, 29-41.
232. Hanson, J. A.; Chang, C. B.; Graves, S. M.; Li, Z.; Mason, T. G.; Deming, T. J., Nanoscale double emulsions stabilized by single-component block copolypeptides. *Nature* **2008,** *455* (7209), 85-88.
233. Pays, K.; Giermanska-Kahn, J.; Pouligny, B.; Bibette, J.; Leal-Calderon, F., Double emulsions: how does release occur? *J. Control. Release* **2002,** *79* (1), 193-205.
234. Ma, F.; Fischer, M.; Han, Y.; Withers, S. G.; Feng, Y.; Yang, G.-Y., Substrate Engineering Enabling Fluorescence Droplet Entrapment for IVC-FACS-Based Ultrahigh-Throughput Screening. *Anal. Chem.* **2016,** *88* (17), 8587-8595.

Chapter 3 Improving single-cell encapsulation efficiency and reliability through neutral buoyancy of suspension*

*Liu, H.; Li, M.; Wang, Y.; Piper, J. A.; Jiang, L., Improving single-cell encapsulation efficiency and reliability through neutral buoyancy of suspension. *Micromachines* **2020**, *11* (1), 94.

To achieve the high-throughput single-cell analysis using droplet-based microfluidics, the efficiency and reliability of single-cell emulsification remain as prerequisites. This is challenging to achieve high-efficiency single-cell encapsulation rate due to cell sedimentation and aggregation. This chapter is to quantitively investigate the influence of neutral buoyancy on single-cell encapsulation and incubation A low-toxicity and non-iconic density-matching reagent, OptiPrep™, was used to achieve neutral buoyancy. An optimal concentration of OptiPrep™ improves single-cell encapsulation rate and facilitates effective single-cell study using microdroplets.

3.1. Introduction

Single-cell analysis has been attracting great interest from both academia and industry as a powerful technique in the field of medical diagnosis, tissue engineering, and cell biology. Conventional biological assays focus on the signals based on large cell populations that normally provide average information about hundreds of thousands of cells; thus, the existence of cell-to-cell variations and the intrinsic and inherent properties of cell populations are obscured[1, 2]. Unlike bulk population analysis, single-cell analysis allows in-depth profiling of cell populations at single-cell resolution and uncovering of rare cell subpopulations.

Furthermore, individual cells of interest can be sorted from the majority of the population for further studies. This technology has been demonstrated as a powerful tool to investigate cancer biology, by profiling marked heterogeneity, development of new diagnostics, and personalised medicine.

Traditional flow cytometry is mostly used in single-cell analysis to scrutinise heterogeneous cell populations in a high throughput and multiplexing manner[3, 4]. However, some limitations have restricted its wide application for single-cell analysis. FACS mainly relies on cell-surface markers for detection, which curb the assay of intracellular interactions, secretions of metabolites, and genetic materials. Moreover, flow cytometry allows only single time point measurements, therefore, the same single cells can neither be observed over long periods nor suitable for repetitive measurements[2, 5].

As an alternative, microfluidic droplet-based assays are fast, cost-effective, and high-throughput methods becoming valuable tools for single-cell analysis. Compartmentalisation of single cells in monodispersed droplets has various advantages for applications across biology and biomedicine, because: (1) microenvironments of cells can be uniformly created and maintained to harmonise the extrinsic influence on cells; (2) droplets provide a unique tool to link genotypes with phenotypes of cells through confinement, as cells and molecules secreted remain trapped inside the droplets and are analysed and sorted in a timeframe [6]; (3) the secreted molecules from single compartmentalised cells quickly reach a detectable limit because of the small volume of the confinement, which enables the rapid detection of molecules of interest; and (4) encapsulated cells can be lysed by cell lysis buffer without membrane rupture, enabling biochemical and genetic analyses of intracellular contents of single cells based on released DNA or RNA amplified in the droplets.

When using microfluidic chips to encapsulate single cells into droplets, the majority of droplets either contain more than one cell or are empty. Although the frequency of droplet

generation and their diameters are tunable to produce more microdroplets containing exactly one cell, cell encapsulation in droplets is a random process limited by the Poisson distribution that is hard to control. Statistical models are established to provide an understanding of the underlying processes and estimation of the relevant parameters, however, high-efficient, reliable, and repeatable control over the encapsulation of single cells in droplets is still difficult to achieve due to the instrumental errors and cell sedimentation and aggregation[7]. Cell sedimentation changes the uniformity of cell distribution within the suspension (in the syringe, tubing, and microchannels), and therefore, increases the chance of aggregation. Ultimately, sedimentation and the resulting aggregation decrease the reliability of the droplet generation system by causing syringe clogging and non-uniform cell count per droplet. Therefore, to achieve higher single-cell encapsulation efficiency and reliability, sedimentation effects must be suppressed in the microfluidic droplet systems.

A variety of methods have been developed to increase the efficiency of single-cell encapsulation in microdroplets. External forces, such as acoustic, magnetic, and optical forces, have been integrated with microfluidic platforms to localise single cells at the droplet formation region, which help to increase the single-cell encapsulation rate. However, cell growth conditions may deteriorate when exposed to external stress, and normally the throughput of external force-assisted droplet generation methods is lower by an order of magnitude than that of methods without the need of external forces (i.e., at kHz rates). Furthermore, external force-assisted methods necessitate more complex experimental setup. In addition to external forces, the intrinsic properties of fluidics in microchannels have been used to enhance single-cell encapsulation efficiency. For example, the introduction of inertial flow coupled with Dean flow can increase the fraction of droplets containing single cells to ~80%[7, 8]. However, the deterministic methods merely suit the encapsulation of homogenous cells, and the velocity of cell perfusion must correspond to that of droplet formation, which requires a meticulous

operation. Moreover, the flow rates are much higher than those typically used in microfluidics chips (i.e., $1 < Re < 300$ and flow velocities on the order of ~ 0.1–1 m s^{-1})[7], and the increased fluid shear stress may induce cell death.

Magnetic stirring has been often used to prevent cell sedimentation and aggregation[9, 10]. However, this method may cause unstable cell volume fraction, cell damage, and cell physiological fluctuations. Compared to the magnetic stirring method, the use of biocompatible density-matching gradient reagents to balance the density of cell suspensions is simpler and gentler. There are a number of different ideal density gradient materials, like sucrose, salts, polysucrose, and colloidal silica[11]. The selection of optimum reagent usually depends on the applications. The optimum should not alter the conditions of cells or particles to be separated and should provide a reliable density range for specific types of suspending cells or particles. OptiPrep™[12, 13] is a non-ionic iodinated solution containing 60% (w/v) iodixanol with a molecular weight of 1550 in water. The density of OptiPrep™ is 1.320 ± 0.001 g/mL and the endotoxins are below 1.0 EU/mL. OptiPrep™ was first developed for clinical purposes in X-ray contrast imaging[12, 14]. Due to its low-toxicity, low osmotic pressure, and no obvious penetration into large particles, OptiPrep™ is extensively used for the isolation of different types of molecules and cells, including peroxisomes, cytokine, DNA, viruses, organelles, exosomes, and a wide range of mammalian cells[13, 15-18].

OptiPrep™ shows advantages when comparing with other density-matching reagents, such as Nycodenz®[19], Metrizamide[20], and Percoll®[11, 21]. For example, Nycodenz® can cause possible contamination when isolating particles[21]; Metrizamide is less cell-friendly due to its ionic nature; and there are concerns about the toxic effects of Percoll®. In addition, the density of Percoll® (1.13 g/mL ± 0.005 g/mL at 25 °C) is lower than that of OptiPrep™, which means that a larger amount of Percoll® is required to make solutions with the same density.

Therefore, its biocompatible and non-invasive properties make OptiPrep™ an ideal additive in the aqueous phase for droplet-based microfluidics. The use of OptiPrep™ has been demonstrated for increasing encapsulation efficiency of single THP-1 cells in microdroplets[22]. The THP-1 cell has a density of 1.05 g/mL, and the sedimentation of this type of cell occurs in a common culture medium. However, the concentration of OptiPrep™ used in the previous article[22] (i.e., 18%) has not been optimised. Moreover, it is noteworthy that time-dependent behaviours of OptiPrep™ and its effect on cell encapsulation efficiency[23] have been only investigated under limited conditions: relatively low cell concentration (3×10^6 cells mL^{-1}), certain cell types (adherent cells), specific period of time (trypsinisation of cells), and limited environment (gel materials with higher viscosity). A detailed study about the impact of Optiprep™ and cell density on the encapsulation rate and cell viability in microdroplets has not yet been reported to date.

In this work, we attempt to mitigate cell sedimentation and improve the efficiency of single-cell encapsulation in microdroplets through neutral buoyancy. Although researchers have mentioned the use of OptiPrep™ for cell encapsulation by droplet-based microfluidics[24-28], to the best of our knowledge, this is the first detailed report quantitatively evaluating the effect of OptiPrep™ on THP-1 cell encapsulation efficiency and cell viability in microdroplets.

3.2. Theory

3.2.1. Stokes' Law

In order to achieve the desired cell suspension dispersion and mitigate the effects of sedimentation, an appropriate medium density that is equivalent to the density of target cells is essential. Theoretical values for sedimentation velocities can be obtained using Stokes' law[29-31], as:

$$v = \frac{(\rho_p - \rho_f)gD_p^2}{18\mu}, \quad (1)$$

where v is the sedimentation velocity, g is the gravitational acceleration, D_p is the particle diameter, ρ_p and ρ_f are the particle and fluid densities, respectively, and μ is the fluid viscosity.

From Equation (1), we know that the sedimentation velocity will increase with effective particle diameter and this indicates that aggregation of cells results in increased sedimentation velocity.

3.2.2. Poisson Distribution

Here, the Poisson distribution is used as an informative predictor for the rate of single-cell encapsulation when the target cells are smaller than the droplets volumetrically and are distributed homogeneously in an aqueous solution. The Poisson distribution, which is a discrete probability distribution, has been used to calculate the probability of a single cell in one droplet during encapsulation, assuming there is random dispersion of cells in the sample and constant flow velocity (shown in Table S3.1). The use of OptiPrep™ can achieve uniform suspension of cells in the sample by tuning the aqueous density to that of cells. The probability of one droplet containing *k* cells can be dictated by

$$P(k, \lambda) = \frac{\lambda^k e^{-\lambda}}{k!}, \quad (2)$$

where λ is the average number of cells per droplet,

$$\lambda = C \cdot V_D, \quad (3)$$

C is the concentration of cells in aqueous solution with unit of cells/mL, and V_D is the volume of each droplet. By replacing λ in Equations (2) with (3), the probability of droplets containing *k* cells at different droplet sizes and cell concentrations can be calculated by Poisson distribution using MATLAB (MathWorks, Natick, MA, USA).

3.3. Materials and Methods

3.3.1. Device design and fabrication

The droplet-based microfluidic device used in this study consists of two inlets for the perfusion of disperse phase and continuous phase, connecting microchannels with an aspect ratio of height/width = 1:2 (height: ~40 μm; width: ~80 μm), a rectangular observation chamber of 2 × 0.65 cm, and one outlet (shown in Fig. S3.1). The geometry we used here was T-junction, in which the oil flowed horizontally towards the observational chamber, and the aqueous phase flowed vertically and sheared into uniform droplets. This droplet-based microfluidic device was fabricated using standard soft-lithography techniques, including: (i) mask design via computer-aided design software; (ii) mylar mask printing; (iii) fabrication of the SU-8 (SU-8 2035 or 2050, MicroChem, Newton, MA, USA) master mold; (iv) casting of PDMS (Sylgard 184, Dow Corning, Midland, MI, USA); and (v) air plasma treatment on the surfaces of the glass substrate and PDMS slabs for irreversible covalent bonding.

3.3.2. Cell culture and preparation

The acute monocytic leukemia THP-1 cell line was obtained from CellBank Australia. Cells were cultured in a vertical T-75 flask filled with 12 mL of the complete growth medium: 90% RPMI-1640 (Sigma-Aldrich, St. Louis, MO, USA), 10% fetal bovine serum (FBS, Thermo Fisher Scientific, Waltham, MA, USA), and supplemented with 1% penicillin-streptomycin (Thermo Fisher Scientific, Waltham, MA, USA); and kept in an incubator (Thermo Fisher Scientific, Waltham, MA, USA) which provides sterile conditions at 37 ℃ with 5% carbon dioxide. THP-1 cells were inoculated in fresh complete growth medium at an initial concentration of 2×10^5 cells/mL. The number and viability of THP-1 cells were measured by the Trypan blue-based TC-20 automated cell counter (Bio-Rad, Hercules, CA, USA). Normally, to acquire enough volume (e.g., 1 mL) of cell suspension (e.g., 6×10^6), two flasks of cells are

cultured for four days simultaneously, then spun down and suspended with fresh medium which adjusts the cell density to the desired value to be used before the viability drops down to 95%. When cell number and viability both satisfied the requirements, THP-1 cells were used to perform encapsulation in microfluidic droplets.

3.3.3. Encapsulation of single cells in water-in-oil droplets

Oil phase, Novec™ 7500 Engineered fluid (3M, St. Paul, MN, USA) mixed with 2% Pico-Surf™ 1 (Sphere Fluidics, Cambridge, UK) as surfactant, and aqueous phase cells in culture medium and OptiPrep™ (Sigma-Aldrich, St. Louis, MO, USA), were delivered via two syringe pumps (PHD 2000, Harvard Apparatus, Holliston, MA, USA; Chemyx, Fusion 200, Stafford, TX, USA) into the microchip to produce cell-encapsulated microdroplets. The fluorinated ethylene propylene (FEP) tubing (IDEX, Lake Forest, IL, USA), with an inner diameter of 0.5 mm, was used for connecting the syringes to the microchip inlets. The microfluidic chip was used to produce uniform cell-laden droplets of different sizes by tuning the flow rate of the oil phase and aqueous phase.

3.3.4. Measurement of cell density and viability with the presence of OptiPrep™

The density gradient centrifugation method is considered as a golden standard to measure individual cell weight [32]. Here, we drew on this idea and mixed different volumes of OptiPrep™ with culture medium to achieve four cell suspensions of different OptiPrep™ concentrations: 4%, 8%, 12%, and 16%. Cells were spiked into the density-tuned media at the concentration of 3×10^6 cells/mL and incubated for at least half an hour to record the cellular precipitation.

Cells at the concentration of ~3×10^6 cells/mL were used to create cell-laden droplets with the medium containing final concentrations 0% OptiPrep™, 8% OptiPrep™, 13.2%

OptiPrep™, and 16% OptiPrep™, individually. Cell viability was monitored after 12 h and 24 h culture at 37 °C with 5% carbon dioxide. For each time point, cells from three replicate experiments were measured. Then 50 μL of cell-laden droplets were pipetted and 2 μL Pico-Break™ (Sphere Fluidics, Cambridge, UK) were added and mixed well by inverting the centrifuge tube five times mildly. After that, the oil phase was spun down at 300 *g* for 1 min at room temperature and the supernatant containing cells was aspirated into a new centrifuge tube. Then, the viability assay kit for animal live and dead cells (Biotium, Hayward, Ca, USA) containing 2 μ M Calcein AM and 4 uM EthD-III was mixed with the released cells at room temperature for 20 minutes. After staining, the cells suspension was imaged by fluorescein isothiocyanate (FITC) channel to see the live cells (green) and mCherry channel to see the dead cells (red) by a fluorescence microscope, IX-83 (Olympus, Tokyo, Japan).

3.3.5. Measurement of OptiPrep™ inducing effect on cell encapsulation

Cell suspensions without OptiPrep™ (0% OptiPrep™), with 8% OptiPrep™, 13.2% OptiPrep™, and 16 % OptiPrep™ were spiked into the aqueous phase, respectively, and then cell encapsulation in microdroplets was performed immediately after the addition and mixing. At least one hundred measurements were performed in the observation chamber for each replicate, and a total of three replicates were conducted for each condition. The experimental results of cell encapsulation in microdroplets were analysed by one-way analysis of variance (ANOVA) to determine whether a significant difference was present between with OptiPrep™ and without OptiPrep™. The experimental data were fitted to the theoretical values based on Poisson statistics to show the effect of OptiPrep™ on cell encapsulation. The ~81 μm diameter droplets were produced to encapsulate single cells at cell density of 2×10^6, 4×10^6, 6×10^6, and 8×10^6 cells/mL, respectively.

3.3.6. Imaging and image analysis

Videos of droplet formation were recorded with a high-speed camera (Phantom Miro M/R/ LC320S, Vision Research, Inc., Wayne, NJ, USA), and a digital camera (DS-Qi1Mc, Nikon, Tokyo, Japan) equipped on an inverted microscope (Eclipse Ti-U, Nikon, Tokyo, Japan) was used to capture images of cell-laden droplets. An observation chamber on the microfluidic chip (Figs. S3.1C, D) was specifically designed for the imaging of droplets. The number of droplets was counted by programs written in MATLAB (Fig. S3.2). In order to show the size distribution of droplets and cell encapsulation rates at different cell and OptiPrep™ concentrations, random frames of at least 100 droplets in the chamber were chosen for counting and statistical analysis using ImageJ (National Institutes of Health (NIH), Bethesda, MD, USA) (see Fig. S3.3).

3.4. Results and Discussion

3.4.1. OptiPrep™ effectively mitigates cell sedimentation

In this work, we developed a medium density matching strategy to improve single-cell encapsulation efficiency and reliability through neutral buoyancy of cell suspension as shown in Fig. 3.1. The two immiscible fluids (continuous phase: oil; dispersed phase: cell, medium, and OptiPrep^{TM}) were simultaneously infused into the droplet generation part, a T-junction, of the fabricated microfluidic chip. The formation of droplets took place when shear force acting on the interface between two fluids overcame the interfacial force (shown in Video S3.1). Cells were encapsulated into microdroplets containing aqueous solutions surrounded by the oil phase.

Many cancer cells are known to aggregate and such aggregation phenomena were observed in many cancer-derived liquid biopsies[33, 34]. Therefore, the suspension always consists of a large number of single cells as well as cell clusters. As seen in Fig. S4A, we observed that cells were mostly clustered at the bottom of inlets and were not able to be perfused into microfluidic

channels in the non-density matched suspension. This was due to the higher density of THP-1 cells (~1.05 g/mL) compared to the cell culture medium (~1.009 g/mL). Using the non-density matched suspension, the single-cell encapsulation rate rarely matches the theoretical value of Poisson statistics. Cell suspension containing 0%, 4%, 8%, 12%, and 16% (v/v) OptiPrep™ were prepared individually to determine the appropriate medium density for preparing neutral buoyancy of THP-1 cell suspension. After 30 min, the THP-1 cells in whole culture medium (left tube) sedimented markedly, whereas density-matched THP-1 cells (right tube) were still well suspended, as shown in Fig. 1. The density of culture media with 12% OptiPrep™ (1.046 g/mL) and 16% OptiPrep™ (1.059 g/mL) is closer to the density of THP-1 cells; neutral buoyancy of THP-1 cell suspension occurs in the media with OptiPrep™ between 12% and 16% (Fig. S4B).

3.4.2. Efficienct single cell encapsulation using neutral buoyancy of suspensions

Some researchers normally adopt the cell seeding of a low λ value to ensure that a large proportion of droplets contain only one cell, but it causes the majority of wasteful empty droplets. Unsurprisingly, the rate of single-cell-encapsulated droplets increases at a higher λ

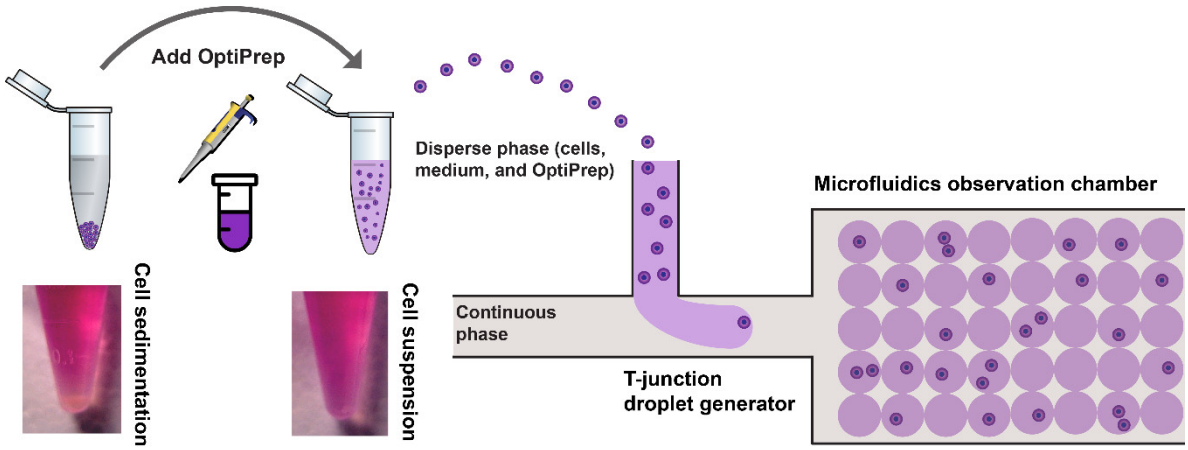

Figure 3.1 Schematic of a droplet-based microfluidic platform for highly efficient single-cell encapsulation using neutral buoyancy of suspension. Using an appropriate concentration of OptiPrep™ in culture medium prevents cell sedimentation.

value. For example, when λ = 1, the rate of droplets containing a single cell is 36.8%, while the rate of empty droplets and droplets containing more than one cell is 36.8% and 26.4%, respectively.

Compared with the laborious change of cell density, droplet size is relatively easy to control. A microfluidic device with T-junction geometry was employed to encapsulate single THP-1 cells in monodisperse microdroplets (Fig. 3.1). With constant flow rates, we produced highly monodisperse droplets, enabling highly reproducible reaction and analysis conditions. Fine tuning of the droplet size for a given channel geometry is accomplished by varying the fluid viscosity, aqueous flow rate or the overall flow rate. This also leads to variations in the drop production frequency. In Fig. 3.2, it can be seen that we generated droplets with a mean diameter of 32.8 µm, and a standard deviation of 3.2%. By increasing the flow rate of the

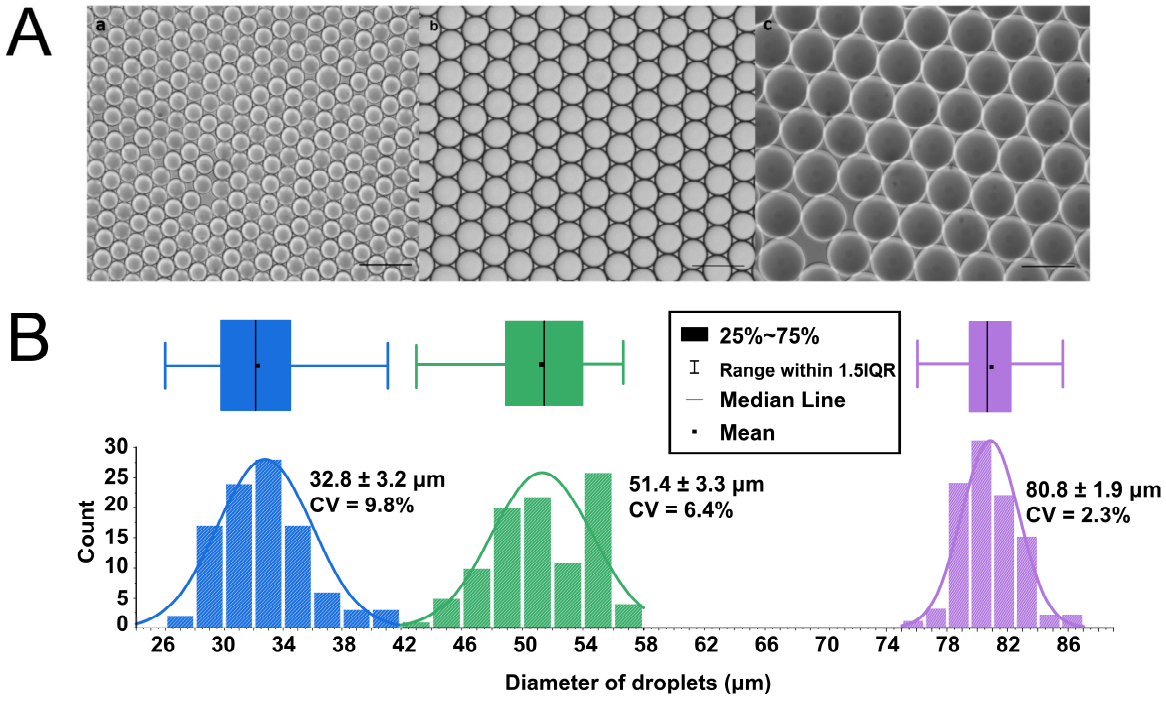

Figure 3.2 Microfluidic T-junction droplet-generator created uniform and stable droplets. (A) The morphology created droplets of three sizes: 32.8 µm, 51.4 µm, and 80.8 µm. Scale bar = 100 µm. (**B**) Plots of size distribution of droplets generated by the microfluidic chip. The limits of the box refer to the 25th and 75th percentiles, the cross line is the mean value, the black square is the median value, and the whiskers extend to 1.5 times the interquartile range (IQR). For each measurement, 100 droplets were counted.

aqueous phase, we were able to generate droplets with a mean diameter of 51.4 μm, and a standard deviation of 6.4%. In order to maintain long-term cell culture in droplets, larger droplets with a mean diameter of 80.8 μm and a standard deviation of 1.9% were formed by decreasing the flow rate of the oil phase using the same device. Therefore, cells can be encapsulated with OptiPrep™ in highly monodisperse droplets for long-term cell culture (i.e., culture in large droplets with affluent nutrients) and assays.

The rate of single-cell encapsulation within microdroplets of three different sizes (with a mean diameter of 32.8 μm, 51.4 μm, and 80.8 μm) at four different cell concentrations (2×10^6 cells/mL, 4×10^6 cells/mL, 6×10^6 cells/mL, and 8×10^6 cells/mL) was calculated by Poisson distribution (Fig. S3.5 and Table S3.1). We used ~81 μm microdroplets to investigate the effect of OptiPrep™ concentration on cell-encapsulation efficiency, because it can achieve a higher rate of droplets containing single cells and lower rate of empty droplets compared to ~33 μm and ~51 μm droplets (see Fig. S5). Moreover, a relatively lower concentration of cells is needed for ~81 μm microdroplets to study single-cell encapsulation. In theory, we assumed that cells are dispersed in culture medium uniformly and the maximum efficiency for encapsulating single cells is 36.6% in the ~81 μm droplets at the cell concentration of 4×10^6 cells/mL. we tested the influence of density matching on the evenness of cell encapsulation rate by using cell suspension with different concentrations of OptiPrep™ (Fig. 3.3A). The single-cell encapsulation is below 10% in the non-density matched suspension at the cell concentration of 4×10^6 cells/mL. The single-cell encapsulation rate increases to ~30% when cell suspension is prepared at the concentration of 8×10^6 cells/mL. This is due to the significant variation between the calculated cell concentration and the real concentration after sedimentation. However, to achieve a high rate of single-cell encapsulation without density matching, an extremely high concentration of cells has to be used initially, which increases the risk of clogging in syringes and microchannels.

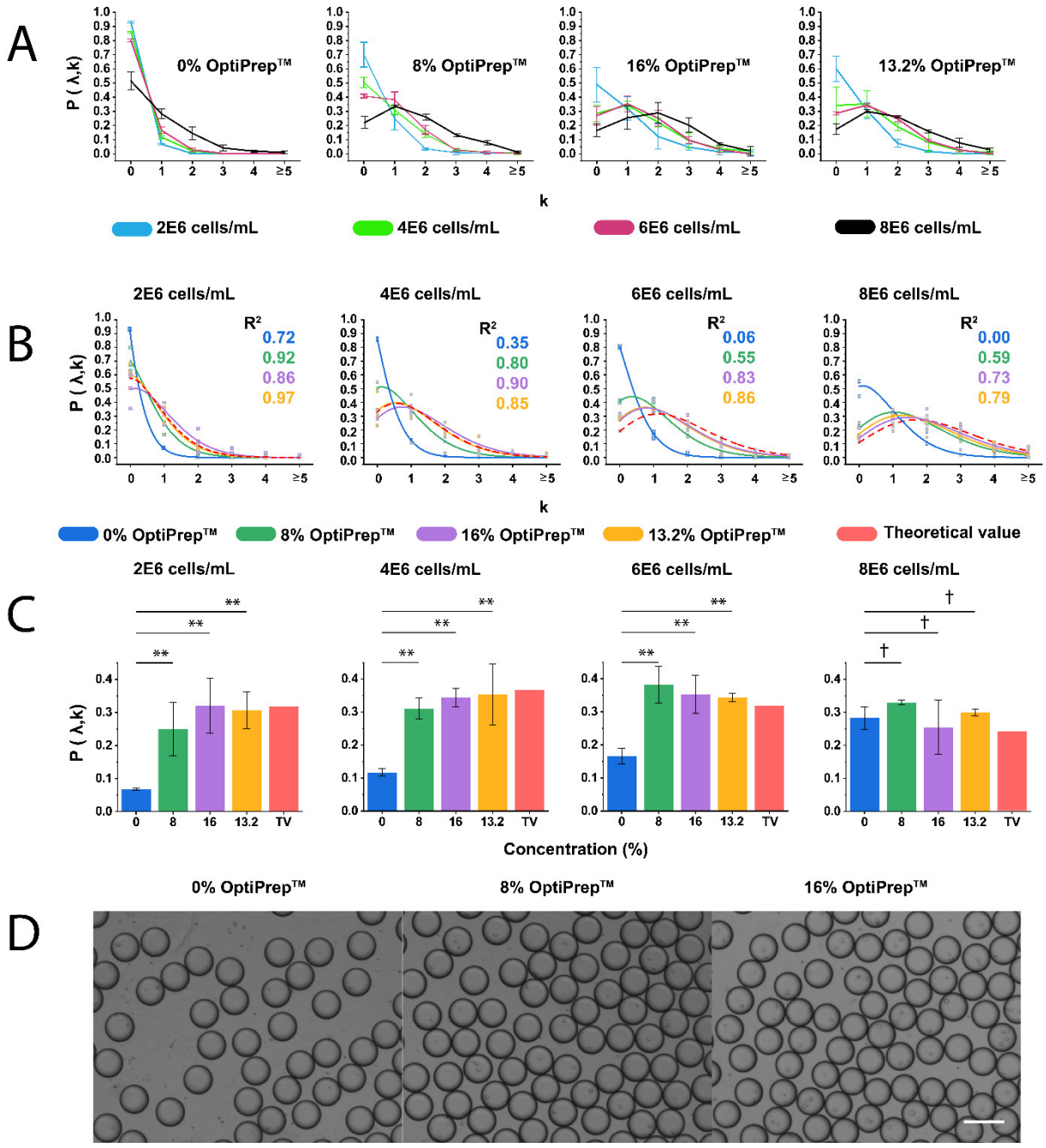

Figure 3.3 Cell encapsulation in microdroplets at different cell and OptiPrep™ concentrations. (A) Plots of probability of THP-1 cell encapsulation in 81 µm droplets at different concentrations of OptiPrep™ (0%, 8%, 13.2%, and 16%) and cells (2×10^6, 4×10^6, 6×10^6, and 8×10^6 cells/mL). From the left to right: experimental values at 0% OptiPrep™, 8% OptiPrep™, 16% OptiPrep™, and optimised OptiPrep™ (13.2%), and theoretical values predicted by Poisson distribution for cell encapsulation of 81 µm droplets. (B) The comparison between the theoretical and experimental results of cell encapsulation in microdroplets.

Plots of the probability P (λ, k) values for droplets containing different number of cells (0, 1, 2, 3, 4, and ≧5) obtained from experiments and Poisson statistics are shown. R^2 refers to the coefficient of determination of different groups fitting Poisson distribution. (**C**) ANOVA test results for the rate of single-cell encapsulation in droplets. A comparison between experimental values and theoretical value (TV) at different concentrations of OptiPrep™ was performed for each cell concentration. ** represents $p < 0.01$; † means no significant difference. $n = 3$, error bars represent the standard deviation. (**D**) Photographs of cell-laden microdroplets generated with the presence of OptiPrep™ at different concentrations. From the top to bottom: 0% OptiPrep™, 8% OptiPrep™, and 16% OptiPrep™ in cell suspensions. Cell concentration was 4×10^6 cells/mL. Scale bar = 100 μm.

Fig. 3.3A also displays the experimental results of cell encapsulation rate in ~81 μm droplets using non-sufficient density matching reagent (8% OptiPrep™). It shows that the single-cell encapsulation rate is ~31.1 ± 3.2%, which is 5.6% lower than the predicted rate by Poisson distribution. Although the increase of cell concentration from 4×10^6 cells/mL to 6×10^6 cells/mL can increase the single-cell encapsulation rate, it leads to an increase rate of droplets containing multiple cells. When using sufficient density matching reagent (16% OptiPrep™), specifically, the rate of droplets containing single cells increases from 34.3 ± 2.8% to 35.3% ± 5.7% (no significant difference), while the rate of droplets containing two cells increases from 22.2 ± 3.2% to 25.1 ± 5.7%. Therefore, cell concentration at 6×10^6 cells/mL is not preferred for single THP-1 cell analysis in 81 μm droplets. In addition, a sudden increase in the rate of droplets containing multiple cells was observed when cell concentration increased to 8×10^6 cells/mL. These results could be attributed to a larger number of cells existing at the T-junction due to sedimentation, or cell clusters injected into the microchannel.

In theory, the rate of droplets containing cells obtained based on the neutral buoyancy of cell suspensions fits better than the ones predicted by Poisson distribution and reduces the amount of OptiPrep™ to lessen its impact on cell physiology. Here we calculated and

experimentally verified that the most appropriate concentration of OptiPrep™ to form THP-1 cell suspension is 13.2%. By using this concentration of OptiPrep™ and the cell density of 4×10^6 cells/mL, experimentally obtained rates of empty droplets (34.1 ± 12.3%), droplets with one cell (35.3 ± 9.2%), droplets with two cells (19.1 ± 2.6%), three cells (8.1 ± 6.6%), and four cells (2.4 ± 2.3%) are in good agreement with the theoretical rates.

Fig. 3.3B shows that the addition of 13.2% OptiPrep™ is optimal to predict the rate of droplets containing different numbers of cells, as the experimental curves of the cell-laden droplet rate under different conditions fit well to the theoretical values.

As shown in Fig. 3.3C, in terms of single-cell droplet rate, all groups but the 8×10^6 cells/mL show a significant difference for 0% OptiPrep™ vs. 8% OptiPrep™, 0% OptiPrep™ vs. 16% OptiPrep™, and 0% OptiPrep™ vs. 13.2% OptiPrep™.

In this study, neutral buoyancy suspensions of THP-1 cells were prepared as a proof-of-concept. Other neutral buoyancy suspensions with specific entities, such as various cancer cells, bacteria, fungi, and particles can be calculated and prepared depending on the density of targets.

3.4.3. Cell viability and proliferation with the presence of OptiPrep™

We examined whether a prolonged period of suspension and incubation would affect cellular viability. This was to ensure that suspending cells in a neutrally buoyant suspension is a feasible and stable approach for long-time single-cell assays. To test the viability of cells in the droplets after 12 h and 24 h culture, we removed the oil layer before performing the live/dead viability stains. As shown in Fig. 4, 91.9 ± 3.0% cells remained alive after 12 h incubation and the cell viability decreased to 88.9% ± 2.0% after 24 h for the 0% OptiPrep™; while 88.1 ± 1.8% cells remained alive after 12 h incubation and slightly decreased to 87.5% ± 5.6% after 24 h with the presence of the 8% OptiPrep™. When the concentration of OptiPrep™ increased to 16%, the cell viability was only 85.6 ± 3.1% after 12 h incubation and significantly decreased to 78.1% ± 2.4% after 24 h. Statistical analysis shows that there is no

significant difference in cell viability between different concentrations of OptiPrep™ after 12 h incubation (see Fig. 3.4). However, after 24 h culture, both measurements of cell viability experienced a significant decrease when 16% OptiPrep™ was present.

Some factors might contribute to the more significant decrease in viability of cells cultured inside droplets: the main ingredient of Pico-Break™, PFOH (1H,1H,2H,2H-Perfluoro-1-octanol), imposed chemical stress on the cells; and the nutrient deficiency due to the dilution from OptiPrep™. However, these factors can be carefully controlled with finer operation during oil removing and regulating the droplets size in the droplet-based cell assay.

OptiPrep™ is a non-ionic solution of 60% iodixanol (w/v) in water. Materials such as sucrose and dextran have also been used to create density gradients for cell separations. In comparison to sucrose solutions at similar concentrations, solutions of OptiPrep™ had a much lower osmolarity and viscosity. The low osmolality of OptiPrep™ solutions allows for its use in cell separation. Dextran, a linear polymer of glucose, has also been used to increase solution

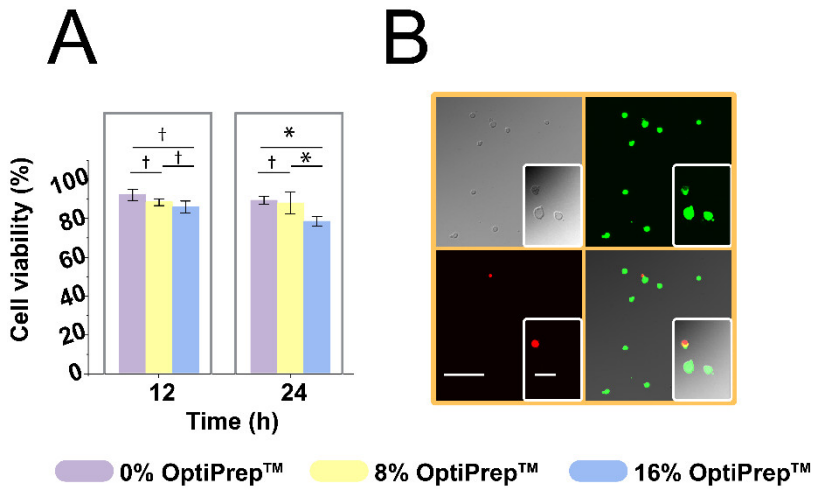

Figure 3.4 THP-1 cells maintained high viability with the presence of OptiPrep™ over 24 h inside the droplets. (A) Cell viability at two time points: 12 h and 24 h; * represents $p < 0.05$; † represents no significant difference; error bars represent the standard deviation. (B) Images showing cell viability. Measurement of cell viability was performed with the live/dead assay, live cells were stained with Calcein-AM (green) and dead cells with EtD-III (red); scale bar = 100 μm for images obtained by a 20× objective; scale bar = 10 μm for insets obtained by a 100× objective.

density; however, it has a much higher viscosity at similar OptiPrep™ solution densities. Thus, OptiPrep™ has the advantages of both low osmotic pressure and low intrinsic viscosity. Preparing neutral buoyancy of suspensions with appropriate concentrations of OptiPrep™ opens up the possibility to improve single-cell encapsulation significantly without affecting cell viability.

3.5. Conclusions

We hypothesised that the influence of physical forces on cells within suspension would lead to stratification of concentrations found within the fluid, and that this would result in unreliable and inaccurate cell counts and manipulations. We reasoned that the single-cell encapsulation rate and reliability over time could increase by mitigating these effects. We alleviated the negative influence of gravity by adding OptiPrep™ to achieve near neutral buoyancy within the suspension. Our hypothesis was confirmed by experimental results: density balancing of cell-based suspensions resulted in an increased rate of single-cell encapsulation in microdroplets and enabled reliable encapsulation distribution that was close to the theoretical values. Among all tested concentrations of OptiPrep™ used in this study, it is demonstrated that the concentration of 13.2% is the optimal one, as it enables reliable encapsulation distribution, when the cells were neutrally buoyant.

We also investigated the effect of initial cell concentrations on single-cell encapsulation in microdroplets with OptiPrep™ of different concentrations. Furthermore, cell viability in microdroplets with the presence of various concentrations of Optiprep™ has been investigated for the first time. This is a pioneering work on evaluating the influence of OptiPrep™ as a density-matching reagent on the efficiency of single-cell encapsulation and culture in microdroplets. It proves that this method can enhance the rate of droplets encapsulated with single cells and has limited adverse effects on THP-1 cell viability when low concentrations of Optiprep™ are used. Interestingly, middle-range concentrations of OptiPrep™ can also be used

to increase cell encapsulation efficiency. However, given that this just reduces the sedimentation velocity of cells, the non-sufficient density matching reagent is only recommended for relatively short time of cell encapsulation.

In conclusion, we demonstrated the feasibility of improving single-cell encapsulation efficiency and reliability using OptiPrep™. We expect this density-matching approach could open the door to realise highly efficient single-cell analysis in a milder and more cost-effective manner. We also envision that this approach can be widely used for a wide variety of applications involving 3D bioprinting.

Supplementary Materials

The following information is available in the Supplementary Materials. Fig. S3.1: Photographs of the microfluidics chips and experimental setup, Fig. S3.2: A photograph of droplets recognised by programs written by MATLAB, Fig. S3.3: Actual images of cells encapsulated within microdroplets under different conditions, Fig. S3.4: A photograph of cell sedimentation at the inlet of a microchannel, Fig. S3.5: Plots of Poisson distribution for droplets of three different sizes, Table S3.1: Poisson statistics for different cell concentrations and droplet sizes, Table S3.2: Data collected from captured images of cell-laden droplets. The data obtained from three duplicates are shown, Table S3.3: Data collected from viability test. The data obtained from three duplicates are shown.

Video S3.1: Droplet formation at the T-junction of a microfluidic droplet generator (see attachment).

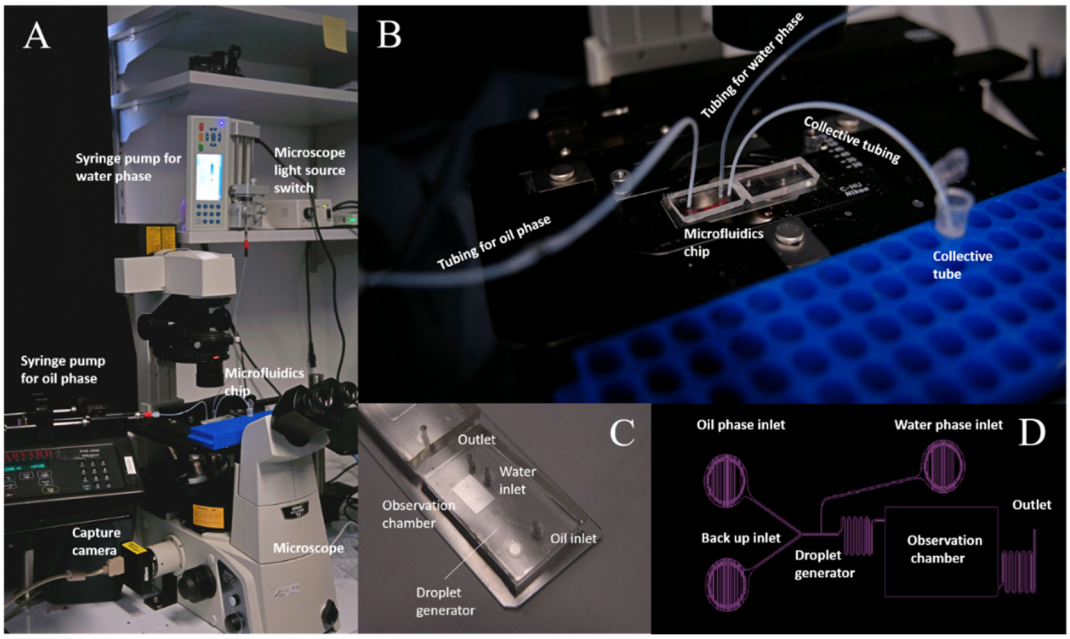

Figure S3. 1 Photographs of the microfluidics chips and experimental setup. (A) A photograph of experimental setup. The external equipment required to generate cell-laden droplets include two syringe pumps for oil phase (continuous phase) and water phase (disperse phase), respectively, a microscope, a light source, a camera to capture images and videos, and a fabricated microfluidic chip. (B) An enlarged view of the device for droplet generation under the microscope. Three tubing for the injection of oil phase and water phase, and sample collection are shown. (C) The actual image of the microfluidic chip, which consists of two inlets for oil phase and a water phase, respectively, a T-junction to create microdroplets, an observation chamber, and an outlet. (D) The CAD file showing the design of the chip.

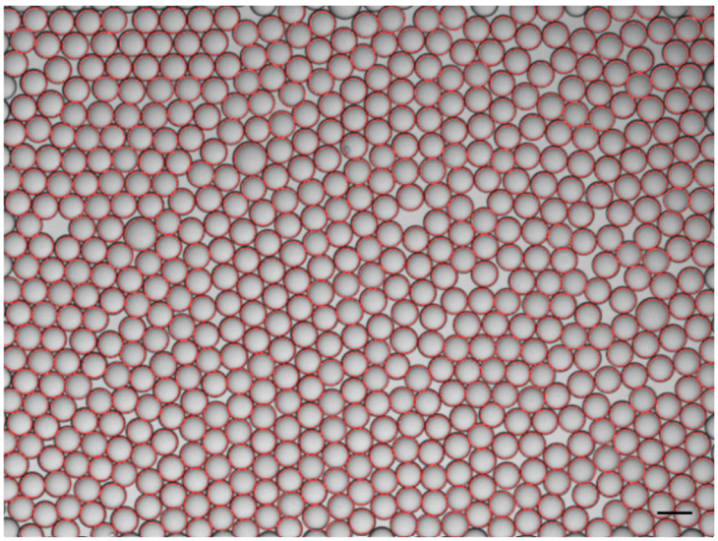

Figure S3.2. A photograph of droplets recognised by programs written by MATLAB. 81 µm droplets were captured and automatically calculated by programs written by MATLAB: count number = 582 droplets; scale bar = 100 µm.

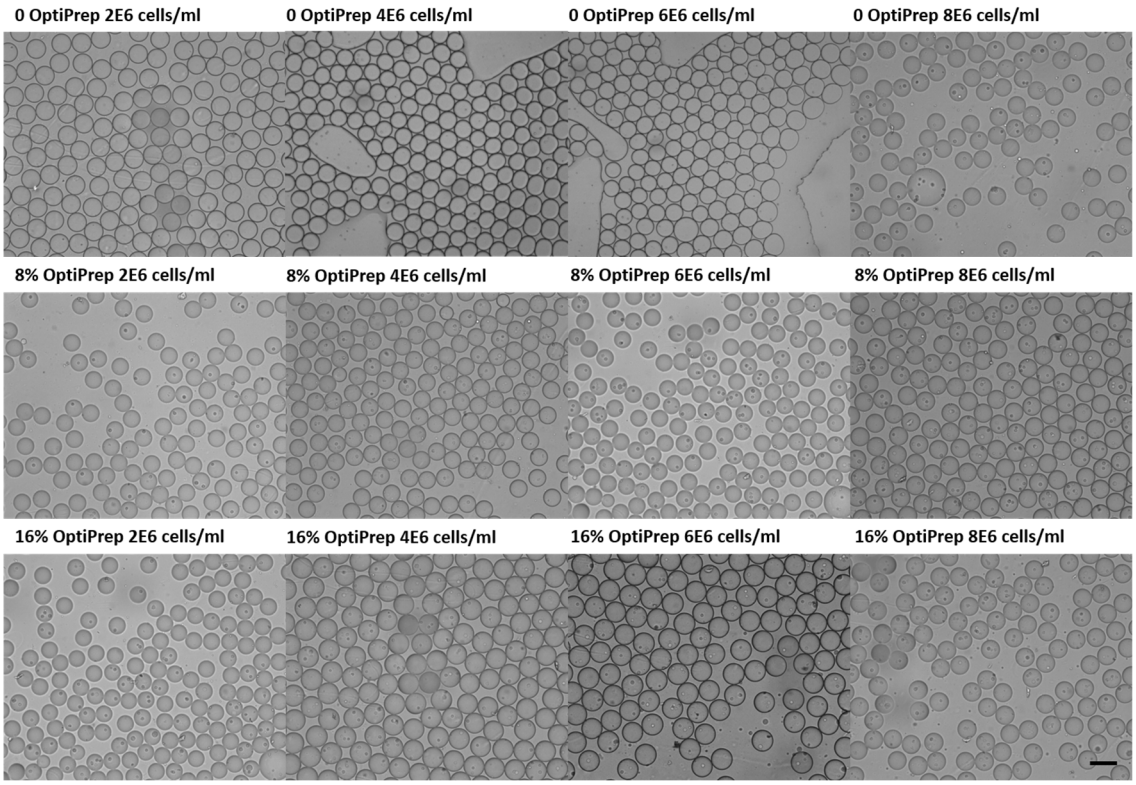

Figure S3.3 Actual images of cells encapsulated within microdroplets under different conditions. Experimental images of cell encapsulation in microdroplets under four different cell concentrations (2×10^6, 4×10^6, 6×10^6 and 8×10^6 cells/mL) and three different OptiPrep™ concentrations (0%, 8% and 16%). Scale bar = 100 µm.

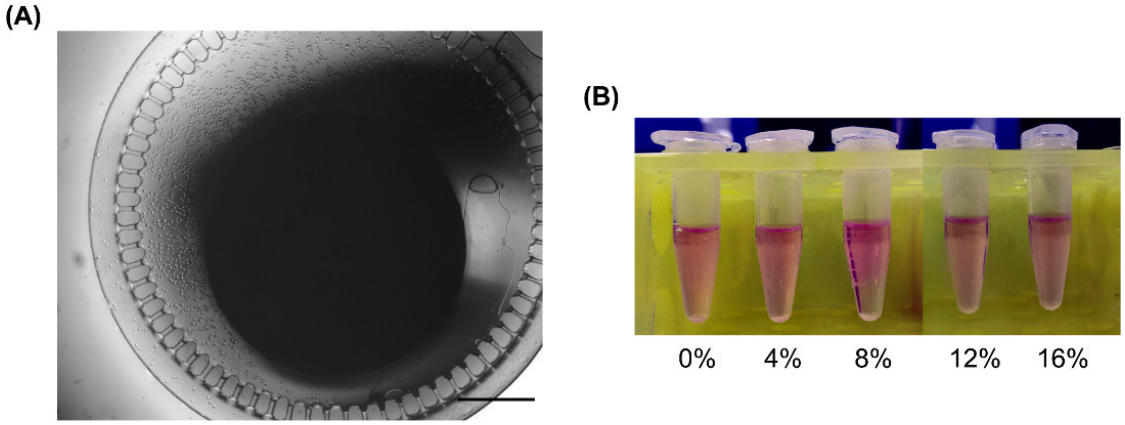

Figure S3.4. A photograph of cell sedimentation at the inlet of a microchannel. Cell sedimentation after 30 min in suspensions containing OptiPrep™ at different concentrations. (**A**) A photograph of cell sedimentation at the inlet of a microfluidic channel. Scale bar = 500 µm. (**B**) Cell sedimentation in culture media with OptiPrep™ at different concentrations of 0%, 4%, 8%, 12% and 16% (from left to right).

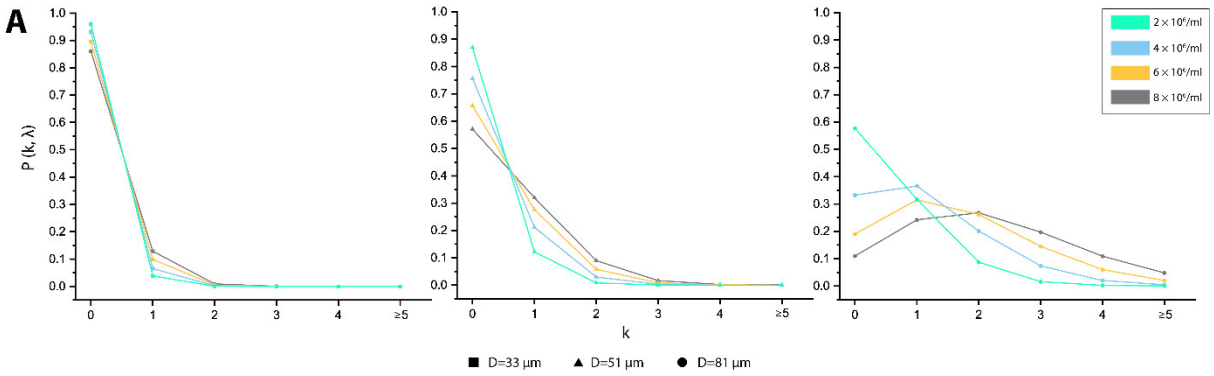

Figure S3.5. The plots of Poisson distribution for droplets of three different sizes (33, 51 and 81 μm). Four cell concentrations (2×10^6, 4×10^6, 6×10^6 and 8×10^6 cells/mL) were used to represent different λ values, and probabilities of droplets capturing different numbers of cells (0, 1, 2, 3, 4 and ≧ 5) were shown.

Table S3.1. Poisson statistics for different cell concentrations and droplet sizes

Cell Conc (cells/mL)	Droplet Size (μm)	λ	Empty	1	2	3	4	5
8.0E + 06	32.8	0.148	0.861	0.129	0.010	0.000	0.000	0.000
6.0E + 06	32.8	0.111	0.896	0.099	0.005	0.000	0.000	0.000
4.0E + 06	32.8	0.074	0.932	0.065	0.002	0.000	0.000	0.000
2.0E + 06	32.8	0.037	0.961	0.038	0.001	0.000	0.000	0.000
8.0E + 06	51.2	0.562	0.571	0.320	0.090	0.017	0.002	0.000
6.0E + 06	51.2	0.422	0.657	0.276	0.058	0.008	0.001	0.000
4.0E + 06	51.2	0.281	0.756	0.212	0.030	0.003	0.000	0.000
2.0E + 06	51.2	0.141	0.869	0.122	0.009	0.000	0.000	0.000
8.0E + 06	80.8	2.210	0.110	0.242	0.268	0.197	0.109	0.048
6.0E + 06	80.8	1.657	0.190	0.316	0.262	0.145	0.060	0.020
4.0E + 06	80.8	1.105	0.333	0.366	0.201	0.074	0.020	0.004
2.0E + 06	80.8	0.552	0.577	0.317	0.087	0.016	0.002	0.000

Table S3.2. The data collected from images of cell-laden droplets

Name	Total	Zero	One	Two	Three	Four	Five or above five
0 OptiPrep 2E6 cells/mL A	180	166	13	1	0	0	0
0 OptiPrep 2E6 cells/mL B	140	131	9	0	0	0	0
0 OptiPrep 2E6 cells/mL C	147	137	10	0	0	0	0
0 OptiPrep 4E6 cells/mL A	166	142	21	3	0	0	0
0 OptiPrep 4E6 cells/mL B	223	191	27	3	0	0	0
0 OptiPrep 4E6 cells/mL C	259	223	27	8	1	0	0
0 OptiPrep 6E6 cells/mL A	123	98	21	4	0	0	0
0 OptiPrep 6E6 cells/mL B	187	148	35	3	1	0	0
0 OptiPrep 6E6 cells/mL C	258	210	36	10	1	1	0
0 OptiPrep 8E6 cells/mL A	163	82	41	24	9	4	3
0 OptiPrep 8E6 cells/mL B	119	66	38	12	2	1	0
0 OptiPrep 8E6 cells/mL C	187	83	52	35	10	4	3
8% OptiPrep 2E6 cells/mL A	205	138	52	6	5	2	2
8% OptiPrep 2E6 cells/mL B	116	73	38	5	0	0	0
8% OptiPrep 2E6 cells/mL C	114	91	19	4	0	0	0
8% OptiPrep 4E6 cells/mL A	258	141	73	29	6	5	4
8% OptiPrep 4E6 cells/mL B	156	75	54	23	4	0	0
8% OptiPrep 4E6 cells/mL C	152	74	46	24	6	2	0
8% OptiPrep 6E6 cells/mL A	234	98	75	48	7	4	2
8% OptiPrep 6E6 cells/mL B	150	59	60	24	5	2	0
8% OptiPrep 6E6 cells/mL C	143	59	61	21	2	0	0
8% OptiPrep 8E6 cells/mL A	293	94	121	45	7	2	24
8% OptiPrep 8E6 cells/mL B	137	23	46	38	18	12	0
8% OptiPrep 8E6 cells/mL C	139	35	46	34	16	8	0
16% OptiPrep 2E6 cells/mL A	85	51	20	3	6	3	2

16% OptiPrep 2E6 cells/mL B	95	34	38	20	3	0	0
16% OptiPrep 2E6 cells/mL C	151	77	49	18	6	1	0
16% OptiPrep 4E6 cells/mL A	145	50	54	28	8	2	3
16% OptiPrep 4E6 cells/mL B	142	33	45	31	22	7	4
16% OptiPrep 4E6 cells/mL C	129	36	44	33	9	6	1
16% OptiPrep 6E6 cells/mL A	114	36	37	22	14	5	0
16% OptiPrep 6E6 cells/mL B	124	24	52	38	9	1	0
16% OptiPrep 6E6 cells/mL C	114	34	36	29	11	4	0
16% OptiPrep 8E6 cells/mL A	203	30	39	62	44	16	12
16% OptiPrep 8E6 cells/mL B	116	25	26	41	17	7	0
16% OptiPrep 8E6 cells/mL C	115	15	40	24	28	8	0

Author Contributions

Conceptualisation, L.J. and J.P.; methodology, L.J; validation, H.L.; formal analysis, H.L. and Y.W.; investigation, H.L.; resources, L.J. and J.P.; data curation, H.L. and Y.W.; writing—original draft preparation, H.L.; writing—review and editing, L.J. and M.L; supervision, L.J., J.P., and M.L.; project administration, L.J. and J.P.; funding acquisition, L.J. and J.P.

References

1. Schmid, A.; Kortmann, H.; Dittrich, P. S.; Blank, L. M., Chemical and biological single cell analysis. *Curr. Opin. Biotechnol.* **2010,** *21* (1), 12-20.
2. Walling, M. A.; Shepard, J. R. E., Cellular heterogeneity and live cell arrays. *Chem. Soc. Rev.* **2011,** *40* (7), 4049-4076.
3. Wilson, Nicola K.; Kent, David G.; Buettner, F.; Shehata, M.; Macaulay, Iain C.; Calero-Nieto, Fernando J.; Sánchez Castillo, M.; Oedekoven, Caroline A.; Diamanti, E.; Schulte, R.; Ponting, Chris P.; Voet, T.; Caldas, C.; Stingl, J.; Green, Anthony R.; Theis, Fabian J.; Göttgens, B., Combined single-cell functional and gene expression analysis resolves heterogeneity within stem cell populations. *Cell Stem Cell* **2015,** *16* (6), 712-724.
4. Adan, A.; Alizada, G.; Kiraz, Y.; Baran, Y.; Nalbant, A., Flow cytometry: basic principles and applications. *Crit. Rev. Biotechnol.* **2017,** *37* (2), 163-176.
5. Eyer, K.; Kuhn, P.; Hanke, C.; Dittrich, P. S., A microchamber array for single cell isolation and analysis of intracellular biomolecules. *Lab Chip* **2012,** *12* (4), 765-72.
6. Eyer, K.; Doineau, R. C. L.; Castrillon, C. E.; Briseño-Roa, L.; Menrath, V.; Mottet, G.; England, P.; Godina, A.; Brient-Litzler, E.; Nizak, C.; Jensen, A.; Griffiths, A. D.; Bibette, J.; Bruhns, P.; Baudry, J.,

Single-cell deep phenotyping of IgG-secreting cells for high-resolution immune monitoring. *Nat. Biotechnol.* **2017,** *35* (10), 977.
7. Collins, D. J.; Neild, A.; deMello, A.; Liu, A.-Q.; Ai, Y., The Poisson distribution and beyond: methods for microfluidic droplet production and single cell encapsulation. *Lab Chip* **2015,** *15* (17), 3439-59.
8. Kemna, E. W. M.; Schoeman, R. M.; Wolbers, F.; Vermes, I.; Weitz, D. A.; van den Berg, A., High-yield cell ordering and deterministic cell-in-droplet encapsulation using Dean flow in a curved microchannel. *Lab Chip* **2012,** *12* (16), 2881-2887.
9. Rotem, A.; Ram, O.; Shoresh, N.; Sperling, R. A.; Schnall-Levin, M.; Zhang, H.; Basu, A.; Bernstein, B. E.; Weitz, D. A., High-Throughput Single-Cell Labeling (Hi-SCL) for RNA-Seq Using Drop-Based Microfluidics. *PLoS ONE* **2015,** *10* (5), e0116328.
10. Sollier, E.; Amini, H.; Go, D. E.; Sandoz, P. A.; Owsley, K.; Di Carlo, D., Inertial microfluidic programming of microparticle-laden flows for solution transfer around cells and particles. *Microfluid. Nanofluidics* **2015,** *19* (1), 53-65.
11. Pertoft, H., Fractionation of cells and subcellular particles with Percoll. *J. Biochem. Biophys. Methods* **2000,** *44* (1-2), 1-30.
12. Bolstad, B.; Borch, K. W.; Grynne, B. H.; Lundby, B.; Nossen, J. O. E.; Kloster, Y. F.; Kristoffersen, D. T.; Andrew, E., Safety and tolerability of iodixanol: a dimeric, nonionic contrast medium: an emphasis on European clinical phases I and II. *Invest. Radiol.* **1991,** *26*, S201-S204.
13. Van Veldhoven, P. P.; Baumgart, E.; Mannaerts, G. P., Iodixanol (Optiprep), an improved density gradient medium for the iso-osmotic isolation of rat liver peroxisomes. *Anal. Biochem.* **1996,** *237* (1), 17-23.
14. Graham, J. M.; Higgins, J. A.; Gillott, T.; Taylor, T.; Wilkinson, J.; Ford, T.; Billington, D., A novel method for the rapid separation of plasma lipoproteins using self-generating gradients of iodixanol. *Atherosclerosis* **1996,** *124* (1), 125-135.
15. Cantin, R.; Diou, J.; Bélanger, D.; Tremblay, A. M.; Gilbert, C., Discrimination between exosomes and HIV-1: purification of both vesicles from cell-free supernatants. *J. Immunol. Methods* **2008,** *338* (1-2), 21-30.
16. Dettenhofer, M.; Yu, X. F., Highly purified human immunodeficiency virus type 1 reveals a virtual absence of Vif in virions. *J. Virol.* **1999,** *73* (2), 1460-1467.
17. Mita, A.; Ricordi, C.; Miki, A.; Barker, S.; Khan, A.; Alvarez, A.; Hashikura, Y.; Miyagawa, S.; Ichii, H., Purification method using iodixanol (OptiPrep)-based density gradient significantly reduces cytokine chemokine production from human islet preparations, leading to prolonged beta-cell survival during pretransplantation culture. *Transplant. Proc.* **2009,** *41* (1), 314-5.
18. Singh, M.; Ugozzoli, M.; Briones, M.; Kazzaz, J.; Soenawan, E.; O'Hagan, D. T., The effect of CTAB concentration in cationic PLG microparticles on DNA adsorption and in vivo performance. *Pharm. Res.* **2003,** *20* (2), 247-251.
19. BØYum, A., Isolation of Human Blood Monocytes with Nycodenz, a New Non-Ionic Iodinated Gradient Medium. *Scand. J. Immunol.* **1983,** *17* (5), 429-436.
20. Rickwood, D.; Birnie, G. D., Metrizamide, a new density-gradient medium. *FEBS Lett.* **1975,** *50* (2), 102-110.
21. Mousset-Siméon, N.; Rives, N.; Masse, L.; Chevallier, F.; Mace, B., Comparison of six density gradient media for selection of cryopreserved donor spermatozoa. *J. Androl.* **2004,** *25* (6), 881-884.
22. Farinas, J.; Chow, A. W.; Wada, H. G., A microfluidic device for measuring cellular membrane potential. *Anal. Biochem.* **2001,** *295* (2), 138-142.
23. Allazetta, S.; Kolb, L.; Zerbib, S.; Bardy, J. a.; Lutolf, M. P., Cell-Instructive Microgels with Tailor-Made Physicochemical Properties. *Small* **2015,** *11* (42), 5647-5656.
24. Headen, D. M.; García, J. R.; García, A. J., Parallel droplet microfluidics for high throughput cell encapsulation and synthetic microgel generation. *Microsyst. Nanoeng.* **2018,** *4*, 17076.
25. Ma, T.; Gao, X.; Dong, H.; He, H.; Cao, X., High-throughput generation of hyaluronic acid microgels via microfluidics-assisted enzymatic crosslinking and/or Diels–Alder click chemistry for cell encapsulation and delivery. *Appl. Mater. Today* **2017,** *9*, 49-59.
26. Mazutis, L.; Gilbert, J.; Ung, W. L.; Weitz, D. A.; Griffiths, A. D.; Heyman, J. A., Single-cell analysis and sorting using droplet-based microfluidics. *Nat. Protoc.* **2013,** *8* (5), 870-91.
27. Lan, F.; Demaree, B.; Ahmed, N.; Abate, A. R., Single-cell genome sequencing at ultra-high-throughput with microfluidic droplet barcoding. *Nat. Biotechnol.* **2017,** *35* (7), 640-646.
28. Shahi, P.; Kim, S. C.; Haliburton, J. R.; Gartner, Z. J.; Abate, A. R., Abseq: Ultrahigh-throughput single cell protein profiling with droplet microfluidic barcoding. *Sci. Rep.* **2017,** *7* (1), 44447.
29. Katta, V. R.; Goss, L. P.; Roquemore, W. M., Numerical investigations of transitional H2/N2 jet diffusion flames. *AIAA J.* **1994,** *32* (1), 84-94.
30. Waite, A.; Fisher, A.; Thompson, P. A.; Harrison, P. J., Sinking rate versus cell volume relationships illuminate sinking rate control mechanisms in marine diatoms. *Mar. Ecol. Prog. Ser.* **1997,** *157*, 97-108.

31. Crowder, T. M.; Rosati, J. A.; Schroeter, J. D.; Hickey, A. J.; Martonen, T. B., Fundamental effects of particle morphology on lung delivery: predictions of Stokes' law and the particular relevance to dry powder inhaler formulation and development. *Pharm. Res.* **2002,** *19* (3), 239-245.
32. Bryan, A. K.; Hecht, V. C.; Shen, W.; Payer, K.; Grover, W. H.; Manalis, S. R., Measuring single cell mass, volume, and density with dual suspended microchannel resonators. *Lab Chip* **2014,** *14* (3), 569-576.
33. Saias, L.; Gomes, A.; Cazales, M.; Ducommun, B.; Lobjois, V., Cell–cell adhesion and cytoskeleton tension oppose each other in regulating tumor cell aggregation. *Cancer Res.* **2015,** *75* (12), 2426-2433.
34. Cheung, K. J.; Ewald, A. J., A collective route to metastasis: Seeding by tumor cell clusters. *Science* **2016,** *352* (6282), 167-169.

Chapter 4 Microdroplet enabled cultivation of single yeast cells correlates with bulk growth and reveals subpopulation phenomena*

* **Liu, H.**; Xu, X.; Peng, K.; Zhang, Y.; Jiang, L.; Williams, T. C.; Paulsen, I. T.; Piper, J. A.; Li, M., Microdroplet enabled cultivation of single yeast cells correlates with bulk growth and reveals subpopulation phenomena. *Biotechnology and Bioengineering* **2021**, 118: 647– 658.

To achieve the ultimate goal of selecting rare yeast cells with desirable phenotypes it is first important to prove the capability of microdroplets for maintaining yeast cell growth and physiology at the single-cell level. This chapter compares single yeast cell growth under various scenarios using microdroplets as bioreactors with growth in bulk. Moreover, yeast cell viability in microdroplets over long-term culture is measured.

4.1 Introduction

Yeast has been widely used as a "cell factory" in industrial fermentation processes to produce a wide range of valuable products, including organic acids that are used extensively in manufacturing, pharmaceutical, cosmetic, food, textile and chemical industries[1-5]. Compared to conventional chemical methods for the production of organic acids based on fossil fuel reserves, microbial production is an attractive approach due to several advantages including sustainability, less environmental pollution and cost-effectiveness[6, 7]. Unlike other hosts that are recalcitrant to genetic manipulation[8, 9], baker's yeast (*S. cerevisiae*) is an ideal organism to discover new gene targets for productivity enhancement, because it is a model eukaryotic organism with high-resolution genomic data. Moreover, the tolerance of yeast to low pH

enables the production of organic acids in their protonated forms, reducing the costs of downstream recovery and purification after fermentation. Due to the economic, environmental and medical importance of organic acid production by yeast, advanced metabolic engineering and synthetic biology technologies have been applied to engineer yeast for improved production of different high-value organic acids, such as lactic acid[10], succinic acid[11], para-hydroxybenzoic acid[12], 3-hydroxypropionic acid[13] and muconic acid[14].

Yeast is also an attractive host for the production of propionic acid (PA) that is commonly used as a food preservative and a chemical intermediate, since PA can be formed as a by-product of yeast fermentation[15]. However, PA is toxic to yeast, especially at relatively low concentrations, causing an important problem of tolerance engineering in yeast PA production. Fortunately, Xu et al.[16] demonstrated significant improvements in yeast tolerance to PA using adaptive laboratory evolution (ALE), a powerful tool in the field of metabolic engineering for the development of superior industrial microbial strains[17-19].

ALE experiments are lab-intensive and time-consuming however, requiring evaluation of growth kinetics of intermediate populations and numerous candidate strains to select an ideal strain with improved phenotypes. The evolution process might be performed over hundreds of generations, and the traditional growth test based on optical density (OD) measurements must be conducted over three repetitions for each population or strain. Moreover, the process lacks the ability to track the growth of yeast at a single-cell level, and cannot consider cell size, morphology and viability that may change during growth. Thus, cell-to-cell variations are obscured and the ability to screen and select single cells with desired characteristics (e.g., high growth rate, high tolerance to acids and high secretion of valuable bio-products) is limited.

In order to address these limitations, an alternative approach is required to quantitatively track the growth of individual cells within a population without perturbation and allows parallel, high-throughput assessment at a single-cell level. Microfluidics can compartmentalise single

cells within monodisperse picolitre-sized droplets in a cost-effective and high-throughput process, for example, screening of 5×10^7 individual reactions requires only 150 μL of reagents and seven hours at an estimated cost of only a few dollars, as demonstrated by Agresti et al.[20]. Over the past decades, droplet microfluidics has enabled single-cell analysis for a wide range of applications across biological science, biomedicine and biochemistry[20-22]. This is because (1) the extracellular environments are accurately mimicked[23, 24]; (2) the genotype-phenotype linkages are established at a single-cell level[25-28] ; (3) the miniaturised confinement improves the detection limit[20, 29]; and (4) massive parallel analysis can be conducted to probe cellular heterogeneity[30-34].

In this study, we quantitatively tracked the growth of single yeast cells under varying conditions by using monodisperse microdroplets. In order to demonstrate the versatility of the microdroplet platform, we used two species of yeast, *S. cerevisiae* (*S. cerevisiae*) and *Pichia pastoris* (*P. pastoris*), and a total of four strains, wild-type *S. cerevisiae* strain (CEN.PK113-7D), the PA evolved mutant *S. cerevisiae* strain (PA-3), GFP-tagged *S. cerevisiae* strain (CEN.PK2-1C-GFP) and GFP-tagged *P. pastoris* strain (CBS7435-GFP). The effects of organic acids, PA and acetic acid (AA), at different concentrations on the growth of yeast at the single-cell level were studied, as well as the effect of K-ions on PA tolerance in yeast. The calculated specific growth rate (μ) of single yeast grown in microdroplets was effectively identical to that for cells in bulk cultures at a pH of 3.5, and yeast cells maintained high viability in microdroplets after 48 hours of culture.

4.2. Materials and Methods

4.2.1 Fabrication of microfluidic devices

The T-junction microfluidic device used in this study consists of two inlets for infusing the disperse (aqueous) phase and continuous (oil) phase, respectively, one outlet for transporting

microdroplets into the collection tube and one rectangular chamber for observation of cell-laden microdroplets. A corona-shaped filter was designed at the inlets to prevent any possible dust entry. The connecting microchannels have an aspect ratio of height/width = 4:5 (height: ~40 μm; width: ~50 μm), and the rectangular observation chamber dimensions of 1.4 × 0.65 cm (Fig. S4.1 & Fig. S4.2).

This droplet-based microfluidic device was fabricated from a silicon wafer patterned with SU-8 mould (SU-8 2035, MicroChem, Newton, MA, USA) using standard soft-lithography techniques[35]. Degassed PDMS (Sylgard 184, Dow Corning, Midland, MI, USA) in liquid form prepared by mixing the base and curing agent at a ratio of 10:1 was poured onto the SU-8 mould and cured in an oven at 80 °C for two hours. Then the PDMS slab with microchannels was peeled off from the mould and the fluidic access holes were created using PDMS biopsy puncher with an outer diameter of 1.5 mm. After cleaning the channel side of PDMS with scotch tape, isopropanol and DI water in order, the PDMS slab and a standard glass slide was treated using an oxygen plasma cleaner to increase the surface energy and immediately pressured to each other for an irreversible bonding. Lastly, the channel was rendered hydrophobic by infusing with 0.02 % Trichloro(octadecyl)silane (OTS, 104817, Sigma-Aldrich, St. Louis, MO, USA) in isopropanol for 5 mins and drying with nitrogen gas followed by drying in an oven at 100 °C for 10 mins.

4.2.2 Cell preparation

We used a total of four yeast strains, the haploid *S. cerevisiae* strain (CEN.PK113-7D), the PA evolved mutant *S. cerevisiae* strain (PA-3), GFP-tagged *S. cerevisiae* strain (CEN.PK2-1C-GFP) and GFP-tagged *P. pastoris* strain (CBS7435-GFP) in the single-cell growth assays (Table S4.1).

CEN.PK113-7D and PA-3 were grown overnight at 30 °C, 200 rpm in 5 mL buffered minimal medium. The overnight culture was washed twice and re-inoculated into 5 mL

buffered minimal medium at three different concentrations of PA: 15 mM, 25 mM and 35 mM. To investigate the effect of K-ions on the tolerance to PA in yeast, CEN.PK2-1C-GFP was pre-cultured overnight at 30 °C, 200 rpm in synthetic drop-out medium, without uracil (contains 1× yeast nitrogen base (YNB) without amino acids mix (Y0626, Sigma-Aldrich, St.Louis, MO, USA), 1% glucose and Yeast Synthetic Drop-out Medium Supplements without uracil (Y1501, Sigma-Aldrich, St.Louis, MO, USA)). Cells were washed twice and re-inoculated into 5 mL uracil drop-out medium containing defined concentrations of potassium (1× translucent K^+ free YNB, 1% glucose, and 0, 1, 10 and 50 mM potassium chloride), supplemented with or without 25 mM PA. CBS7435-GFP was pre-cultured overnight in the same drop-out medium as the one used for CEN.PK2-1C-GFP at 25 °C, 200 rpm, and the culture was washed twice and re-inoculated into 5 mL uracil drop-out medium. All the cultures were reinoculated at an initial OD_{600} of 0.2. Before injecting cell suspensions into the microfluidic device, we also counted the number of cells using hemocytometer (Boeco, Hamburg, Germany) to ensure that cell concentration is about 3×10^6 cells/mL.

4.2.3 Generation and storage of microdroplets

In the T-shaped droplet generator of 50 × 50 μm (width × depth), continuous phase flowed to the observation chamber and the disperse phase flowed and sheared at the interface to generate monodisperse microdroplets with a diameter of ~65 μm. Continuous phase used here was Novec™ 7500 Engineered Fluid (3M, St. Paul, MN, USA) containing 2% Pico-Surf™ 1 (Sphere Fluidics, Cambridge, UK). Disperse phase used here was culture medium added with 20% OptiPrep™ (D1556, Sigma-Aldrich, St. Louis, MO, USA). Cells were diluted to an OD_{600} of 0.1 for the disperse phase. Two syringe pumps (Fusion 100, Chemyx, Stafford, TX, USA) were used to inject the two phases, respectively. When the ratio of the flow rates of the two phases reached 4:1 (continuous phase: 16 μL/min vs disperse phase: 4 μL/min), ~ 144 pL monodisperse microdroplets were created in a high-throughput fashion (~116 droplets per

second). By Poisson distribution, this size of droplet can ensure substantial droplets containing single cells (28.0%) and maintain relatively low ratio of droplets containing two cells (6.0%) and less than 1.0% droplets containing more than two cells, and the rest 65.0% droplets are empty (Fig. S4.3). A FEP tubing (IDEX, Lake Forest, IL, USA) with an inner diameter of 0.5 mm was used to transfer microdroplets into a 2 mL Eppendorf™ safe-lock tube (Hamburg, Germany) pre-filled with 100 µl continuous phase (Fig. S4.4).

4.2.4 Image acquisition and analysis

An initial observation of microdroplets containing single cells was performed at a rectangular chamber of the microdevice before microdroplets were transported into the collection tube. Bright-field snapshots of the generated microdroplets were captured by a digital camera (DS-Qi1Mc, Nikon, Tokyo, Japan) installed on an inverted microscope (Eclipse Ti-U, Nikon, Tokyo, Japan). After images were taken, the number of cells per droplet was counted using ImageJ® (NIH, Bethesda, MD, USA). In order to avoid errors when counting the number of *S. cerevisiae* cells that formed cell clusters in the droplets, we dropped 10 µL of oil on the hydrophobic glass slides, spread 1 µL of droplets onto the oil, and covered this mixture with coverslips. Such gentle manipulation enables droplets to be squeezed into a thin flat layer, resulting in a monolayer of cells in the droplets, therefore, the number of cells per droplet could be easily counted.

To quantify the growth of single yeast cells, the values for the specific growth rate µ were determined based on the number of counted cells per droplet at hourly time points up to 10 hours. The number of cells per droplet (N) was converted into the logarithmic scale as ln(N), and the estimation of the biokinetic constant, µ, over time of culture, t, was obtained by the equation below:

$$\mu = \frac{dln(N)}{dt} \quad (1)$$

To determine whether the single yeast cells in droplets possess similar growth behaviour to those in bulk culture, the number of cells per droplet at each time points were fitted by nonlinear regression to a sigmoidal logistic function using OriginPro 2019 program (OriginLab Co., Northampton, MA, USA)

$$y = {a}/{1 + e^{-k(x-x_c)}} \quad (2)$$

where a is the maximum value of the sigmoid, x_c is the midpoint, and k is the coefficient.

Fluorescence images of GFP-tagged cells were obtained at FITC channel by a confocal microscope FV3000 (Olympus, Tokyo, Japan). The number of yeast cells in a complex cluster were more easily counted from the fluorescence images compared to bright-field images. Regarding uncountable agglomeration, images of eight slices were stacked up and the corresponding fluorescence intensity was measured by ImageJ®. The image processing includes the following four main steps: 1) the bit depth of images was reduced to 8 bits; 2) area of each droplet was recognised; 3) The threshold was set by Yen's algorithm to remove noise; and 4) “limit to threshold” was chosen and the mean fluorescence intensity within the area of each droplet was measured.

4.2.5 Cell viability test

To measure the viability of yeast cells in microdroplets, live/dead staining tests were performed at three selected time points: before encapsulation, at 24 hours of culture and 48 hours of culture. At each time point, 50 µl emulsion microdroplets in oil were collected into a centrifuge tube, and 2 µL Pico-Break™ (Sphere Fluidics, Cambridge, UK) was added subsequently to release yeast cells from the microdroplets. After a short centrifugation at 2000 rpm for 30 s, the oil phase was kept at the bottom and the supernatant was transferred into a new centrifuge tube. 30 µl staining solution consisting of 2 µM SYTO 9 (Thermo Fisher Scientific, Waltham, MA, USA) and 4 µM EthD-III (Biotium, Hayward, Ca, USA) was added into the suspension of released yeast and co-cultured for 20 mins. Fluorescence images were

taken when excited at a wavelength of ~495 nm and ~530 nm, respectively: live cells showed green fluorescence in ~515 nm channel while dead cells showed red fluorescence in ~635 nm channel and yellow colour in merged images. The cell viability over time was tested based on three random frames for each measurement, and a total of 100 cells were tested for each measurement. The viability test results were analysed by one-way repeated measures analysis of variance (ANOVA) to determine whether a significant difference was existed among different time points.

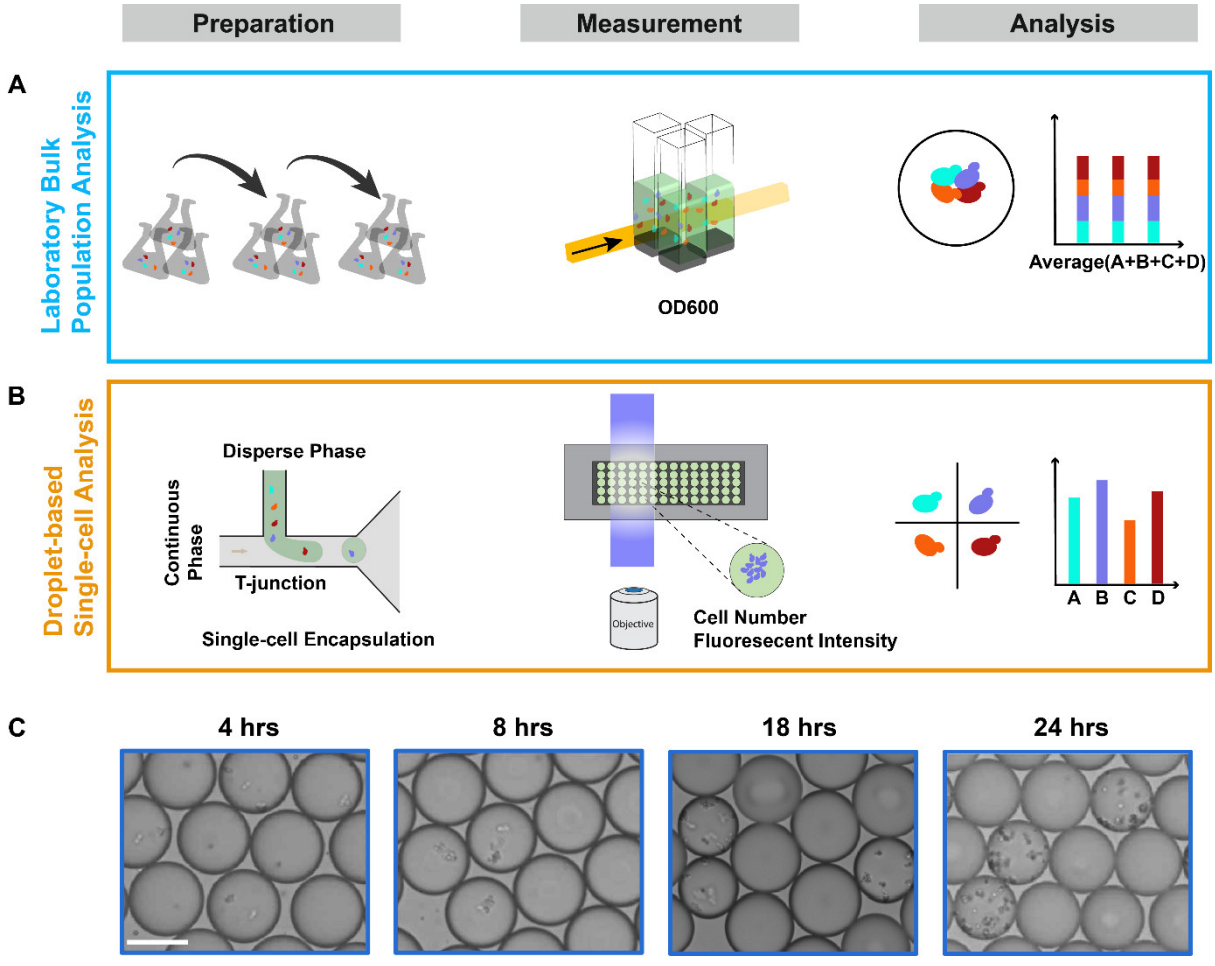

Figure 4.1 Schematic illustration of conventional laboratory approach (A) and droplet-based microfluidics (B) for tracking the growth of yeast at population level and the single-cell level, respectively. (C) Bright-field microscope images of CEN.PK 113-7D growth without organic acid stress in ~144 pL microdroplets. Scale bar = 50 µm.

3. Results and Discussion

4.3.1 The encapsulation and cultivation of single yeast cells

Similar to the standard method used to measure the average growth rate of bulk populations, the procedure for the microfluidic droplet technique used in this study to measure the growth of single yeast cells includes three main steps: 1) preparation, 2) measurement and 3) analysis (Figs. 4.1A and 4.1B). 1) Uniformly distributed microdroplets containing single cells and a small volume of culture medium, subject to a range of different environmental conditions, are generated; 2) the number of cells per droplet and fluorescence intensity of GFP-tagged cells are tracked as cells grow over time; and 3) the growth rate of each cell within the microdroplet is obtained and single-cell growth under varying environmental conditions (with PA, AA and K-ions at different concentrations) is investigated and compared.

Before cell encapsulation within microdroplets, the overnight culture and preculture protocols were successively performed to ensure yeast cells were rapidly proliferating but this also results in an asynchronous culture, containing single cells, single cells with small buds, and cells with large buds. In practise, the budded cells were counted as single cells when the buds did not exceed the one-half the size of the mother cell. Cell concentration was diluted to 3×10^6 cells/mL with fresh medium and density-matching reagent to ensure the substantial majority (~80.0%) of cell-laden droplets contained just one cell (Fig S4.3). According to the Poisson distribution, this concentration of cells theoretically maintains high efficiency of single-cell encapsulation[24]. It is worth noting that under these conditions the majority (65.0%) of droplets do not contain any cells. The density-matching reagent used here is 20% OptiPrep™, which prevents the sedimentation of yeast cells at the inlet and guarantees the neutral buoyancy of cell suspensions for ~30 mins[36]. The asynchronous nature of the cell population combined with the small statistical probability for more than one cell per droplet leads inevitably to some experimental uncertainties in measured cell growth notionally arising from a single cell origin.

The growth of single *S. cerevisiae* CEN.PK 113-7D cells in ~ 144 pL microdroplets without acid stress is illustrated by the images of Fig. 4.1C. After culture of 18 hrs, the droplets shrank from ~ 144 pL (empty droplets) to ~ 65 pL (yeast-containing droplets) driven by osmosis. The yeast cells kept consuming the glucose from the medium in droplets and the continuous phase is slightly permeable to water, allowing a net diffusion of water through the oil into droplets of higher osmolarity[37-39]. No significant size differences were detected between the same types of droplets. Apart from this, the yeast-containing droplets cells did not experience any noticeable disruption, such as merging and burst, after long-term storage, thus the single yeast growth can be quantitatively and accurately tracked over 24 hours within this type of droplet. Noteworthy, to ensure the encapsulated cells can grow with sufficient oxygen, fluorinated oil was used to give high oxygen permeability so as to avoid anaerobic cultivation. Moreover, nutrient-rich fresh medium was used within droplets, to provide enough nutrients for single-cell growth within the timeframe of the measurements.

4.3.2 The effect of acid stress on the growth of single wild-type *S. cerevisiae* cells

First, we tracked the growth of the single *S. cerevisiae* CEN.PK 113-7D cells in ~144 pL microdroplets without acid stress over 24 hours. In Fig. 4.2A, we plotted the number of cells per droplet at a logarithmic scale based on the first ten hours of culture, assumed during exponential phase. The μ_{max} for single *S. cerevisiae* cells in microdroplets was calculated to be 0.23 h^{-1}, identical to that reported for bulk populations (0.21 h^{-1}) within experimental uncertainty. Then we plotted the number of cells per droplet at eight selected time points: 0 hr, 2 hrs, 4 hrs, 6 hrs, 8 hrs, 10 hrs, 18 hrs and 24 hrs (Fig. 4.2B). In general, the number of cells per droplet increases over time: single yeast cells (at 0 hrs) grow to 3.2 ± 1.4 cells at 2 hrs, 5.7 ± 2.0 cells at 4 hrs, 8.7 ± 2.2 cells at 6 hrs, 11.6 ± 2.7 cells at 8 hrs, 14.6 ± 3.1 cells at 10 hrs, 42.2 ± 7.0 cells at 18 hrs and 50.0 ± 8.0 cells at 24 hrs. The number of cells per droplet is seen

to increase monotonically over time, but with an increasing spread of cell-counts for the later time (18 hrs and 24 hrs). Also, the heterogeneity in the proliferation of single yeast cells is

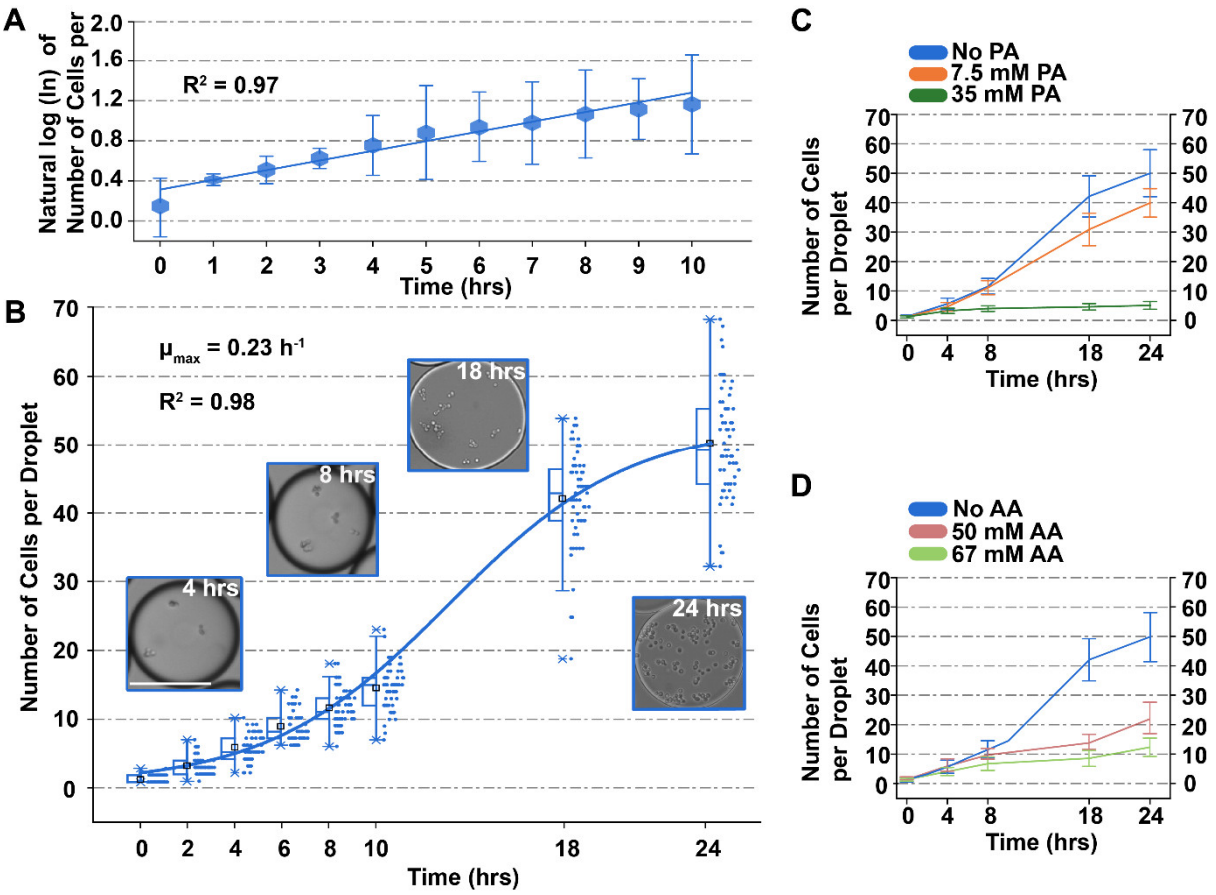

Figure 4.2 The growth of single wild-type *S. cerevisiae* (CEN.PK 113-7D) cells in microdroplets over 24 hours under different concentrations of organic acids: PA (0 mM, 7.5 mM and 35 mM) and AA (0 mM, 50 mM and 67 mM). (A) Plots of the natural logarithms of the number of cells per droplets at every hour without acid stress over the culture of 10 hrs. The coefficient of determination (R^2) is 0.97 for the linear fit. (B) Plots of the number of cells per droplet without acid stress at eight selected time points: 0 hr, 2 hrs, 4 hrs, 6 hrs, 8 hrs, 10 hrs, 18 hrs and 24 hrs. 60 cell-laden droplets were measured for each time point. The top and bottom edges of the box refer to the 25th and 75th percentiles, the cross line represents the median value, the black square represents the mean value, the whiskers extend to 1.5 times the interquartile range (IQR) and the asterisks represent upper and lower limits. The μ_{max} was calculated as 0.23 h^{-1}. The R^2 is 0.98 for the fitted growth curve. Scale bar = 50 μm. (C, D) Comparison of the growth of single CEN.PK 113-7D cells at different concentrations of (C) PA: 0 mM, 7.5 mM and 35 mM, and (D) AA: 0 mM, 50 mM and 67 mM. 60 cell-laden droplets were measured for each time point and for each condition.

demonstrated (Fig. S4.5). At 24 hrs, a small portion (i.e., 5.0%) of microdroplets contain more than 60 cells, whereas another small proportion (i.e., 6.7%) of microdroplets has less than 40 cells. This is evidence of subpopulations exhibiting diverse traits that are obscured in bulk assays at the population level. It is noteworthy that after the culture of 18 hrs, the amount of yeast cells in droplets altered slightly compared to the previous growth, indicating that the yeast cells had reached the stationary phase due to the scarce nutrient and limited space. Droplet size can be tuned to enable different scales of cell culture and has been seen in other studies[37, 40].

Secondly, we investigated the effect of acid stress on cell growth by tracking and comparing the growth of single *S. cerevisiae* cells with the addition of PA (at 7.5 mM and 35 mM, Fig. 4.2C) and AA (at 50 mM and 67 mM, Fig. 4.2D). The study of yeast growth and responses to PA and AA is of great importance, because PA is a valuable organic acid produced by yeast during fermentation, and AA is a main growth inhibitor found in lignocellulose hydrolysate for lignocellulose-based biofuel production. Experimental results show that microdroplets enable cell growth in all conditions. In more detail, at 7.5 mM PA, single cells in microdroplets grow to 31.0 ± 5.5 and 40.0 ± 4.8 cells, respectively, at 18 hrs and 24 hrs; while at 35 mM PA, single cells grow to 3.1 ± 1.4 cells at 18 hrs and 3.8 ± 1.4 cells at 24 hrs (Fig. 4.2C). At 50 mM AA, single cells in microdroplets grow to 13.9 ± 2.6 and 22.0 ± 5.84 cells, respectively, at 18 hrs and 24 hrs; while at 67 mM AA, single cells grow to 8.6 ± 2.7 cells at 18 hrs and 12.4 ± 3.1 cells at 24 hrs (Fig. 4.2D). Moreover, we found that growth of single *S. cerevisiae* cells responds sensitively to both acids, and cell numbers per droplet decrease as the concentration of acids increases. At 24 hrs, the number of yeast cells per microdroplet under 7.5 mM PA (40.0 ± 4.8 cells) and 35 mM PA (3.8 ± 1.4 cells) declined, respectively, to 80.0% and 7.6% of that for no acid control (50.0 ± 8.0 cells) (Fig. 4.2C). Additionally, at 24 hrs, the number of yeast cells per microdroplet decreased to 44.0% (22.0 ± 5.84 cells) and 24.8% (12.4 ± 3.1 cells) of cell number of the control group (no AA), respectively, when the concentration of AA

increased to 50 mM and 67 mM (Fig. 2D). It is noteworthy that only the number of cells per droplet with the addition of 7.5 mM PA can be well fitted to sigmoid growth curve, indicating the low concentration of PA, like 7.5 mM, did not affect yeast growth much but the high concentration of that, like 35 mM, and AA will impose negative effect since the beginning of cell growth. We also compared the values of μ between cell cultures in microdroplets ($\mu_{droplet}$) and in bulk (μ_{bulk}) under different concentrations of PA (Table S4.2). These results indicate that the growth and physiology of single cells in microdroplet experience the same trend with those of yeast populations grown in bulk[16], although microdroplet culture reveals subpopulation phenomena that are obscured by population average measurements.

4.3.3 The effect of K^+ on the growth of single GFP-tagged *S. cerevisiae* cells

Since biochemical assays are typically measured using fluorescence detection techniques, we investigated the growth of fluorescent GFP-tagged *S. cerevisiae* strain (CEN.PK2-1C) to demonstrate the capability of our platform for fluorescence-based quantification and detection of single-cell features. Both bright-field and fluorescence images show that the number of fluorescent cells per droplet increases over time (Figs. 4.3A and 4.3B). We counted the number of cells per droplet (Fig. 4.3C) and measured the total fluorescence intensity of cells per droplet (Fig. 4.3D) at five selected time points: 2 hrs, 6 hrs, 10 hrs, 18 hrs and 24 hrs. The data shows that growth from single cells has a high degree of variability: although the average cell number per droplet is 14.4 ± 3.3 cells at 24 hrs, a few microdroplets (i.e., 3.3%) contain more than 20 cells, whereas some microdroplets (i.e., 15.0%) contain less or equal to 10 cells. This is further evidence of cellular subpopulation with different growth growth rates which are obscured in bulk assays. Moreover, we plotted the total fluorescence intensity of cells per droplet versus the number of cells per droplet (see Fig. S4.6). As expected, the fluorescence intensity of cell-laden droplets increases with the number of cells per droplet, thus the fluorescence measurement can be used to quantify cell growth as well. In *S. cerevisiae*, potassium uptake

has been shown to stabilise membrane potential, and mediate intracellular pH, protein synthesis and function[41-43]. In previous studies, potassium supplementation was also demonstrated to be beneficial to PA-tolerance behaviours of *S. cerevisiae*[16]. We firstly tracked the growth of single

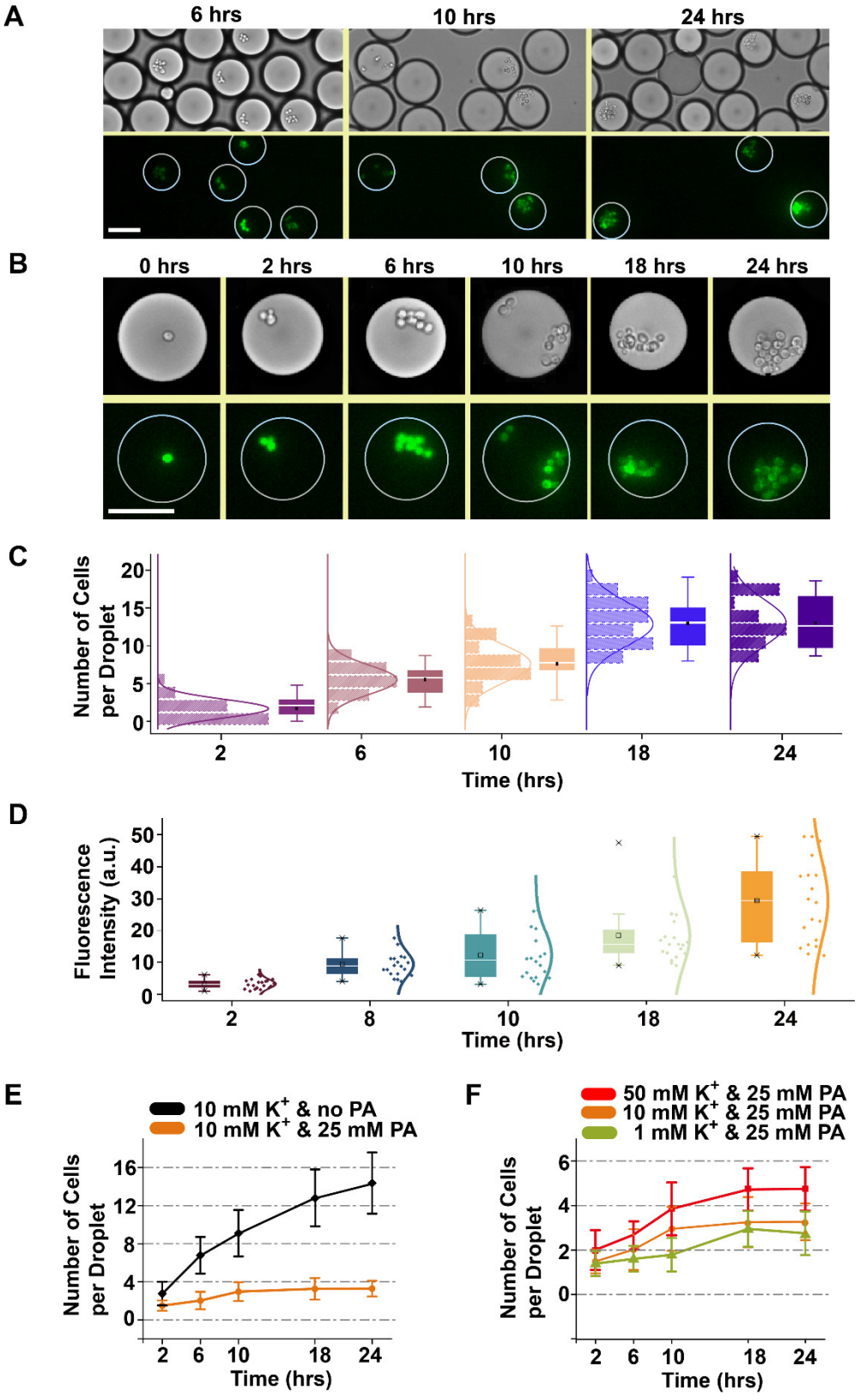

Figure 4.3 The growth of single CEN.PK2-1C cells in microdroplets over 24 hours under different concentrations of K^+ (1 mM, 10 mM and 50 mM) with (25 mM) or without PA. (A) Bright-field and fluorescence microscope images of CEN.PK2-1C growth without environmental stress in microdroplets at 6 hrs, 10 hrs and 24 hrs. Scale bar = 50 μm. (B) Enlarged bright-field fluorescence images showing the growth of CEN.PK2-1C in microdroplets over time. Scale bar = 50 μm. (C) Plots of the number of cells per droplet at five selected time points: 2 hrs, 6 hrs, 10 hrs, 18 hrs and 24 hrs. 60 cell-laden droplets for each time point were measured, and the number of cells per droplet were counted from bright-field images. The top and bottom edges of the box refer to the 25^{th} and 75^{th} percentiles, the cross line represents the median value, the black square represents the mean value and the whiskers extend to 1.5 times the IQR. (D) Plots of total fluorescence intensity of cells per droplet. 20 cell-laden droplets were measured for each time point. The top and bottom edges of the box refer to the 25th and 75th percentiles, the cross line represents the median value, the black square represents the mean value, the whiskers extend to 1.5 times the IQR and the asterisks represent upper and lower limits. (E) Comparison of the growth of single CEN.PK2-1C cells under different concentrations of K^+, 1, 10 and 50 mM, when the concentration of PA is fixed at 25 mM.

CEN.PK2-1C cells in microdroplets under a fixed potassium defined condition (10 mM K^+) with or without 25 mM PA (Fig. 4.3E). The results show that yeast growth in microdroplets was inhibited under PA stress condition when the medium contains 10 mM K^+.

We then applied another two concentrations of K^+, excessive supply of 50 mM and a scant supply of 1 mM, when the concentration of PA is fixed at 25 mM (Fig. 4.3F). Compared to the μ under 10 mM K^+ at 24 hrs, there is a 38.9% increase when 50 mM K^+ was used, and no significant decrease when the concentration of K^+ reduces to 1 mM. These results agree with the previous findings that extracellular supplementation of K^+ can increase PA tolerance in yeast, and potassium influx is important to increase organic acid tolerance in *S. cerevisiae.*

By using the GFP-tagged strain and supplementing K^+ under PA stress conditions, we have shown that single-cell culture in microdroplets demonstrates the same phenotype and

experience the same trend as bulk cultures[16], although cell-to-cell variations in proliferation are observed. We conclude therefore that the microdroplet platform can reliably quantify the effects of external factors on cell growth and complex physiology under varying conditions.

4.3.4 The growth of wild-type and PA evolved mutant *S. cerevisiae* strains

ALE has previously been employed to improve PA tolerance in yeast, and PA-3 is one of the isolated strains with increased PA tolerance after performing ALE. The non-synonymous mutation in potassium transporter encoding gene *TRK1*, has been confirmed to be the cause of the increased PA tolerance[16]. To demonstrate that microdroplets could be used to track the growth of yeast mutant strains, we monitored and compared the growth of PA evolved mutant strain (PA-3) and its parental strain (CEN.PK 113-7D) when 15 mM PA was applied (Fig. 4.4). The experimental data confirm that PA-3 grows faster and reaches a significantly higher average number of cells per droplet, i.e., 18.0 ± 3.0 cells at 24 hrs, whereas the average number of cells per droplet for wild-type strain is 5.2 ± 1.3 cells at 24 hrs (Fig. 4.4). Moreover, we have tracked and compared the growth of PA-3 and CEN.PK 113-7D in microdroplets when PA of

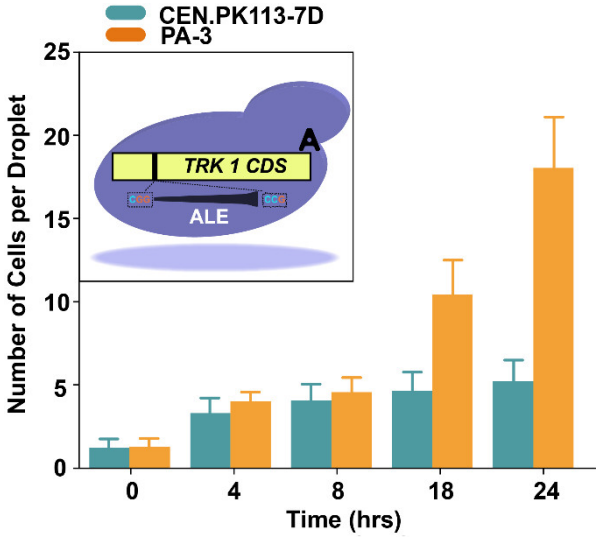

Figure 4.4 The growth of wild-type (CEN.PK 113-7D) and PA evolved mutant *S. cerevisiae* strain (PA-3) in microdroplets over 24 hours when 15 mM PA is applied. 60 cell-laden microdroplets were measured for each time point. The inset represents the causal mutation for the acquired PA tolerance identified in PA-3.

two different concentrations (25 mM and 35 mM) are applied (see Fig. S4.7). Mutant strain (PA-3) shows a higher tolerance to PA than its parental strain under all PA concentrations and the growth rate of both mutant and wild type strains are shown to decrease with the increase of PA concentration. This agrees with our previous findings when both strains are grown in bulk[16]. This result demonstrates that the microdroplet reactor approach is effective for both normal and mutant strains of *S. cerevisiae* and holds their difference in cell growth and physiology at the population level when single cells are tracked in microdroplets[16].

In addition, the $\mu_{droplet}$ and μ_{bulk} of these two strains under different concentrations of PA were compared (Table S4.2), which follow the same trend. Moreover, we noticed that value of $\mu_{droplet}$ is smaller than that of μ_{bulk} under the same external environments. This may be due to some factors, e.g., limited nutrients available to individual cells, relatively low moisture and gas permeability of surrounding environment; local accumulation of metabolic wastes; and limited capability to form clusters to resist starvation or acid stress[44-46].

4.3.5 The growth of single *P. pastoris* cells in picoliter microdroplets

In order to demonstrate that this platform can be applied to species other than *S. cerevisiae*, we tracked the growth of GFP-tagged *P. pastoris* strain (CBS7435-GFP) at a single-cell level in ~144 pL microdroplets. *P. pastoris* has a similar cell size to *S. cerevisiae*, but the proliferation behaviour is different. The CBS7435-GFP cells used here tended to aggregate and form large clusters in the microdroplets. This trait might help cells uptake more carbon source and survive environmental stress[44], but cause difficulty in counting the number of cells per droplet under microscope. The bright-field and fluorescence images (stacks of eight slices) show that single *P. pastoris* cells are able to grow in microdroplets over time (Fig. 4.5A). The distribution of total fluorescence intensity of cells per droplet at five selected time points demonstrated the variations between individual cells (Fig. 4.5B). Although some outliers exist, the growth curve of *P. pastoris* shows a similar profile over 24 hours to that of *S. cerevisiae*

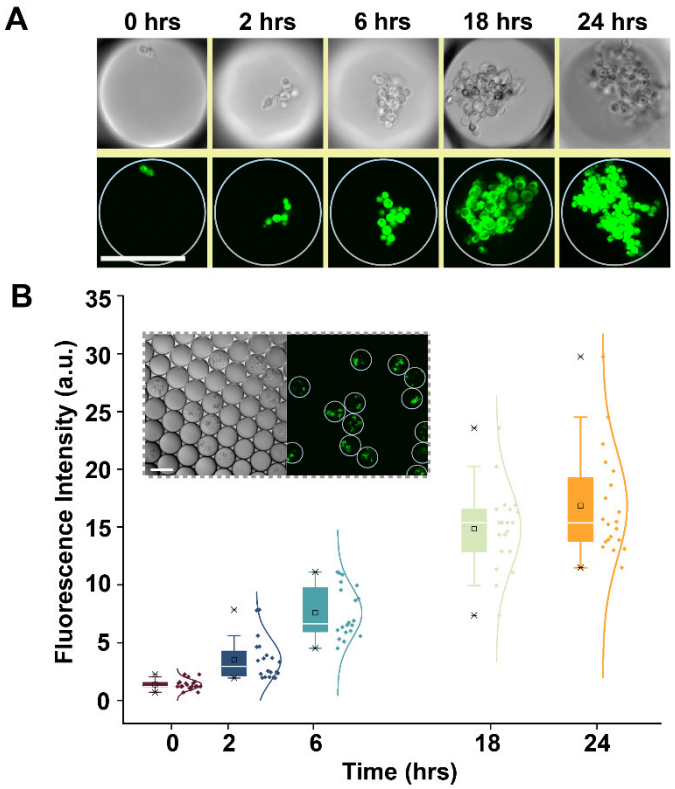

Figure 4.5 The growth of GFP-tagged *P. pastoris* strain (CBS7435-GFP) at the single-cell level in microdroplets over 24 hours. (A) Bright-field and fluorescence images showing the growth of single CBS7435-GFP cells in microdroplets over time. Scale bar = 50 µm. (B) Plots of total fluorescence intensity of cells per droplet. 20 cell-laden droplets were measured for each time point. The top and bottom edges of the box refer to the 25th and 75th percentiles, the cross line represents the median value, the black square represents the mean value, the whiskers extend to 1.5 times IQR and the asterisks represent upper and lower limits. The insets are bright-field and fluorescence images of *P. pastoris* after 24 hours of culture in microdroplets. Scale bar = 50 µm.

under normal conditions. This indicates that the fluorescence measurement can quantitively indicate the growth of single cells in microdroplets and demonstrates that the microdroplet bioreactors used in this study can maintain and screen of growth of single yeast cells of different species.

4.3.6 Viability assays of *S. cerevisiae* and *P. pastoris* grown in microdroplets

We used the cell staining live/dead kit to investigate whether 24 hours or a prolonged period of culture will affect the viability of *S. cerevisiae* and *P. pastoris*. This is to ensure that

encapsulation and cultivation of cells in microdroplets is a feasible and stable method for long-time single-cell assays.

The viability tests were performed and compared at three time points: before encapsulation, after 24 hrs and 48 hrs of encapsulation. The bright-field and fluorescence images show that both *S. cerevisiae* and *P. pastoris* cells maintain a high level of viability after 24 hours of culture (Fig. 4.6A). For *S. cerevisiae*, 94.4 ± 1.3% cells remain alive after 24 hours of culture, and cell viability slightly decreases to 93.6% ± 1.7% after 48 hours of culture; while for *P. pastoris*, 97.8 ± 0.8% and 95.5% ± 1.1% cells remain alive after 24 hours and 48 hours of culture, respectively (Fig. 4.6B).

Considering that the oil-removing reagent, pico-break™, contains PFOH which is a potential chemical hazard for yeast cells, the measured viability of encapsulated cells may

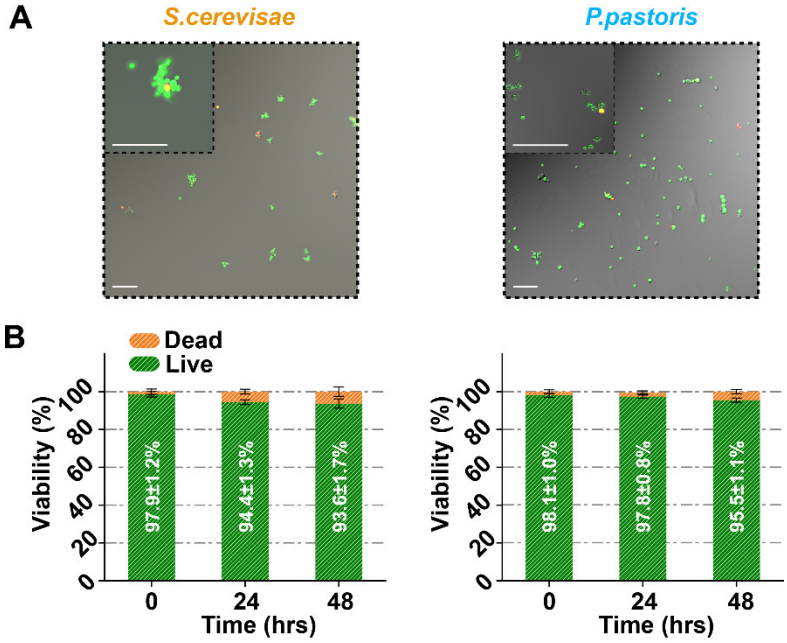

Figure 4.6 The viability of *S. cerevisiae* and *P. pastoris* grown in the microdroplets experiences no noticeable reduction over 48 hours. (A) Fluorescence images showing the viability of *S. cerevisiae* (left) and *P. pastoris* (right) recovered from microdroplets after 48 hours of culture. Scale bars are 50 μm for images obtained by a 20× objective and the insets obtained by a 40× objective. (B) Bar plots showing cell viability at three time points: 0 hrs (before encapsulation), 24 hrs and 48 hrs (after encapsulation). Three repetitions, each of 100 cells, were measured for each time point.

represent an underestimate of the true viability. Moreover, the result of one-way repeated measures ANOVA ($P < 0.005$) shows that there is no significant difference in cell viability among that before encapsulation, that for 24 hours and 48 hours of culture. This demonstrates that the viability of yeasts cultured in microdroplets is not significantly affected and the method is capable of prolonged assays of live yeast cells.

In this study, we explored the feasibility of using microdroplets as bioreactors to measure growth kinetics of single yeast cells and revealed the variations of growth at the single-cell level. It is noteworthy that the genetically identical cells in bulk cultures can always show phenotypic variations under the influence of various factors, such as cell cycle progression, cell ageing, and the biological noise that is attributed to stochastic variations in the concentrations of various biomolecules within individual cells[47-50]. In the meanwhile, two main factors in bulk culture conditions can make the growth of yeast cell populations appear homogenous: 1) external environmental factors, as there is no gradients of nutrients and oxygen supply exist due to constant mixing; and 2) quorum sensing that occurs through the sending and receiving message molecules in the extracellular environment[51].

Thus, the complexity inside the bulk cultures makes the detection of cell-to-cell heterogeneity extremely difficult, which always requires to employ the genetically and chemically external control, high-throughput cell assays and high-throughput sequencing of yeast growth and gene expression. In our study, the droplet-based culture of single cells was used to reveal subpopulation phenomena in a simple and cost-effective manner.

Cell encapsulation in microdroplets is a random process limited by the Poisson distribution but affected by cell sedimentation, leading to a majority of droplets that are empty. To maximise the proportion of single cell-encapsulated microdroplets without any noticeable damage, we used a non-ionic solution of 60% iodixanol, OptiPrep™, which has proved to be biocompatible, has low osmotic pressure and low intrinsic viscosity suitable for the culture of

cells in microdroplets[36, 52]. We used a relatively low concentration (20%) of OptiPrep™ (a non-ionic solution of 60% iodixanol) here, which has proved to be biocompatible, has low osmotic pressure and low intrinsic viscosity, and suitable for the culture of multiple types of cells in microdroplets[53, 54] . Researchers have used 50% OptiPrep™ to isolate quiescent yeast cells, and the results show that the isolated cells have growth behaviour similar to untreated cells and remain resist to heat shock and zymolyase treatment[55]. Here, we used the addition of 20% OptiPrep™ to reduce the effect of cell sedimentation (the density of yeast cells is 1.1 g/mL, which is higher than that of culture medium), and to temporarily create neutrally buoyant cell suspensions without noticeable adverse effects. This concentration of OptiPrep™ (i.e., 20%) enables the generation of a total of 830,000 microdroplets (~ 28.0% containing single yeast cells) in 30 mins. We note, however, that for studies that require a continuous generation of large amounts of cell-laden microdroplets, a higher concentration of OptiPrep™ or an alternative density-matching reagent of higher density may be necessary.

Moreover, we demonstrated the capability of droplet microfluidic platform for quantitatively tracking of single yeast cell growth of different species, genotypes and phenotypes, and also under different environmental conditions. When single cells are contained in isolated environments, not only can the growth rate of cells be screened, but also the phenotypes to secrete multiple high-value bioproducts (e.g., organic acids, antibodies and cellulases), since all the secreted products are confined within the microdroplet compartments. We can also obtain further understanding of genetic and molecular mechanisms underpinning beneficial phenotypes due to the genotype-phenotype linkages provided by the microdroplets. By combining with high-throughput screening and sorting technologies, e.g., FACS and IFC[56], this platform can accelerate the progress of development of yeast strains with desirable properties (e.g., high yield of valuable products, high environmental tolerance and high growth rate) for industrial applications.

4.4. Conclusions

This study demonstrated the use of microdroplets for quantitative, high-throughput and low-cost assessment of growth of single yeast cells. The results from single-cell assays showed that PA and AA inhibit cell growth, the uptake of K^+ improves PA tolerance in yeast, and *TRK*1 mutant exhibits increased PA tolerance, agreeing with previous findings obtained by analysis of cells in bulk populations. Neither were cells in microdroplets seen to experience noticeable loss in viability over 48 hours. Moreover, the microdroplet approach reveals subpopulation phenomena that are obscured by population average measurements, opening avenues to probe cell-to-cell variations under different environmental conditions.

Supplementary Materials

The following information is available in the Supplementary Materials. Fig, S4.1: Design of microfluidics device, Fig, S4.2: A photograph of the microfluidic device used in experiments, Fig, S4.3: Probability of cell encapsulation in droplets at different cell concentrations, Fig, S4.4: A photograph of experimental setup, Fig. S4.5: Distribution of number of cells per droplet at 24 hrs, Fig. S4.6 Plot of correlation between fluorescence intensity of all cells per droplet and number of cells per droplet, Fig. S4.7 Comparison of specific growth rates between two strains under 25 and 35 mM PA, Table S4.1: Details of yeast strains used in this study, Table S4.2: Comparison of specific growth rates between culture in microdroplet and culture in bulk.

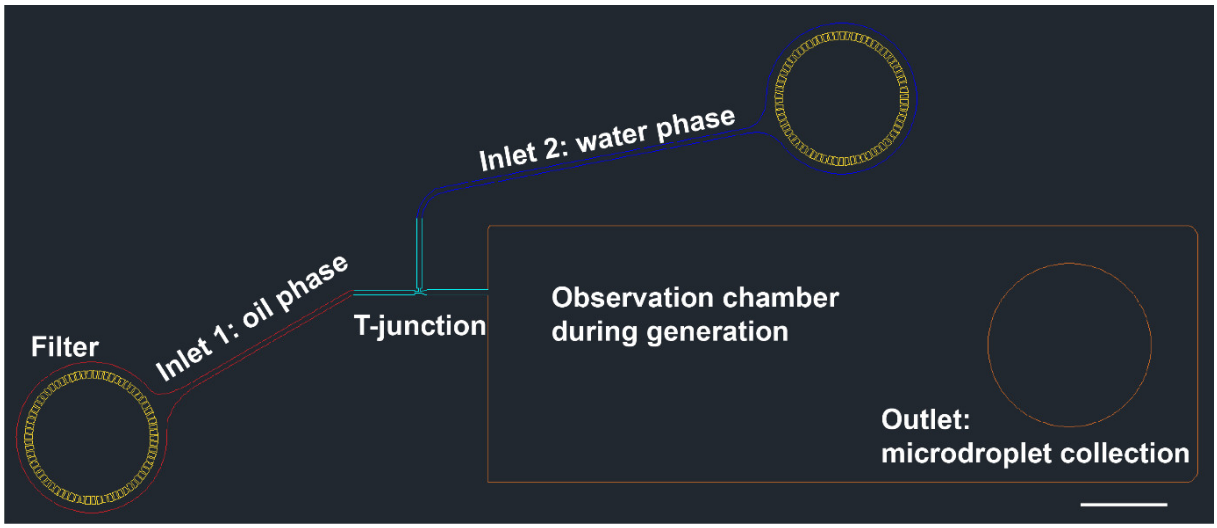

Figure S4.1 A CAD file showing the design of the microfluidic device used in this study, which consists of two inlets for injecting oil (continuous) phase and water (disperse) phase, a T-junction for generating microdroplets, a rectangular observation chamber and an outlet for collecting microdroplets. Scale bar = 100 mm.

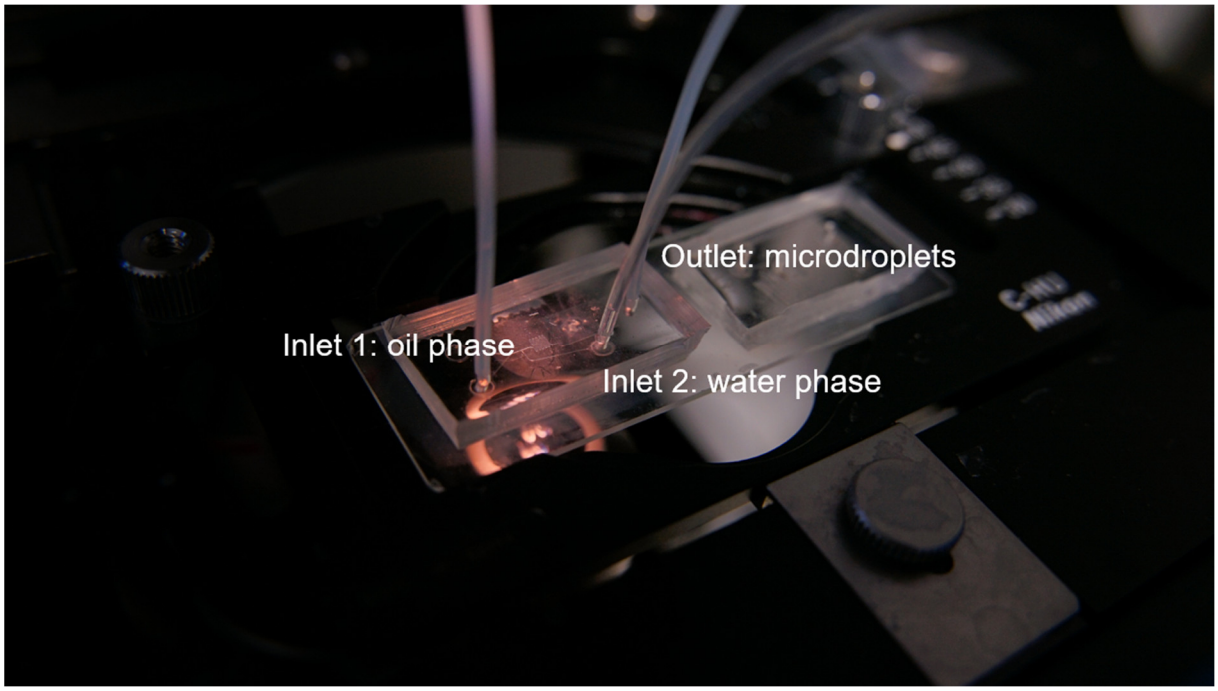

Figure S4.2 An enlarged view of the microfluidic device used in experiments for quantitatively tracking the growth of single yeast cells.

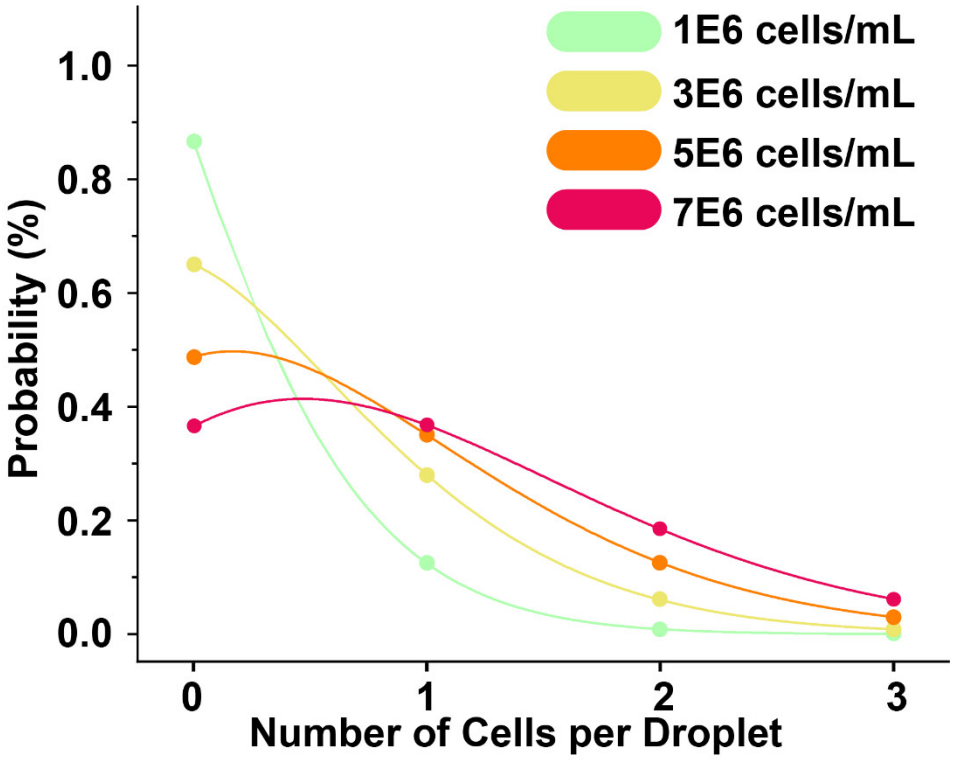

Figure S4.3 The probability of microdroplets containing different numbers of cells (0, 1, 2, 3) predicted by Poisson distribution.

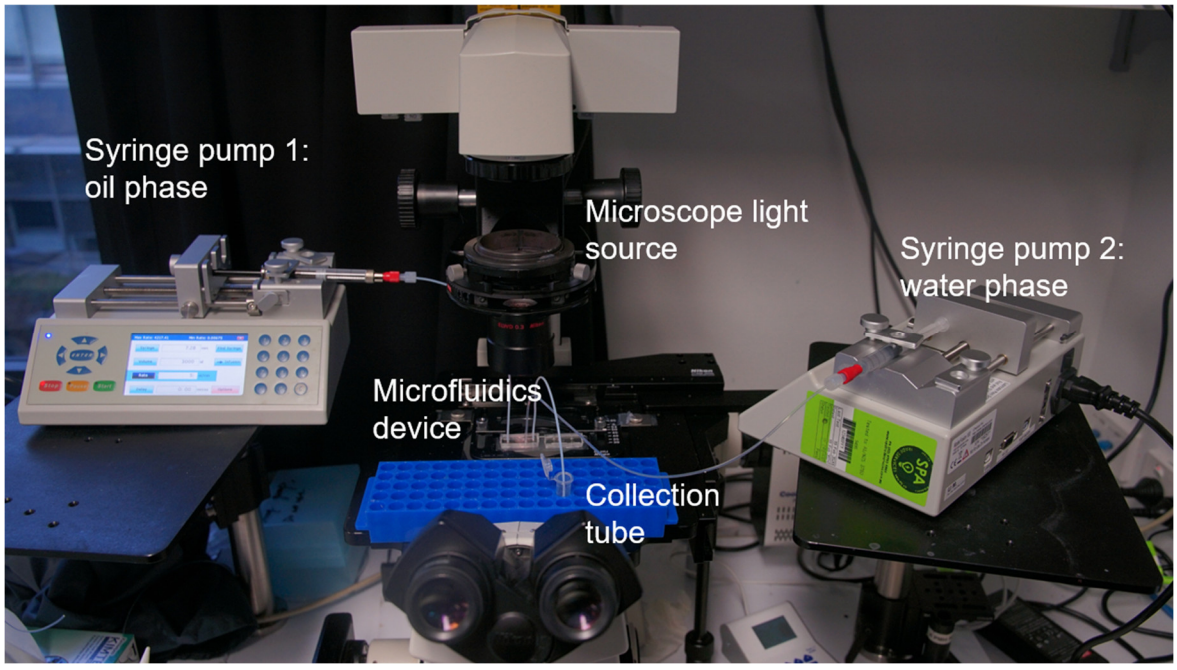

Figure S4.4 An actual image of experimental setup. The external equipment required to create cell-laden microdroplets include two syringe pumps for oil (continuous phase) and water (disperse phase), respectively, and an inverted fluorescence microscope equipped with a light source and a camera.

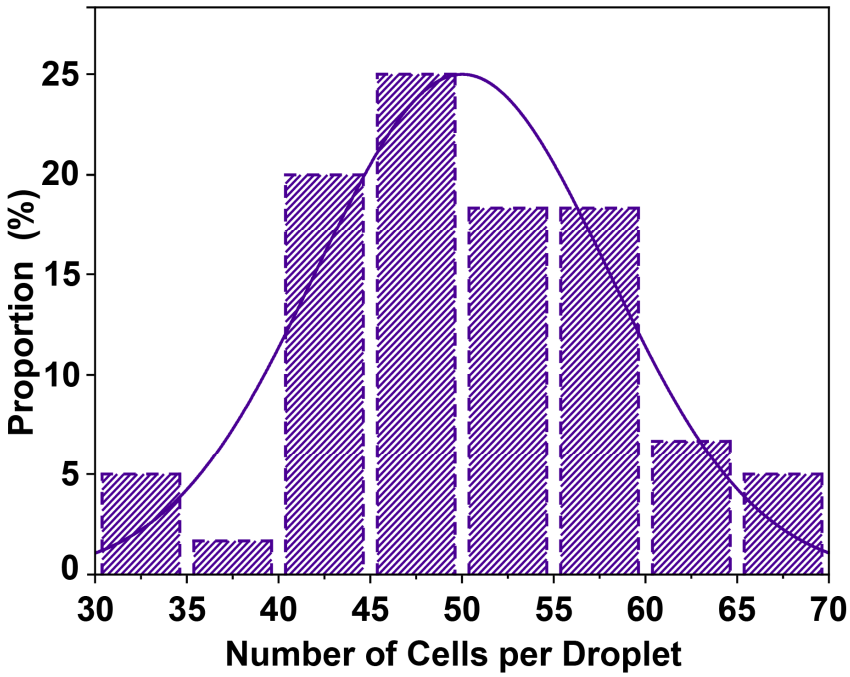

Figure S4.5 Distribution of the number of cells per droplet at 24 hrs for *S. cerevisiae* CEN.PK 113-7D. 60 cell-laden droplets were counted for this time point.

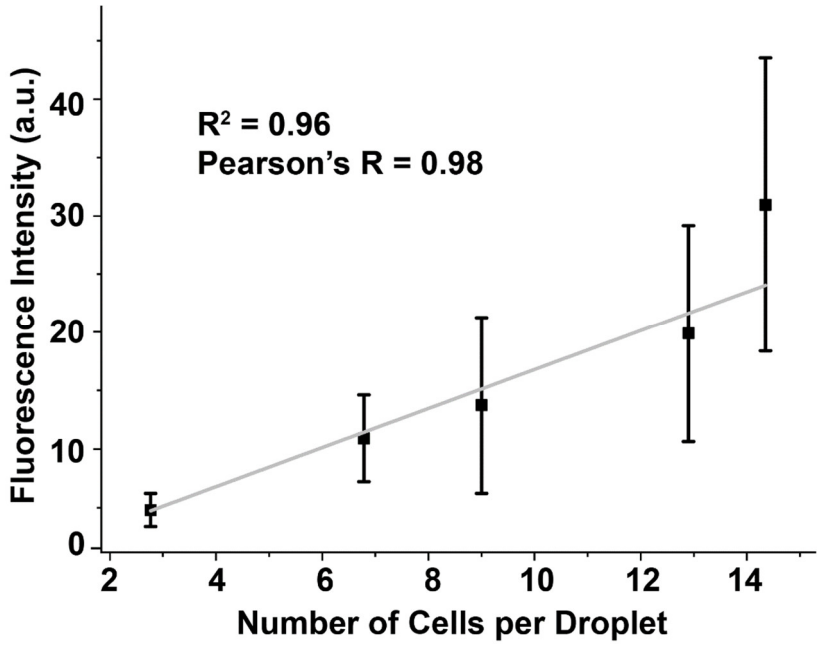

Figure S4.6. Plots of the total fluorescence intensity of all *S. cerevisiae* cells per droplet versus the number of cells per droplet. For the analysis of the relationship between total fluorescence intensity and the number of yeast cells per droplet, the coefficient of determination (R^2) is 0.96 for the linear fit and the Pearson correlation coefficient (Pearson's R) is 0.98.

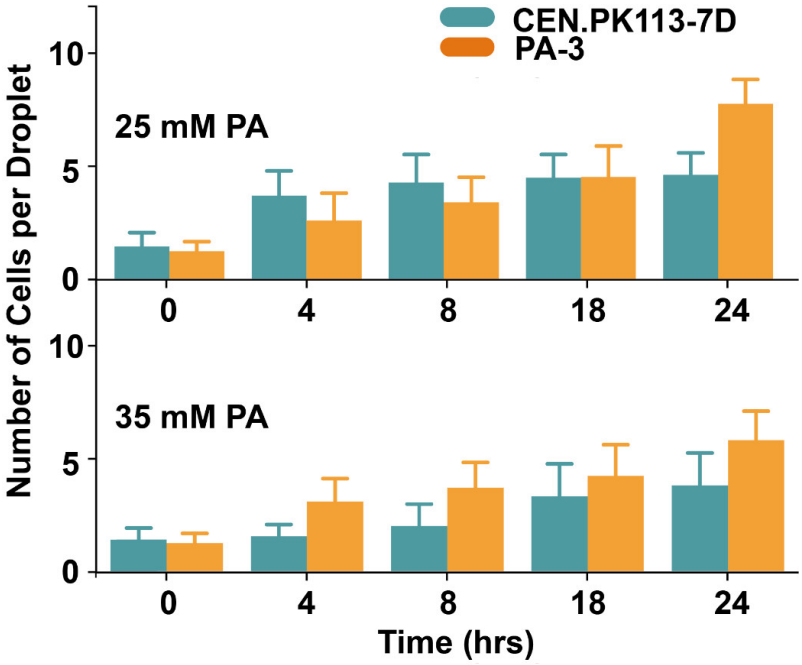

Figure S4.7 The growth of wild-type (CEN.PK 113-7D) and PA evolved mutant *S. cerevisiae* strain (PA-3) in microdroplets over 24 hours when 25 mM and 35 mM PA is applied. 60 cell-laden microdroplets were measured for each time point.

Table S4.1 Details of yeast strains used in this study

Name	Note	Origin
CEN.PK113-7D	Haploid prototrophic laboratory strain, mating type 'a'	Euroscarf
PA-3	The strain isolated after adaptive laboratory evolution of CEN.PK113-7D under the PA treated condition	Xin et al., 2019
CEN.PK2-1C-GFP	Laboratory strain of *S. cerevisiae* engineered with pRS416 vector expressing GFP under the *PGK1* promoter	Peng et al., unpublished
CBS7435-GFP	Laboratory strain of *P. pastoris* with GFP expressing cassette controlled by the *KAR2* promoter, integrated to the *RGI2* promoter region	Peng et al., unpublished

Table S4.2 Comparison of specific growth rates between culture in droplet and culture in bulk

Strain	PA concentration (mM)	$\mu_{droplet}$ (h^{-1})	μ_{bulk} (h^{-1})
CEN.PK 113-7D	0	0.23	0.21
	7.5	0.13	0.16
	15	0.05	0.07
	25	0.04	0.05
	35	0.04	0.03
PA-3	0	0.14	0.20
	15	0.10	0.17
	25	0.07	0.12
	35	0.05	0.10

Author Contributions

H.L. carried out the experiment. X.X. and K.P. prepared the yeast sample. H.L and Y.Z. fabricated the microfluidic device. H.L., X.X. L.J., T.W., I.P., J.P. and M.L. interpreted of the results. H.L. and M.L. wrote the manuscript with input from all authors. J.P. and M.L. conceived the study and supervised this project.

References

1. Hong, K.-K.; Nielsen, J., Metabolic engineering of Saccharomyces cerevisiae: a key cell factory platform for future biorefineries. *Cell. Mol. Life Sci.* **2012,** *69* (16), 2671-2690.
2. de Jong, B. W.; Shi, S.; Siewers, V.; Nielsen, J., Improved production of fatty acid ethyl esters in Saccharomyces cerevisiae through up-regulation of the ethanol degradation pathway and expression of the heterologous phosphoketolase pathway. *Microb. Cell Fact.* **2014,** *13* (1), 39.
3. Chen, Y.; Daviet, L.; Schalk, M.; Siewers, V.; Nielsen, J., Establishing a platform cell factory through engineering of yeast acetyl-CoA metabolism. *Metab. Eng.* **2013,** *15*, 48-54.
4. Álvarez-Chávez, C. R.; Edwards, S.; Moure-Eraso, R.; Geiser, K., Sustainability of bio-based plastics: general comparative analysis and recommendations for improvement. *J. Clean. Prod.* **2012,** *23* (1), 47-56.
5. Gonzalez-Garcia, R. A.; McCubbin, T.; Navone, L.; Stowers, C.; Nielsen, L. K.; Marcellin, E., Microbial Propionic Acid Production. *Fermentation* **2017,** *3* (2).
6. Steen, E. J.; Kang, Y.; Bokinsky, G.; Hu, Z.; Schirmer, A.; McClure, A.; del Cardayre, S. B.; Keasling, J. D., Microbial production of fatty-acid-derived fuels and chemicals from plant biomass. *Nature* **2010,** *463* (7280), 559-562.
7. Sauer, M.; Porro, D.; Mattanovich, D.; Branduardi, P., Microbial production of organic acids: expanding the markets. *Trends Biotechnol.* **2008,** *26* (2), 100-108.

8. Zhuge, X.; Liu, L.; Shin, H.-d.; Chen Rachel, R.; Li, J.; Du, G.; Chen, J., Development of a Propionibacterium-Escherichia coli Shuttle Vector for Metabolic Engineering of Propionibacterium jensenii, an Efficient Producer of Propionic Acid. *Appl. Environ. Microbiol.* **2013,** *79* (15), 4595-4602.
9. Kiatpapan, P.; Murooka, Y., Genetic manipulation system in propionibacteria. *J. Biosci. Bioeng.* **2002,** *93* (1), 1-8.
10. Ishida, N.; Saitoh, S.; Tokuhiro, K.; Nagamori, E.; Matsuyama, T.; Kitamoto, K.; Takahashi, H., Efficient Production of l-Lactic Acid by Metabolically Engineered Saccharomyces cerevisiae with a Genome-Integrated l-Lactate Dehydrogenase Gene. *Appl. Environ. Microbiol.* **2005,** *71* (4), 1964-1970.
11. Otero, J. M.; Cimini, D.; Patil, K. R.; Poulsen, S. G.; Olsson, L.; Nielsen, J., Industrial Systems Biology of Saccharomyces cerevisiae Enables Novel Succinic Acid Cell Factory. *PLoS ONE* **2013,** *8* (1), e54144.
12. Williams, T. C.; Averesch, N. J. H.; Winter, G.; Plan, M. R.; Vickers, C. E.; Nielsen, L. K.; Krömer, J. O., Quorum-sensing linked RNA interference for dynamic metabolic pathway control in Saccharomyces cerevisiae. *Metab. Eng.* **2015,** *29*, 124-134.
13. Borodina, I.; Kildegaard, K. R.; Jensen, N. B.; Blicher, T. H.; Maury, J.; Sherstyk, S.; Schneider, K.; Lamosa, P.; Herrgård, M. J.; Rosenstand, I.; Öberg, F.; Forster, J.; Nielsen, J., Establishing a synthetic pathway for high-level production of 3-hydroxypropionic acid in Saccharomyces cerevisiae via β-alanine. *Metab. Eng.* **2015,** *27*, 57-64.
14. Curran, K. A.; Leavitt, J. M.; Karim, A. S.; Alper, H. S., Metabolic engineering of muconic acid production in Saccharomyces cerevisiae. *Metab. Eng.* **2013,** *15*, 55-66.
15. Eglinton, J. M.; Heinrich, A. J.; Pollnitz, A. P.; Langridge, P.; Henschke, P. A.; de Barros Lopes, M., Decreasing acetic acid accumulation by a glycerol overproducing strain of Saccharomyces cerevisiae by deleting the ALD6 aldehyde dehydrogenase gene. *Yeast* **2002,** *19* (4), 295-301.
16. Xu, X.; Williams, T. C.; Divne, C.; Pretorius, I. S.; Paulsen, I. T., Evolutionary engineering in Saccharomyces cerevisiae reveals a TRK1-dependent potassium influx mechanism for propionic acid tolerance. *Biotechnol. Biofuels* **2019,** *12* (1), 97.
17. Kildegaard, K. R.; Hallström, B. M.; Blicher, T. H.; Sonnenschein, N.; Jensen, N. B.; Sherstyk, S.; Harrison, S. J.; Maury, J.; Herrgård, M. J.; Juncker, A. S.; Forster, J.; Nielsen, J.; Borodina, I., Evolution reveals a glutathione-dependent mechanism of 3-hydroxypropionic acid tolerance. *Metab. Eng.* **2014,** *26*, 57-66.
18. González-Ramos, D.; Gorter de Vries, A. R.; Grijseels, S. S.; van Berkum, M. C.; Swinnen, S.; van den Broek, M.; Nevoigt, E.; Daran, J.-M. G.; Pronk, J. T.; van Maris, A. J. A., A new laboratory evolution approach to select for constitutive acetic acid tolerance in Saccharomyces cerevisiae and identification of causal mutations. *Biotechnol. Biofuels* **2016,** *9* (1), 173.
19. Almario, M. P.; Reyes, L. H.; Kao, K. C., Evolutionary engineering of Saccharomyces cerevisiae for enhanced tolerance to hydrolysates of lignocellulosic biomass. *Biotechnol. Bioeng.* **2013,** *110* (10), 2616-2623.
20. Agresti, J. J.; Antipov, E.; Abate, A. R.; Ahn, K.; Rowat, A. C.; Baret, J.-C.; Marquez, M.; Klibanov, A. M.; Griffiths, A. D.; Weitz, D. A., Ultrahigh-throughput screening in drop-based microfluidics for directed evolution. *Proc. Nat.l Acad. Sci. U. S. A.* **2010,** *107* (9), 4004.
21. Yu, Z.; Boehm, C. R.; Hibberd, J. M.; Abell, C.; Haseloff, J.; Burgess, S. J.; Reyna-Llorens, I., Droplet-based microfluidic analysis and screening of single plant cells. *PLoS ONE* **2018,** *13* (5), e0196810.
22. Brouzes, E.; Medkova, M.; Savenelli, N.; Marran, D.; Twardowski, M.; Hutchison, J. B.; Rothberg, J. M.; Link, D. R.; Perrimon, N.; Samuels, M. L., Droplet microfluidic technology for single-cell high-throughput screening. *Proc. Nat.l Acad. Sci. U. S. A.* **2009,** *106* (34), 14195.
23. Hosokawa, M.; Nishikawa, Y.; Kogawa, M.; Takeyama, H., Massively parallel whole genome amplification for single-cell sequencing using droplet microfluidics. *Sci. Rep.* **2017,** *7* (1), 5199.
24. Liu, H.; Li, M.; Wang, Y.; Piper, J.; Jiang, L., Improving Single-Cell Encapsulation Efficiency and Reliability through Neutral Buoyancy of Suspension. *Micromachines* **2020,** *11* (1).
25. Li, M.; van Zee, M.; Riche, C. T.; Tofig, B.; Gallaher, S. D.; Merchant, S. S.; Damoiseaux, R.; Goda, K.; Di Carlo, D., A Gelatin Microdroplet Platform for High-Throughput Sorting of Hyperproducing Single-Cell-Derived Microalgal Clones. *Small* **2018,** *14* (44), 1803315.
26. Li, M.; van Zee, M.; Goda, K.; Di Carlo, D., Size-based sorting of hydrogel droplets using inertial microfluidics. *Lab Chip* **2018,** *18* (17), 2575-2582.
27. Fischlechner, M.; Schaerli, Y.; Mohamed, M. F.; Patil, S.; Abell, C.; Hollfelder, F., Evolution of enzyme catalysts caged in biomimetic gel-shell beads. *Nat. Chem.* **2014,** *6* (9), 791-796.
28. Bowman, E. K.; Alper, H. S., Microdroplet-Assisted Screening of Biomolecule Production for Metabolic Engineering Applications. *Trends Biotechnol.* **2020,** *38* (7), 701-714.
29. Zhu, Z.; Zhang, W.; Leng, X.; Zhang, M.; Guan, Z.; Lu, J.; Yang, C. J., Highly sensitive and quantitative detection of rare pathogens through agarose droplet microfluidic emulsion PCR at the single-cell level. *Lab Chip* **2012,** *12* (20), 3907-3913.

30. Zinchenko, A.; Devenish, S. R. A.; Kintses, B.; Colin, P.-Y.; Fischlechner, M.; Hollfelder, F., One in a Million: Flow Cytometric Sorting of Single Cell-Lysate Assays in Monodisperse Picolitre Double Emulsion Droplets for Directed Evolution. *Anal. Chem.* **2014,** *86* (5), 2526-2533.
31. Ostafe, R.; Prodanovic, R.; Lloyd Ung, W.; Weitz, D. A.; Fischer, R., A high-throughput cellulase screening system based on droplet microfluidics. *Biomicrofluidics* **2014,** *8* (4), 041102.
32. Klein, Allon M.; Mazutis, L.; Akartuna, I.; Tallapragada, N.; Veres, A.; Li, V.; Peshkin, L.; Weitz, David A.; Kirschner, Marc W., Droplet Barcoding for Single-Cell Transcriptomics Applied to Embryonic Stem Cells. *Cell* **2015,** *161* (5), 1187-1201.
33. Hindson, B. J.; Ness, K. D.; Masquelier, D. A.; Belgrader, P.; Heredia, N. J.; Makarewicz, A. J.; Bright, I. J.; Lucero, M. Y.; Hiddessen, A. L.; Legler, T. C.; Kitano, T. K.; Hodel, M. R.; Petersen, J. F.; Wyatt, P. W.; Steenblock, E. R.; Shah, P. H.; Bousse, L. J.; Troup, C. B.; Mellen, J. C.; Wittmann, D. K.; Erndt, N. G.; Cauley, T. H.; Koehler, R. T.; So, A. P.; Dube, S.; Rose, K. A.; Montesclaros, L.; Wang, S.; Stumbo, D. P.; Hodges, S. P.; Romine, S.; Milanovich, F. P.; White, H. E.; Regan, J. F.; Karlin-Neumann, G. A.; Hindson, C. M.; Saxonov, S.; Colston, B. W., High-Throughput Droplet Digital PCR System for Absolute Quantitation of DNA Copy Number. *Anal. Chem.* **2011,** *83* (22), 8604-8610.
34. Headen, D. M.; García, J. R.; García, A. J., Parallel droplet microfluidics for high throughput cell encapsulation and synthetic microgel generation. *Microsyst. Nanoeng.* **2018,** *4* (1), 17076.
35. Xia, Y.; Whitesides, G. M., Soft lithography. *Annu. Rev. Mater. Sci.* **1998,** *28* (1), 153-184.
36. Allazetta, S.; Kolb, L.; Zerbib, S.; Bardy, J. a.; Lutolf, M. P., Cell-Instructive Microgels with Tailor-Made Physicochemical Properties. *Small* **2015,** *11* (42), 5647-5656.
37. Siedler, S.; Khatri, N. K.; Zsohár, A.; Kjærbølling, I.; Vogt, M.; Hammar, P.; Nielsen, C. F.; Marienhagen, J.; Sommer, M. O. A.; Joensson, H. N., Development of a Bacterial Biosensor for Rapid Screening of Yeast p-Coumaric Acid Production. *ACS Synth. Biol.* **2017,** *6* (10), 1860-1869.
38. Joensson, H. N.; Uhlén, M.; Svahn, H. A., Droplet size based separation by deterministic lateral displacement—separating droplets by cell-induced shrinking. *Lab Chip* **2011,** *11* (7), 1305-1310.
39. Hofmann, T. W.; Hänselmann, S.; Janiesch, J.-W.; Rademacher, A.; Böhm, C. H. J., Applying microdroplets as sensors for label-free detection of chemical reactions. *Lab Chip* **2012,** *12* (5), 916-922.
40. Pan, J.; Stephenson, A. L.; Kazamia, E.; Huck, W. T. S.; Dennis, J. S.; Smith, A. G.; Abell, C., Quantitative tracking of the growth of individual algal cells in microdroplet compartments. *Integr. Biol.* **2011,** *3* (10), 1043-1051.
41. Yenush, L.; Mulet, J. M.; Ariño, J.; Serrano, R., The Ppz protein phosphatases are key regulators of K+ and pH homeostasis: implications for salt tolerance, cell wall integrity and cell cycle progression. *EMBO J.* **2002,** *21* (5), 920-929.
42. Kahm, M.; Navarrete, C.; Llopis-Torregrosa, V.; Herrera, R.; Barreto, L.; Yenush, L.; Ariño, J.; Ramos, J.; Kschischo, M., Potassium Starvation in Yeast: Mechanisms of Homeostasis Revealed by Mathematical Modeling. *PLoS Comput. Biol.* **2012,** *8* (6), e1002548.
43. Ariño, J.; Ramos, J.; Sychrová, H., Alkali Metal Cation Transport and Homeostasis in Yeasts. *Microbiol. Mol. Biol. Rev.* **2010,** *74* (1), 95-120.
44. Ratcliff, W. C.; Travisano, M., Experimental Evolution of Multicellular Complexity in Saccharomyces cerevisiae. *Bioscience* **2014,** *64* (5), 383-393.
45. Köster, S.; Angilè, F. E.; Duan, H.; Agresti, J. J.; Wintner, A.; Schmitz, C.; Rowat, A. C.; Merten, C. A.; Pisignano, D.; Griffiths, A. D.; Weitz, D. A., Drop-based microfluidic devices for encapsulation of single cells. *Lab Chip* **2008,** *8* (7), 1110-1115.
46. Guo, M. T.; Rotem, A.; Heyman, J. A.; Weitz, D. A., Droplet microfluidics for high-throughput biological assays. *Lab Chip* **2012,** *12* (12), 2146-2155.
47. Komin, N.; Skupin, A., How to address cellular heterogeneity by distribution biology. *Curr. Opin. Syst. Biol.* **2017,** *3*, 154-160.
48. Campbell, K.; Vowinckel, J.; Ralser, M., Cell-to-cell heterogeneity emerges as consequence of metabolic cooperation in a synthetic yeast community. *Biotechnol. J.* **2016,** *11* (9), 1169-1178.
49. Altschuler, S. J.; Wu, L. F., Cellular Heterogeneity: Do Differences Make a Difference? *Cell* **2010,** *141* (4), 559-563.
50. Li, S.; Giardina, D. M.; Siegal, M. L., Control of nongenetic heterogeneity in growth rate and stress tolerance of Saccharomyces cerevisiae by cyclic AMP-regulated transcription factors. *PLoS Genet.* **2018,** *14* (11), e1007744.
51. Avbelj, M.; Zupan, J.; Raspor, P., Quorum-sensing in yeast and its potential in wine making. *Appl. Microbiol. Biotechnol.* **2016,** *100* (18), 7841-7852.
52. Ma, T.; Gao, X.; Dong, H.; He, H.; Cao, X., High-throughput generation of hyaluronic acid microgels via microfluidics-assisted enzymatic crosslinking and/or Diels–Alder click chemistry for cell encapsulation and delivery. *Appl. Mater. Today* **2017,** *9*, 49-59.

53. Hsu, M. N.; Wei, S.-C.; Guo, S.; Phan, D.-T.; Zhang, Y.; Chen, C.-H., Smart Hydrogel Microfluidics for Single-Cell Multiplexed Secretomic Analysis with High Sensitivity. *Small* **2018,** *14* (49), 1802918.
54. Brower, K. K.; Khariton, M.; Suzuki, P. H.; Still, C.; Kim, G.; Calhoun, S. G. K.; Qi, L. S.; Wang, B.; Fordyce, P. M., Double Emulsion Picoreactors for High-Throughput Single-Cell Encapsulation and Phenotyping via FACS. *Anal. Chem.* **2020,** *92* (19), 13262-13270.
55. Quasem, I.; Luby, C. J.; Mace, C. R.; Fuchs, S. M., Density separation of quiescent yeast using iodixanol. *Biotechniques* **2017,** *63* (4), 169-173.
56. Nitta, N.; Sugimura, T.; Isozaki, A.; Mikami, H.; Hiraki, K.; Sakuma, S.; Iino, T.; Arai, F.; Endo, T.; Fujiwaki, Y.; Fukuzawa, H.; Hase, M.; Hayakawa, T.; Hiramatsu, K.; Hoshino, Y.; Inaba, M.; Ito, T.; Karakawa, H.; Kasai, Y.; Koizumi, K.; Lee, S.; Lei, C.; Li, M.; Maeno, T.; Matsusaka, S.; Murakami, D.; Nakagawa, A.; Oguchi, Y.; Oikawa, M.; Ota, T.; Shiba, K.; Shintaku, H.; Shirasaki, Y.; Suga, K.; Suzuki, Y.; Suzuki, N.; Tanaka, Y.; Tezuka, H.; Toyokawa, C.; Yalikun, Y.; Yamada, M.; Yamagishi, M.; Yamano, T.; Yasumoto, A.; Yatomi, Y.; Yazawa, M.; Di Carlo, D.; Hosokawa, Y.; Uemura, S.; Ozeki, Y.; Goda, K., Intelligent Image-Activated Cell Sorting. *Cell* **2018,** *175* (1), 266-276.e13.

Chapter 5 Rapid, simple and inexpensive spatial patterning of wettability in microfluidic devices for double emulsion generation*

*Liu, H.; Piper, J. A.; Li, M., Rapid, simple and inexpensive spatial patterning of wettability in microfluidic devices for double emulsion generation. *Analytical Chemistry* **2021,** 93, 31, 10955–10965.

Although the yeast cell phenotypes can be screened using w/o single emulsions under a microscope, the throughput is too low. Therefore, the w/o/w DE is introduced to engulf single emulsions with an aqueous outer layer, which is compatible with commercial flow cytometrical instruments for high-throughput single-cell analysis. Unfortunately, DEs formed by conventional emulsion generation approaches in most cases are highly polydisperse; moreover, conventional methods for DE generation are labour intensive, expensive, complex and always require external bulky instruments. Thus, a rapid, simple, and inexpensive method to spatially pattern wettability in microfluidic devices for the continuous generation of monodisperse DEs is proposed. To demonstrate the biological capability of generated DEs, the DEs containing single yeast cells before and after culture are screened with a FC. This also lays a foundation for the high-throughput screening and sorting of yeast phenotypes using FACS at the single-cell level.

5.1 Introduction

A DE is a complex soft colloidal system consisting of an aqueous core encapsulated within an immiscible shell, dispersed in an external aqueous carrier fluid [1, 2]. A DE has a highly

adjustable core-shell structure, which allows for a substantial degree of control over the encapsulation and release of active ingredients[3]. The middle phase (shell) can be selectively gelled or hardened to create solid capsules[4, 5], and the minimised oil volume prevents the oil from diffusing to and affecting the inner content directly[6]. Moreover, unlike water-in-oil (w/o) single emulsion, DE is compatible with commercial flow cytometers and FACS instruments that require an aqueous carrier flow, allowing user-friendly quantitative high-throughput assays[7-12]. Due to these significant advantages, DE has been widely used in various food, cosmetic, pharmaceutical, chemical, and biological applications, such as encapsulation and release of nutrients and flavours, production of low-calorie food, controlled release and targeted delivery of drugs, chemical extraction, synthesis of functional particles, medical diagnostics, and directed cellular and molecular evolution[10, 13-23].

Traditional batch emulsification generation methods, such as stirring, high shear homogenisation, and membrane extrusion[9, 19, 24, 25], can be used to rapidly generate DEs, but they have limited controllability of the resulting DEs in respect of size distribution and tendency for coalescence due to high shear rates[26, 27]. These issues are problematic for downstream quantitative assays and controlled reactions where DEs with high uniformity and stability are required. With rapid growth in advanced manufacturing sector, microfluidic devices have been developed to hierarchically generate monodisperse DEs by selectively controlling the wettability of microchannels[7, 8, 10, 11, 14, 20, 25-31]. Wettability, a physical property of channel surface, plays a vital role in the types of emulsion droplets generated, as hydrophobic and hydrophilic surfaces are necessary to generate w/o emulsions and O/W emulsions, respectively[26, 31-34].

Two main strategies, multi-module and single-module, have been used to generate DEs by microfluidic devices. The first multi-module strategy is based on the combination of two or three devices, each of which can be either entirely hydrophobic or entirely hydrophilic[3, 6, 10, 20,

[21, 28, 35-37]. Although this strategy allows easy surface modification, turbulent shear occurring at the connection between two devices results in unstable generation of DEs with an uncertain number of embedded inner cores[27]. The process of DE generation using co-axial flow-focusing capillaries is inefficient, as high flow rate of sheath is required to prevent the dispersed phases from touching the channel walls[36]. Moreover, the manufacture of capillaries suffers from the lack of flexible and reproducible methods for capillary alignment and sealing[8, 31, 33], and glass capillaries need extra hydrophobic silane coatings compared with intrinsically hydrophobic PDMS devices.

The other single-module strategy allows DE generation in a single microfluidic device with microchannels having different hydrophilic and hydrophobic sections. A variety of methods, including LbL assembly[8, 38, 39], UV treatment[33], flow confinement by inert phases[30, 40, 41], and oxygen plasma polymerisation[7, 11, 31], have been used to selectively modify the wettability of microchannel surfaces in a single device.

However, these generally require multiple complex processing steps, bulky external laboratory instrumentation, or use of different chemical solvents. Layer-by-layer assembly methods are based on the alignment bonding of two PDMS slabs, but the process requires extra fabrication costs of the additional layer and the outcome is largely dependent on the skills and experience of the fabricator. The process of UV treatment needs a silane (e.g., OTS) coating to render the whole glass device hydrophobic and a long exposure time (i.e., 60 min), which induces PDMS fragility. Although flow confinement by inert nitrogen (N_2) or fluid is a commonly used method to achieve the spatial patterning of wettability in microchannels, it is relatively slow and has a relatively high failure rate. This is because it is difficult to keep the interface between the reactive region and inert region steady in a microchannel,[32] thereby resulting in easy contamination of microchannels. In addition, the process of photo-initiated or thermal-initiated polymerisation at reactive regions requires repeated cycles to produce

uniform surface properties due to the ill-defined boundaries of treated areas, which also require UV or high temperature (i.e., 120 °C) treatment.

Plasma treatment has been used for surface wettability modification. This is because that O_2/air plasma can effectively render a PDMS surface hydrophilic by oxidizing surface siloxane groups to silanols[42]. Several researchers have embedded electrodes within microchannels to confine plasma for targeted treatment[43]. However, accurate alignment of the injected electrodes and bulky external equipment are required, making this process comparatively complex. Tan et al firstly demonstrated that oxygen plasma can effectively alter localised PDMS surface from hydrophobic to hydrophilic in a sealed microchannel[44]. Kim *et al.* and Brower *et al.* have used a narrow microchannel as a barrier to prevent plasma from entering into hydrophobic regions[7, 11, 31]. This method avoids the use of chemicals for surface functionalisation but lacks the capacity to precisely control the targeted regions for plasma treatment. Moreover, it also requires the use of bulky external apparatus, high gas pressure (1 mbar), and relatively long treatment time (3 to 10 min).

To overcome the limitations of existing methods, we have developed a unique method employing localised corona discharge, which is further confined by a narrow, serpentine corona resistance microchannel, to achieve spatial patterning of wettability in a single microfluidic device for generating extremely monodisperse DEs (Fig. 1A). The microchannel surface of the corona resistor as well as the upstream T-junction droplet generator remains hydrophobic, ideal for w/o single emulsion generation. The electrode tip for the corona discharge is inserted via the microchannel outlet so that the localised corona treatment renders the flow-focusing droplet generator hydrophilic for w/o/w DE generation. The purpose-optimised corona resistor (Fig. 1A inset, red square), which is narrower than the expansive channels flanking the flow-focusing droplet generator, effectively prevents the corona

discharge from entering the hydrophobic channel; thus, the corona discharge is confined to the selected microchannel zone for DE generation, and the spatial patterning of wettability is easily and robustly achieved.

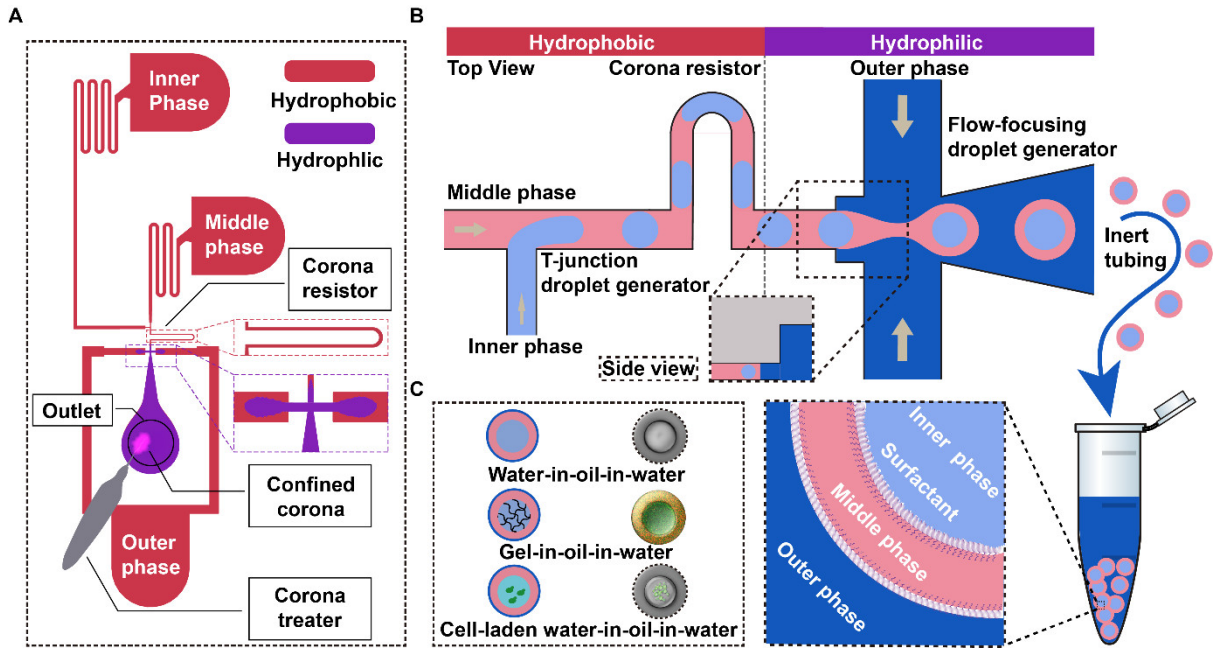

Figure 5.1 Schematic illustration of DE generation in a microfluidic device with spatial wettability patterned by the proposed approach. A) Schematic illustration of spatial wettability patterns in the device after corona treatment. After natural recovery or surface modification, the whole microfluidic device is hydrophobic (red). Then linear corona discharge is introduced into the expansion region by the electrode of the corona treater, which is further confined by the corona resistance channel (red enlarged region). This corona discharge precisely modifies the inside surfaces of the flow-focusing droplet generator (purple enlarged region) and outlet to become hydrophilic (blue). B) Schematics of continuous DE generation. At the hydrophobic T-junction droplet generator, the inner phase (light blue) is sheared by middle phase (red) into water-in-oil single emulsions, which are further encapsulated by the outer phase (dark blue) at the hydrophilic flow-focusing droplet generator, creating monodisperse water-in-oil-in-water DEs. The generated DEs are further transported into and stored in a centrifuge tube prefilled with an aqueous buffer. C) Schematics and real images of three types of DEs with different inner cores: PBS solution, thermo-responsive hydrogel solution, and cell-laden culture medium.

Compared with O_2/air plasma treatment, corona treatment is cost-effective, and can generate very localised corona discharge directly at the surfaces of targeted regions using a low-cost hand-held instrument at atmospheric air pressure[45]. Although corona treatment has been used for wettability patterning in microchannels, inert chemicals are always needed to retain the hydrophobicity of blocked region surfaces[14, 26, 32]. To the best of our knowledge, this is the first report of forming spatially-resolved wettability patterns in a single microfluidic device by one step, within a few seconds under room air without any solvents or strict conditions.

To quantitatively assess the effectiveness of this method for wettability modification, we characterised the properties of PDMS surfaces under different levels of corona treatment. We have then examined the controllability of size and morphology of generated DEs by adjusting the flow rates of inner, middle, and outer phase media of the microfluidic DE generator. In order to demonstrate the versatility of DEs produced by this method, we used DEs as intermediate templates for fabricating monodisperse gelatin microgels, and as bioreactors for culturing yeast cells by high-throughput flow cytometric screening.

5.2 Methods and Materials

5.2.1 Device design and fabrication

The microfluidic device consists of two layers: a shallow channel having a depth of ~25 μm with a hydrophobic T-junction microdroplet generator (Fig. S5.1A); and a deep channel having ~35 μm with a hydrophilic flow-focusing microdroplet generator (Fig. S5.1B). The T-junction droplet generator used to create w/o single emulsions has widths of 16 μm and 18 μm for an inner aqueous phase and a middle phase, respectively, whilst the flow-focusing droplet generator used to produce DEs has widths of 30 μm and 35 μm for an outer phase and single emulsion introduction, respectively. A narrow serpentine microchannel (22.5 μm in width 3.4 mm in length, and an inner radius of 72 μm) separates the two droplet generators to confine the

injected corona discharge to the deep (hydrophilic) layer. There are three inlets for injecting an inner phase, a middle phase, and an outer phase, respectively, and an outlet for injecting the electrode of the corona treater and collecting the formed DEs (Fig. S5.1C).

The two-layer SU-8 2025 (MicroChem, Newton, MA, USA) master was fabricated using standard soft-lithography by a direct-write optical lithography machine (MicroWriter ML3, Durham Magneto Optics, Durham, UK). The PDMS (Sylgard 184, Dow Corning, Midland, MI, USA) was prepared by mixing the PDMS base and the curing agent with a weight ratio of 10:1 and was degassed under vacuum for 15 min. The PDMS mixture was then poured over the SU-8 master and baked at 60 °C for 2 h, after which the PDMS slab was peeled off from the master. A 1.5-mm puncher was used to punch the three inlets and one outlet. Standard glass slides were cleaned with isopropanol (I9516 Sigma-Aldrich, St. Louis, MO, USA) and water followed by drying at 60°C for 10 min to remove moisture. The side of the PDMS slab with microchannel patterns was cleaned with scotch tape to remove PDMS scraps and dust. The cleaned side of the glass slides and the channel side of PDMS slab were treated with oxygen plasma (PX 250, March Instruments, Concord, CA, USA) for 22 s at 300 mbar and then immediately bonded together. The bonded device was baked at 120°C for 5 min.

5.2.2 Spatial wettability patterning

In order to make the microfluidic device suitable for generating DEs, the whole device was first placed in an oven at least 60 °C for 48 h to recover the intrinsic hydrophobicity of PDMS. To render the flow-focusing droplet generator hydrophilic while maintaining the T-junction droplet generator hydrophobic, a hand-held corona treater (BD-20AC, Electrotechnic Products, Chicago, IL, USA) was employed. First, the corona metal electrode tip was inserted into the microchannel outlet in contact with the glass substrate. The corona discharge power level was set to the minimum (~10,000 V at a frequency of 4.5 MHz), and the penetration of the electrode tip was adjusted to ensure the corona discharge extended only to the end of the deep channel

(i.e., the entrance to the corona resistor). The corona discharge was sustained for approximately 5 to 10 s.

5.2.3 Surface wettability characterisation

Three types of characterisation were performed to assess the effectiveness of this method under three scenarios of treatment: untreated, partially treated (2 s), and sufficiently treated (5 s). Contact angle (CA) measurements were performed using a static sessile drop method. 3 μL droplets of Milli-Q water were positioned on PDMS surfaces, and after 10 min the shapes of the CAs were captured. To visualise the wettability patterns within the microchannels, a hydrophobic fluorescence dye, 20 μM SYTO 9® (Thermo Fisher Scientific, Waltham, MA, USA), was continuously flowed through the channel for 3 min. The microchannel was then flushed by Milli-Q water and dried by N_2. In addition, the DEs formation behaviour was monitored and recorded at the flow-focusing section.

5.2.4 Device operation

Solutions for inner phase, middle phase, and outer phase were loaded into three different syringes that were connected to the corresponding inlets via FEP tubing (IDEX, Lake Forest, IL, USA) with an inner diameter of 0.5 mm. The plastic syringes were mounted on syringe pumps (Fusion 100, Chemyx, Stafford, TX, USA) for smooth and controllable infusion. After the device was treated to create spatially patterned wettability, an outer phase solution was immediately injected into the deep channel and kept flowing for up to 2 min; the middle phase solution was subsequently injected to prevent the outer phase from coating at the T-junction droplet generator; then the inner phase was injected (Fig. S5.2). All three phases were fine-tuned to desired volumetric flow rates to generate stable monodisperse DEs of different properties according to applications. After stable DEs are generated, a 2 mL Eppendorf™ safe-lock tube (Hamburg, Germany) prefilled with 250 μL collection buffer, 1% v/v Tween® 20

(P9416, Sigma-Aldrich, St. Louis, MO, USA) added 1 × phosphate-buffered saline (PBS, 10010023, Thermo Fisher Scientific, Waltham, MA, USA) was used to collect DEs.

5.2.5 DE generation

To investigate of the size and morphology of DEs, we used 1% v/v tween® 20 added PBS as an inner phase, 2% v/v Pico-Surf™ 1 (Sphere Fluidics, Cambridge, UK) added Novec™ 7500 Engineered Fluid (3M, St. Paul, MN, USA) as a middle phase, and 2% w/v Pluronic-127®, 2% v/v Tween® 20 added PBS as an outer phase.

To generate gelatin microgels using DEs as templates, we mixed 0.001% w/v 200 kDa FITC-dextran, (FD2000S, Sigma-Aldrich, St. Louis, MO, USA) with gelatin from porcine skin (Type B, G6650 Sigma-Aldrich, St. Louis, MO, USA) dissolved in PBS at a temperature of 50 °C and used this solution as the inner phase. The middle phase was prepared by adding 0.001% w/v Nile Red (19123, Sigma-Aldrich, St. Louis, MO, USA) and 1% v/v Span® 80 (85548, Sigma-Aldrich, St. Louis, MO, USA) to mineral oil (M5904, Sigma-Aldrich, St. Louis, MO, USA); The outer phase and the collection buffer were the same as aforementioned. During the generation of DEs, the ambient temperature was maintained above 30 °C. After the collection of DEs, the collection tube was kept at 4 °C to make sure that the inner gelatin core undergoes phase transition to gel.

To effectively encapsulate yeast cells with a density of ~1.11 g/mL) in DEs, we used 30% v/v OptiPrep™ (D1556, Sigma-Aldrich, St. Louis, MO, USA)[41] with added cell culture medium containing yeast cells as the inner phase[46], Bio-Rad droplet generation oil for probes (1863005, Bio-Rad, Hercules, CA, USA) as the middle phase, and the same outer phase and collection buffer as before. The procedures for the preparation of GFP-tagged *S. cerevisiae* strain (CEN.PK2-1C-GFP), determination of concentration, and *in vitro* culture, were detailed in our previous study[47]. GFP-tagged *S. cerevisiae* cells at four different concentrations: 5×10^6,

1×10^7, 2×10^7, and 8×10^7 cells/mL were used in inner phase. Cell concentration of 1×10^7 cells/mL was used for the screening of single-cell growth in DEs.

5.2.6 Flow cytometric screening

The yeast cell-laden DEs were screened using a CytoFLEX flow cytometer (Beckman Coulter Life Sciences, Miami, FL, USA) with a 100 μm nozzle. The FC was equipped with a 488 nm excitation laser and a FITC (λ_{ex} = 488 nm/λ_{em} = 525 nm) bandpass filter for the screening of DEs encapsulating *S. cerevisiae* cells. For each measurement, 30 μL DEs were pipetted from the top of the centrifuge tube and resuspended in 90 μL sheath buffer containing 1% v/v Tween® 20 in PBS. Monodisperse DEs were selected from 8,000 events, using FSC vs SSC log-log scatter plots for analysis (Fig. S5.3). Fluorescence intensity was then used to identify the DE droplets encapsulating *S. cerevisiae* cells. Screening rate was set to below 500 events/s to avoid high shear turbulence.

5.2.7 Data acquisition and analysis

The formation and behaviour of DEs were monitored and recorded using an inverted microscope (Eclipse Ti-U, Nikon, Tokyo, Japan) equipped with a high-speed camera (Phantom Miro 320, Vision Research, Wayne, NJ, USA). The images were captured with an exposure time of 10 μs, and frame rates were varied according to channel regions for measurements. A portable microscope (AM4113T, Dino-Lite, New Taipei City, Taiwan) was used to visualise the shape of droplets on PDMS surfaces, measure CAs, and monitor the performance of corona resistors having different features. The fluorescence images used to characterise spatially patterned wettability within microchannels were recorded by a digital camera (DS-Qi1Mc, Nikon, Tokyo, Japan) installed on the inverted microscope. The bright-field and fluorescence images of gelatin microgels in and out of DEs as well as cell-laden DEs were acquired by a confocal microscope (FV3000, Olympus, Tokyo, Japan). All recorded videos and image sequences were processed using Phantom Camera Control Software (PCC 3.5, Vision Research,

Wayne, NJ, USA) and Image J (NIH, Bethesda, MD, USA). Flow cytometric data were recorded and analysed by software CytExpert 2.4 (Beckman Coulter Life Sciences, Miami, FL, USA).

5.3 Results and discussion

5.3.1 Design and preparation of the microfluidic device with spatial wettability patterning

The microfluidic device employed here includes two separate microdroplet generators, a T-junction and a sequential flow-focusing geometry for hierarchical encapsulation of single emulsions (see Fig. 5.1B). At the hydrophobic T-junction droplet generator, the inner phase meets a stream of carrier oil and then is encapsulated into regularly-spaced w/o single emulsions. We use T-junction instead of flow-focusing geometry for single emulsion generation to minimise the possibilities of bubble adhesion. At the hydrophilic flow-focusing droplet generator, single emulsions are subsequently entrapped by the aqueous outer phase, resulting in stable DEs. Using different inner and middle phases in the same microfluidic devices, we can generate different types of DEs having different inner cores (Fig. 5.1C), which can be used for multiple applications, such as templates to fabricate and spontaneously release gelatin microgels, and bioreactors to encapsulate and culture single cells.

The resultant DEs in this study can maintain the core-shell structure for more than one month, when they are stored in a normal centrifuge tube under ambient conditions. Please note that that our approach can generate highly uniform, with a coefficient of variation (C.V.) < 1.4% (see Fig. S5.4). This value is comparable to or smaller than those for the DEs generated by other methods, e.g., multi-module co-axial flow-focusing capillaries (C.V. = 2.5~3.0%[3, 4, 6]), multi-module connected microfluidics chips (C.V. = 2.5~3.0%)[10, 48], layer-by-layer assembly (C.V. = 5.2~7.3%)[38, 39], chemical functionalisation by flow confinement (C.V. = 1.3 ~ 4.2%)[27,

[40, 49-51], plasma oxidation (C.V. = 2.1~2.5%)[7, 14, 31], and localised UV treatment of glass (C.V. < 8.0%)[33]. We noted that the stability of generated DEs can be further improved by different approaches, such as using proper surfactants[7, 52] and maintaining the balance of the osmotic pressure between the inner phase and the outer phase[39]. Moreover, there are some potential approaches which can be used to further enhance the cost-effectiveness of our system for DE generation, such as using a balloon-based pressure pump for liquid injection[53], and constructing a customised system based on a DC high voltage supply and metal tips to generate corona discharge[54]. It's worth noting that the distribution and real-time intensity of corona discharge during the wettability patterning process can be observed by a smartphone, which has recently been adopted for highly sensitive and quantitative analysis in microfluidics[55].

5.3.2 Characterisation of spatial wettability patterns

The surface properties of the microfluidic channels determine the polarity of the emulsions formed and the types of DE generated. A hydrophobic surface is required for w/o single emulsion generation at the T-junction droplet generator, while localised corona treatment is applied to modify the inside surface area of the flow-focusing droplet generator to hydrophilic for w/o/w DE generation (see Figs. S5.5A and 5.5B). Using the controllable corona discharge with the purpose-optimised corona resistance microchannel, a defined area of spatial patterning of wettability is achieved in one step within 10 s, without the necessity for repeated treatments or any external blocking phases. Noteworthy, this can be acquired by visual instead of microscope-assisted observation because the corona discharge induced by a high voltage can result in a highly distinct flare in PDMS channels.

We achieved continuous generation of DEs for at least 6 hours. Moreover, the capacity of the device for generating DEs can be extended to at least three days in optimal conditions. After prefilling the hydrophilic region with DI water, we stored the treated device in a petri dish filled with DI water and covered all openings on the device with a waterproof tape. DEs were found

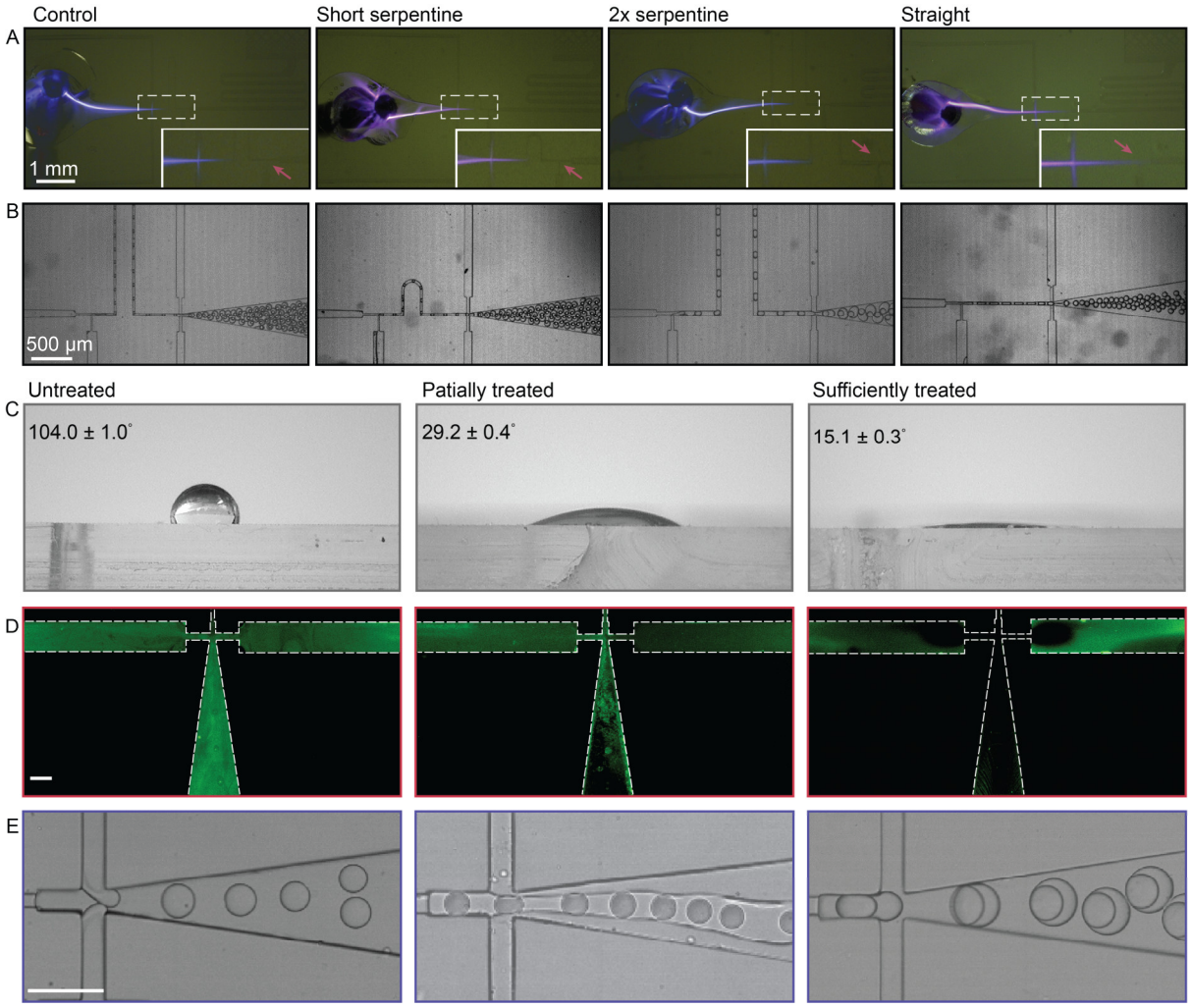

Figure 5.2 Characterisation of PDMS surface properties within the microfluidic devices having spatially resolved wettability patterns. A and B) Experimental images of A) microchannels being treated by localised corona discharge, and B) droplet generation in microchannels after sufficient treatment. Different types of corona resistors: control, short serpentine, 2 times serpentine and straight channel, are presented. The white dashed frame represents the enlarged area including two droplet generators. The red arrow indicates the T-junction droplet generator. C) Bright-field images of contact angles (CAs) of 3 µL water droplets positioned on the surfaces of untreated, partially treated (2 s), and sufficiently treated (5 s) PDMS. D) Fluorescent images of the flow-focusing droplet generator, which is flushed with SYTO 9 dye. E) Experimental images of DE generation at the flow-focusing junction under different levels of treatment. Scale bars represent 100 µm.

to be successfully generated in the corona discharge treated device after three days of storage (see Fig. S5.6). This agrees with previous findings that the hydrophilicity of PDMS can remain stable for one week by storing the sealed PDMS channels in DI water[44, 56]. Although,

hydrophilicity was observed to remain for several hours without sealing by water, however exposing the treated channel to air for long times was not desirable since this may reduce the performance of devices for continuous generation of monodisperse DEs[44].

This method can be used to achieve desired balance or higher levels of complexity of hydrophilicity and hydrophobicity in specific microfluidic devices for the generation of droplets of different sizes, morphology, or higher order of emulsions.

The key concept of this approach is when the unwanted regions are protected by a narrow channel acting as a corona resistor, to achieve a highly hydrophilic surface at target regions. Thus, we have optimised the performance of this method from two aspects: the geometry of microchannels and the treatment time. First, the microchannel (which can resist the entry of ionised air) can be an analogy of the resistor to electric currents, where the geometry plays an important role in resistance performance. Second, the treatment time is positively correlated with the ability to remove hydrocarbon groups and increase hydrophilic groups. Moreover, it is reported that a relatively long plasma treatment time renders a much smoother surface by AFM surface analysis[44].

For the optimisation of dimensions of microchannels, the effects of shape, size, and length of the corona resistors on DE generation have been investigated by observing the localised distribution of corona discharge (see Fig. 5.2A) and droplet generation in devices having different resistance channels treated with corona discharge of the same intensity (see Fig. 5.2B). All corona resistor channels have a uniform height of ~25 μm. The control is the corona resistance microchannel used in this study. 2 × serpentine corona resistor has a width and a length twice those of the control, while short serpentine corona resistor has a length one-third of that of the control. The straight corona resistor is 0.85 mm in length. The results showed that the serpentine microchannels used in our study are more effective for preventing the corona discharge from entering the hydrophobic droplet generation region. In the device with a straight

channel as a corona resistor, corona discharge distribution gets in contact with the hydrophobic droplet generation region (see Fig. 5.2A). We also found out that devices with serpentine corona resistance channels can successfully generate monodisperse DEs. However, the one with a straight corona resistor can only form o/w droplets at the T-junction droplet generator and fail to generate DEs afterwards (see Fig. 5.2B). This indicates that the corona discharge is able to travel through the straight corona resistor to enter the T-junction droplet generator region, where hydrophobic surfaces are required.

Notably, a serpentine microchannel as a corona resistor is cost-effective to extend the length of the resistance channel that directly affects its resistance in limited space. In some single-module microfluidic devices for DE generation, a long straight channel (i.e., 1.45 mm[26] and 2.43 mm[27] in length) between the first and the second droplet generators generally acts as a barrier to prevent the surface treatment in a region from disturbing the other one. In contrast, our design of a serpentine channel is very compact and saves up ~20% space, which has also been adopted by other studies[7, 11, 31, 41] to increase the distance between hydrophobic and hydrophilic regions during the process of spatial patterning of wettability. Although a short serpentine channel sometimes works for DE generation as well (see Fig. 5.2B), it bears a high risk with a failure rate of ~ 25%.

Another parameter that plays an important role in confining corona discharge is the width of the channels (i.e., cross-sectional area). Since the resistance of a rectangular channel is inversely proportional to the cross-sectional area[57-60], a decrease in the channel width could increase the resistance to the ionised air in this study and improve the performance of the corona resistor. However, the dimensions of the resistance channel have to be approximately equal to the required inner core diameter (D_{in}) of DEs. This is to ensure 1) the generated w/o droplets (i.e., inner cores of DEs) can pass through the corona resistance channel in an ordered manner, otherwise, the generation of DEs containing multiple cores might unintentionally occur at the

flow-focusing droplet generator, and 2) the inner cores can pass through the corona resistance channel in the form of spherical droplets rather than plug-like shaped ones, which might come in contact with hydrophilic region and rupture[14]. This is also demonstrated by the device with a 2 × serpentine corona resistor (with a width of 45 μm), which generates DEs with inner cores having a diameter (i.e., 49 μm) twice that of the ones generated in the control device (see Fig. 5.2B).

Furthermore, to qualitatively and quantitatively verify the effectiveness of this approach for surface modification, we set three scenarios: untreated (0 s), partially treated (2 s, can render low or part hydrophilicity at target regions and cannot induce DE generation), and sufficiently treated (5 s, can render strong or full hydrophilicity at target regions and can induce successful DE generation). We first performed CA measurements to characterise surface wettability by placing 3 μL water droplets on PDMS surfaces prepared under these three scenarios. A significant difference is observed for CAs measured for treated and untreated surfaces: the calculated CAs were 104.0°, 29.2°, and 15.1°, respectively, for untreated, partially treated, and sufficiently treated PDMS surfaces (see Fig. 5.2C). It is worth noting that a method has been reported to measure the CAs of sealed PDMS channels, in which DI water was pumped into a channel and formed a static and water/air interface for hydrophilicity measurement. This can further provide a more accurate measurement of surface hydrophilicity at the treated regions[44]. Compared with sufficient treatment, partial treatment renders the PDMS surface hydrophilic only to a limited extent (with a relatively high CA, ~70% of treated area are still hydrophobic, and failure to generate DEs). Next, we investigated surface wettability at the flow-focusing droplet generator. 20 μM SYTO 9® staining dye was continuously introduced into microchannels and then flushed out by DI water. SYTO 9® fluorescent dye is hydrophobic and is typically strongly adsorbed at hydrophobic interfaces, similar to rhodamine B[61, 62]. The results show that the untreated PDMS channel is fluorescent, while almost no fluorescence is

observed in sufficiently treated PDMS regions (see Fig. 5.2D). As expected, partial treatment is too weak to properly modify the intended PDMS regions. In addition, no residual dye is found inside or beyond the boundary of the wall at the minimal intensity of corona discharge (i.e., ~10,000 V at a frequency of 4.5 MHz), indicating that the low intensity of corona meets the need. If the corona discharge intensity is excessive, cracking or local swelling of the PDMS channel occurs, and the loaded dye diffuses into and remains trapped in the wall[61]. Moreover, the beginning part of the corona resistor is prone to be treated, rending a super hydrophilic surface. This can result in instable droplet generation, as the aqueous phase for w/o droplets has a higher affinity than the middle phase[32]. The rupture of the droplets may occur as well, especially when the oil shell is very thin[14].We noted that these adverse effects can also be caused if the position of the electrode tip is placed too close to the treated regions. Thirdly, we observe DE formation at the flow-focusing droplet generator (see Fig. 5.2E): only w/o single emulsions are generated in untreated channels, while stable w/o/w DEs are generated for at least 3 h in sufficiently treated channels. Finally, we failed to see DE generation in partially treated channels. This is because the oil middle phase wets the walls, causing it to flow as a parallel stream with the aqueous carrier flow (see Fig. 5.2E middle)[31].

5.3.3 Generation of DEs with controllable size and morphology

We have further investigated the effects of flow rates of different phases on the size and morphology of generated DEs, including D_{in}, shell thickness, and the number of inner cores. Note that monodisperse w/o droplet formation at the T-junction droplet generator and w/o/w DEs at the flow-focusing droplet generator in dripping regime[63] were consistently observed under all tested experimental conditions. The corresponding Capillary number (Ca) of the disperse phase and continuous phase for stable and continuous droplet generation is below 0.1[32, 64].

We found that D_{in} increased with decreasing ratio of inner phase flow rate (Q_{in}) to middle phase flow rate (Q_{mi}), Q_{mi}/Q_{in}, the oil shell thickness decreasing correspondingly, when the total flow rates (Q_{total}) of Q_{in} and Q_{mi} were kept constant (see Fig. 5.3A and Fig. S5.7). Moreover, we can increase the outer diameter of DEs (D_{out}) and consequently increase the number of encapsulated cores by decreasing Q_{Out}/Q_{total} while keeping Q_{total}, $Q_{in}+Q_{mi}$, constant (see Fig. 5.3B). The value of D_{out} is roughly constant at 58.9, 56.8, and 52.2 μm, respectively, when Q_{total} is 4 μL/min, 6 μL/min, or 8 μL/min. Our results agree with findings of previous studies: under the dripping regime, when the geometry of droplet generators and properties of different phases are fixed, the diameter of resultant droplets relies on the flow rate ratio between different phases, i.e., $D_{in} \propto (\mathrm{Ca} \times \mathrm{a})^{-1}$, $\mathrm{a} = Q_{mi}/Q_{total}$[64]. Moreover, when D_{out} is kept constant, the thickness of the oil shell is inversely proportional to D_{in}, which, therefore, is also dependent on the flow rate ratios.

D_{in} and middle-phase (oil) shell thickness were measured for three different Q_{total}, when Q_{mi}/Q_{in} was varied from 1 to 5 (Fig. 5.3C). The results show that D_{in} can be adjusted independently of other droplet dimensions by varying flow rate ratios, i.e., Q_{mi}/Q_{in}. In general, the inner core dimeter increases while the shell thickness decreases with the increase of Q_{mi}/Q_{in}.The dimensions of generated DEs show greatest variability for the highest Q_{Out} (i.e., 8 μL/min): D_{in} can be chosen in a range from the largest (41.9 μm) to the smallest (27.5 μm) size, with the thinnest oil shell (i.e., 5.2 μm). It is noteworthy that when Q_{mi}/Q_{in} declines to below 1, the inner phase is forced to contact the hydrophilic walls of the channels, resulting in the rupture of DE.[17]

In addition, we varied Q_{Out} while maintaining Q_{in} and Q_{mi} constant at 1 and 3 μL/min, respectively, to investigate the effect of Q_{Out} on D_{out} and the number of inner cores (see Fig. 5.3D). When Q_{Out}/Q_{total} declines from 1.26 to 0.13, D_{out} increases and the number of encapsulated inner cores consequently changes from 1 to 5. It is noteworthy that the

monodispersity of generated DEs is highly dependent on the synchronisation of three phases. When the values of Q_{Out}/Q_{total} are between these values, DEs having different core numbers co-exist. When Q_{Out}/Q_{total} is increased to slightly over 1.26, D_{out} subsequently declines, and DEs are generated more rapidly. We note that DEs with single cores can be generated when

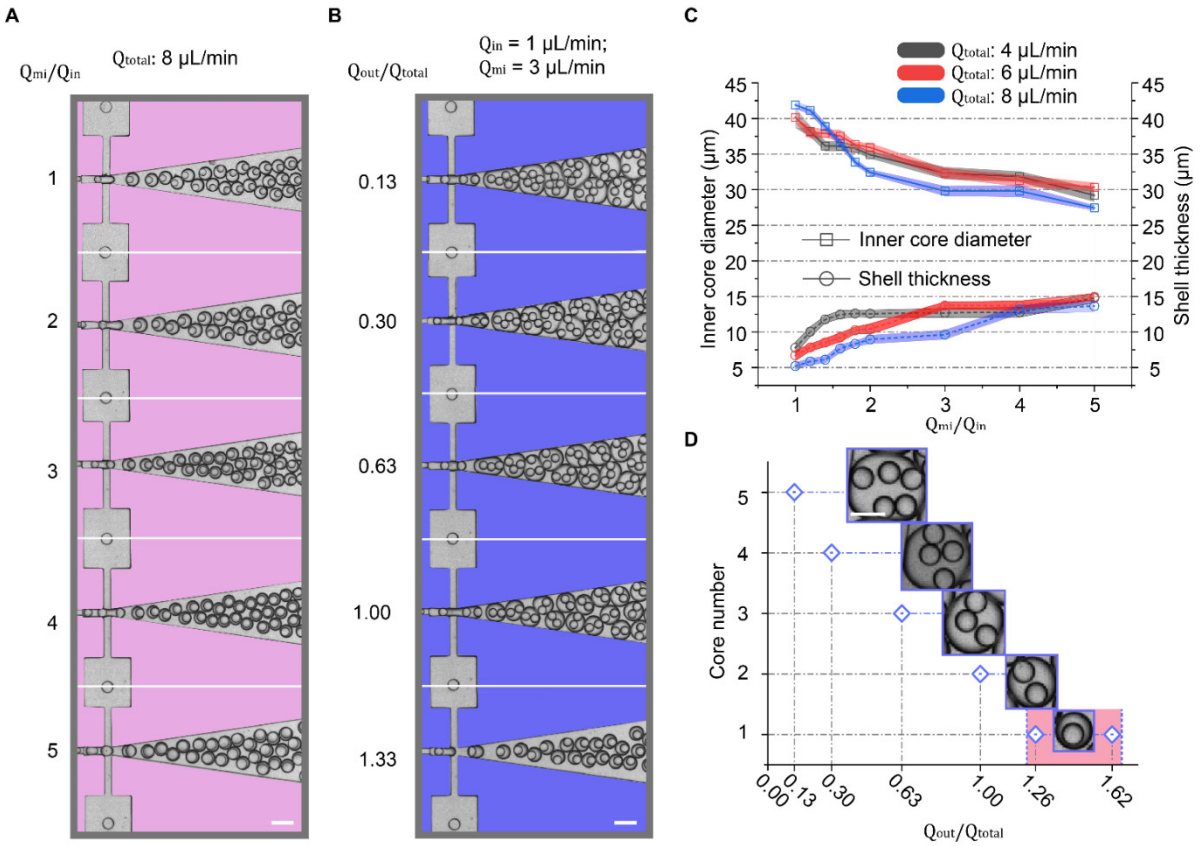

Figure 5.3 Control of the inner core diameter (D_{in}), oil shell thickness, and the core number of DEs. A) Experimental images of generated DEs at five different ratios of the middle and inner phase flow rates, Q_{mi}/Q_{in}: 1, 2, 3, 4, and 5, when the total flow rate, Q_{total}, sum of Q_{in} and Q_{mi}, is set constant at 8 μL/min. B) Experimental images of generated DEs at five different ratios of outer phase flow rate and total flow rate, Q_{out}/Q_{total}: 1.33, 1.00, 0.63, 0.30, and 0.13, when the Q_{total} is fixed at 4 μL/min (Q_{in} = 1 μL/min; Q_{mi} = 3 μL/min). Scale bars represent 100 μm. C) A plot of D_{in} and shell thickness versus Q_{mi}/Q_{in} at three different Q_{total}: 4, 6, and 8 μL/min. The outer diameters of DEs are roughly constant in these cases for each outer diameter of DEs (D_{out}). The standard deviation is indicated by the shaded area. D) A plot of core number versus Q_{Out}/Q_{total}, when Q_{total} is fixed at 4 μL/min. The red highlighted area indicates the range of Q_{Out}/Q_{total}, for the generation of DEs encapsulating single cores. The insets are images showing DEs have different numbers of inner cores. Scale bar represents 50 μm.

Q_{Out}/Q_{total} varies with the range of 1.26 to 1.62 (Fig. 5.3D, red lighted region). If Q_{Out}/Q_{total} increased significantly to over 1.62, empty oil droplets appear. The number of inner cores is dependent on the outer diameter of DEs as $\mathrm{d} \propto (\mathrm{Ca} \times \mathrm{a})^{-1}, a = Q_{out}/Q_{out} + Q_{total}$, where D_{out} is the outer diameter of DEs[64].

5.3.4 Generation of monodisperse gelatin microgels using DEs as templates

We have also demonstrated that the DE technique can be used as a template to generate spherical microgels of highly uniform size. Such microgels have significant potential for application in tissue engineering and cell therapy due to their ability to provide a physiologically relevant 3D microenvironment for living cells[15, 22, 65]. Traditionally, w/o single emulsions are used for producing monodisperse microgels with a variety of polymerisation approaches. However, such methodologies require the use of large volumes of oil for the carrier phase, prolonged exposure to the oil and surfactants (which can be cytotoxic to the encapsulated cells), and an additional washing step for phase transfer. Alternatively, DE can be used as an intermediate template to produce microgels in an aqueous solution, avoiding the use of oil and the extra washing step[6, 14, 35, 37]. Using the microfluidic device described here, we have created monodisperse gelatin-in-oil-in-water DEs with different sizes and compositions. Gelatin is a cross-linked natural protein with thermally responsive sol-gel transition properties and is commonly used food and pharmaceutical industries[47].

We used FITC-dextran added gelatin in PBS at three different concentrations, 1, 2 and, 4% w/v, as the inner phase, mineral oil as the middle phase, and PBS with 2% w/v Pluronic-127® and 2% v/v Tween® 20 as the outer phase. The FITC-dextran added gelatin is pre-dissolved in PBS at ~50 °C. By controlling the ambient temperature at above 30 °C, we encapsulated aqueous gelatin solution in DEs as core (see Fig. 5.4A). Since the viscosity of mineral oil is higher than that of fluorocarbon HFE-7500 engineering oil, a higher middle-phase flow rate, Q_{mi}, (requiring higher pressure delivery) is needed to overcome the resistance in the channel,

otherwise, a jetting regime[45] occurs at the T-junction droplet generator. Thus, we use Q_{mi}/Q_{in} a factor around three times greater than those used in the previous experiment, notably 4, 6, 8, 10, and 12, to investigate the effect on D_{in}. The results show that D_{in} can be easily controlled by adjusting Q_{mi}/Q_{in}, when the Q_{total} of gelatin solution (inner phase) and mineral oil (middle phase) is fixed at 8 μL/min. In general, D_{in} decreases with the increase of Q_{mi}/Q_{in}, regardless

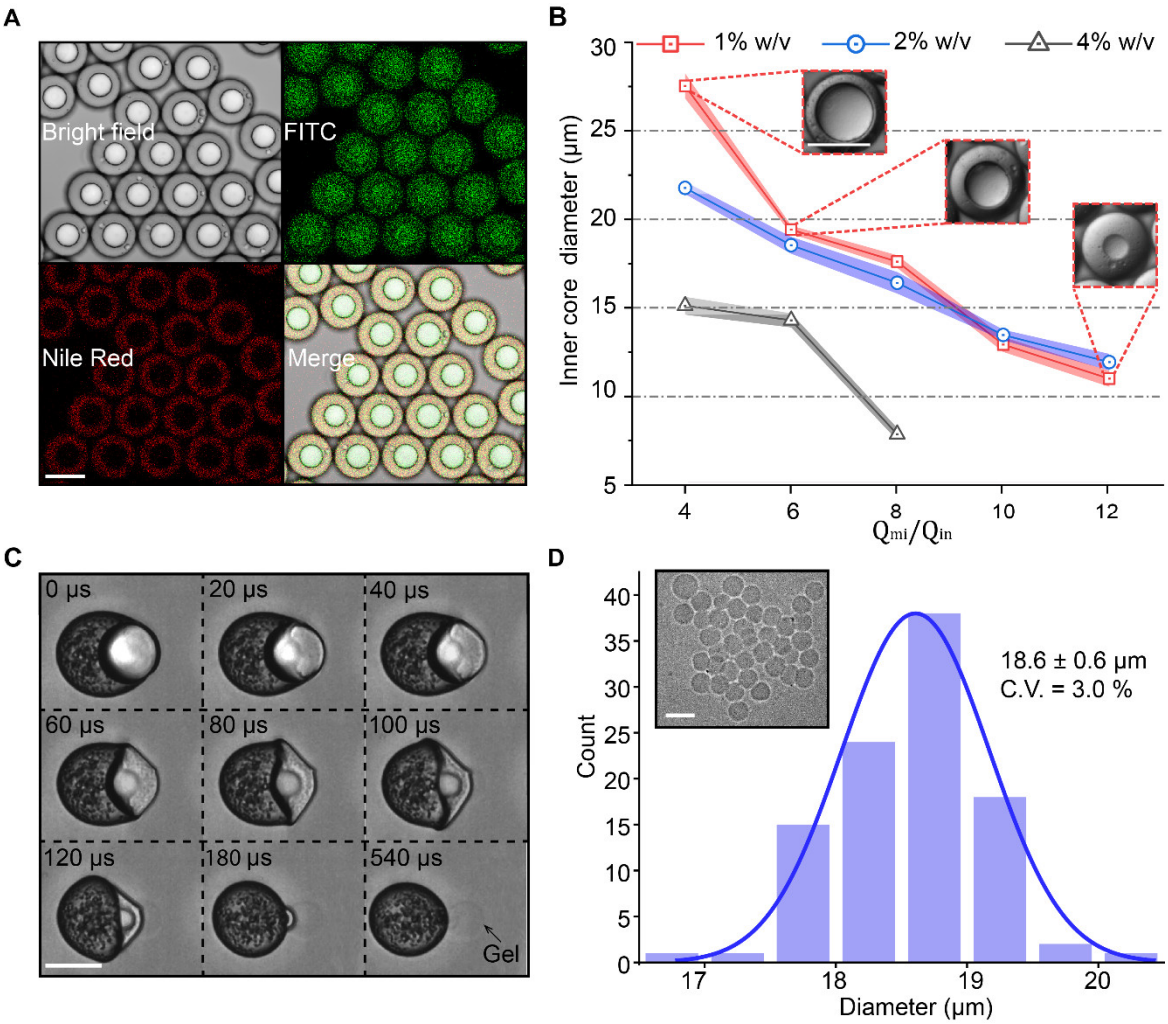

Figure 5.4 Generation of monodisperse gelatin microgels using DEs as templates. A) Brightfield and confocal images of FITC-dextran added gelatin-in-oil-in-water DEs surrounded by Nile-Red labelled mineral oil. B) A plot of D_{in} versus Q_{mi}/Q_{in}, when gelatin solutions have three different concentrations: 1, 2, and 4 % w/v. The standard deviation is indicated by the shaded area. The insets are images showing DEs with different sized inner cores. C) A series of high-speed images showing the release of a microgel from a DE into an aqueous solution (DI water). D) A histogram of size distribution of the released gelatin microgels. The inset shows the resultant microgels. Scale bars represent 30 μm.

of gelatin concentration (see Fig. 5.4B). When Q_{mi} / Q_{in} increases from 4 to 12, D_{in} significantly decreases from 27.5 ± 0.7 to 10.9 ± 0.4 μm and from 21.7 ± 0.3 to 11.8 ± 0.5 μm, respectively, when gelatin concentrations are 1 and 2% w/v. When the concentration of gelatin increases to 4% w/v, D_{in} declines from 15.0 ± 0.5 to 7.7 ± 0.4 μm with the increase of Q_{mi}/Q_{in} from 4 to 8 (though injection into the channels remains satisfactory). However, when we further increase Q_{mi}/Q_{in}, to over 8, the inner phase containing 4% w/v gelatin fails to enter the T-junction droplet generator. This is because the resistance to flow in PDMS channel significantly increases when injecting the fluids of high viscosity. A lower flow rate is necessary to inject high viscosity liquids, otherwise, the high pressure in the microchannel might lead to inconsistent flow, fluid leakage, and channel deformation[66, 67].

After solidification of gelatin solution at a low temperature (i.e., 4 °C), DEs were transferred to DI water without any surfactants. It has been noted that there are significant changes in the interfacial tension and density among the difference phases of gel-in-oil-in-water DEs[6]. In this case the oil shell destabilises and dewets the solid surface of the inner gelatin microgel, and spontaneous release of gelatin microgels from DEs to outer phase occurs[6, 37, 68]. Fig. 5.4C shows that the release of the gelatin microgel from DE into DI water without any surfactants, within the course of 540 μs. Using DEs as sacrificial payload carriers, monodisperse gelatin microgelwith a C.V. of 3.0% can be generated (Fig. 5.4D).

5.3.5 Flow cytometric screening of encapsulation and growth of yeast *S. cerevisiae* cells in DEs

To demonstrate that the generated w/o/w DEs in this study can act as microbioreactors, we encapsulated and cultured GFP-tagged *S. cerevisiae* cells in DEs.

The microfluidic device can generate monodisperse (C.V. < 1.5%) DEs having D_{in} of 28.3 μm and D_{out} of 46.3 μm (see Fig. S5.4), which are compatible with FC. We first encapsulated *S. cerevisiae* cells of three different concentrations, 5×10^6, 2×10^7, and 8×10^7 cells/mL, within

monodisperse DEs (see Fig. 5.5A). Using FC, we performed screening of empty DEs as a negative control, and samples of both empty DEs and cell-laden DEs prepared at different cell concentrations (Fig. 5.5B). Although empty DEs have low but detectable auto-fluorescence, we are able to isolate the population of cell-laden DEs based on measured parameters (i.e., FSC-H and SSC-H). The gating strategy is shown in Fig. S5.3. Around 6,000 events representing monodisperse DEs are selected in all the conditions. As expected, we observed an increase in the fluorescence intensity as well as the proportion of cell-laden DEs (FL positive events in Fig. 5.5B) with the increase of cell concentration. The percentages of empty DEs in total events are 95.1 ± 0.2%, 80.5 ± 3.3%, and 46.7 ± 6.0% when the cell concentrations are 5 × 10^6, 2 × 10^7, and 8 × 10^7 cells/mL, respectively. These practical values determined by FC screening agree well with the theoretical ones predicted by Poisson distribution (see Fig. S5.8).

To show that the generated DEs are capable for yeast growth assays, we first confirmed that single *S. cerevisiae* cells grow to clusters in DEs after a culture of 8 h under a microscope (Fig. 5.5C). Additionally, we performed FC screening of DE samples before and after culture, where two main populations of empty DEs and cell-laden DEs are observed in both scatter plots (Fig. 5.5D). The proportions of cell-laden DEs are determined as 9.3 ± 0.5% and 10.5 ± 1.0%, respectively, for samples before and after culturing, effectively the same within experimental error. Using the defined gate, we selected at least 500 cell-laden DEs from each sample and compared their fluorescence intensity (Fig. 5.5E). There exists a clear shift of fluorescence intensity values between before culture and after culture samples. The median fluorescence intensity increases from 1.1 × 10^5 to 1.6 × 10^5 due to cell growth and the corresponding increase in the number of *S. cerevisiae* cells in DEs. These results demonstrate that DEs can be used to perform high-throughput cell screening at the population level, where different growth characteristics of individual cells within a phenotypically heterogeneous population can be detected.

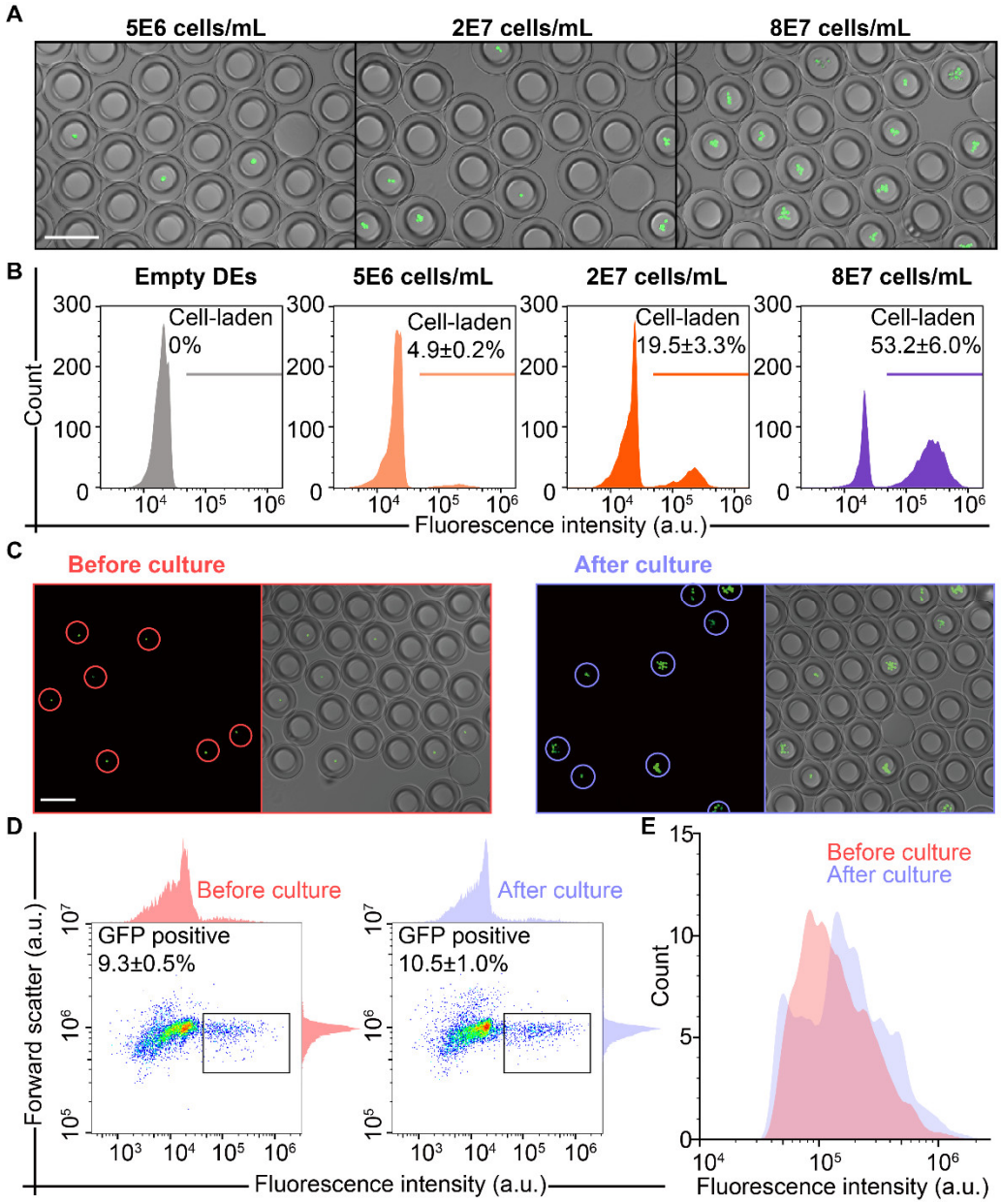

Figure 5.5 Encapsulation and growth of GFP-tagged *S. cerevisiae* cells in monodisperse DEs. A) Merged brightfield and confocal images showing the encapsulation of *S. cerevisiae* cells at three different initial concentrations, 5E6, 2E7, and 8E7 cells/mL, into DEs. Scale bar represents 50 μm. B) Fluorescence (FITC-H) histograms of empty DEs and samples containing both empty DEs and DEs containing *S. cerevisiae* cells of different concentrations obtained by flow cytometric screening. C) Experimental images showing the growth of single *S. cerevisiae* cells in DEs over a culture of 8 h. Scale bar represents 50 μm. D) Forward scatter (FSC-H) vs FITC-H of DE samples before and after culture obtained by flow cytometric screening. The square gate encircles DEs containing fluorescence-positive *S. cerevisiae* cells. E) Comparison of the fluorescence intensity of cell-laden DEs in the defined gate before culture and after culture.

In addition to characterisation of cell growth, DEs can be used to investigate cellular responses to environmental stimuli at a single-cell level. Enzymatic activity analysis might also be performed inside DEs by adding fluorogenic substrates to the medium. Since DEs can circumvent the shear-induced destabilisation in FC instruments, we can use FACS to sort multiple sub-populations exhibiting important phenotypes of interest using DEs as compartments. For instance, we have achieved the high-throughput screening and sorting for an artificial library containing cells of different levels of enzyme secretion. This will achieve *in vitro* compartmentalisation and directed evolution of molecules and cells based on iterative rounds of randomisation and selection, at a higher throughput than on-chip processes, i.e., FADS. The versatility of DEs makes them potentially applicable to a wide range of applications, including but not limited to drug discovery, disease diagnostics, and synthetic biology.

5.4 Conclusions

In this study, we have demonstrated a rapid, simple, and inexpensive method to selectively pattern wettability in a single PDMS microfluidic device using localised corona discharge combined with a purpose-designed serpentine corona resistance microchannel (corona resistor). The method affords greatly enhanced flexibility in generating monodisperse DEs of different components, with a high degree of control over their size and morphology. Moreover, we have successfully generated gelatin microgels using DEs as templates and performed high-throughput FC screening of DEs that allow single yeast cell growth. This approach can be more easily extended to create different hydrophilic and hydrophobic patterns in microfluidic devices for generating inverted DEs, i.e., oil-in-water-in-oil emulsions, and high-order multiple emulsions, than previously-reported approaches requiring complex fabrication or difficult manipulation of blocking phases. We believe that these developments offer major advantages in improved efficiency, simplicity, cost-effectiveness, robustness, and versatility, with the

potential to further accelerate the evolution of DE applications in industry and fundamental research.

Supporting Information

Fig. S5.1 Design of the microfluidic device used in the experiments, Fig. S5.2 Actual image of the experimental setup, Fig. S5.3 Scatter plot of DE samples obtained by a flow cytometer, Fig. S5.4 Droplet monodispersity measurements, Fig. S5.5 Photograph of the device and the device being treated by corona discharge, Fig. S5.6 Droplet generation within devices stored in DI water for 3 days, Fig. S5.7 DE generation at different ratios of the middle and inner phase flow rates, and Fig. S5.8 Comparison of the probability of empty DEs obtained by experiments and predicted by the Poisson distribution.

Video S5.1 Generation of highly monodisperse single emulsions and double emulsions and Video S5.2 Encapsulation of single yeast *S. cerevisiae* cells in DEs (see attachment).

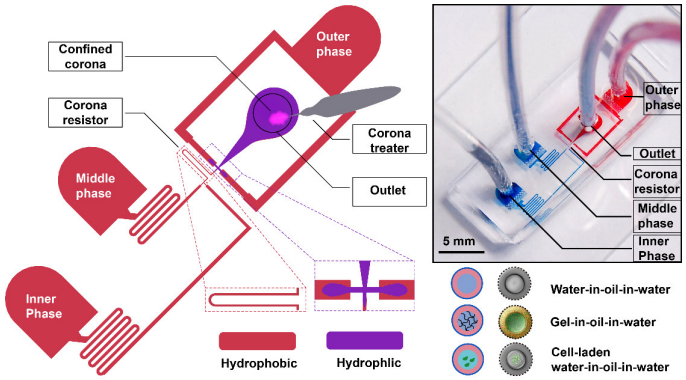

Table of content

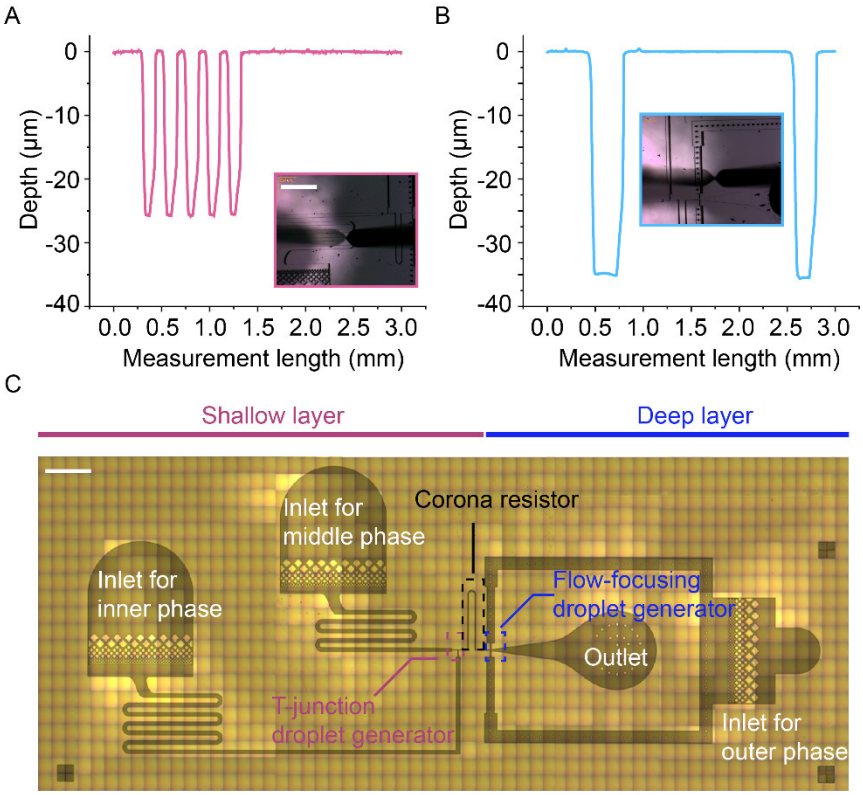

Figure S5.1 The design of the microfluidic device used in this study. Thickness measurement of the (A) shallow and (B) deep layers of the microfluidic device used in this study. Insets are images of the measured regions. Measurement length is set at 3 mm. (C) An actual image of SU-8 master showing the elements integrated in this microfluidic device. The microfluidic device consists of three inlets for injecting an inner phase, a middle phase, and an outer phase; a T-junction droplet generator for generating water-in-oil single emulsions; a flow-focusing junction for generating DEs; a serpentine channel as a corona resistor; and an outlet for injecting corona discharge and collecting DEs. Scale bars represent 1 mm.

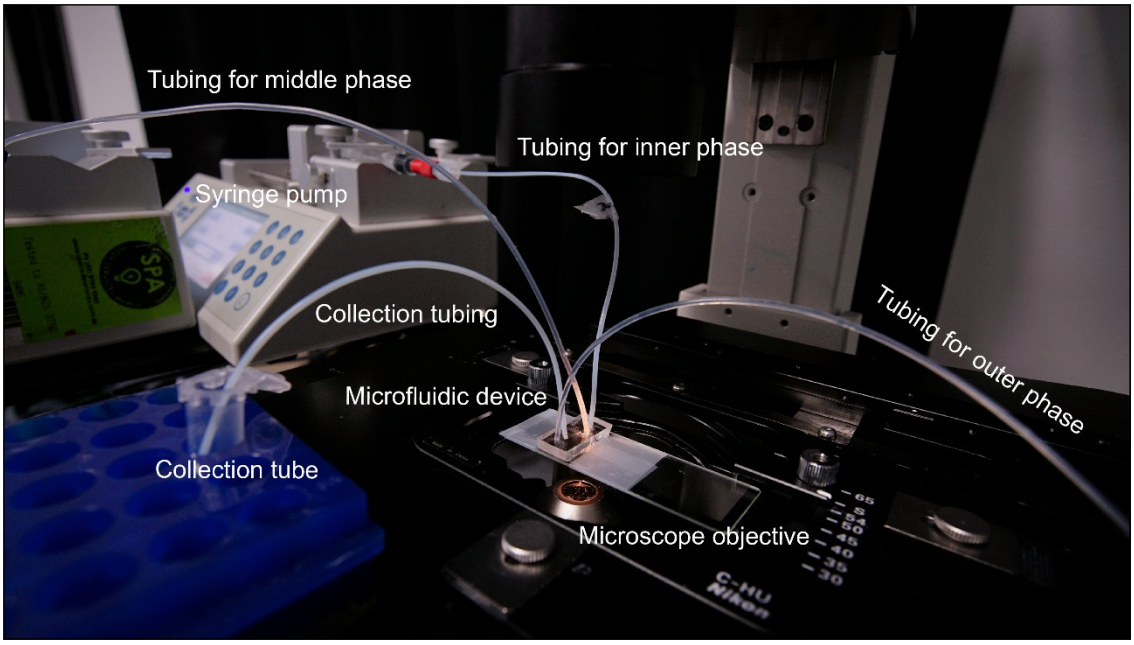

Figure S5.2 An actual image of the experimental setup. The external instruments required for the experiment include three syringe pumps for inner phase, middle phase, and outer phase, respectively, an

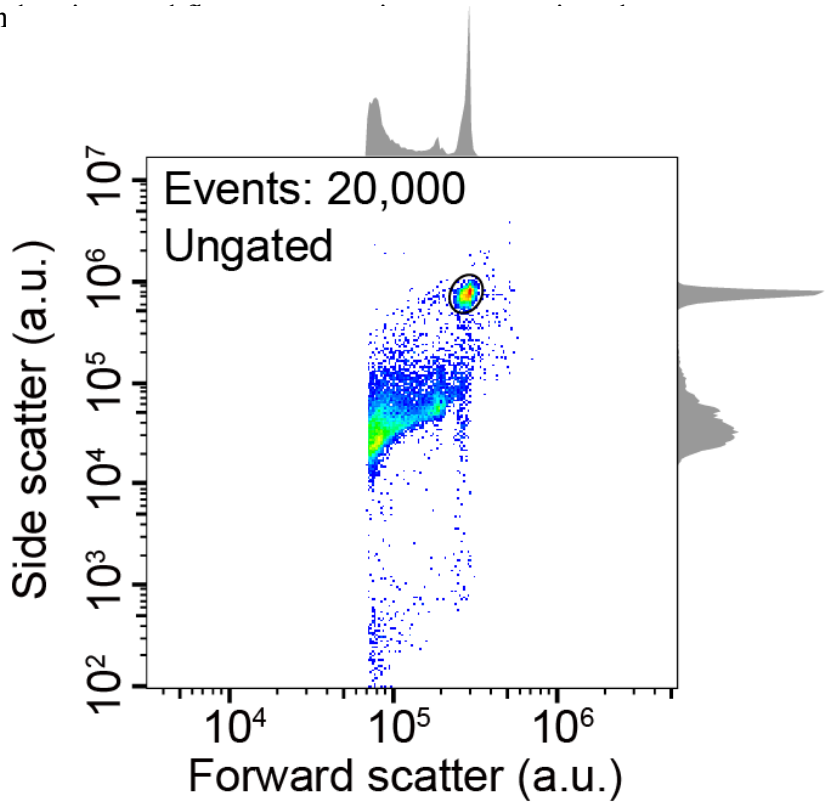

Figure S5.3 Side scatter (SSC-H) vs Forward scatter (FSC-H) of samples obtained by flow cytometric screening. There exists a distinct main population of double emulsion droplets that are highly uniform in term of size and inner structure.

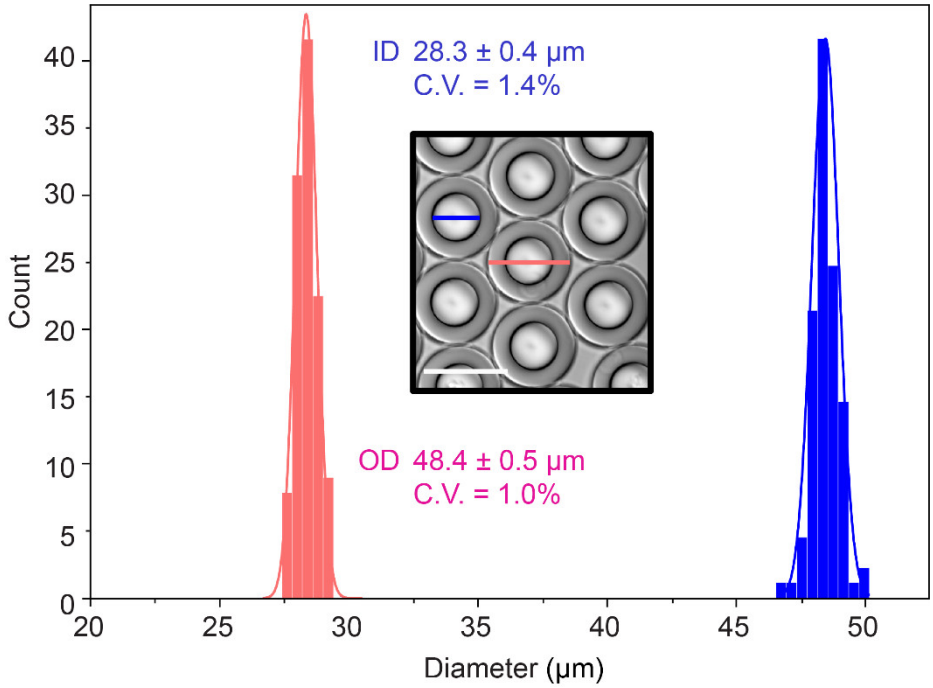

Figure S5.4 A histogram of size distribution of the inner core diameter (D_{in}, red) and the outer diameter (D_{out}, blue) of DEs, which are generated when the flow rates for inner phase, middle phase, and outer phase are 1.2, 2.5, and 8 μL/min, respectively. Scale bar represents 50 μm.

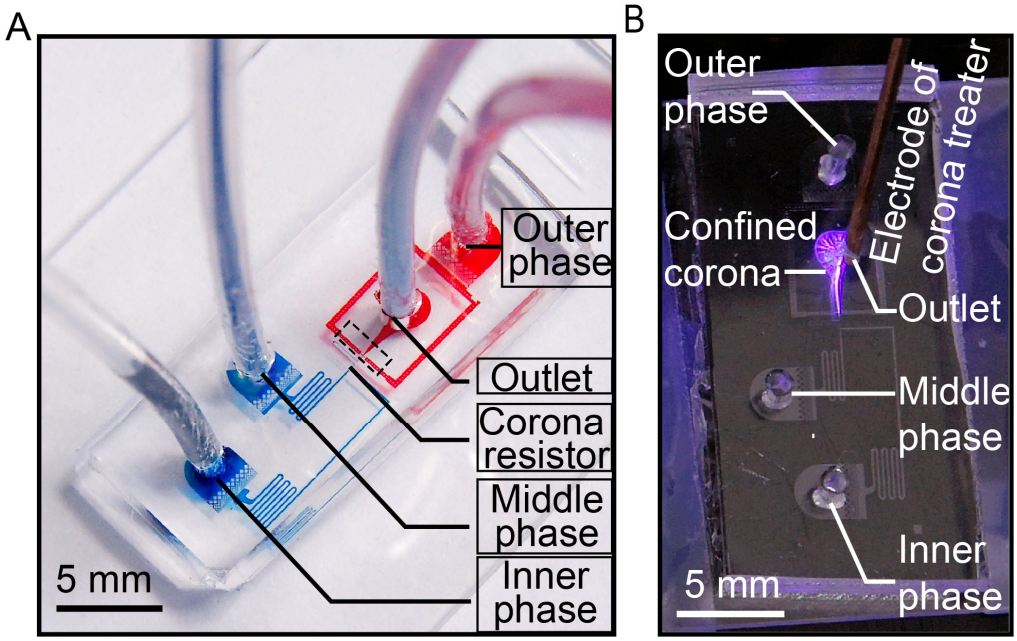

Figure S5.5 A) A photograph of the microfluidic device used in the experiment for DE generation. Shallow channels with a height of 25 μm are infused with blue ink, whereas deep channels with a height of 35 μm are infused with red ink. The black dashed line frame represents the flow-focusing droplet generator. B) An enlarged view of the microfluidic device that is being treated by corona treater to obtain spatially patterned wettability.

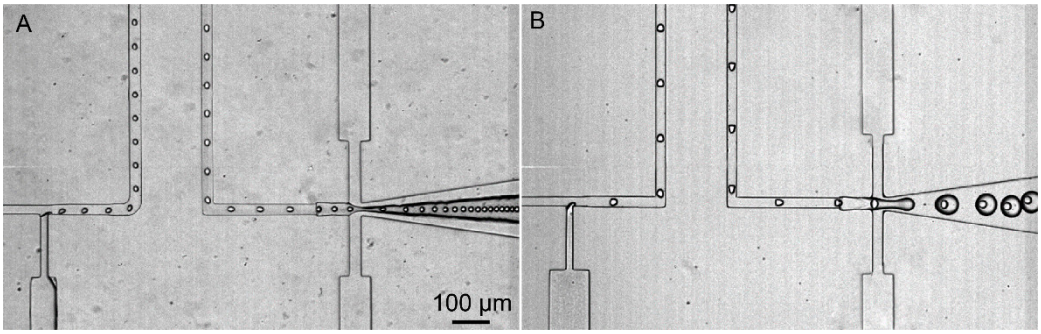

Figure S5.6 Comparison of droplet generation within devices stored in different conditions for three days. (A) Only the generation of water-in-oil droplets is achieved at the first hydrophobic droplet generator, when the hydrophilic region of the device is not filled with DI water. (B) The generation of water-in-oil-in-water droplets is achieved, when the hydrophilic region of the device is filled with DI water. In both cases, the device for droplet generation is placed in a petri dish filled with DI water, and all openings on the device are covered with a waterproof tape.

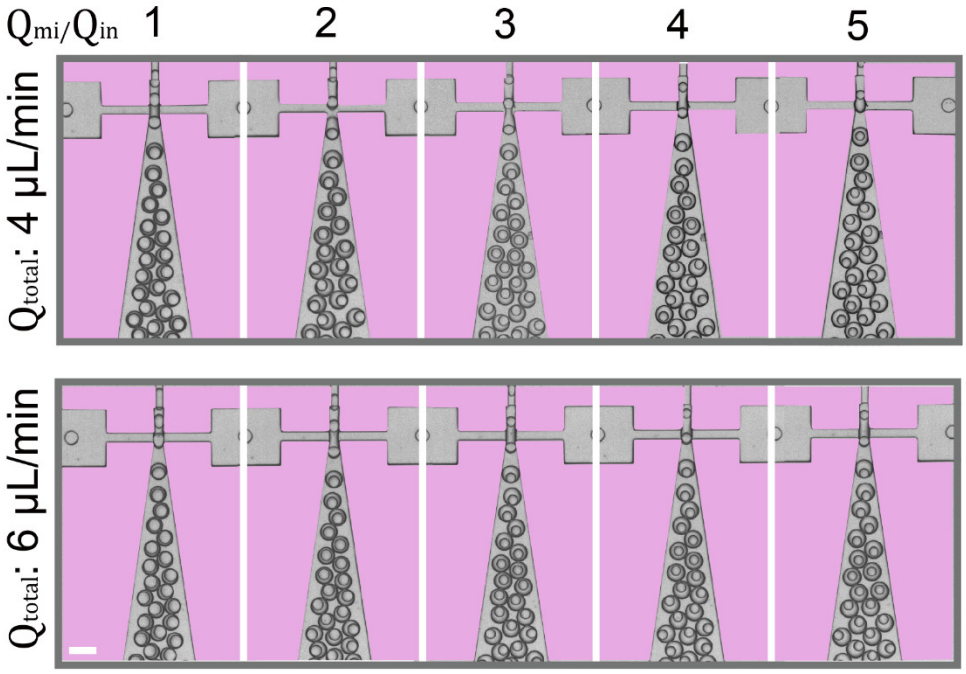

Figure S5.6 Experimental images of DE generation at five different ratios of the middle and inner phase flow rates, Q_{mi}/Q_{in}: 1, 2, 3, 4, and 5, when the total flow rate, Q_{total}, sum of $Q_{in}$and Q_{mi}, are set constant at 6 µL/min and 8 µL/min. Scale bar represents 100 µm.

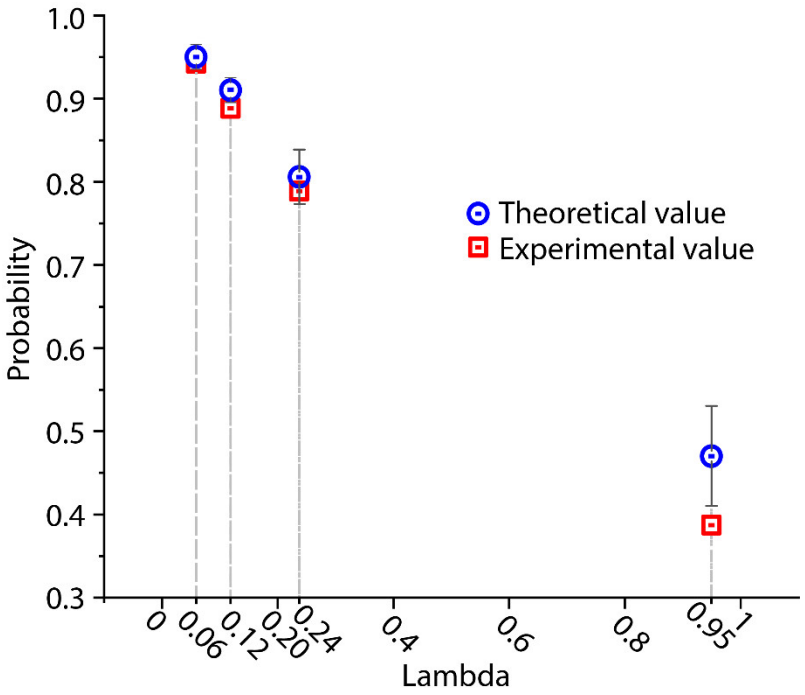

Figure S5.7. Comparison of probability of empty DEs with a D_{in} of 28.3 μm, obtained from Poisson distribution and experiments for four lambdas, 0.06 (5×10^6 cells/mL), 0.12 (1×10^7 cells/mL), 0.24 (2×10^7 cells/mL), and 0.95 (8×10^7 cells/mL).

Author Contributions

H. L. proposed the project and conceived the idea. H. L. and M. L. designed the experiments. H. L. performed the experiments. H. L., J. A. P., and M. L. analysed the results. J. A. P. and M. L. supervised the project. H. L., J. A. P., and M. L. wrote the manuscript.

References

1. Florence, A.; Whitehill, D., The formulation and stability of multiple emulsions. *Int. J. Pharm.* **1982,** *11* (4), 277-308.
2. Garti, N., Double emulsions—scope, limitations and new achievements. *Colloids Surf. A Physicochem. Eng. Asp.* **1997,** *123*, 233-246.
3. Kim, B.; Jeon, T. Y.; Oh, Y. K.; Kim, S. H., Microfluidic Production of Semipermeable Microcapsules by Polymerization-Induced Phase Separation. *Langmuir* **2015,** *31* (22), 6027-34.
4. Liu, L.; Wu, F.; Ju, X. J.; Xie, R.; Wang, W.; Niu, C. H.; Chu, L. Y., Preparation of monodisperse calcium alginate microcapsules via internal gelation in microfluidic-generated double emulsions. *J. Colloid Interface Sci.* **2013,** *404*, 85-90.

5. Volpatti, L. R.; Shimanovich, U.; Ruggeri, F. S.; Bolisetty, S.; Muller, T.; Mason, T. O.; Michaels, T. C. T.; Mezzenga, R.; Dietler, G.; Knowles, T. P. J., Micro- and nanoscale hierarchical structure of core-shell protein microgels. *J. Mater. Chem. B* **2016,** *4* (48), 7989-7999.
6. Choi, C. H.; Wang, H.; Lee, H.; Kim, J. H.; Zhang, L.; Mao, A.; Mooney, D. J.; Weitz, D. A., One-step generation of cell-laden microgels using double emulsion drops with a sacrificial ultra-thin oil shell. *Lab Chip* **2016,** *16* (9), 1549-55.
7. Brower, K. K.; Carswell-Crumpton, C.; Klemm, S.; Cruz, B.; Kim, G.; Calhoun, S. G. K.; Nichols, L.; Fordyce, P. M., Double emulsion flow cytometry with high-throughput single droplet isolation and nucleic acid recovery. *Lab Chip* **2020,** *20* (12), 2062-2074.
8. Li, S.; Gong, X.; Mc Nally, C. S.; Zeng, M.; Gaule, T.; Anduix-Canto, C.; Kulak, A. N.; Bawazer, L. A.; McPherson, M. J.; Meldrum, F. C., Rapid preparation of highly reliable PDMS double emulsion microfluidic devices. *RSC Adv.* **2016,** *6* (31), 25927-25933.
9. Mastrobattista, E.; Taly, V.; Chanudet, E.; Treacy, P.; Kelly, B. T.; Griffiths, A. D., High-throughput screening of enzyme libraries: in vitro evolution of a beta-galactosidase by fluorescence-activated sorting of double emulsions. *Chem. Biol.* **2005,** *12* (12), 1291-300.
10. Zinchenko, A.; Devenish, S. R.; Kintses, B.; Colin, P. Y.; Fischlechner, M.; Hollfelder, F., One in a million: flow cytometric sorting of single cell-lysate assays in monodisperse picolitre double emulsion droplets for directed evolution. *Anal. Chem.* **2014,** *86* (5), 2526-33.
11. Brower, K. K.; Khariton, M.; Suzuki, P. H.; Still, C., 2nd; Kim, G.; Calhoun, S. G. K.; Qi, L. S.; Wang, B.; Fordyce, P. M., Double Emulsion Picoreactors for High-Throughput Single-Cell Encapsulation and Phenotyping via FACS. *Anal. Chem.* **2020,** *92* (19), 13262-13270.
12. Li, M.; Liu, H.; Zhuang, S.; Goda, K., Droplet flow cytometry for single-cell analysis. *RSC Adv.* **2021,** *11* (34), 20944-20960.
13. Vasiljevic, D.; Parojcic, J.; Primorac, M.; Vuleta, G., An investigation into the characteristics and drug release properties of multiple W/O/W emulsion systems containing low concentration of lipophilic polymeric emulsifier. *Int. J. Pharm.* **2006,** *309* (1-2), 171-177.
14. Samandari, M.; Alipanah, F.; Haghjooy Javanmard, S.; Sanati-Nezhad, A., One-step wettability patterning of PDMS microchannels for generation of monodisperse alginate microbeads by in Situ external gelation in double emulsion microdroplets. *Sens. Actuators B Chem.* **2019,** *291*, 418-425.
15. Chung, B. G.; Lee, K.-H.; Khademhosseini, A.; Lee, S.-H., Microfluidic fabrication of microengineered hydrogels and their application in tissue engineering. *Lab Chip* **2012,** *12* (1), 45-59.
16. Sapei, L.; Naqvi, M. A.; Rousseau, D., Stability and release properties of double emulsions for food applications. *Food Hydrocoll.* **2012,** *27* (2), 316-323.
17. Wang, K.; Qin, K.; Wang, T.; Luo, G., Ultra-thin liquid film extraction based on a gas–liquid–liquid double emulsion in a microchannel device. *RSC Adv.* **2015,** *5* (9), 6470-6474.
18. van Tatenhove-Pel, R. J.; Hernandez-Valdes, J. A.; Teusink, B.; Kuipers, O. P.; Fischlechner, M.; Bachmann, H., Microdroplet screening and selection for improved microbial production of extracellular compounds. *Curr. Opin. Biotechnol.* **2020,** *61*, 72-81.
19. Korfer, G.; Pitzler, C.; Vojcic, L.; Martinez, R.; Schwaneberg, U., In vitro flow cytometry-based screening platform for cellulase engineering. *Sci. Rep.* **2016,** *6*, 26128.
20. Terekhov, S. S.; Smirnov, I. V.; Stepanova, A. V.; Bobik, T. V.; Mokrushina, Y. A.; Ponomarenko, N. A.; Belogurov, A. A., Jr.; Rubtsova, M. P.; Kartseva, O. V.; Gomzikova, M. O.; Moskovtsev, A. A.; Bukatin, A. S.; Dubina, M. V.; Kostryukova, E. S.; Babenko, V. V.; Vakhitova, M. T.; Manolov, A. I.; Malakhova, M. V.; Kornienko, M. A.; Tyakht, A. V.; Vanyushkina, A. A.; Ilina, E. N.; Masson, P.; Gabibov, A. G.; Altman, S., Microfluidic droplet platform for ultrahigh-throughput single-cell screening of biodiversity. *Proc. Natl. Acad. Sci. U. S. A.* **2017,** *114* (10), 2550-2555.
21. Li, W.; Zhang, L.; Ge, X.; Xu, B.; Zhang, W.; Qu, L.; Choi, C.-H.; Xu, J.; Zhang, A.; Lee, H.; Weitz, D. A., Microfluidic fabrication of microparticles for biomedical applications. *Chem. Soc. Rev.* **2018,** *47* (15), 5646-5683.
22. Moshksayan, K.; Kashaninejad, N.; Warkiani, M. E.; Lock, J. G.; Moghadas, H.; Firoozabadi, B.; Saidi, M. S.; Nguyen, N.-T., Spheroids-on-a-chip: Recent advances and design considerations in microfluidic platforms for spheroid formation and culture. *Sens. Actuators B Chem.* **2018,** *263*, 151-176.
23. Dinh, N.-D.; Kukumberg, M.; Nguyen, A.-T.; Keramati, H.; Guo, S.; Phan, D.-T.; Ja'Afar, N. B.; Birgersson, E.; Leo, H. L.; Huang, R. Y.-J.; Kofidis, T.; Rufaihah, A. J.; Chen, C.-H., Functional reservoir microcapsules generated via microfluidic fabrication for long-term cardiovascular therapeutics. *Lab Chip* **2020,** *20* (15), 2756-2764.
24. Iqbal, M.; Valour, J.-P.; Fessi, H.; Elaissari, A., Preparation of biodegradable PCL particles via double emulsion evaporation method using ultrasound technique. *Colloid Polym. Sci.* **2014,** *293* (3), 861-873.
25. Sukovich, D. J.; Kim, S. C.; Ahmed, N.; Abate, A. R., Bulk double emulsification for flow cytometric analysis of microfluidic droplets. *Analyst* **2017,** *142* (24), 4618-4622.

26. Bashir, S.; Bashir, M.; Solvas, X.; Rees, J.; Zimmerman, W., Hydrophilic Surface Modification of PDMS Microchannel for O/W and W/O/W Emulsions. *Micromachines* **2015,** *6* (10), 1445-1458.
27. Nisisako, T.; Okushima, S.; Torii, T., Controlled formulation of monodisperse double emulsions in a multiple-phase microfluidic system. *Soft Matter* **2005,** *1* (1), 23-27.
28. Zhang, Y.; Ho, Y. P.; Chiu, Y. L.; Chan, H. F.; Chlebina, B.; Schuhmann, T.; You, L.; Leong, K. W., A programmable microenvironment for cellular studies via microfluidics-generated double emulsions. *Biomaterials* **2013,** *34* (19), 4564-72.
29. Abate, A. R.; Weitz, D. A., High-order multiple emulsions formed in poly(dimethylsiloxane) microfluidics. *Small* **2009,** *5* (18), 2030-2.
30. Abate, A. R.; Thiele, J.; Weinhart, M.; Weitz, D. A., Patterning microfluidic device wettability using flow confinement. *Lab Chip* **2010,** *10* (14), 1774-6.
31. Kim, S. C.; Sukovich, D. J.; Abate, A. R., Patterning microfluidic device wettability with spatially-controlled plasma oxidation. *Lab Chip* **2015,** *15* (15), 3163-9.
32. Davies, R. T.; Kim, D.; Park, J., Formation of liposomes using a 3D flow focusing microfluidic device with spatially patterned wettability by corona discharge. *J. Micromech. Microeng.* **2012,** *22* (5).
33. Bai, Z.; Wang, B.; Chen, H.; Wang, M., Spatial wettability patterning of glass microchips for water-in-oil-in-water (W/O/W) double emulsion preparation. *Sens. Actuators B Chem.* **2015,** *215*, 330-336.
34. Thurgood, P.; Baratchi, S.; Arash, A.; Pirogova, E.; Jex, A. R.; Khoshmanesh, K., Asynchronous generation of oil droplets using a microfluidic flow focusing system. *Sci. Rep.* **2019,** *9* (1), 10600.
35. Martinez, C. J.; Kim, J. W.; Ye, C.; Ortiz, I.; Rowat, A. C.; Marquez, M.; Weitz, D., A microfluidic approach to encapsulate living cells in uniform alginate hydrogel microparticles. *Macromol. Biosci.* **2012,** *12* (7), 946-51.
36. Tran, T. M.; Cater, S.; Abate, A. R., Coaxial flow focusing in poly(dimethylsiloxane) microfluidic devices. *Biomicrofluidics* **2014,** *8* (1), 016502.
37. Liu, E. Y.; Jung, S.; Weitz, D. A.; Yi, H.; Choi, C. H., High-throughput double emulsion-based microfluidic production of hydrogel microspheres with tunable chemical functionalities toward biomolecular conjugation. *Lab Chip* **2018,** *18* (2), 323-334.
38. Cole, R. H.; Tran, T. M.; Abate, A. R., Double Emulsion Generation Using a Polydimethylsiloxane (PDMS) Co-axial Flow Focus Device. *J. Vis. Exp.* **2015,** (106), e53516.
39. Chang, F.-C.; Su, Y.-C., Controlled double emulsification utilizing 3D PDMS microchannels. *J. Micromech. Microeng.* **2008,** *18* (6).
40. Bauer, W. A.; Fischlechner, M.; Abell, C.; Huck, W. T., Hydrophilic PDMS microchannels for high-throughput formation of oil-in-water microdroplets and water-in-oil-in-water double emulsions. *Lab Chip* **2010,** *10* (14), 1814-9.
41. Trantidou, T.; Elani, Y.; Parsons, E.; Ces, O., Hydrophilic surface modification of PDMS for droplet microfluidics using a simple, quick, and robust method via PVA deposition. *Microsyst. Nanoeng.* **2017,** *3* (1), 16091.
42. Bodas, D.; Khan-Malek, C., Formation of more stable hydrophilic surfaces of PDMS by plasma and chemical treatments. *Microelectron. Eng.* **2006,** *83* (4-9), 1277-1279.
43. Priest, C.; Gruner, P. J.; Szili, E. J.; Al-Bataineh, S. A.; Bradley, J. W.; Ralston, J.; Steele, D. A.; Short, R. D., Microplasma patterning of bonded microchannels using high-precision "injected" electrodes. *Lab Chip* **2011,** *11* (3), 541-4.
44. Tan, S. H.; Nguyen, N. T.; Chua, Y. C.; Kang, T. G., Oxygen plasma treatment for reducing hydrophobicity of a sealed polydimethylsiloxane microchannel. *Biomicrofluidics* **2010,** *4* (3), 32204.
45. Haubert, K.; Drier, T.; Beebe, D., PDMS bonding by means of a portable, low-cost corona system. *Lab Chip* **2006,** *6* (12), 1548-1549.
46. Liu, H.; Li, M.; Wang, Y.; Piper, J.; Jiang, L., Improving Single-Cell Encapsulation Efficiency and Reliability through Neutral Buoyancy of Suspension. *Micromachines* **2020,** *11* (1).
47. Liu, H.; Xu, X.; Peng, K.; Zhang, Y.; Jiang, L.; Williams, T. C.; Paulsen, I. T.; Piper, J. A.; Li, M., Microdroplet enabled cultivation of single yeast cells correlates with bulk growth and reveals subpopulation phenomena. *Biotechnol. Bioeng.* **2021,** *118* (2), 647-658.
48. Wang, B. L.; Ghaderi, A.; Zhou, H.; Agresti, J.; Weitz, D. A.; Fink, G. R.; Stephanopoulos, G., Microfluidic high-throughput culturing of single cells for selection based on extracellular metabolite production or consumption. *Nat. Biotechnol.* **2014,** *32* (5), 473-8.
49. Jankowski, P.; Ogończyk, D.; Derzsi, L.; Lisowski, W.; Garstecki, P., Hydrophilic polycarbonate chips for generation of oil-in-water (O/W) and water-in-oil-in-water (W/O/W) emulsions. *Microfluid. Nanofluidics* **2012,** *14* (5), 767-774.
50. Zhu, X.-D.; Shi, X.; Wang, S.-W.; Chu, J.; Zhu, W.-H.; Ye, B.-C.; Zuo, P.; Wang, Y.-H., High-throughput screening of high lactic acid-producing Bacillus coagulans by droplet microfluidic based flow cytometry with fluorescence activated cell sorting. *RSC Adv.* **2019,** *9* (8), 4507-4513.

51. Yan, J.; Bauer, W.-A.; Fischlechner, M.; Hollfelder, F.; Kaminski, C.; Huck, W., Monodisperse Water-in-Oil-in-Water (W/O/W) Double Emulsion Droplets as Uniform Compartments for High-Throughput Analysis via Flow Cytometry. *Micromachines* **2013,** *4* (4), 402-413.
52. Ma, S.; Huck, W. T. S.; Balabani, S., Deformation of double emulsions under conditions of flow cytometry hydrodynamic focusing. *Lab Chip* **2015,** *15* (22), 4291-4301.
53. Thurgood, P.; Suarez, S. A.; Chen, S.; Gilliam, C.; Pirogova, E.; Jex, A. R.; Baratchi, S.; Khoshmanesh, K., Self-sufficient, low-cost microfluidic pumps utilising reinforced balloons. *Lab Chip* **2019,** *19* (17), 2885-2896.
54. Julák, J.; Kříha, V.; Scholtz, V., Corona discharge: A simple method of its generation and study of its bactericidal properties. *Czechoslov. J. Phys.* **2006,** *56* (2), B1333-B1338.
55. Boyd-Moss, M.; Baratchi, S.; Di Venere, M.; Khoshmanesh, K., Self-contained microfluidic systems: a review. *Lab Chip* **2016,** *16* (17), 3177-92.
56. Teo, A. J. T.; Malekpour-galogahi, F.; Sreejith, K. R.; Takei, T.; Nguyen, N.-T., Surfactant-free, UV-curable core–shell microcapsules in a hydrophilic PDMS microfluidic device. *AIP Adv.* **2020,** *10* (6).
57. Choi, S.; Lee, M. G.; Park, J.-K., Microfluidic parallel circuit for measurement of hydraulic resistance. *Biomicrofluidics* **2010,** *4* (3), 034110.
58. Godwin, L. A.; Deal, K. S.; Hoepfner, L. D.; Jackson, L. A.; Easley, C. J., Measurement of microchannel fluidic resistance with a standard voltage meter. *Anal. Chim. Acta* **2013,** *758*, 101-107.
59. Mach, A. J.; Di Carlo, D., Continuous scalable blood filtration device using inertial microfluidics. *Biotechnol. Bioeng.* **2010,** *107* (2), 302-311.
60. Wu, C.-Y.; Liao, W.-H.; Tung, Y.-C., Integrated ionic liquid-based electrofluidic circuits for pressure sensing within polydimethylsiloxane microfluidic systems. *Lab Chip* **2011,** *11* (10), 1740-1746.
61. Wells, R.; Badyal, J.; Drummond, I.; Robinson, K.; Street, F., A comparison of plasma-oxidized and photo-oxidized polystyrene surfaces. *Polymer* **1993,** *34* (17), 3611-3613.
62. Niepa, T. H. R.; Hou, L.; Jiang, H.; Goulian, M.; Koo, H.; Stebe, K. J.; Lee, D., Microbial Nanoculture as an Artificial Microniche. *Sci. Rep.* **2016,** *6* (1), 30578.
63. Utada, A. S.; Chu, L. Y.; Fernandez-Nieves, A.; Link, D. R.; Holtze, C.; Weitz, D. A., Dripping, Jetting, Drops, and Wetting: The Magic of Microfluidics. *MRS Bull.* **2007,** *32* (9), 702-708.
64. Cubaud, T.; Mason, T. G., Capillary threads and viscous droplets in square microchannels. *Phys. Fluids* **2008,** *20* (5).
65. Li, M.; van Zee, M.; Riche, C. T.; Tofig, B.; Gallaher, S. D.; Merchant, S. S.; Damoiseaux, R.; Goda, K.; Di Carlo, D., A Gelatin Microdroplet Platform for High-Throughput Sorting of Hyperproducing Single-Cell-Derived Microalgal Clones. *Small* **2018,** *14* (44), 1803315.
66. Perry, S. L.; Roberts, G. W.; Tice, J. D.; Gennis, R. B.; Kenis, P. J. A., Microfluidic Generation of Lipidic Mesophases for Membrane Protein Crystallization. *Cryst. Growth Des.* **2009,** *9* (6), 2566-2569.
67. Perry, S. L.; Higdon, J. J. L.; Kenis, P. J. A., Design rules for pumping and metering of highly viscous fluids in microfluidics. *Lab Chip* **2010,** *10* (22), 3112-3124.
68. Wang, D.; Huang, X.; Wang, Y., Managing the phase separation in double emulsion by tuning amphiphilicity via a supramolecular route. *Langmuir* **2014,** *30* (48), 14460-8.

Chapter 6 High-throughput microfluidics for the screening and sorting of superior cellulase activity in yeast*

***Liu, H.**; Piper, J. A.; Li, M., High-throughput microfluidics for the screening and sorting of superior cellulase activity in yeast. Palm Springs, California, USA, *MicroTAS* **2021.**

To satisfy the requirements of metabolic engineering for improving yeast strains, the recovery, regrowth, and sequencing of yeast cells exhibiting desired properties encapsulated in DEs are necessary. As a proof-of-concept study, we present the screening and sorting of S. cerevisiae factories that can produce the industrial enzyme, β-Glucosidase (BGL), using integrated DE-FACS technology. The formed DEs allows long-term culture (i.e., 4.5 hours) of encapsulated cells without any leakage or coalesce, and flow cytometric quantification and sorting. This opens avenues for synthetic biology of yeast for enzyme production at the industrial scale.

6.1 Introduction

The microbial enzymes play an import role in food, biofuel, and energy industries, which offer numerous advantages compared to traditional chemical catalysts, such as cost-effectiveness, biodegradability, specificity to substrate, and mild work conditions[1]. However, the complexity of cell metabolism has highly hindered the engineering of industrial microbes for discovery or improvement of enzyme characteristics[2]. High-throughput droplet microfluidics has enabled the evolution of microbial enzymes but calls for techniques that can analyse enzyme activity of yeast (*S. cerevisiae*), an important cell factory. Here, we present a study on the screening and sorting of β-Glucosidase (BGL) activity in single yeast cells using an integrated DE and FACS approach (see Fig. 6.1). In this study, we encapsulated single yeast

cells that can secrete BGL and fluorogenic substrates in uniform DEs (C.V.< 2%) acting as bioreactors. After culture and enzyme reaction, flow cytometric screening and sorting of DEs were performed based on BGL activity. Sorted cells can recover from DEs and remain viable, enabling further downstream analysis (e.g., re-culture and sequencing).

6.2 Methods and Materials

The PDMS microfluidic device (see Fig. S6.1A) employed for single-cell laden DEs generation (see Fig. S6.1B) consists of two separate droplet generators, which possess the reverse surface properties. The device design is similar to the one of Fig. S5.1, whereas the depths are 15 and 25 μm for the two respective layers, resulting in smaller DEs suitable for FACS processing (see Fig. S6.1C). The method to prepare the spatial patterning of wettability is reported in our previous study[3]. We mixed yeast cell population (at a concentration of 1 × 10^7 cells/mL) and 100 μM Fluorescein Di-β-D-Glucopyranoside as an inner phase, surfactant-added fluorinated oil as a middle phase, and surfactant-added PBS as an outer phase. The

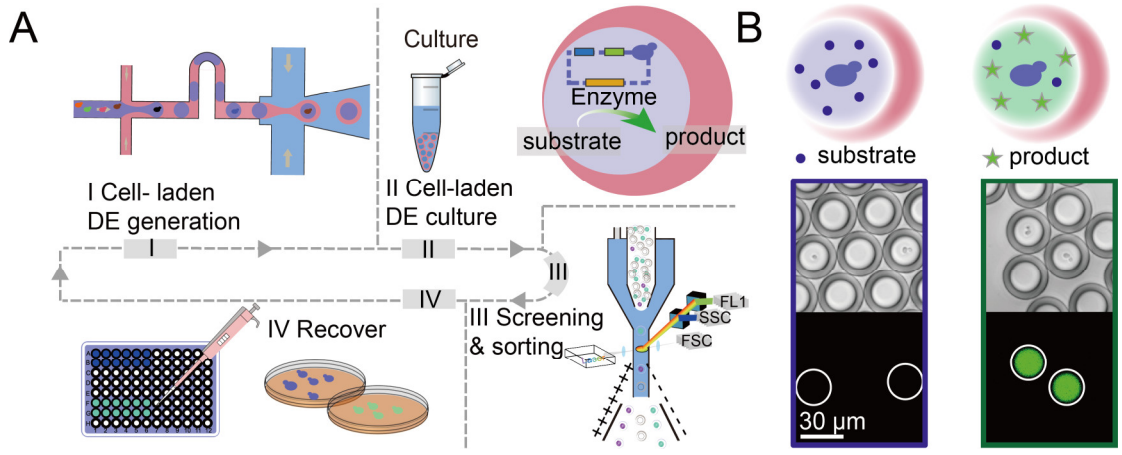

Figure 6.1 Illustration of the workflow and fluorescence-based enzymatic assays. A) A workflow for the screening and sorting of enzyme activity in single yeast cells using an integrated DE-FACS method. (I) Individual yeast cells and fluorogenic substrate are encapsulated into DEs. (II) Cell-laden DEs incubation for enzyme reactions. (III) Screening and sorting of DEs based on yeast enzyme activity using FACS. (IV) Yeast cells can be recovered from sorted DEs for downstream analysis. B) Comparison of DEs containing yeast cells without (left) and with (right) significant enzyme activity after 4.5h culture.

generated DEs were cultured over 4.5 hours for the screening and sorting based on enzyme activity by FACS (BD FACSMelody™).

6.3 Results and discussion

DEs enabled the trapping of small molecules (i.e., fluorescein) inside the compartments over 6 h (see Fig. S6.2). Bright-field and fluorescence images showing the increase in BGL activity of *S. cerevisiae* single cells in DEs over 4.5 h are presented in Fig. S6.3. We achieved the screening of BGL activity of *S. cerevisiae* after culture of 0.5, 1.5, 3, and 4.5 h, using FACS (see Fig. 6.2A). At least 30,000 events and 1,000 fluorescence-positive events were recorded for each experiment. We found that DEs containing wild-type *S. cerevisiae* cells that do not secrete BGL have almost no fluorescence signal, even after 4.5 h culture; and the BGL activity of single yeast cells (a BGL3 mutant) can be detected even after 0.5 h culture. Also, the fluorescence intensity of DEs containing mutant cells gradually increases over time (see Fig. 6.2B). Furthermore, as a proof-of-concept study of the sorting of cells secreting BGL, we mixed mutant cells that secret BGL (positive) and wild-type cells at a ratio of 1:1. The initial

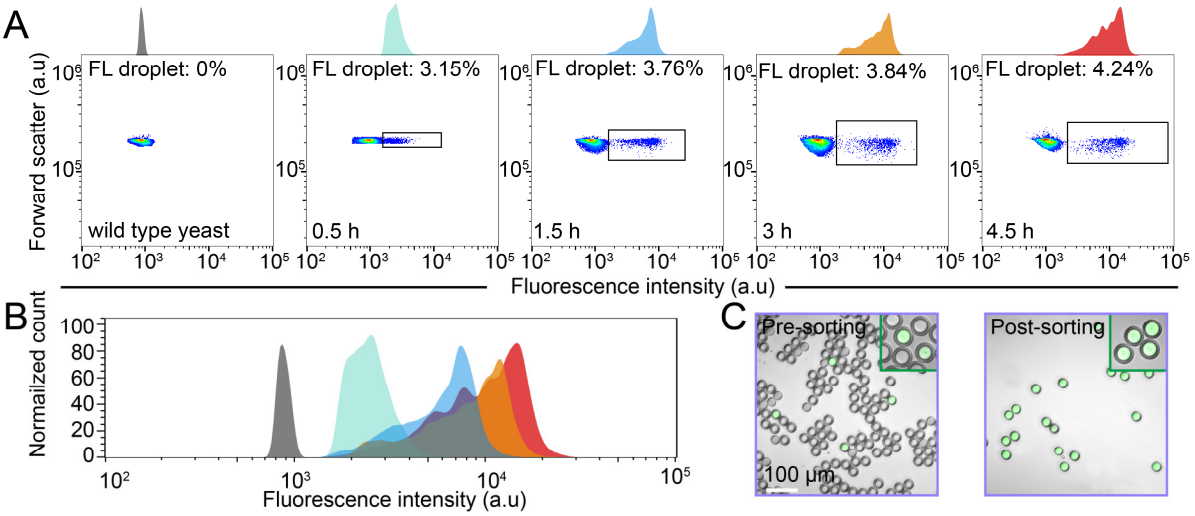

Figure 6.2: Screening and sorting of yeast cells BGL activity using FACS. A) Forward scatter vs fluorescence intensity of mixed DEs containing wild-type cells and mutant cells secreting BGL at different time points. The square gate encircles DEs containing BGL-secreting cells. B) Comparison of the fluorescence intensity of positive DEs in the defined gates at different time points. C) Enrichment of DEs containing BGL secreting cells after 4.5h culture.

percentage of positive DEs are less than 2% of the total. After a 4.5 h culture, 8,000 DEs containing positive cells were isolated from ~550,000 events at a frequency of ~ 2,000 Hz. 92% of the sorted DEs are positive, yielding a 46-fold enrichment (Fig. 6.2C).

6.4 Conclusions

The integrated DE-FACS method is firstly used for the screening and sorting of cellulase activity.in single yeast cells. We showed quantitative tracking of the BGL activity of single yeast cells in DEs over time and sorting of yeast cells showing high BGL activity We envision that this method can be readily applied for the development and improvement of enzymes produced by yeast based on a mutagenesis library containing millions of variants.

Supporting Information

Fig. S6.1 Generation of highly monodisperse DEs containing yeast single cells, Fig. S6.2 Trapping of fluorescein inside DEs over 6 h, Fig. S6.3 Images showing the increase in BGL activity of *S. cerevisiae* single cells over 4.5 h.

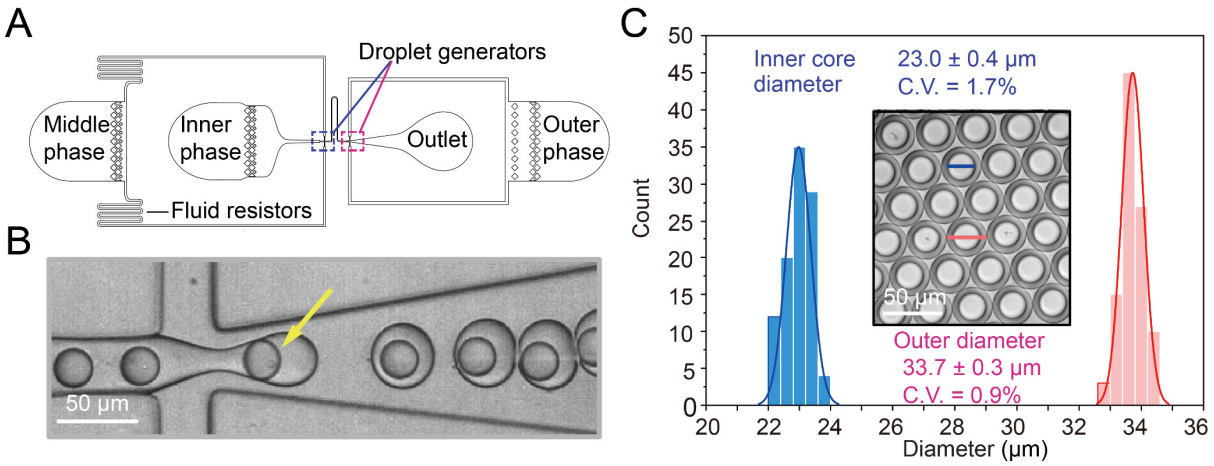

Figure S6.1 Generation of highly monodisperse DEs containing yeast single cells. A) Design of the microfluidic device used in this study, B) Encapsulation of yeast single cells in DEs. C) Size distribution of the inner core diameter and the outer diameter of generated DEs.

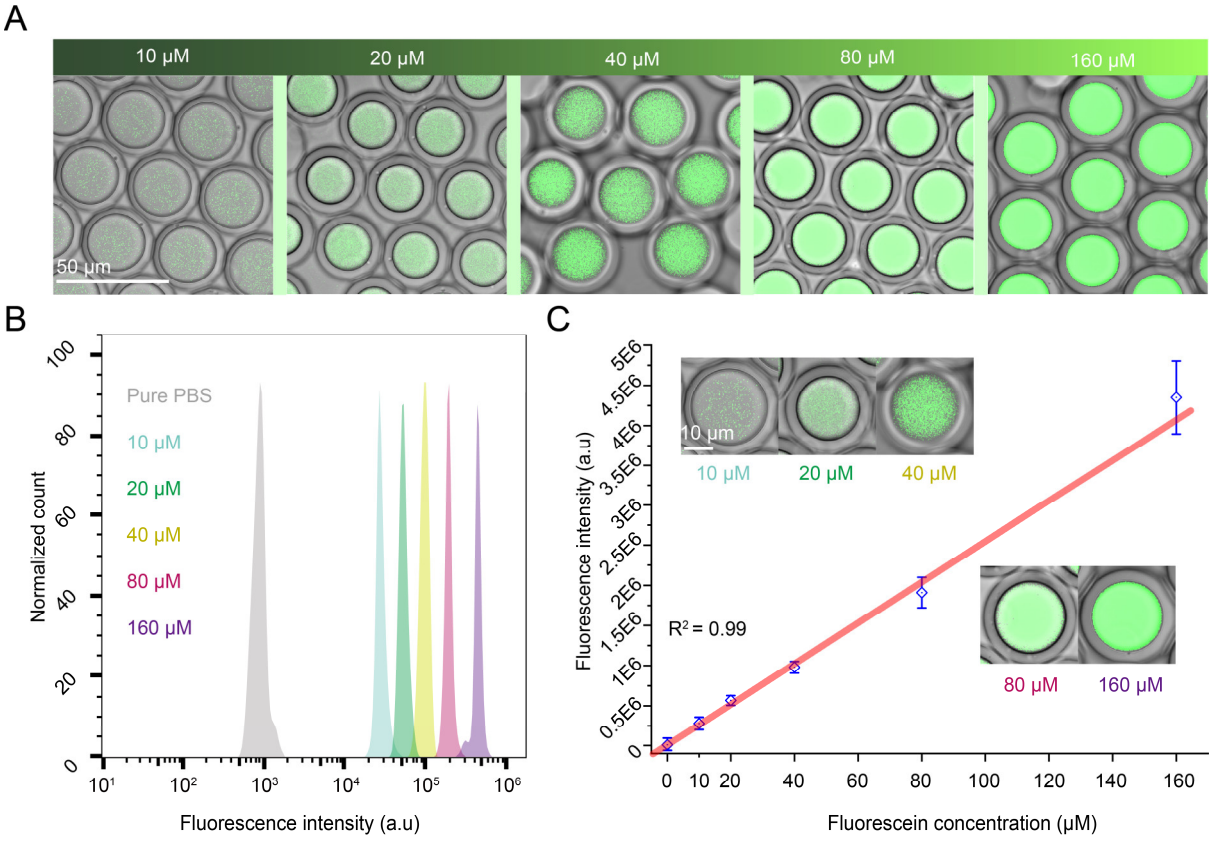

Figure S6.2 Trapping fluorescein inside DEs over 6 h. A) Confocal images of different concentrations of fluorescein trapped in DEs. B) A histogram of fluorescence intensity of DEs containing different concentrations of fluorescein measured by FACS. C) Plots of the fluorescence intensity of DEs containing different concentrations of fluorescein versus the concentrations of fluorescein. R^2 is 0.99 for the linear fit.

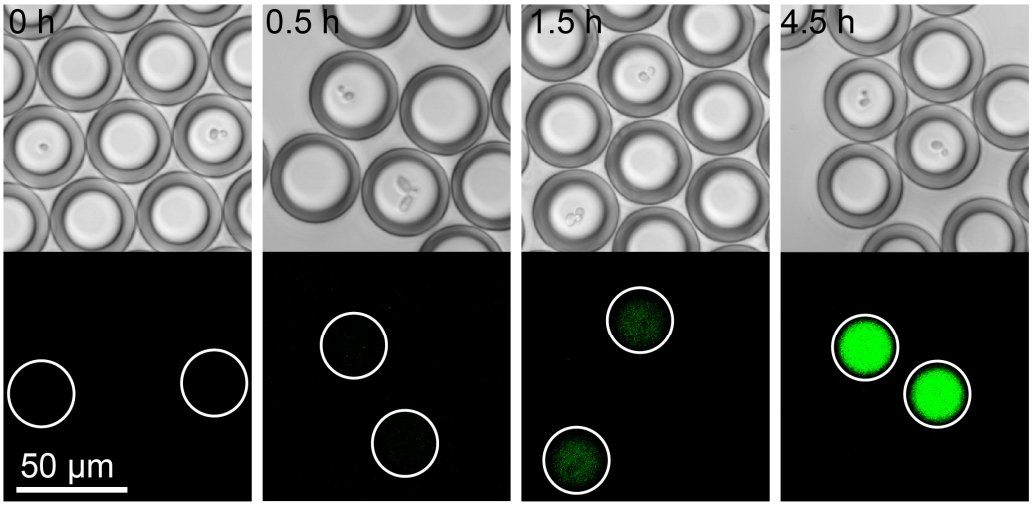

Figure S6.3 Bright-field and fluorescence images showing the increase in BGL activity of *S. cerevisiae* single cells in DEs over 4.5 h.

Author Contributions

M. L. proposed the project and conceived the idea. H. L. and M. L. designed the experiments. K. P. prepared the biological samples. H. L. performed the experiments. J. A. P. and M. L. supervised the project. All authors analysed the date and wrote the manuscript.

References

1. Dietrich, J. A.; McKee, A. E.; Keasling, J. D., High-Throughput Metabolic Engineering: Advances in Small-Molecule Screening and Selection. *Annu. Rev. Biochem.* **2010,** *79* (1), 563-590.
2. Baker, D., An exciting but challenging road ahead for computational enzyme design. *Protein Sci.* **2010,** *19* (10), 1817-1819.
3. Liu, H.; Piper, J. A.; Li, M., Rapid, Simple, and Inexpensive Spatial Patterning of Wettability in Microfluidic Devices for Double Emulsion Generation. *Anal. Chem.* **2021**.

Chapter 7 Conclusions and future work

7.1. Conclusions

This thesis describes research aimed at improving the precision, efficiency, and cost-effectiveness of DE-FACS approach for high-throughput single-cell assays, particularly the directed evolution of extracellular enzyme in yeast. The explorations are built on four existing challenges that have prevented further widespread applications of integrated DE-FACS platform technology, including 1) unreliable passive encapsulation of single cells; 2) lack of a comprehensive correlation between single-cell culture in microdroplets and bulk cultures; 3) inefficiency of current methods to generate monodisperse DEs; and 4) lack of studies on the direction evolution of extracellular enzymatic activities of yeast single cells by DE-FACS.

First, I improved the encapsulation efficiency of single cells in microdroplets using a density-match approach. Cell sedimentation and aggregation in suspensions that occurred before or during cell injection into microfluidic chips can cause either a limited number of droplets containing single cells or excessive droplets encapsulated with multiple cells. To alleviate this negative influence of gravity, a biocompatible, non-ionic density-matching reagent, OptiPrep™, was added to the culture medium to acquire a neutral buoyancy of cell suspensions. I performed a detailed quantitative study of the effect of OptiPrep™ on the single-cell encapsulation efficiency using THP-1 cells encapsulated in ~81 μm w/o droplets. It is found that the distribution of droplets containing cells is best fitted to Poisson distribution when 13.2% OptiPrep™ is added into the aqueous phase. Additionally, no significant differences in cell viability were found among droplets containing 0%, 8%, and 16% OptiPrep™ within 12 h, while the cells in droplets with 16% OptiPrep™ has lower viability than the rest at 24 h.

Second, I performed multiple yeast single-cell cultures in microdroplets using different cell strains and environmental conditions. At first, the growth of *S. cerevisiae* single cells in

microdroplets was tracked over 24 h. The number of cells per droplet generally increased over time, from 3.2 cells at 2 h to 50 cells at 24h, with a μ_{max} of 0.23 of the first 10 hours, which is comparable to that of 0.21 for bulk culture. Moreover, the effect of acids (e.g., PA and AA) with different concentrations on the growth of yeast single cells were assessed. Not only an evolved mutant strain showed high resistance to PA stress, but also the addition of K^+ was found to significantly increase the resistance of wild-type cells. These growth and physiological phenomena of yeast single cells observed in microdroplets experience the same trend with those of yeast grown in bulk. Notably, the cell-to-cell variation was revealed in all experiments, which has been obscured in previous bulk cultures.

Third, I developed a rapid, simple, and low-cost method to spatially pattern wettability in a singular PDMS microfluidic device for DE generation. The microfluidic device is designed with two sequential droplet generators, separated by a narrow, serpentine microchannel acting as a corona resistor. This approach adopts an inexpensive hand-held corona treater to generate localised plasma at targe regions, which is further confined by the corona resistor. The generation of highly monodisperse DEs with tunable structures and morphologies was achieved. To prove the versatility of DEs generated by this method, I used the generated DEs as templates for preparing gelatin microgels and for culturing GFP-tagged yeast single cells.

Lastly, based on the above achievements, I demonstrated, for the first time, the use of the integrated DE-FACS approach for high-throughput (> 2,000 events/s) screening and sorting of DEs encapsulated with yeast single cells exhibiting a high yield of BGL3 cellulase. As a proof of concept, an artificial library was prepared by mixing wild type and mutant strains at a ratio of 1:1. By encapsulating and cultivating individual cells from the library with a fluorogenic substrate in DEs, BGL3 secreting cells can be identified and isolated by FACS. As a result, 8,000 DEs from 550,000 DEs were isolated with a sorting accuracy of 92%, leading to a 46-fold enrichment of BGL3 secreting cells.

7.2. Future work

In this thesis, I optimised integrated DE-FACS platform technology from different aspects for yeast extracellular enzymatic activity assays. These achievements validate the potentials of this integrated platform technology for the directed evolution of extracellular enzymes in yeast, which has not yet been reported. Nevertheless, an establishment of a high-impact microfluidic single-cell analytical platform normally includes knowledge from various fields[1-4], e.g., physics, engineering, microbiology, genetics, bioinformatics, and so on. Therefore, several future investigations need to be performed to achieve the claimed goal in this study and to extend the applications of DE-FACS technology.

Mutagenesis is needed to create a mutant variant library for the directed evolution of enzymes produced by yeast. A mutant library consisting of a large number of mutants exhibiting different levels of from extracellular enzymatic activities will be screened and isolated by DE-FACS. To date, several mutagenesis approaches have been developed, e.g., error-prone PCR, chemical mutagenesis, UV-induced mutagenesis, atmospheric and room temperature plasma. Notably, a novel method named Synthetic Chromosome Rearrangement and Modification by LoxPsym-mediated Evolution (SCRaMbLE) has been demonstrated to generate a wide range of mutations in the chromosome structure of yeast. Compared with conventional methods, this approach can induce mutations in cells with a high positive mutation rate and high cell viability. In the subsequent study, I plan to use SCRaMbLE to generate yeast variants and use developed DE-FACS technology to select mutants exhibiting high BGL3 activity.

Downstream analysis. After the sorting of the desired variants exhibiting desired properties, a wide range of assays can be performed on the isolated variants (e.g., sequencing and bioinformatic analysis). This genome mining provides new insights into the underlying mechanisms of the molecular evolution of enzymes. Expectedly, I will identify new gene

clusters and protein regions contributing to the secretion or activity of enzymes and further apply this knowledge in the synthesis of yeast genomes.

Applications. This developed DE-FACS approach is not limited to *S. cerevisiae*. In the future, I will expand the use of this approach for the functional and genomic profiling for other microorganisms of industrial and biomedical importance at the single-cell level, including fungus (e.g., *Y. lipolytica*, *Trichoderma reeseia*, *Aspergillus sp*., *Hansenula polymorpha*), prokaryotic cells (e.g., *E. coli*, *Cyanobacteria*, *Bacillus sp*, and *Lactococcus lactis*), microalgal cells (e.g., *Haematococcus pluvialis* and *Chlamydomonas reinhardtii*), etc.

With further advances of DE-FACS, I foresee that this integrated platform technology will be adopted by wider communities for a wider range of industrial and biomedical applications.

References

1. Terekhov, S. S.; Smirnov, I. V.; Stepanova, A. V.; Bobik, T. V.; Mokrushina, Y. A.; Ponomarenko, N. A.; Belogurov, A. A., Jr.; Rubtsova, M. P.; Kartseva, O. V.; Gomzikova, M. O.; Moskovtsev, A. A.; Bukatin, A. S.; Dubina, M. V.; Kostryukova, E. S.; Babenko, V. V.; Vakhitova, M. T.; Manolov, A. I.; Malakhova, M. V.; Kornienko, M. A.; Tyakht, A. V.; Vanyushkina, A. A.; Ilina, E. N.; Masson, P.; Gabibov, A. G.; Altman, S., Microfluidic droplet platform for ultrahigh-throughput single-cell screening of biodiversity. *Proc. Natl. Acad. Sci. U. S. A.* **2017,** *114* (10), 2550-2555.
2. Terekhov, S. S.; Smirnov, I. V.; Malakhova, M. V.; Samoilov, A. E.; Manolov, A. I.; Nazarov, A. S.; Danilov, D. V.; Dubiley, S. A.; Osterman, I. A.; Rubtsova, M. P.; Kostryukova, E. S.; Ziganshin, R. H.; Kornienko, M. A.; Vanyushkina, A. A.; Bukato, O. N.; Ilina, E. N.; Vlasov, V. V.; Severinov, K. V.; Gabibov, A. G.; Altman, S., Ultrahigh-throughput functional profiling of microbiota communities. *Proc. Natl. Acad. Sci. U. S. A.* **2018,** *115* (38), 9551-9556.
3. Romero, P. A.; Tran, T. M.; Abate, A. R., Dissecting enzyme function with microfluidic-based deep mutational scanning. *Proc. Nat.l Acad. Sci. U. S. A.* **2015,** *112* (23), 7159.
4. Agresti, J. J.; Antipov, E.; Abate, A. R.; Ahn, K.; Rowat, A. C.; Baret, J.-C.; Marquez, M.; Klibanov, A. M.; Griffiths, A. D.; Weitz, D. A., Ultrahigh-throughput screening in drop-based microfluidics for directed evolution. *Proc. Nat.l Acad. Sci. U. S. A.* **2010,** *107* (9), 4004.

Appendix

Biosafety letter 1

OFFICE OF THE DEPUTY VICE-CHANCELLOR (RESEARCH)
Research Office | Biosafety

MACQUARIE University
SYDNEY·AUSTRALIA

24 October 2019

Dear Lianmei Jiang,

Re: Microfluidic based cancer biomarker analysis - 0905

Your Project Amendment request for the above mentioned project has been approved effective 24 October 2019.

Please note this amendment will not change the project expiration date 14/09/2023.

Kind Regards,
Biosafety Secretariat

Research Services
Level 3 Research Hub, Building C5C East
Macquarie University, NSW 2109 Australia
T: +61 2 9850 4063
E: biosafety@mq.edu.au
W: mq.edu.au/research

Biosafety letter 2

OFFICE OF THE DEPUTY VICE-CHANCELLOR (RESEARCH)
Research Office | Biosafety

MACQUARIE University
SYDNEY·AUSTRALIA

29/06/2020

Dear Dr Ming Li,

Re:" High-throughput single-cell manipulation and analysis using microfluidics" - 52020610117282

Your notification application has been documented effective 29/06/2020. The risk assessment portion of this project is valid for 5 years.

Please ensure a hard copy of this project is made available in your laboratory for reference.

A final report for this project will be due by 29/06/2025 .

Kind Regards
Claudia Huang

Biosafety Secretariat - Research Services Level 3
Research Hub, Building C5C East
Macquarie University, NSW 2109 Australia
T: +61 2 9850 4063
E: biosafety@mq.edu.au
W: mq.edu.au/research